Dynamic Incompressible Navier-Stokes Model of Catalytic Converter in 1-D Including Fundamental Oxidation Reaction Rate Expressions

By
Sudarshan Loya

Submitted to the graduate degree program in Mechanical Engineering and the Graduate Faculty of the University of Kansas in partial fulfillment of the requirements for the degree of Master of Science.

_____
Chairperson Dr. Christopher Depcik

_____
Dr Bedru Yimer

_____
Dr. Peter TenPas

Date Defended: 06/20/11

The Thesis Committee for Sudarshan Loya
certifies that this is the approved version of the following thesis:

Dynamic Incompressible Navier-Stokes Model of Catalytic Converter in 1-D Including Fundamental Oxidation Reaction Rate Expressions

_____
Chairperson Dr. Christopher Depcik

_____
Dr Bedru Yimer

_____
Dr. Peter TenPas

Date approved: 08/23/11

Abstract

Classical one-dimensional (1D) models of automotive catalysts are effective in designing catalyst systems that meet current emission standards. These models use various assumptions in order to simplify the mathematical formulation. Although these postulations have been effective in the past, they might not work with new versions of catalytic converters and the architectures being proposed. In particular, classical models neglect viscosity, conductivity and diffusion in the bulk gas phase. However, in low flow rate regenerative catalysts, these terms might become important. In order to account for these phenomena, an updated model is proposed for the dynamically incompressible flow in the converter. At the same time, derivation and utilization of these terms is studied for proper inclusion in the model.

Furthermore, it is evident from the history of catalyst modeling that precise reaction rate expressions are needed for accurate predictions. In order to determine the correct reaction rate expression, this work includes the history of the fundamental reactions of automotive catalysts including carbon monoxide (CO), hydrogen (H_2) and nitric oxide (NO) oxidation on a widely used material formulation (platinum catalyst on alumina washcoat). A detailed report of these reactions is incorporated for the reader in order to understand the reaction mechanism along with the creation of a reaction rate expression. Using this review, the CO oxidation reaction is modeled in order to validate the changes proposed in the updated flow model. Moreover, the importance of using the model for determining the characteristics of the catalyst in low flow conditions is presented. This work ends by describing the success and failures of the revised model as compared to the classical model.

Acknowledgement

After realizing the dream of being master in Mechanical engineering, I understand that it was not me, but support of so many people that helped me reach this stage. Had this people not shared their time, happiness and enthusiasm with me, being here would have never been possible.

First and foremost a sincere thanks to Dr. Depcik (Dr. D) for sharing his thoughts, passion, guidance and enthusiasm with me. His constant support and confidence helped me to overcome innumerable hurdles. I thank you from bottom of my heart to drive me till here and hope to get your support in future also.

I will like to express a sincere gratitude towards Dr. Yimer and Dr. TenPas for their support and time. I have learned a lot from you and my knowledge in the field of mechanical engineering would have never reached this stage without your support and guidance.

A special thanks to all my lab mates, Anand, Michael, Travis, Austin, Charles and Eric. I thoroughly enjoyed the time working in lab because of all you guys. I would also like to thanks my friends at Lawrence for helping me in my time of frustration and installing confidence in me.

Last but not the least; I thank the almighty god, my parents and family members for their blessings and understanding. I hope to receive your blessings all life long. I have no words to express my gratitude towards you and just want to say “THANK YOU” from bottom of my heart.

Table of Contents

List of Figures

List of Tables

Chapter 1: Introduction & Literature Review

1.1 Introduction:

The internal combustion engine, either rotary or piston cylinder, is the primary power plant of today's world. Although it is used in both an on- and off-road capacity, automobiles are typically their primary customer. Because of their versatility, flexibility and low initial cost, automobiles dominate the market for passenger and transport freight [1]. Furthermore, economic growth in developing countries like India, China, Brazil, and Chile has triggered an increase in the number of automobiles on the road [1-3].

The combustion of carbonaceous fuel in these engines leads to the formation of various byproducts, released in air as exhaust gases. Since combustion occurs at a high temperature and pressure in fractions of a second, dissociation and incomplete combustion lead to partial and complete products of combustion [4]. Exhaust species like carbon monoxide (CO), carbon dioxide (CO_2), particulate matter (PM), water (H_2O), oxides of nitrogen (NO_x), oxides of sulfur (SO_x) and hydrocarbons (HC) resulting from combustion pollutes the air and has drastic effects on human life and nature. When these pollutants are near the earth surface, they cause various health issues like asthma, respiratory problems, and irritation to the eyes and damage to the lungs [1, 5-7]. Away from the surface, they are directly responsible for acid rain and global warming. For example, Figure 1 and Figure 2 illustrate how the increasing number of automobiles around the globe has increased the total carbon dioxide footprint in the atmosphere. As a result, before irreparable damage is done to nature and mother earth, pollution must be controlled.

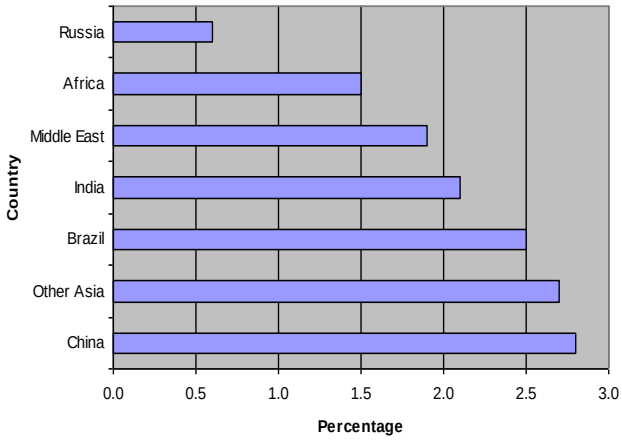

Figure 1: Average Annual Growth in Carbon Dioxide Emissions [2].

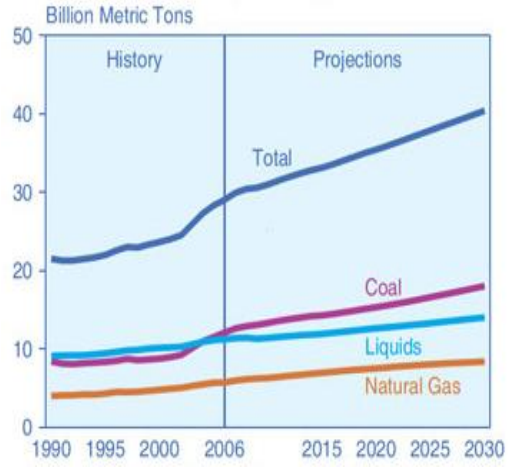

Figure 2: Carbon Dioxide Emissions by Fuel Type [2].

When the effects of pollution became visible in the 1950's, the federal government conducted research on its source. It was found that automobiles are one of the biggest sources of emissions, which led to the formulation of various laws in order to enforce pollution control from the automobile [4, 8-9]. In specific, the Clean Air Act of 1970 gave the environmental protection agency (EPA) authority to regulate motor vehicle pollution; hence, dictating the allowed quantity of each species emitted [8-10].

The creation of pollutants can be controlled inside the cylinder through modifying engine design or by using alternative fuels. In the beginning, fundamental improvements in engine design were enough to meet the emission norms through in-cylinder techniques like Exhaust Gas Recirculation (EGR) and fuel injection over carburetion. However, progressively over a number of years, emission standards became increasingly stringent, which led to implementation of catalytic converters. Catalytic converters are small chemical reactors that convert the hazardous combustion by-products to

Figure 3: Methodologies in Order to Reduce Pollution from Automobiles [11].

less toxic substances [12]. They utilize expensive metals like platinum, palladium and rhodium in order to achieve the desired reactions. As a result, by 1975 all three techniques were being utilized to reduce emissions as illustrated by Figure 3 [13].

In 1990, the Clean Air Act introduced new emission standards that include carbon monoxide emission limits at relatively low temperatures (20 degrees Fahrenheit). Moreover, stringent emission standards were set for diesel engines and emission regulations were enacted for all vehicle weight categories irrespective of size or fuel [8, 11, 14]. To comply with this continual standard revision, catalytic converters have undergone various modification and improvements in order to perform both the oxidation and reduction of exhaust gases. Current systems reduce nitrogen oxides to elemental nitrogen and oxygen while oxidizing carbon monoxide and hydrocarbons to carbon dioxide and water. In order to achieve these stringent norms, new designs and operation methodologies have been proposed [15].

Since, catalytic converters use expensive platinum group metals (PGM), this significantly increases the overall cost of automobile. Therefore, it becomes important to simulate the flow of exhaust gases over the catalytic converter in order to minimize the use of these metals without compromising on tailpipe emission levels. Over the years, catalytic converters have been updated with various physical and chemical improvements in order to make the simulations more predictive and practically applicable. Moving ahead, because catalytic converters involve chemical reactions, it is necessary to have adaptive and predictive reaction rate expressions in order to create a better model that can be used to further reduce the cost of the device while increasing its effectiveness. Moreover, with the continual development of new designs and changes to their operation, the governing equations of these models need further adaptation for accuracy and predictability.

1.2 Catalytic Converter:

In order to understand the need to modify current models of catalytic converters, one must understand the basic catalytic converter, its workings along with the existing fundamentals of the model.

1.2.1 COMPONENTS OF CATALYTIC CONVERTER:

A catalytic converter consists of three components: Substrate, washcoat and the catalyst. The substrate is a ceramic, stainless steel or silicon carbide honeycomb structure, which supports the washcoat and the catalyst. A honeycomb structure is employed in order to increase the surface area providing a significant region for catalytic reactions. In addition, the small channels used in the converter (on the order of 1mm in width and height) create laminar flow increasing residence time [16]. A silica or alumina washcoat is added to the substrate in order to make the surface irregular or rough. This further increases the surface area enhancing effectiveness. This washcoat supports the catalyst and sometimes helps in the reaction process through secondary reactions. Moreover, reactants are sometimes adsorbed on the washcoat and then diffused over the catalytic material in order to increase the reaction rate of the converter. The catalyst is a precious metal, dispersed over the washcoat and acts as the active site for the reaction. As exhaust gases flow through a catalyst, they adsorb onto the catalyst, undergo various reactions with subsequent release as non-toxic gases back in the gas flow. The catalyst used depends on the engine type and different levels of exhaust species. For spark ignition (SI) engines, a three-way catalytic converter (TWC) is used, which consists of platinum group metals (PGM) as the primary reactive material. Whereas, for compression ignition (CI) engines, one option is to use lean NO_x traps (LNT) consisting of alkali and alkali earth metals along with platinum group metals. The reason for this

differentiation between options relates to the different engine types explained in the next section.

1.2.2 CATALYTIC CONVERTER USED FOR SI ENGINE:

Spark Ignition (SI) engines typically operate around a stoichiometric ratio of fuel and air. Stoichiometry involves the relative quantity of the products and reactants such that, on completion of the reaction there is no shortfall or excess of the reactants. For example, in the following equation, one mole of carbon monoxide and a half mole of oxygen is required in order to form one complete mole of carbon dioxide:

$CO + 0.5O_2 \rightarrow CO_2$	(1)

If either of the reactants are not in the desired amount, then the reactant available in a lower quantity will undergo complete conversion; whereas, the species in excess will appear in the products.

Typically for an SI engine, the goal is to provide the exact amount of oxygen necessary for complete conversion of a hydrocarbon fuel into only water and carbon dioxide. As a part of the air, ideally nitrogen gas should not undergo any reactions. However, since the combustion reaction inside the cylinder happens at high temperatures and pressures, some of the nitrogen reacts with oxygen to form nitrogen oxides through dissociation and chemical kinetics. Moreover, since an engine is not a perfect combustor, hydrocarbon species are left over from incomplete combustion (crevices, oil, wall quenching, etc…). Furthermore, incomplete combustion, dissociation and kinetics all influence the production of carbon monoxide in the engine. As a result, these engines produce a relatively moderate amount of CO, HC and NO_x emissions [17-18].

Of importance, catalysts are unable to convert NO_x in the exhaust stream into elemental nitrogen and oxygen through an oxidation process over a catalyst. This is because

the oxidation process of NO leaving the engine (the main constituent) prefers to form NO_2 rather than N_2. However, since NO_x is a significant oxidizer, it reacts with CO and HC to reduce all species to benign products (CO_2, H_2O and N_2). Any left over CO and HC species then convert via oxidation using any available oxygen left in the exhaust stream or through a secondary-air injection [19]:

$C_aH_b + (a + 0.25b)O_2 \rightarrow aCO_2 + 0.5bH_2O$	(2)
$C_aH_b + \left(\frac{2a}{x} + \frac{0.5b}{x}\right)NO_x \rightarrow aCO_2 + 0.5bH_2O + \left(\frac{a}{x} + \frac{0.5b}{2x}\right)N_2$	(3)
$CO + \left(\frac{1}{x}\right)NO_x \rightarrow CO_2 + \left(\frac{1}{2x}\right)N_2$	(4)

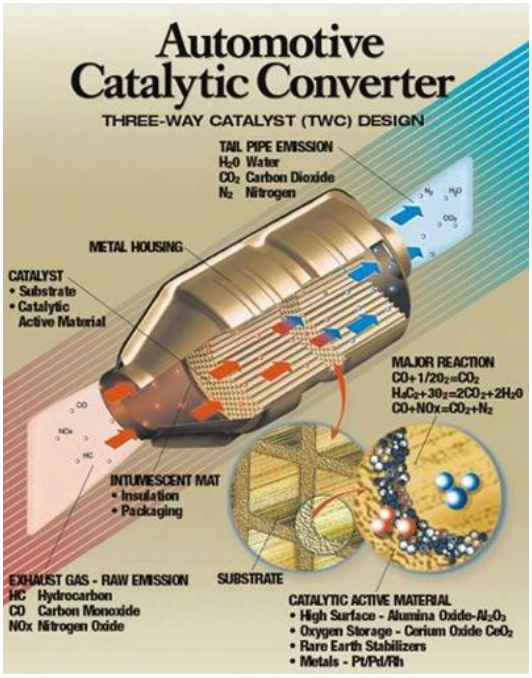

Figure 4: General Design of Three Way Catalyst [20].

The aftertreatment device that produces these three reactions is called a TWC because the three main constituents (CO, HC and NO_x) are converted. In this device, platinum and palladium are utilized as the oxidizing catalyst for conversion of CO and HC; whereas, platinum and rhodium are used as a reducing catalyst to convert NO_x with CO and HC. In the

end, only water, carbon dioxide and nitrogen are released as exhaust from the tailpipe as illustrated in Figure 4.

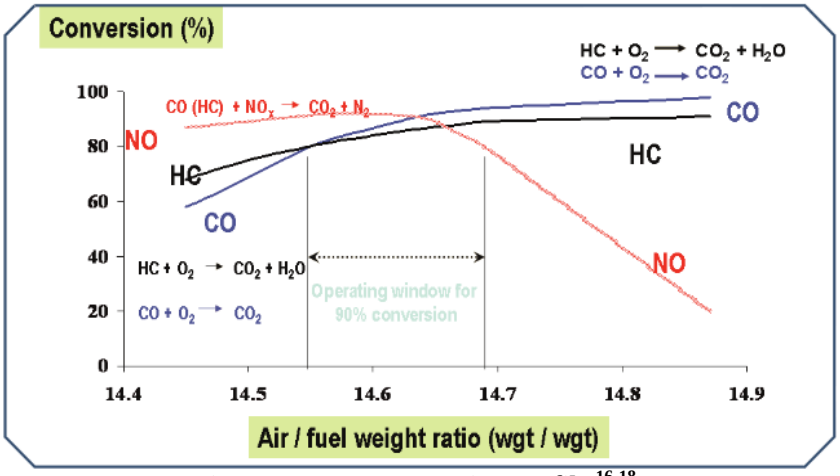

Figure 5: TWC Conversion Profile [16-18].

1.2.3 CATALYTIC CONVERTER USED FOR CI ENGINES:

Compression Ignition (CI) engines run lean in that excess oxygen is supplied as compared to the hydrocarbon fuel. In this case, the engine operates with surplus air resulting in nearly complete combustion of the fuel ending in relatively low CO and HC emissions. However, the engine produces relatively high nitrogen oxide emissions as the excess air coupled with high temperatures promotes N_2 and O_2 dissociation. As a result, this engine produces significant NO_x emissions and relatively low HC and CO emissions. Yet, a TWC is most effective when the engine is running near stoichiometry (approximately an air-to-fuel mass ratio of 14.6) as shown in Figure 5 [1, 9, 17]. This is because in this range enough CO and HC are produced in order to reduce the oxides of nitrogen into its basic elements. Due to a lack of CO and HC available under lean conditions, and the fact that NO_x cannot be oxidized by itself, the TWC fails to meet required NO_x standards. As a result, different catalyst formulations are used for CI engines in order to achieve emission standards.

The first such option is a Selective Catalytic Reduction (SCR) aftertreatment device. An SCR operates by converting nitrogen oxides to diatomic nitrogen using a reductant like ammonia or urea, with the aid of catalyst. The reductant is added to the exhaust gas stream and passed over a catalyst, like vanadium, in order reduce the nitrogen oxides [9, 21]. Using SCR to eliminate NO_x offers an important advantage of optimizing the engine for fuel economy by adjusting injection timing and reducing the amount of EGR [22-23]. As explained earlier, both EGR and injection timing were techniques used by engine manufacturers in order to reduce the amount of pollutants formed. While effective, using this methodology robs the device of its potential. For example, EGR is used to reduce the amount of NO_x generated by the engine through recirculation of exhaust gas back into the engine intake. This modification reduces the operating temperature for the engine and results in low NO_x formation (NO_x growth is exponential with temperature). This results in a power loss resulting in an increase of fuel consumption in order to generate the same output [24]. SCR eliminates the requirement of EGR and hence, the engine can run to its full potential. However, this system needs extra hardware in order to store the reductant, spray it in the exhaust, along with correct control and tuning in order to operate. Moreover, it can introduce a new pollutant to the environment; i.e., the reductant. Finally, infrastructure is needed for widespread adoption of this device as the reductant tanks will need to be periodically refilled. No such infrastructure is currently available; however, plans are underway for the United States. In the meantime, another option exists that does not require a secondary reductant.

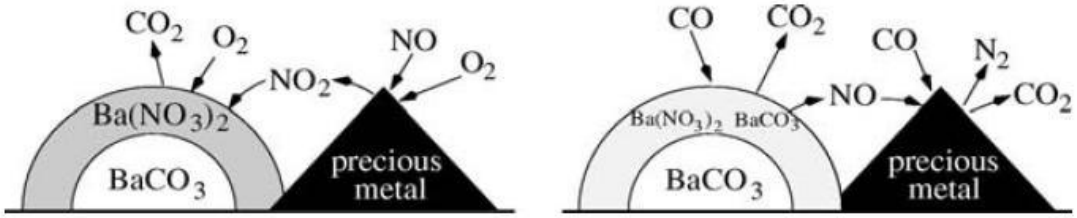

Figure 6: LNT Operation During Lean Storage (Left) and Rich Regeneration (Right) [25]

This option is a Lean NO_x Trap (LNT) where the NO_x generated during combustion is stored during lean exhaust conditions [9, 17, 26-27]. Of importance, engine exhaust mainly contains two types of nitrogen oxides in the forms of nitric oxide (NO) and nitrogen dioxide (NO_2). During the lean phase, nitrogen dioxide adsorbs on alkali or alkali earth metals forming respective metal nitrates. In addition, nitric oxide is oxidized to nitrogen dioxide using the excess oxygen in presence of precious platinum group metals on the catalyst surface. This NO_2 is then subsequently adsorbed on alkali or alkali earth metals as shown in Figure 6. During a subsequent rich phase, nitrogen oxides are liberated from the surface in order to react with CO, hydrogen or hydrocarbons creating nitrogen through the same reactions as the TWC converter utilized for SI engines (illustrated in Figure 6).

As mentioned, typically diesel engines operate lean, during which time the nitrogen oxides are stored on alkali or alkaline earth metal. Intermittently, the exhaust gas is switched to rich conditions, by either reducing intake airflow to the engine and/or a late fuel injection in-cylinder. While the LNT device has its own advantage over the SCR device by virtue of little additional hardware, it can effect engine durability and reduce fuel economy by shifting the engine to less thermodynamically attractive conditions. Another method for creating the correct exhaust conditions is to inject fuel directly into the exhaust gases. However, this has a relatively large toll on fuel economy as a significant amount of fuel is oxidized, but this methodology does not interfere with the inner workings of the engine. The LNT is attractive

to the internal combustion engine community because of the possibility to achieve the same conversion capability as SCR devices without the need of a secondary fluid on board the vehicle.

After understanding the nature and operation of different catalytic converters, it becomes important to simulate their effectiveness using a model that can predict its performance. Use of the model will help reduce the overall price of the catalyst by optimizing the placement of the PGM materials. Past research documents a model that has been effective in predicting the workings of a catalytic converter. However, recent developments required the author to revisit its original assumptions in order to determine if they are still valid.

1.3 Modeling of Catalytic Converters:

The flow of exhaust gases in an aftertreatment device is inherently three-dimensional (3D), with different species and temperatures entering each channel [28]. While a 3D model will accurately simulate a catalytic converter, the amount of overhead needed in modeling a complete system combined with the slow computational time makes it impractical for everyday use with chemical reactions [29-31]. Hence, the literature illustrates that a 1D model is preferred, in which the temperature and reaction rate changes only along the length of the catalyst and not in the radial direction. Although this model cannot simulate the mal-distribution of temperature and species, it has been proven to have good accuracy.

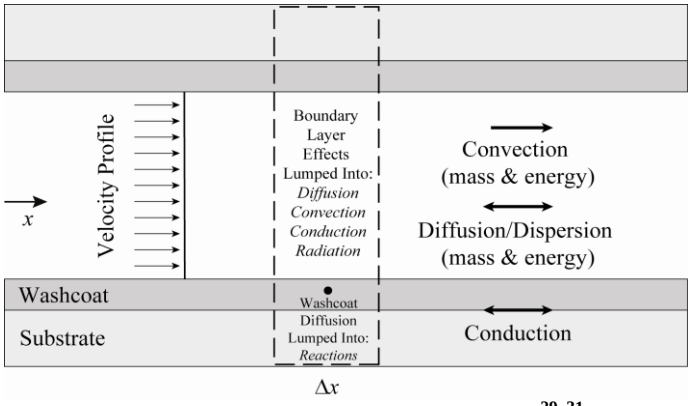

Figure 7: Classical 1D Catalyst Model [29, 31].

In a 1D model, only a single channel is modeled in order to represent the entire converter. There are two sets of equation that capture bulk and surface phases in the channel as shown in Figure 7. The bulk phase represents the flow of gases in the channel, while the surface phase models the reactions occurring on the surface and the monolith temperature. In order to understand the model's capabilities, it is necessary to first review the common assumptions made.

1.3.1 ASSUMPTIONS IN 1D CATALYST MODEL:

The historical review of 1D catalyst modeling showcases various assumption made in order to decrease modeling time and effort. These assumptions, their basis and conditions at which they fail are explained in this section.

1.3.1.1 Dynamically Incompressible Flow:

Gases are invariably compressible. However, for low flow velocities (< 0.3 Mach), along with relatively small changes in pressure and temperature in the axial direction, flow can be assumed dynamically incompressible [32-36]. With respect to the flow of gas entering a catalytic converter, it is significantly less than 100 m/s (i.e. < 0.3 Mach) and the pressure variation across the catalyst is insignificant [34, 37]. While the catalytic converter does operate in a large temperature range of 300 to 1000K, temperature variation at given instant across

the catalyst in the axial direction is often not considerable. However, during catalyst light-off when the temperature variation does increase, it is reasonable to assume dynamic incompressibility for modeling purposes.

For dynamic incompressibility, the change in density of a particle is negligible and therefore is assumed constant. In mathematical form, this is represented as:

$$\frac{D\rho}{Dt} = 0 = \frac{1}{\rho}\frac{D\rho}{Dt} = \frac{1}{\rho}\frac{\partial\rho}{\partial p}\bigg|_T \frac{Dp}{Dt} + \frac{1}{\rho}\frac{\partial\rho}{\partial T}\bigg|_p \frac{DT}{Dt} \quad (5)$$

where *D/Dt* represents the substantial derivative. Since density is governed by the thermodynamic equation of state, it can be represented as a function of temperature and pressure [35]. In addition, Eqn. (5) can be written as:

$$\frac{1}{\rho}\frac{D\rho}{Dt} = \alpha\frac{Dp}{Dt} - \beta\frac{DT}{Dt} = 0 \quad (6)$$

where the isothermal compressibility, α, and thermal expansion coefficient, β, are the characteristic of fluid and hence cannot be set to zero [38-39]. However, if the change in pressure and change in temperature is sufficiently small, then Eqn. (6) is equal to zero. By assuming the density is constant, this significantly reduces computational time and overhead [29]. This is because the fundamentals laws of fluid dynamics can be solved independently of each other [32].

1.3.1.2 Adiabatic Modeling of Converter:

Although the catalytic converter exchanges heat with the atmosphere, 1D modeling assumes it to be adiabatic [40]. This is because the model requires radial heat transfer to be neglected when moving from a 3D representation into 1D [16]. However, the literature illustrates that the 1D model works well in predicting the conversion performance during its warm up in comparison to 2D and 3D models [31, 41]. Moreover, the computational effort of including a second or third-dimension to account for heat transfer to the ambient is

significant making it unattractive for modeling purposes as the reaction kinetics play a much larger role in its effectiveness [29, 42].

1.3.1.3 Laminar Flow in Channels:

The number of channels in a catalytic converter is given by channel density which ranges from 100 to 600 channels per square inch (CPSI) [18]. As this value increases, so does the surface area that acts to increase the conversion rate of the converter [18]. Modern day converters typically have a density of 400 CPSI with wall thicknesses of about 0.01 inches and a channel diameter of approximately 1mm [18]. For this size of a channel, flow quickly becomes laminar [16, 43].

1.3.1.4 Negligible Storage Terms in Bulk Phase (No Time Derivative):

The thermal response of the monolith substrate is three times slower than that of bulk gas [29, 44]. Hence, monolith thermal behavior dominates the dynamic behavior of the catalytic converter. The bulk gas phase quickly reaches an asymptotic equilibrium condition with that of solid phase and hence, time derivatives in the bulk gas fluid dynamics are omitted. This assumption has been used and verified by numerous researchers [16, 26, 29, 44-47].

1.3.1.5 Diffusion and Heat Transfer Coefficients Equal to Fully Developed Flow:

Young and Finlayson showed that Nusselt and Sherwood numbers (heat transfer and mass transfer coefficients) do vary along the length of catalyst depending upon the initial entry length and reaction zones [47]. However, this entry length is short and the channel diameter is small as compared to the catalytic converter length [16, 48-50]. As a result, the fluid dynamics soon become fully developed within a negligible time and length change. Hence, for simplicity, researchers often calculate heat and mass transfer coefficients using fully-developed values.

1.3.1.6 Negligible Heat Conduction and Diffusion in Bulk Phase:

Axial diffusion in bulk gas phase is often neglected based on a Peclet number analysis. The Peclet number is a dimensionless variable that can represents either heat or mass transfer in fluid flow. For heat transfer, it is ratio of heat transferred by advection to that of conduction [51-52]. The Peclet number for mass transfer is ratio of particle displacement due to advection to that of diffusion [53]. In a catalytic converter, the rate of advection for both heat and mass transfer is much higher as compared to conduction and diffusion. For example, the typical value of the Peclet number for both heat and mass transfer is above fifty; whereas, diffusion and conduction become important when the value is near unity.

1.3.2 1D CATALYTIC CONVERTER MODEL:

Fundamental fluid dynamic laws of energy and species characterize both the phases for a dynamically incompressible understanding of a catalyst model. The species equation for the bulk gas phase is represented as [30-31]:

$$\underbrace{\frac{\partial \bar{C}_j}{\partial t}}_{neglect} + u\frac{\partial \bar{C}_j}{\partial x} = \frac{\kappa_j G_a}{\varepsilon}\left(\bar{C}_{s,j} - \bar{C}_j\right) \qquad (7)$$

where the left hand side of the above equation represents the species flow through the channel, while right hand side provides the mass transfer of species from the bulk to surface under laminar flow conditions. Since modeling of the bulk phase is performed in 1D, the multi-dimensional diffusion of species from the bulk to the surface is not directly included in the model. Instead, a source term is added on the right hand side effectively simulating the boundary layer interaction. The diffusion of species from the bulk to the surface and vice versa is given by κ_j, which depends on the Sherwood number, diffusion coefficient and the diameter of the channel as will be presented later.

The energy equation is written as function of temperature in the bulk phase as:

$$\rho c_p \left(\underbrace{\frac{\partial T}{\partial t}}_{neglect} + u \frac{\partial T}{\partial x} \right) = \frac{h_c G_a}{\varepsilon} \left(T_m - T \right) \quad (8)$$

Where the left hand side of the equation simulates the temperature profile through the channel, and right hand side describes the heat transfer between the gas and the surface. Similar to the species equation, heat transfer from the bulk gas to surface is included as a source term in a 1D model. This source term, h_c, depends on the Nusselt number, thermal conductivity of the gas along with the diameter of the channel and will be described in detail later in this thesis.

The species equation governing the surface phase is:

$$\frac{d\bar{C}_{s,j}}{dt} = \frac{\kappa_j G_a}{1-\varepsilon} \left(\bar{C}_j - \bar{C}_{s,j} \right) - \frac{G_{ca} \bar{R}_j}{1-\varepsilon} \quad (9)$$

Where the left hand side represents the storage of gas on the surface. Although it is negligible, writing in this format allows use of an ordinary differential equation solver aiding in numerical efficiency. The first term on the right hand side represents mass transfer of species between surface and bulk; whereas, the second term accounts for reactions occurring on the surface.

The monolith or surface energy equation is:

$$\rho_m c_m \frac{\partial T_m}{\partial t} = \lambda_m \frac{\partial^2 T_m}{\partial x^2} + \frac{h_c G_a}{1-\varepsilon} \left(T - T_m \right) + \frac{G_{ca}}{1-\varepsilon} \sum_{j=1}^{NM} \bar{R}_j \bar{h}_j \quad (10)$$

Where the left hand side accounts for the storage of energy on the surface. The first term on the right hand side represents conduction along the monolith, while second term describes the heat transfer between monolith and the bulk phase. The third term is the energy generated by the endothermic or exothermic reactions happening on the surface.

The model described above is the most common version of the 1D catalyst model as it has evolved over various years of research and understanding [29]. Many authors have tried

to incorporate various effects present in catalyst modeling like non-adiabatic formulation, mal-distributed temperature and species concentration across various cells of the catalyst, 3D modeling, and surface intermediates [41-42, 45]. In a review paper by Depcik and Assanis, they support the use of dynamically incompressible flow citing its advantage in mathematical modeling for chemical reaction optimization given its reduced simulation time. In this paper, they additionally provide a compressible formulation of the model if the need arises for its usage. However, since this thesis is concerned with the assumptions present in 1D incompressible flow catalytic modeling, the compressible flow equations are omitted and left to the reader's review. Moreover, Depcik and Assanis provide information for modeling the converter with detailed chemical kinetics instead of global reaction rate expressions (discussed later). This inclusion is omitted here for simplification and to avoid confusion.

The above model description illustrates that the effectiveness of the catalytic converter depends significantly on temperature. In particular, the reaction rate expression described in a later chapter is exponentially dependent on temperature; hence, catalytic converters are only effective within a certain temperature range. With increasingly stringent regulations covering low temperature operation of catalysts, certain modifications to the system are made to overcome this temperature requirement. At the same time, alternative arrangements for NO_x emissions have their own issues as explained earlier. As a result, modifications are necessary so as to provide a solution for the effective working of the catalytic converter without influencing engine performance. Failures of existing catalytic converters, along with proposed modifications and their change on the modeling assumptions of the catalytic converter are discussed below.

1.4 Drawbacks and Solutions for SI Engine Catalytic Converter (TWC):

The TWC has proven its effectiveness in the reduction of emissions of CO, HC and NO_x [17]. Any drawbacks associated with this device are not particularly failures of its design and catalyst formulation, but instead its inability to meet zero emission levels.

1.4.1 COLD START

The effectiveness of a catalyst is largely a function of its operating temperature [16]. As its temperature increases, the conversion rate of hazardous emissions to non-toxic products slowly increases. After certain temperature, the conversion rate suddenly amplifies and reaches its peak. The temperature at which the conversion rate jumps is called the light-off temperature. Below this temperature, the conversion rate is negligible. During a cold start event after the engine has been sitting in cold weather, a TWC requires a certain amount of time to warm up to reach light-off. During this time, there is negligible conversion of toxic exhaust gases. For example, in a typical engine a large portion of HC (up to 80%) is released during the cold start time [18, 54]. As a result, the emission released during this time can result in disqualification of the engine in meeting emission regulations; like Euro III or Euro IV [55].

1.4.1.1 Solution:

Various solutions have been proposed to solve this problem like electrically heated catalysts, close-coupled catalysts or hydrocarbon absorbers [9, 54, 56]. Out of these possibilities, close coupled catalysts became the main option as it is similar in operation to a TWC but includes an enhanced thermal stability washcoat [55]. In order to modify the current version of the catalyst model to enhance its effectiveness for these options, one must understand the solutions posed.

1.4.1.2 Modification Required in 1D Catalyst Modeling:

An electrically heated TWC uses electricity in order to warm up the catalyst to its light-off temperature. In such a case, no major modification is needed in the modeling of the catalytic converter except the inclusion of a heat generation term provided in Depcik and Assanis's paper. Since typical TWC devices do not include this external heating source, this term is neglected in this effort.

Hydrocarbon absorbers absorb emitted hydrocarbons at low temperatures and release them under high temperatures. When placed in front of a TWC, they will absorb hydrocarbons during the cold start event and release them (ideally) when the TWC has reached the correct temperature. For this situation, no modification is required in the modeling of a catalytic converter. Instead, the time required for the TWC to reach light-off can be calculated and one can measure the amount of hydrocarbons released upstream. The primary issue for the engine designer is to ensure a sufficient amount of zeolite material is present in the adsorber in order to capture the hydrocarbons until the TWC device is ready for conversion.

Close coupled catalysts are placed next to the exhaust manifold of the engine and contain a thermally stable washcoat, similar in design and operation as a TWC. This close proximity allows them to warm up to light-off temperature faster before any heat is lost to atmosphere as the exhaust gases transverse through the system. This results in a quicker light-off, subsequently reducing cold start emissions. Since they are placed next to engine, the pulsating flow of engine exhaust, along with the geometry of exhaust manifold generate non-uniform inlet conditions [28-29]. Hence, the assumption of uniform temperature and species concentration across all the channels may fail in the modeling of this catalyst. As a result, a

2D or 3D model is required in order to simulate the different inlet conditions for unique channels. Since this thesis is concerned only with one-dimensional modeling, this avenue of research is omitted and left to future efforts.

It is important to note that it is not always the temperature that influences cold start emissions. Instead, a better understanding of the catalytic converter can help in reducing these problematic emissions. As seen in Eqn. (9) and (10), a physically correct reaction rate expression can generate a better model, which in turn can help reduce these species. For example, in case of CO oxidation, better dispersion of the PGM on the surface can yield a better conversion at lower temperatures. Thus, it is necessary to determine the correct rate expressions for each reaction happening on the catalyst. This is one area the author has chosen to focus his research.

1.4.2 AGEING

TWC devices operate over a wide range of conditions depending upon personal driving habits, local climate, type of use, etc… [9, 16]. This leads to the ageing of the catalyst as it loses its effectiveness over time. This may happen due to sintering of catalytic material, reduction of surface area and poisoning by sulfur or oil additives. However, current TWC are over designed in order to overcome this ageing effect. They can successfully reduce emissions for nearly 150,000 miles [17]. With respect to this thesis, the proper modeling of the reactions on the surface will allow researchers to increase the lifetime of the catalyst.

1.4.3 COST

TWC devices use platinum, palladium and rhodium as the main catalysts in order to achieve the desired conversion. These platinum group metals are significantly expensive and increase the cost of the automobile. One solution for this problem is to use another, less

expensive catalyst that can provide the same performance. However, research illustrates that this is not currently feasible given the effectiveness of PGM in comparison to cheaper alternatives in combination with the extremely low emission standards. Another possibility is to reduce the amount of PGM by improving the predictability of the chemical reaction rate expressions. With respect to this thesis, a better understanding of chemical kinetics can result in more efficient use of the catalytic material subsequently reducing the costs associated with the device.

1.5 Drawbacks and Solutions for CI Engine Catalytic Converter (LNT):

A LNT has the same cold start, cost and ageing issues as a TWC; hence, the discussion in the previous section holds true for LNT catalyst modeling needs. Apart from this, the major consideration for LNT implementation is its impact on fuel economy. As previously discussed, CI engines typically run lean, during which time it stores the NO_x generated by the engine. In order to regenerate this device, engine modulation, late in-cylinder injection or exhaust fuel injection is needed in order to create a rich charge that is utilized to convert the stored NO_x similar in manner to TWC devices. It has been found by researchers that this change in operation causes approximately a 5-8% fuel economy penalty [57-59].

In order to avoid a loss in fuel economy, a dual path approach as shown in Figure 8 may be utilized. In this system, exhaust flow is divided in two paths with the major portion (about 95%) of exhaust gases flows through the pathway in which NO_x is being absorbed. Only a relatively small fraction (5%) of exhaust gases traverses the regeneration path. When the absorbing path is completely filled with NO_x, flow is switched and the regeneration leg becomes the storage leg and vice versa.

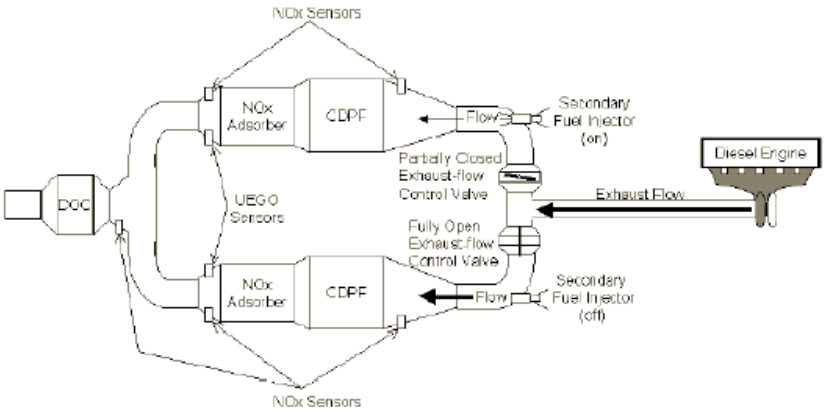

Figure 8: Dual Path System for LNT Regeneration [27].

Because of the small flow rate through the regenerative leg, less fuel is required to create the needed rich regeneration species. Moreover, this system does not interfere with engine operation and results in a less than 3% impact on fuel economy. However, a large quantity of additional hardware and a second LNT is required for proper functioning. While simulation of the absorbing path can utilize the traditional catalyst model, due to the low flow rate of exhaust in the regenerative path, axial conduction and diffusion might become of the same order to that of flow velocity. Hence, these physics will need to be incorporated in the catalyst model [27, 60-63].

1.6 Conclusion:

This chapter briefly describes why a catalyst is needed along with its inner workings. After reviewing the current state of catalyst modeling along with its inherent assumptions, further refinement requires a review of these assumptions along with a better understanding of the reaction rate expression. As discussed for LNTs, it is necessary to review axial conduction and diffusion in the low flow regeneration path. As a result, the next chapter develops the catalytic model from the fundamental laws of fluid dynamics including axial conduction and diffusion. Following this effort, the third chapter provides a formulation of

reaction rate expressions from the fundamentals of chemical reactions happening on the surface as a function of the history of these reactions. This helps provide fundamentally correct reaction rate expressions for better chemical species modeling. Finally, the classical and modified models are compared for reduced flow rates using literature found experimental data.

Chapter 2: Modified 1D Model for Regeneration Leg in LNT Catalytic Converter

As explained in the previous chapter, nearly all of the assumptions present in the 1D catalyst model will work during low mass flow rate conditions within the catalytic converter. However, in a dual leg system, it is feasible that if the flow becomes sufficiently low, axial diffusion and conduction might become important as indicated by the Peclet number. As mentioned previously, in such a system the flow of exhaust species during the regeneration phase is only 5% of the total exhaust flow. This equals a corresponding drop in the flow velocity of approximately twenty fold.

In order to study this phenomenon in further detail, axial diffusion and conduction terms have to be incorporated in the bulk gas phase governing equations. This is accomplished in this chapter through derivation from the basis of first principles. Although the bulk gas phase governing equations will be modified, the surface phase equations do not require adjustment. This is because the surface phase equations do not include a direct velocity dependency in their formulation. Hence, flow speed does not influence their solution, except for residence time that is a function of the bulk equations. As elucidated earlier, for dynamically incompressible flow only the energy and species equations are utilized in catalytic converter modeling efforts. However, in order to derive the correct versions of these equations, the mass and momentum balances must be included in the formulation. Therefore, this chapter investigates dynamic incompressibility utilizing the four fundamental laws of fluid dynamics.

2.1 Law of Conservation of Mass:

In order to derive the conservation of mass, one must first consider an infinitesimally small mass of fluid moving along with the flow as shown in Figure 9. The mass of the fluid

element is constant; however, its shape and volume can change as it moves. Let δm represent the mass of moving fluid element and $\delta \forall$ describe its volume.

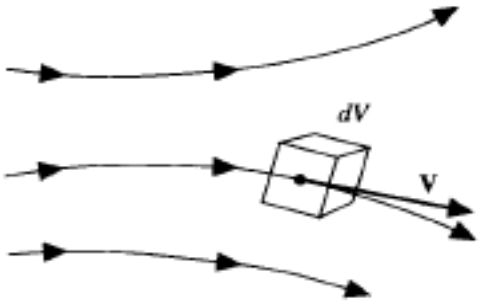

Figure 9: Flow of Infinitesimally Small Mass of Fluid Moving with Velocity Equal to Local Flow Velocity[32].

Mass is given as product of density and volume:

$\delta m = \rho \delta \forall$	(11)

Mass must be conserved in the absence of nuclear reactions; hence, there will not be a change in mass across the flow, which means the substantial derivative of mass is equal to zero:

$\frac{D(\delta m)}{Dt} = 0$	(12)

Substituting Eqn. (11) in Eqn. (12),

$\frac{D(\rho \delta \forall)}{Dt} = \delta \forall \frac{D(\rho)}{Dt} + \rho \frac{D(\delta \forall)}{Dt} = 0$	(13)

while dividing by the volume of the fluid element

$\frac{D(\rho)}{Dt} + \rho \left[\frac{1}{\delta \forall} \frac{D(\delta \forall)}{Dt} \right] = 0$	(14)

and incorporating the definition of divergence in velocity, results in:

$\frac{D(\rho)}{Dt} + \rho \nabla \cdot V = 0$	(15)

The above equation represents the law of conservation of mass in non-conservation format. Using the assumption of dynamically incompressible flow where $\rho \approx 0$, this equation is simplified using Eqn. (15) as follows:

$$\frac{1}{\rho}\frac{D\rho}{Dt} = -\nabla \cdot V = -\lim_{\forall \to 0}\frac{1}{\forall}\frac{D\forall}{Dt} = 0 \qquad (16)$$

The divergence of velocity in this equation $(\nabla \cdot V)$ is the time rate change of volume of a moving fluid element, per unit volume. This means that the change in volume (volume dilation) of the fluid element is zero. This is consistent with Eqn. (11); i.e., if density and mass are constant, the volume is required to be constant. Written out explicitly using directional variables, the divergence of velocity is given as:

$$\nabla \cdot V = \frac{\partial u}{\partial x} + \frac{\partial v}{\partial y} + \frac{\partial w}{\partial z} = 0 \qquad (17)$$

where *u, v* and *w* represents the velocity component in *x, y* and *z* direction respectively.

2.2 Law of Conservation of Momentum:

Note that the derivation of the law of conservation of momentum is available in various books on fluid dynamics [32-35, 64-65]. A brief derivation is presented here for convenience; however, the reader might wish to review the referenced books for a more complete understanding. Consider a fluid element moving with the flow as shown in Figure 10. This element is subjected to body forces caused by gravitation, and surface forces like pressure and shear stresses due to the friction caused by flow. From Newton's second law of motion, the net forces acting on the fluid element must be equal to mass times acceleration, represented here using spatial components as:

$$F_x = ma_x; F_y = ma_y; F_z = ma_z \qquad (18)$$

The net surface forces in the *x*-direction are:

$$\text{Surface Force} = \left[p - \left(p + \frac{\partial p}{\partial x}dx\right)\right]dydz + \left[\left(\tau_{zx} + \frac{\partial \tau_{zx}}{\partial z}dz\right) - \tau_{zx}\right]dxdy + \left[\left(\tau_{xx} + \frac{\partial \tau_{xx}}{\partial x}dx\right) - \tau_{xx}\right]dydz + \left[\left(\tau_{yx} + \frac{\partial \tau_{yx}}{\partial y}dy\right) - \tau_{yx}\right]dxdz \qquad (19)$$

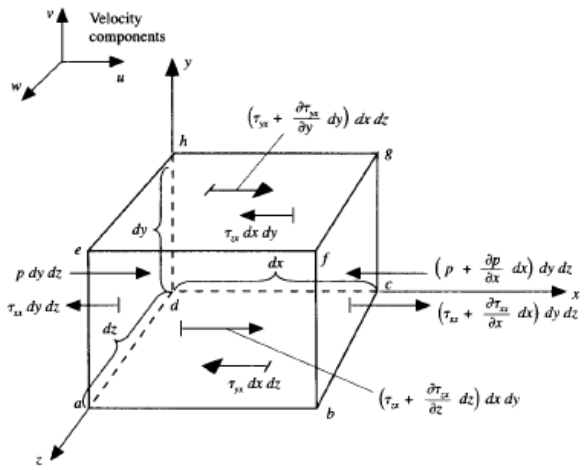

Figure 10: Forces Acting on Body with only *x*-direction Forces Shown [32].

The total force acting on the fluid element is equal to the body force plus the surface forces as:

$$F_x = \left[-\frac{\partial p}{\partial x} + \frac{\partial \tau_{xx}}{\partial x} + \frac{\partial \tau_{yx}}{\partial y} + \frac{\partial \tau_{zx}}{\partial z} \right] dxdydz + \rho g_x dxdydz \quad (20)$$

with mass and acceleration in *x*-direction given as:

$$m = \rho dxdydz; a_x = \frac{Du}{Dt} \quad (21)$$

Substituting Eqn. (20) and Eqn. (21) into Eqn. (18):

$$\rho \frac{Du}{Dt} = \left[-\frac{\partial p}{\partial x} + \frac{\partial \tau_{xx}}{\partial x} + \frac{\partial \tau_{yx}}{\partial y} + \frac{\partial \tau_{zx}}{\partial z} \right] + \rho g_x \quad (22)$$

where the above equation gives the momentum balance in the *x*-direction. Through a similar tactic, the momentum balances in the *y* and *z* directions are represented as:

$$\rho \frac{Dv}{Dt} = \left[-\frac{\partial p}{\partial y} + \frac{\partial \tau_{xy}}{\partial x} + \frac{\partial \tau_{yy}}{\partial y} + \frac{\partial \tau_{zy}}{\partial z} \right] + \rho g_y \quad (23)$$

$$\rho \frac{Dw}{Dt} = \left[-\frac{\partial p}{\partial z} + \frac{\partial \tau_{xz}}{\partial x} + \frac{\partial \tau_{yz}}{\partial y} + \frac{\partial \tau_{zz}}{\partial z} \right] + \rho g_z \quad (24)$$

In the case of catalyst modeling, gases can be considered a Newtonian fluid; hence, shear stress is formulated using Newton's postulation that the shear stress needed to deform the fluid is linearly proportional to the velocity gradient. Stokes extended Newton's idea for

1D flow to multidimensional flows, resulting in the shear stress equation in velocity gradient form as follows [32, 64, 66-67]:

$$\tau_{xx} = \lambda_v \left(\nabla \cdot V\right) + 2\mu \frac{\partial u}{\partial x}; \tau_{yy} = \lambda_v \left(\nabla \cdot V\right) + 2\mu \frac{\partial v}{\partial y}; \tau_{zz} = \lambda_v \left(\nabla \cdot V\right) + 2\mu \frac{\partial w}{\partial z} \quad (25)$$

$$\tau_{xy} = \tau_{yx} = \mu\left[\frac{\partial v}{\partial x} + \frac{\partial u}{\partial y}\right]; \tau_{xz} = \tau_{zx} = \mu\left[\frac{\partial u}{\partial z} + \frac{\partial w}{\partial x}\right]; \tau_{zy} = \tau_{yz} = \mu\left[\frac{\partial v}{\partial z} + \frac{\partial w}{\partial y}\right] \quad (26)$$

Since the flow is assumed to be dynamically incompressible, the velocity gradient via Eqn. (17) is approximately equal to zero. Therefore, the influence of Lame's constant (λ_v) is ignored as it is multiplied by a negligible term; e.g. viscosity is much smaller in magnitude than other flow parameters, like pressure, which results in the multiplication of a relatively small term by a negligible term.

Solving for the momentum equation in the *x*-direction by substituting Eqn. (25) and (26), while assuming a constant viscosity results in:

$$\rho \frac{Du}{Dt} = -\frac{\partial p}{\partial x} + 2\mu \frac{\partial^2 u}{\partial x^2} + \mu\left[\frac{\partial^2 v}{\partial y \partial x} + \frac{\partial^2 u}{\partial y^2} + \frac{\partial^2 w}{\partial z \partial x} + \frac{\partial^2 u}{\partial z^2}\right] + \rho g_x \quad (27)$$

For a Newtonian fluid, viscosity depends on temperature and pressure. In the case of a dynamically incompressible fluid, as discussed later, the change of temperature and pressure across the region must be relatively small in order for the assumption of dynamic incompressibility to hold. Hence, there is a negligible change in viscosity as a function of these parameters and the assumption of constant viscosity is valid.

Further simplification results in:

$$\rho \frac{Du}{Dt} = -\frac{\partial p}{\partial x} + \mu\left[\underbrace{\frac{\partial^2 u}{\partial x^2} + \frac{\partial^2 u}{\partial y^2} + \frac{\partial^2 u}{\partial z^2}}_{\nabla^2 u}\right] + \mu\left[\frac{\partial^2 u}{\partial x^2} + \frac{\partial^2 v}{\partial y \partial x} + \frac{\partial^2 w}{\partial z \partial x}\right] + \rho g_x \quad (28)$$

Where Eqn. (28) represents law of conservation of momentum for dynamically incompressible flow. By collecting the derivative in the second to last term on the right hand side, this results in:

$$\rho\frac{Du}{Dt}=-\frac{\partial p}{\partial x}+\mu\nabla^2 u+\mu\frac{\partial}{\partial x}\left[\underbrace{\frac{\partial u}{\partial x}+\frac{\partial v}{\partial y}+\frac{\partial w}{\partial z}}_{\nabla\cdot V=0}\right]+\rho g_x \tag{29}$$

As a result, this term disappears since the velocity gradient is set as zero from dynamic incompressibility. Similarly, the momentum equations for dynamic incompressible flow in the *y* and *z* directions can be obtained as:

$$\rho\frac{Du}{Dt}=-\frac{\partial p}{\partial x}+\mu\nabla^2 u+\rho g_x \tag{30}$$

$$\rho\frac{Dv}{Dt}=-\frac{\partial p}{\partial y}+\mu\nabla^2 v+\rho g_y \tag{31}$$

$$\rho\frac{Dw}{Dt}=-\frac{\partial p}{\partial z}+\mu\nabla^2 w+\rho g_z \tag{32}$$

2.3 Law of Conservation of Energy:

The physical principle governing the law of conservation of energy is that the total energy of the system must be conserved. Similar to the last two sections, consider a small fluid element moving with the fluid flow as in Figure 11. The rate of change of energy inside the fluid element will be equal to the addition of the net heat flux into the element and rate of work done on the fluid element due to body and shear forces. In mathematical form, this is represented as:

$$dE_t=dQ_t+dW_t \tag{33}$$

The change in total energy inside the fluid element is a function of its internal energy and the change in kinetic energy due to the translational motion of fluid element:

$$dE_t=\rho\frac{D\left(e+V^2/2\right)}{Dt}dxdydz \tag{34}$$

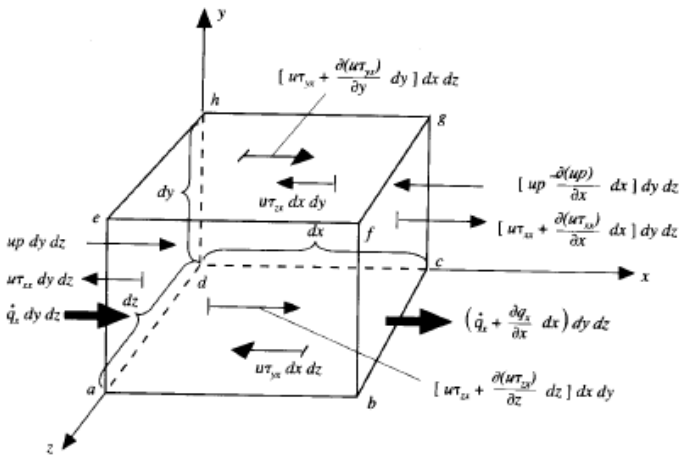

Figure 11: Energy Fluxes Through an Infinitesimally Small Fluid Element with only the Fluxes in the *x*-direction Illustrated [32].

The net heat flux in the *x*-direction is derived from Figure 11 as:

$$\text{Net Heat Flux} = \left[\dot{q}_x - \left(\dot{q}_x + \frac{\partial \dot{q}_x}{\partial x} dx \right) \right] dydz = -\frac{\partial \dot{q}_x}{\partial x} dxdydz \quad (35)$$

And the net heat transfer into the fluid element will be the addition of heat fluxes from all three directions:

$$\text{Net Heat Transfer} = -\left[\frac{\partial \dot{q}_x}{\partial x} + \frac{\partial \dot{q}_y}{\partial y} + \frac{\partial \dot{q}_z}{\partial z} \right] dxdydz \quad (36)$$

Heat flux is a function of the thermal conduction inside the fluid and using Fourier's law of heat conduction, it is proportional to the local temperature gradient:

$$\dot{q}_x = -\lambda \frac{\partial T}{\partial x}; \dot{q}_y = -\lambda \frac{\partial T}{\partial y}; \dot{q}_z = -\lambda \frac{\partial T}{\partial z} \quad (37)$$

Substituting Eqn. (36) recovers:

$$\text{Net Heat Transfer} = \left[\frac{\partial}{\partial x}\left(\lambda \frac{\partial T}{\partial x} \right) + \frac{\partial}{\partial y}\left(\lambda \frac{\partial T}{\partial y} \right) + \frac{\partial}{\partial z}\left(\lambda \frac{\partial T}{\partial z} \right) \right] dxdydz \quad (38)$$

The work done on a fluid element is a function of the forces acting on this element. As indicated in the momentum equation, there are two forces (body and shear) evident. The rate of work done by a force is the product of this force and the component of velocity in the direction of the force. Hence, the work done by the body force is represented as:

$$\text{Body Work} = \rho\left(g \cdot V\right) dxdydz \tag{39}$$

The rate of work done by pressure and shear forces are the product of pressure and shear stresses with the component of velocity in the corresponding direction. As a result, the rate of work done in the *x*-direction by pressure forces is:

$$\text{Pressure Work} = \left[up - \left(up + \frac{\partial\left(up\right)}{\partial x} dx \right) \right] dydz = -\frac{\partial\left(up\right)}{\partial x} dxdydz \tag{40}$$

Similarly, net rate of work done by shear stresses in the *x*-direction is:

$$\text{Shear Work} = \left[\frac{\partial\left(u\tau_{xx}\right)}{\partial x} + \frac{\partial\left(u\tau_{xy}\right)}{\partial y} + \frac{\partial\left(u\tau_{xz}\right)}{\partial z} \right] dxdydz \tag{41}$$

Including the work done by pressure and surface forces in all three directions, the net rate of work done is equal to:

$$dW_t = \left[\begin{array}{l} -\left(\frac{\partial\left(up\right)}{\partial x} + \frac{\partial\left(vp\right)}{\partial y} + \frac{\partial\left(wp\right)}{\partial z} \right) + \frac{\partial\left(u\tau_{xx}\right)}{\partial x} + \frac{\partial\left(v\tau_{yy}\right)}{\partial y} + \frac{\partial\left(w\tau_{zz}\right)}{\partial z} \\ + \frac{\partial\left(v\tau_{xy}\right)}{\partial x} + \frac{\partial\left(u\tau_{yx}\right)}{\partial y} + \frac{\partial\left(u\tau_{zx}\right)}{\partial z} + \frac{\partial\left(w\tau_{xz}\right)}{\partial x} + \frac{\partial\left(w\tau_{yz}\right)}{\partial y} + \frac{\partial\left(v\tau_{zy}\right)}{\partial z} \\ + \rho\left(g \cdot V\right) \end{array} \right] dxdydz \tag{42}$$

Substituting Eqns. (34), (38) and (42) into Eqn. (33):

$$\frac{D\left(e + \frac{V^2}{2} \right)\rho}{Dt} = \left[\begin{array}{l} -\left(\frac{\partial\left(up\right)}{\partial x} + \frac{\partial\left(vp\right)}{\partial y} + \frac{\partial\left(wp\right)}{\partial z} \right) + \frac{\partial\left(v\tau_{zy}\right)}{\partial z} + \rho\left(g \cdot V\right) + \\ + \frac{\partial\left(u\tau_{xx}\right)}{\partial x} + \frac{\partial\left(v\tau_{yy}\right)}{\partial y} + \frac{\partial\left(w\tau_{zz}\right)}{\partial z} + \frac{\partial\left(v\tau_{xy}\right)}{\partial x} \\ + \frac{\partial\left(u\tau_{yx}\right)}{\partial y} + \frac{\partial\left(u\tau_{zx}\right)}{\partial z} + \frac{\partial\left(w\tau_{xz}\right)}{\partial x} + \frac{\partial\left(w\tau_{yz}\right)}{\partial y} \\ \left[\frac{\partial}{\partial x}\left(\lambda \frac{\partial T}{\partial x} \right) + \frac{\partial}{\partial y}\left(\lambda \frac{\partial T}{\partial y} \right) + \frac{\partial}{\partial z}\left(\lambda \frac{\partial T}{\partial z} \right) \right] \end{array} \right] \tag{43}$$

For a further understanding of this derivation, the reader can refer to the following references [32, 34-35, 64-65, 68]. As a result, the energy equation governing fluid flow consists of

two energy sources. Work through the body forces act to accelerate the fluid and increase its kinetic energy, while thermal energy conduction (heat flux) increases its internal energy [35].

Of importance, when the mechanical work component is subtracted from the total energy equation, the remaining part is called the thermal energy equation. As discussed earlier, mechanical work is equal to product of force and velocity. All the forces acting on the body are described via the momentum equation. Hence, in order to obtain the mechanical energy equation in the *x*-direction, one can multiply the momentum equation by the respective velocity component *u* as follows:

$$\rho\frac{D\left(u^2/2\right)}{Dt}=\left[-u\frac{\partial p}{\partial x}+u\frac{\partial \tau_{xx}}{\partial x}+u\frac{\partial \tau_{yx}}{\partial y}+u\frac{\partial \tau_{zx}}{\partial z}+\rho u g_x\right] \tag{44}$$

Similarly, the mechanical energy equations for the *y* and *z* directions can be found as:

$$\rho\frac{D\left(v^2/2\right)}{Dt}=\left[-v\frac{\partial p}{\partial y}+v\frac{\partial \tau_{xy}}{\partial x}+v\frac{\partial \tau_{yy}}{\partial y}+v\frac{\partial \tau_{zy}}{\partial z}+\rho v g_y\right] \tag{45}$$

$$\rho\frac{D\left(w^2/2\right)}{Dt}=\left[-w\frac{\partial p}{\partial z}+w\frac{\partial \tau_{xz}}{\partial x}+w\frac{\partial \tau_{yz}}{\partial y}+w\frac{\partial \tau_{zz}}{\partial z}+\rho w g_z\right] \tag{46}$$

Through adding these equations, the total mechanical energy is obtained:

$$\rho\frac{D\left(\frac{V^2}{2}\right)}{Dt}=\left[\begin{array}{l}-\left(u\frac{\partial p}{\partial x}+v\frac{\partial p}{\partial y}+w\frac{\partial p}{\partial z}\right)+u\left(\frac{\partial \tau_{xx}}{\partial x}+\frac{\partial \tau_{yx}}{\partial y}+\frac{\partial \tau_{zx}}{\partial z}\right)\\ +v\left(\frac{\partial \tau_{xy}}{\partial x}+\frac{\partial \tau_{yy}}{\partial y}+\frac{\partial \tau_{zy}}{\partial z}\right)+w\left(\frac{\partial \tau_{xz}}{\partial x}+\frac{\partial \tau_{yz}}{\partial y}+\frac{\partial \tau_{zz}}{\partial z}\right)\\ +\underbrace{\rho u g_x+\rho v g_y+\rho w g_z}_{\rho(g\cdot V)}\end{array}\right] \tag{47}$$

Subtracting this equation from the total energy Eqn. (43), the thermal energy equation is derived:

$$\rho\frac{De}{Dt}=\begin{bmatrix}-p\left(\frac{\partial u}{\partial x}+\frac{\partial v}{\partial y}+\frac{\partial w}{\partial z}\right)+\left(\tau_{xx}\frac{\partial u}{\partial x}+\tau_{yx}\frac{\partial u}{\partial y}+\tau_{zx}\frac{\partial u}{\partial z}\right)\\+\left(\tau_{xy}\frac{\partial v}{\partial x}+\tau_{yy}\frac{\partial v}{\partial y}+\tau_{zy}\frac{\partial v}{\partial z}\right)+\left(\tau_{xz}\frac{\partial w}{\partial x}+\tau_{yz}\frac{\partial w}{\partial y}+\tau_{zz}\frac{\partial w}{\partial z}\right)\\+\left[\frac{\partial}{\partial x}\left(\lambda\frac{\partial T}{\partial x}\right)+\frac{\partial}{\partial y}\left(\lambda\frac{\partial T}{\partial y}\right)+\frac{\partial}{\partial z}\left(\lambda\frac{\partial T}{\partial z}\right)\right]\end{bmatrix} \quad (48)$$

In vector form, Eqn. (48) is represented as:

$$\rho\frac{De}{Dt}=-p\left(\nabla\cdot V\right)+\tau:\nabla V+\nabla\cdot\left(\lambda\nabla T\right) \quad (49)$$

In order to utilize the thermal energy equation for modeling purposes, it is customary to convert it to utilize temperature as the dependant variable [34]. This can be accomplished using either of the following two methods.

2.3.1 METHOD 1:

Internal energy is a thermodynamic property and can be expressed by two fundamental properties of state. This is accomplished here using temperature and specific volume:

$$de=\underbrace{\left(\frac{\partial e}{\partial T}\right)\Big|_{v}}_{c_v}dT+\left(\frac{\partial e}{\partial v}\right)\Big|_{T}dv \quad (50)$$

Note that the first term on the right hand side is the definition of the constant volume specific heat.

Substituting Eqn. (50) in Eqn. (49) finds:

$$\rho c_v\frac{DT}{Dt}+\rho\left(\frac{\partial e}{\partial v}\right)\Big|_{T}\frac{Dv}{Dt}=-p\left(\nabla\cdot V\right)+\tau:\nabla V+\nabla\cdot\left(\lambda\nabla T\right) \quad (51)$$

However, the specific volume is reciprocal of density and, therefore, results in:

$$\rho c_v\frac{DT}{Dt}+\left(\frac{\partial e}{\partial v}\right)\Big|_{T}\left(-\frac{1}{\rho}\right)\frac{D\rho}{Dt}=-p\left(\nabla\cdot V\right)+\tau:\nabla V+\nabla\cdot\left(\lambda\nabla T\right) \quad (52)$$

However, equation (52) is further simplified applying law of incompressibility. But before applying incompressibility equation it is necessary to understand it applicability for each term in the above equation.

Any gaseous flow is assumed to be incompressible if the velocity is less than a Mach number of 0.3 and there is not a large local change in temperature and pressure. For such a flow condition, density is assumed to be constant $(\rho = \text{constant})$ and the divergence of velocity is set equal to zero $(\nabla \cdot V = 0)$. However, in actuality, there is a negligible change in density $(\rho \approx \text{constant})$ and divergence of velocity is not quite zero $(\nabla \cdot V \approx 0)$. As a result, when the temperature gradient is not large, the conduction and advection of gases are relatively small and nearly of same magnitude as the divergence of velocity. Hence, in the thermal energy equation, any term containing the divergence of velocity or substantial derivative of pressure, temperature or density cannot be set immediately to zero without a thorough review.

2.3.1.1 Viscous Dissipation:

Viscous dissipation is always positive and acts to create internal energy [35]. This is irreversible and it is written as a dyadic product of two tensors, shear stress and gradient of velocity $(\tau : \nabla V)$ resulting in scalar work [67]. Viscous dissipation describes rate of work for shape change at constant volume. For dynamically incompressible flow, change in shape at constant volume is negligible as density is assumed to be constant; hence, viscous dissipation is relatively small [67]. Moreover, viscous dissipation becomes important when the fluid is highly viscous or turbulent [69]. In a catalytic converter, the fluid is a gas with low viscosity and the flow is laminar. Therefore, the change in internal energy due to viscous dissipation

will not influence the internal energy significantly and, subsequently, the temperature. As a result, it can be neglected in Eqn. (52).

2.3.1.2 Substantial Derivative of Density:

For dynamically incompressible flow, the change in density is negligible. Moreover, any change in internal energy corresponding to a change in volume is marginal. This is because the change in volume itself is small as indicated in Eqn. (17). Since this component is a product of two trivial terms $\left[-\left(\partial e/\partial \forall\right)_T \left(1/\rho\right)\frac{D\rho}{Dt}\right]$, it is neglected in Eqn. (52).

2.3.1.3 Pressure Times Divergence of Velocity:

Although the divergence of velocity may be small, pressure across the flow is significant in magnitude [67]. Hence, this term is not inconsequential as the product is on the same order of scale as that of conduction: $p\left(\nabla\cdot V\right)$. As a result, applying the above discussions and the influence of this component, the final thermal energy equation is obtained as:

$$\rho c_{\forall} \frac{DT}{Dt} = \nabla\cdot\left(\lambda\nabla T\right) - p\left(\nabla\cdot V\right) \quad (53)$$

From Eqns. (6) and (17):

$$-\left(\nabla\cdot V\right) = \alpha\left(\frac{Dp}{Dt}\right) - \beta\left(\frac{DT}{Dt}\right) \quad (54)$$

As a result, Eqn. (53) is modified to equal:

$$\rho c_{\forall} \frac{DT}{Dt} = \nabla\cdot\left(\lambda\nabla T\right) + p\left[\alpha\left(\frac{Dp}{Dt}\right) - \beta\left(\frac{DT}{Dt}\right)\right] \quad (55)$$

For ideal gas, isothermal compressibility, α, is the reciprocal of pressure and the thermal expansion coefficient, β, is the reciprocal of temperature [68, 70-71]. Incorporating these simplifications into Eqn. (62) results in:

$$\rho\left(c_{v}+\frac{\beta}{\rho\alpha}\right)\frac{DT}{Dt}=\nabla\cdot\left(\lambda\nabla T\right)+\frac{Dp}{Dt} \quad (56)$$

As explained earlier, the change in pressure across the flow is negligible and the substantial derivative of pressure in this Eqn. is set to zero. Moreover, the specific heat of gases are related by the gas constant as:

$$c_p=c_{v}+R\Rightarrow c_{v}+\frac{p}{\rho T} \quad (57)$$

Using the property of isothermal compressibility and thermal expansion coefficient for ideal gases, Eqn. (57) converts to:

$$c_p=c_{v}+\frac{p}{\rho T}=c_{v}+\frac{\beta}{\rho\alpha} \quad (58)$$

Substituting Eqn. (65) into Eqn. (56), finds that:

$$\rho c_p\frac{DT}{Dt}=\nabla\cdot\left(\lambda\nabla T\right) \quad (59)$$

As a result, the thermal energy equation for dynamically incompressible flow shows that the advection of enthalpy is balanced by conduction.

2.3.2 METHOD 2:

Another option is to utilize internal energy expanded in terms of enthalpy as:

$$e=h-p/\rho \quad (60)$$

Written in derivative format, this becomes:

$$de=dh-dp/\rho+p\left(d\rho/\rho^2\right) \quad (61)$$

Since enthalpy is a thermodynamic property, it can additionally be expressed by two fundamental state variables; here it is expressed as a function of temperature and pressure:

$$dh=\underbrace{\left(\frac{\partial h}{\partial T}\right)_p}_{c_p}dT+\left(\frac{\partial h}{\partial p}\right)_T dp \quad (62)$$

where the first term on the right hand side is the definition of the constant pressure specific heat of a fluid.

Using the basic law of thermodynamics along with Maxwell's relation,

$$\left(\frac{\partial h}{\partial p}\right)_T = \left[\cancel{v} + T\left(\frac{\partial s}{\partial p}\right)_T\right] = \left[\cancel{v} + T\left(\frac{\partial \cancel{v}}{\partial T}\right)_p\right] = \frac{1}{\rho}\left[1 - \frac{T}{\rho}\left(\frac{\partial \rho}{\partial T}\right)_p\right] \tag{63}$$

And substituting Eqns. (62) and (63) into Eqn. (61), one can write the internal energy as a function of the constant pressure specific heat:

$$de = c_p dT + \frac{1}{\rho}\left[1 - \frac{T}{\rho}\underbrace{\left(\frac{\partial \rho}{\partial T}\right)_p}_{\beta}\right] dp - \frac{dp}{\rho} + \frac{p}{\rho^2} d\rho \tag{64}$$

Note that the derivative of density with respect to temperature is the definition of the thermal expansion coefficient.

Furthermore, incorporating (64) into Eqn. (49),

$$\rho\left[c_p \frac{DT}{Dt} - \frac{T\beta}{\rho}\frac{Dp}{Dt} + \frac{p}{\rho^2}\frac{D\rho}{Dt}\right] = -p\left(\nabla \cdot V\right) + \tau : \nabla V + \nabla \cdot \left(\lambda \nabla T\right) \tag{65}$$

and modifying the result equals:

$$\rho c_p \frac{DT}{Dt} = T\beta \frac{Dp}{Dt} - p\left[\frac{1}{\rho}\frac{D\rho}{Dt} + \left(\nabla \cdot V\right)\right] + \tau : \nabla V + \nabla \cdot \left(\lambda \nabla T\right) \tag{66}$$

Note that the second term on the right hand side is the continuity equation for dynamically incompressible flow in non-conservative format and equals zero. As a result, the final thermal equation following this procedure equals:

$$\rho c_p \frac{DT}{Dt} = T\beta \frac{Dp}{Dt} + \tau : \nabla V + \nabla \cdot \left(\lambda \nabla T\right) \tag{67}$$

As a result, Eqn. (52) and Eqn. (67) both represent the thermal energy equation utilizing temperature as the dependant variable. Similar to method 1, the assumption of dynamic incompressibility $\left(\nabla \cdot V \approx 0\right)$ is applied to the above equation, after evaluation of each term.

2.3.2.1 Substantial Derivative of Pressure

The substantial derivative of pressure factor $\left[T\beta\left(Dp/Dt\right)\right]$ includes the thermal expansion coefficient, β. For an ideal gas, this coefficient is the reciprocal of temperature; hence, it cancels out the temperature component leaving just the material pressure derivative [68]. For incompressible flow, thermodynamics properties (like λ, c_p, μ) are often considered constant. Although they fundamentally change with temperature, one of the overriding assumptions for dynamic incompressibility is that there is not a substantial temperature change otherwise the flow must be treated as compressible [35, 72]. This allows decoupling of the continuity and momentum equations from the thermal energy equation. Hence, all three velocities and pressure can be solved without needing to compute the temperature simultaneously. Therefore, the velocity field and pressure are unaffected by thermal changes in incompressible flow, since they are derived from the mass and momentum equations. Thus, pressure is represented as a force and not as a property influencing temperature. This illustrates that if the pressure increases or decreases across the incompressible flow region, the level of all pressures increases or decreases respectively. As a result, the change in pressure across the flow is negligible and it can be eliminated from Eqn. **Error! Reference source not found.**.

Viscous dissipation can be neglected by using the same argument as used in method 1. Using the above discussion in Eqn. (67), results in

$$\rho c_p \frac{DT}{Dt} = \nabla \cdot \left(\lambda \nabla T\right) \qquad (59)$$

Thus, both methods yield the same result for thermal energy equation and this form is what will be utilized in modeling a catalytic converter.

In case of truly incompressible liquids and solids, the difference between the specific heat at constant volume and specific heat at constant pressure vanishes. Hence, Eqn. (59) reduce to equation:

$$\rho c \frac{DT}{Dt} = \nabla \cdot (\lambda \nabla T) \qquad (68)$$

However, in case of gases, these specific heats have distinct values and, therefore, the specific heat at constant pressure must be used for simulation purposes [34-35].

2.4 Law of Conservation of Species:

The law of conservation of species follows the same principles as the law of conservation of mass. In modeling a catalytic converter, the species equation is typically written in mole fraction or molar concentration format. This is because the reaction rate expression utilized in surface species equation is expressed in terms of the number of moles of reactants converting to products. Since both the surface and bulk gas species equation share a common mass transfer source term, it is numerically advantageous to model the species equation in mole fraction or molar concentration form.

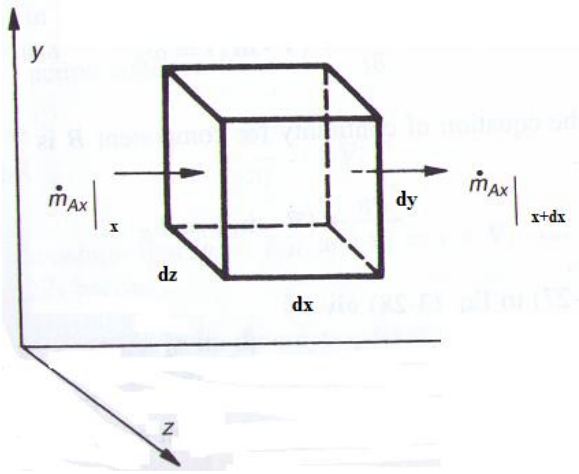

Figure 12: Species Flux Through an Infinitesimally Small Fluid Element Represented only in the *x*-direction [73].

First, one must consider a mixture of gases flowing through a differential control volume of size *dx*, *dy*, and *dz* as indicated in Figure 12. In this control volume, a chemical species *A* is produced by a chemical reaction at a rate equal to $\dot{\omega}_A$ (kg $m^{-3}s^{-1}$). If $\dot{\omega}_A$ is negative, then the species *A* is consumed. The rate of accumulation of this species in the control volume is written as a change in density of the particular species:

$$\text{Rate Accumulation} = \frac{\partial \rho_A}{\partial t} dxdydz \tag{69}$$

The rate of mass entering in the *x*-direction is equal to:

$$\text{Mass Input} = \dot{m}_{Ax}\big|_x \, dydz \tag{70}$$

Whereas, the rate of mass leaving in the *x*-direction is:

$$\text{Mass Output} = \dot{m}_{Ax}\big|_{x+dx} \, dydz + \frac{\partial \dot{m}_{Ax}}{\partial t} dxdydz \tag{71}$$

and the rate of production of species *A* by chemical reaction is:

$$\text{Production} = \dot{\omega}_A dxdydz \tag{72}$$

Similarly, the fluxes in the *y* and *z* directions can be obtained with the entire mass balance given by:

$$\frac{\partial \rho_A}{\partial t} + \left(\underbrace{\frac{\partial \dot{m}_{Ax}}{\partial x} + \frac{\partial \dot{m}_{Ay}}{\partial y} + \frac{\partial \dot{m}_{Az}}{\partial z}}_{\nabla \cdot \dot{m}_A} \right) = \dot{\omega}_A \tag{73}$$

This equation is the law of conservation of species *A*. In this equation, the mass flux rate of individual species is the product of the specific density of that species and velocity in the given direction. However, the velocity of individual species not only depends on the bulk velocity of the flow, but also on concentration gradients. If there is a difference in concentration of species at various points across the flow, the species will move from regions of high concentrations to that of low concentrations. This is analogous to the phenomena of

heat conduction from high temperatures to low temperatures. The velocity induced by a concentration gradient is called the diffusion velocity.

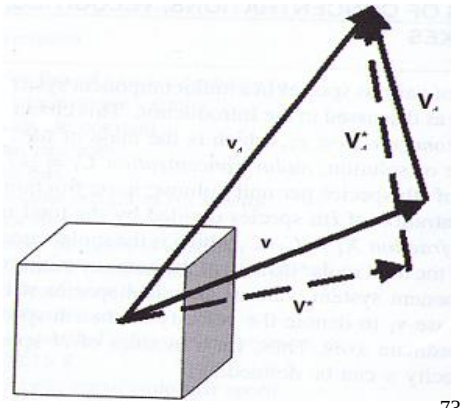

Figure 13: Diagram of Velocity Vectors [73].

Consider a multicomponent system with different species in the mixture moving with different velocities in different directions. As shown in Figure 13, V represents the mass averaged bulk velocity of the flow ($V = u\mathbf{i} + v\mathbf{j} + w\mathbf{k}$) and V^* represents the molar averaged flow velocity. Both V and V^* will differ in magnitude and direction as they contain unique weighing factors. Letting v_A be the velocity of species A, this value is independent on the molar weight or mass of the species A as it represents only that species. The difference between velocity of individual species and the mass averaged velocity is called the mass diffusion velocity of that species respectively. In this case, it is V_A. Similarly, the difference between individual species velocity and the molar averaged velocity of the flow is called the molar diffusion velocity.

Therefore, the velocity of individual species A is given as:

$v_A = V + V_A$	(74)

with the mass flux rate of this species now represented as:

$\dot{m}_A = \rho_A v_A = \rho_A \left(V + V_A\right)$	(75)

In this analysis, V represents the total bulk flow velocity and not the velocities in the individual directions; hence, the x subscript is dropped.

Adolf Fick investigated the diffusion velocity in the above equation in significant detail. He explained that this term could be expressed using diffusion coefficients (δ). The use of this coefficient in the mass flux expression was later called Fick's law of diffusion and is written in mathematical format as:

$$\rho_A V_A = -\rho_A \delta_{Am} \nabla \left(\ln Y_A \right) \tag{76}$$

where the mass fraction is given by

$$Y_A = \frac{\rho_A}{\rho} \tag{77}$$

with the m subscript on the diffusion coefficient indicating the value of species A with respect to the entire mixture as described in a later section.

Substituting this expression back into Fick's law of diffusion:

$$\rho_A V_A = -\rho_A \delta_{Am} \nabla \left(\ln \frac{\rho_A}{\rho} \right) \tag{78}$$

Solving for the logarithmic derivative,

$$\rho_A V_A = -\delta_{Am} \rho \nabla \left(\frac{\rho_A}{\rho} \right), \tag{79}$$

and applying dynamic incompressibility results in:

$$\rho_A V_A = -\delta_{Am} \nabla \rho_A \tag{80}$$

Since the mass fraction of A is expressed as:

$$Y_A = \frac{\rho_A}{\rho} = \frac{\bar{C}_A M W_A}{\rho} \tag{81}$$

Substituting Eqns. (75), (80), and (81) into Eqn. (73) finds:

$$\frac{\partial \rho_A}{\partial t} + \nabla \rho_A V - \nabla \left(\rho \delta_{Am} \nabla Y_A \right) = \dot{\omega}_A \tag{82}$$

which can also be written as:

$$\frac{\partial(\rho Y_A)}{\partial t} + \nabla \rho Y_A V - \nabla\left(\rho \delta_{Am} \nabla Y_A\right) = \dot{\omega}_A \quad (83)$$

This equation is further modified as per the assumptions of catalytic converter modeling by using dynamic incompressibility along with neglecting purely gas phase reactions, aka homogeneous, in the bulk phase; e.g. $\dot{\omega}_A$=0:

$$\rho\left[\frac{\partial Y_A}{\partial t} + \nabla Y_A V - \nabla\left(\delta_{Am} \nabla Y_A\right)\right] = 0 \quad (84)$$

Through incorporation of Eqn. (81) into Eqn. (84),

$$\rho MW_A\left[\frac{\partial \bar{C}_A}{\partial t} + \nabla \bar{C}_A V - \nabla\left(\delta_{Am} \nabla \bar{C}_A\right)\right] = 0, \quad (85)$$

and dividing by density and molecular weight, along with expanding the middle term equals:

$$\frac{\partial \bar{C}_A}{\partial t} + V\nabla \cdot \bar{C}_A + \bar{C}_A \underbrace{\nabla \cdot V}_{=0} - \nabla\left(\delta_{Am} \nabla \bar{C}_A\right) = 0 \quad (86)$$

This results in the law of conservation of species in molar concentration format for dynamically incompressible flow:

$$\frac{\partial \bar{C}_A}{\partial t} + V\nabla \cdot \bar{C}_A - \nabla\left(\delta_{Am} \nabla \bar{C}_A\right) = 0 \quad (86)$$

2.4.1 DIFFUSION COEFFICIENT OF THE MIXTURE:

Fick's law expresses the diffusion velocities in terms of diffusion coefficients. However, calculation of these coefficients has always been subject to interpretation in the literature. The standard method of calculating these values is a three-step process. First, the diffusion coefficient for one species is calculated as in a binary mixture consisting of two gases with one gas is held as the base. The binary diffusion coefficient is then calculated for all other gases in the mixture keeping the base gas constant. Then, the diffusion coefficient of the base gas is calculated for the mixture from all of the calculated binary diffusion

coefficients. This method is then repeated for all the gases in the mixture keeping one gas as the base each time.

There are many ways proposed to calculate the binary diffusion coefficient in the mentioned procedure [67, 73-75]. After studying the referenced literature, the author feels that binary diffusion is best calculated by the following [67, 74]:

$$\delta_{AB} = \frac{0.00186T^{1.5}\left(\frac{1}{MW_A}+\frac{1}{MW_B}\right)^{0.5}}{p\sigma_{AB}^2\Omega} \quad (87)$$

Although this equation has a limitation in that it assumes all gases to be non polar and values of σ (Collision diameter of the molecule) and Ω (dimensionless energy integral based on temperature and Boltzmann constant) are not available for all gases, it provides for a relatively high accuracy within an eight percent error range with experimental data [74]. This accuracy is appreciable as it is the closest any equation predicting binary diffusion coefficient can get. Even the commercial software program, transport CHEMKIN, supports the same equation for calculating these values [76]. From these binary coefficients, the mixture averaged diffusion coefficients can be calculated. The most accurate method to accomplish this is to utilize a full multi-component system that involves inverting an L by L matrix, where L is number of species [67, 74-75, 77]. However, this is computationally expensive and not required in most numerical models. As a result, most researchers utilize approximate formulas as follows.

When the mass diffusion velocity is given as a function of mass fractions,

$$V_A = \frac{-1}{Y_A}\delta_{Am}\nabla Y_A \quad (88)$$

The mixture-averaged diffusion coefficient is represented as:

$$\frac{1}{\delta_{Am}} = \sum_{j \neq A}^{L} \frac{X_A}{\delta_{Aj}} + \frac{X_A}{1-Y_j} \sum_{j \neq A}^{L} \frac{Y_j}{\delta_{Aj}} \quad (89)$$

However, when the mass diffusion velocity is written using mole fractions,

$$V_A = \frac{-1}{X_A} \delta'_{Am} \nabla X_A \quad (90)$$

The mixture-averaged diffusion coefficient is now written as:

$$\delta'_{Am} = \frac{1-Y_A}{\sum_{j \neq A}^{L} \frac{X_j}{\delta_{Aj}}} \quad (91)$$

Ideally, in order for these two equations to synchronize, the velocities in Eqns. (88) and (90) must be equal. As an attempt to derive the relationship between these two diffusion coefficients, the author utilizes the fundamental equations of mole and mass fractions respectively as:

$$X_A = \frac{Y_A / MW_A}{\sum_j Y_j / MW_j} \quad (92)$$

$$Y_A = \frac{X_A MW_A}{\sum_j X_j MW_j} \quad (93)$$

Substituting Eqns. (91) and (92) into Eqn. (90),

$$V_A = \frac{-\sum_j Y_j / MW_j}{Y_A / MW_A} \frac{1-Y_A}{\sum_{j \neq A}^{L} X_j / \delta_{Aj}} \nabla \left(\frac{Y_A / MW_A}{\sum_j Y_j / MW_j} \right) \quad (94)$$

and simplifying it further results in:

$$V_A = \frac{-(1-Y_A)}{Y_A} \frac{\sum_j Y_j / MW_j}{\sum_{j \neq A}^{L} X_j / \delta_{Aj}} \nabla \left(\frac{Y_A}{\sum_j Y_j / MW_j} \right) \quad (95)$$

Through equating Eqns. (95) and (88)

$$\delta_{Am}\nabla Y_A = \left(1-Y_A\right)\frac{\sum_j Y_j/MW_j}{\sum_{j\neq A}^{L} X_j/\delta_{Aj}}\nabla\left(\frac{Y_A}{\sum_j Y_j/MW_j}\right) \quad (96)$$

the diffusion coefficient for velocity as function of mass fractions is deduced as:

$$\delta_{Am} = \frac{\left(1-Y_A\right)}{\nabla Y_A}\frac{Y_j/MW_j}{\sum_{j\neq A}^{L} X_j/\delta_{Aj}}\nabla\left(\frac{Y_A}{\sum_j Y_j/MW_j}\right) \quad (97)$$

Eqn. (97) should be equal to reciprocal of Eqn. (89); however, it cannot be solved further as there is mass fraction term inside the derivative, which cannot be taken outside. Hence, future work should involve further investigation into velocities via Eqn. (88) and (90) for rectification.

2.5 Modified 1D Catalyst Model:

After investigating the four conservation laws, the modified catalyst model utilizing dynamically incompressible flow under low flow conditions for the bulk gas phase can be derived. Eqn. **Error! Reference source not found.** presents the energy equation involving conduction, while Eqn. (86) represents the species equation including diffusion. However, both of these equations are in three-dimensional format and require simplification into one dimension. In order to accomplish this effectively, source terms are required to account for phenomenon typically considered in two- (2D) and three-dimensional (3D) fluid dynamics. In other words, flow from the bulk gas to the surface can be modeled using the governing equations in multi-dimensions; however, in 1D it requires the inclusion of a term that effectively simulates the same physics.

2.5.1 SOURCE TERMS:

The governing equations of flow provide the foundation equations of modeling. Incorporating source terms makes them unique and applicable to a specific purpose. For

simple modeling of catalytic converters, 3D flow is converted into 1D. Hence, to account for 3D phenomena, source terms are used that incorporate boundary layer effects. The source terms for catalytic converter modeling are given in literature and have been widely accepted [29, 31, 78-79]. In this section, they are presented from first principles.

2.5.1.1 Source Term for Energy Equation:

While the energy equation in 1D simulates advection and conduction of energy in the bulk phase, there is heat transfer between the surface and bulk neglected by this equation. To consider this phenomenon, Newton's law of convection is used. From this, the heat transfer by convection from the bulk to the monolith surface is given by [80]:

$$\dot{q} = h_c \cdot Area \cdot (T - T_m) \quad (98)$$

where h_c is the convective heat transfer coefficient that depends on the physical properties of the fluid and the physical situation in which convection occurs. In this equation, T is the bulk gas temperature and T_m is the monolith temperature.

The surface area involved in this equation is not just the area of one channel, but also the area of the entire catalytic converter that trades heat with the bulk surface. This is because the catalytic converter model simulates the entire catalyst as a function of one representative channel. For this component, a concept called geometric surface area is introduced which takes into consideration the entire surface area. The concept of geometric surface area and the void fraction are explained in detail in Appendix II for a better understanding of the model. As a result, the final rate of heat transfer becomes:

$$\dot{q} = h_c \frac{G_a}{\varepsilon}(T - T_m) \quad (99)$$

with the heat transfer coefficient given by [78-79]:

$$h_c = \frac{\mathrm{Nu}\lambda}{d} \quad (100)$$

where *d* is the diameter of the channel and the Nusselt (Nu) number (ratio of convective to conductive heat transfer across the boundary layer) is calculated for square channel as [50, 80-81]:

$$\mathrm{Nu} = 2.98 \tag{101}$$

For fully developed flow, the Nusselt number is constant and independent of Reynolds and Prandtl numbers. As a result, it does not change with axial distance. This number is calculated initially, when the wall temperature is constant and equal to room temperature.

2.5.1.2 Source Term for Species Equation:

Similar to the energy equation, the 1D species equation models advection and diffusion in the bulk gas phase. However, there exists the mass transfer of species from the bulk gas to the surface and vice versa as a function of Fick's law. In other words, the transfer of mass (species flux) depends on the concentration gradient between the surface and bulk phase:

$$\text{Species Flux} = \frac{\kappa_i G_a}{\varepsilon}\left(\bar{C}_{s,i} - \bar{C}_i\right) \tag{102}$$

with the mass transfer of each individual species given by [79]:

$$\kappa_i = \frac{\mathrm{Sh}_i \delta_{im}}{d} \tag{103}$$

where Sh is the Sherwood number (the ratio of convective to diffusive mass transport) and is calculated for square channel as[82]:

$$\mathrm{Sh}_i = 2.98\left(1 + 0.095\frac{du}{\delta_{im}}\right)^{0.45} \tag{104}$$

Sherwood number is analogous to Nusselt number for mass transfer [50, 67, 82]. For fully developed flow it is also a constant, independent of Schmidt and Reynolds numbers and does not depend on axial distance.

2.5.2 FINAL ENERGY EQUATION:

Utilizing these source terms and the discussion regarding dynamically incompressible flow, the final thermal energy equation for the bulk gas is formulated. The source term is added to the equation in order to account (effectively) for multi-dimensional effects. Moreover, the author utilizes a constant thermal conductivity of the gas since the temperature gradient is not significant (and is one of the requirements of dynamic incompressibility). Finally, the storage term (time derivative) is neglected as per the assumptions of 1D modeling presented in the first chapter:

$$\rho c_p u \frac{\partial T}{\partial x} = \lambda \frac{\partial^2 T}{\partial x^2} + \frac{h_c G_a}{\varepsilon}\left(T_m - T\right) \quad (105)$$

Hence, conduction and heat transfer to the monolith incorporating a correct surface area understanding balance the advection of the gas moving through the catalyst.

2.5.3 FINAL SPECIES EQUATION:

Similar to the energy equation, the final species model is formulated using dynamic incompressibility and a source term. In this equation, the storage term is neglected similar to the thermal energy equation and the diffusion coefficient is assumed to be independent of direction and taken as a constant. The diffusion coefficient is a function of temperature, pressure and species concentration. For dynamic incompressibility to hold, the pressure and temperature changes across the catalyst must be negligible. Although species mole fractions do change along the length of the catalyst, the mole fractions of the participating species are relatively small. Hence, the change in diffusion as a function of concentration changes can be neglected [67].

In order to understand this assumption, consider the regenerative arm of the dual leg catalyst system described in Chapter 1. Exhaust gases from the engine mainly contain (about

75%) nitrogen that acts as an inert gas inside the catalytic converter. Other species include carbon dioxide and water, which are not directly involved in the reduction of nitrogen oxides and, hence, the composition of the gas does not vary significantly across the catalytic converter. As compared to these species, oxides of nitrogen are less than 1% of the total composition. This results in a negligible impact of these mole fractions on the diffusion values. Hence, diffusion values can be assumed relatively constant in the axial direction resulting in the following equation of chemical species in the bulk gas:

$$u\frac{\partial \bar{C}_i}{\partial x} - \delta_{im}\frac{\partial^2 \bar{C}_i}{\partial x^2} = \frac{\kappa_i G_a}{\varepsilon}\left(\bar{C}_{s,i} - \bar{C}_i\right) \quad (106)$$

As a result, mass transfer to and from the monolith surface balances the advection and diffusion of the gas through the catalyst.

2.6 Conclusion:

This chapter developed a modified catalyst model from the laws of conservation of fluid mechanics applicable for the regenerative leg of dual leg LNT systems. In particular, the model now includes axial conduction and diffusion in the bulk phase equations. While using the principle of dynamic incompressibility, the author addresses the energy equation paradox and provides expressions in order to calculate diffusion coefficients. Building on this fundamental development of the model, the next chapter develops reaction rate equations for a number of the more important reactions occurring within a catalytic converter. This is needed as catalyst models are only as accurate as their reaction rate expressions, no matter the level of detail of fluid mechanics. This is because their non-linear nature and large temperature dependency have a significant impact on simulation prediction characteristics. Hence, an extensive study of the literature for three pertinent reactions is performed in order to deduce the predictive reaction rate expression for each respective reaction.

Chapter 3: Global Reaction Rate Expression

After investigation of the governing equations for catalytic converter modeling, one understands the importance of including a physically accurate reaction rate expression. For any model to work, this expression needs to be accurate and depict the phenomena happening on the surface as the gas interacts with the catalytic material. Since chemical reactions within the catalytic converter are function of catalyst formulation, dispersion, age and particle diameter; this leads to an immeasurable number of kinetic possibilities. In addition, there are multiple reactions happening simultaneously with each reaction having its own expression [19]. This further adds nonlinearity in the model and makes simulation difficult as each reaction is influenced by dispersion, age and washcoat formulation. Investigation of all variations simultaneously is a logistical nightmare; hence, this chapter involves understanding one reaction at a time in order to build the proper knowledge. Future efforts will include linking these results to create a complete mechanistic model.

There are numerous reactions occurring inside a catalytic converter; like carbon monoxide oxidation, hydrogen oxidation, hydrocarbon oxidation, nitrogen oxide reduction with carbon monoxide and hydrocarbons and so on. The framework of all reaction mechanism efforts, for both SI and CI engines, are the basic oxidation reactions; namely carbon monoxide, hydrogen and nitric oxide oxidation. Moreover, the most widely used catalyst formulation provides the basis for this study; platinum catalyst on alumina washcoat. A review of these three reactions is presented in this chapter along with determination of the reaction rate expressions from first principles basis for inclusion in the catalyst model.

3.1 Review of Detailed and Global Reaction Mechanism for CO Oxidation on Platinum and Platinum/Alumina Catalysts:

All engines contain after engine exhaust treatment devices to directly either reduce CO or eliminate it as a side effect of other desired reactions. Catalyst modelers must therefore include the CO oxidation reaction to CO_2 in their set of chemical reactions. In addition, because of the increasingly stringent standards requiring near zero tailpipe CO emissions for all engines, these models must be accurate and predictive.

3.1.1 REACTION HISTORY:

This section describes the history of the formulation of the CO oxidation mechanism by thoroughly searching all available references on the subject. To indicate global reactions when found, the authors include a "G" in order for the reader to distinguish these separately of the detailed reactions.

In 1922, Langmuir found that the reaction rate of CO oxidation is proportional to oxygen pressure but inversely related to CO pressure [83]. He determines that oxygen and CO molecules compete with each other for adsorption on free platinum surface sites. CO orients in such a way that the carbon monoxide molecule will combine with platinum with two bonds or pair of electrons (duplets). This is a covalent chemisorption bond, but Langmuir does not mention it as a covalent bond with the platinum surface:

$CO + Pt \underset{k_{-107}}{\overset{k_{107}}{\rightleftarrows}} Pt \cdot CO$	(107)

Oxygen bonds with the surface via physical or van der Waals forces in this model:

$O_2 + Pt \underset{k_{-108}}{\overset{k_{108}}{\rightleftarrows}} Pt \cdot O_2$	(108)

Once the molecular oxygen bonds, it dissociates into atomic oxygen that remains connected to the surface:

$\mathrm{Pt\cdot O_2 + Pt \underset{k_{-109}}{\overset{k_{109}}{\rightleftarrows}} 2Pt\cdot O}$	(109)

The mechanism proposed was of the Eley-Rideal (E-R) type where gaseous CO reacts with the atomic oxygen on the surface:

$\mathrm{Pt\cdot O + CO \overset{k_{110}}{\rightarrow} CO_2 + Pt}$	(110)

Langmuir considers CO bonded to the surface as inert and does not contribute to the reaction.

In 1969, Sklyarov proposes that the oxidation reaction happens as a function of a Langmuir-Hinshelwood (L-H) mechanism. In this model, adsorbed CO reacts with adsorbed molecular oxygen and any dissociation into atomic oxygen does not factor in the mechanism [84]:

$\mathrm{Pt\cdot O_2 + 2Pt\cdot CO \overset{k_{111}}{\rightarrow} 2CO_2 + 3Pt}$	(111)

In 1972, Bonzel and Ku present a detailed kinetic model involving CO oxidation as a function of an E-R mechanism where gaseous CO reacts with both adsorbed atomic, Eqn. (110), and molecular oxygen [85]:

$\mathrm{Pt\cdot O_2 + CO \overset{k_{112}}{\rightarrow} CO_2 + Pt\cdot O}$	(112)

In this mechanism, they describe the Rate Determining Step (RDS) as desorption of CO from the surface. Consistent with Langmuir's early hypothesis, Bonzel states that adsorbed CO does not take part in reaction and its only impact is to block available oxygen adsorption sites. Hence, in order for the reaction to proceed, desorption of CO is required to make the sites available to capture oxygen via Eqn.(107). From this detailed model, they write a global kinetic reaction mechanism under steady state conditions:

$R = 2k_3\left(\frac{k_1}{k_{-1}}\right)p_{O_2}p_{CO}\left[1+\frac{k_1}{k_{-1}}\left(1+\frac{k_3}{k_4}\right)p_{O_2}+\left(\frac{k_2}{k_{-2}}+\frac{k_3}{k_{-1}}\right)p_{CO}+\left(\frac{k_2}{k_{-2}}\right)\left(\frac{k_3}{k_{-1}}\right)p_{CO}^2\right]^{-1}$	(G1)

In the following year, Voltz et al. verifies that CO bonds strongly to platinum through chemisorption and inhibits its own oxidation [86]. As the temperature increases, this inhibition decreases owing to CO desorbing from the surface. This was modeled through a global reaction mechanism as a function of an L-H dual site reaction mechanism including the inhibition effects of propene and NO; terms omitted from following Equation since this paper concentrates on modeling CO oxidation without any other species present:

$R = \frac{k\bar{C}_{CO}\bar{C}_{O_2}}{\left(1+K_{CO}\bar{C}_{CO}\right)^2}$	(G2)

where k is an Arrhenius rate expression, $k = Ae^{-E_a/(R_u T)}$, and K_{CO} utilizes the absorption heat of CO; e.g. $K_{CO} = k_{107}/k_{-107} = Ae^{-\Delta H_{CO}/(R_u T)}$. The "dual site" nomenclature indicates that the adsorbed reactants interact with another site; in this case, the CO bonded to one site reacts with the molecular oxygen bonded to the second or dual site represented by Eqn. (111). At this point in the literature, there are competing thoughts on whether it proceeds via an E-R or L-H pathway. This is again seen in the next year, where Firth et al. reference Bonzel and Ku's paper and state that the reaction proceeds via the E-R atomic and molecular oxygen pathway of Eqns. (110) and (112) [87]. The next year finds Shishu and Kowalczyk supporting Sklyarov's finding that oxidation of CO involves adsorbed molecular oxygen and adsorbed carbon monoxide [88].

A slight deviation to either approach occurs in 1975, when Hori and Schmidt represent the reaction including a carbon platinum complex in order to explain its conversion in a transient setting [89]:

$2CO + Pt \underset{k_{-113}}{\overset{k_{113}}{\rightleftarrows}} Pt\cdot C + CO_2$	(113)
$O_2 + Pt\cdot C \overset{k_{114}}{\rightarrow} CO_2 + Pt$	(114)

resulting in the formation of a global reaction rate expression:

$$R = \frac{kK_{CO}p_{CO}K'^{1/2}_{O_2}p^{1/2}_{O_2}}{\left(1+K_{CO}p_{CO}+K'^{1/2}_{O_2}p^{1/2}_{O_2}\right)^2} \quad \text{(G3)}$$

along with a simplified version used to curve-fit the data taken based on the observation that CO adsorption was much stronger than oxygen adsorption: $K_{CO}p_{CO} >> K'_{O_2}p_{O_2}$:

$$R = \frac{kp_{CO}p^{1/2}_{O_2}}{\left(1+K_{CO}p_{CO}\right)^2} \quad \text{(G4)}$$

In this case, K'_{O_2} utilizes the adsorption heat of molecular oxygen; e.g. $K'_{O_2} = k_{108}/k_{-108} = Ae^{-\Delta H'_{O2}/(R_u T)}$. Consistent with the thoughts to date, CO adsorption was determined to be faster than the oxygen adsorption rate.

In the same year, McCarthy et al. find that at low CO concentrations oxygen largely covers platinum, whereas at high CO concentrations it is mainly CO [90]. As a result, at low concentrations, the reaction rate is proportional to CO whereas at high concentrations it becomes inversely proportional. Hence, the oxidation reaction rate might have different RDS as a function of the relative CO levels. They decide on an E-R mechanism as the pathway for both concentration options expressed as Eq. (110) but in reversible format. They state that an E-R mechanism is not possible between adsorbed CO and gaseous molecular oxygen; however, they do not mention anything on the reaction between adsorbed oxygen and molecular CO. In addition, they do not say anything about the possibility of an L-H mechanism.

In McCarthy et al.'s paper, the RDS in the high concentration case is oxygen adsorption, Eq. (109), whereas through inference the E-R reaction between gaseous CO and adsorbed atomic oxygen is the RDS for the low concentration case. This finding is of

particular importance with respect to engines operating part-time in LTC combustion modes. Because the exhaust levels of CO can be significantly different between conventional and LTC combustion, the RDS for the CO oxidation reaction might change during engine operation. Hence, the models might over predict the conversion for the LTC mode because of missing inverse CO dependence at high concentrations.

In 1976, Nicholas and Shah find that the CO oxidation reaction self-inhibits through the adsorbed CO covering the surface [91]. For conversions less than 80%, the rate is inversely proportional to CO concentration while directly related to oxygen concentration. They present a few different global models to model the rate expression with the first such being a power law version when the CO conversion rates were lower than 13%:

$$R = k\bar{C}_{CO}^{a}\bar{C}_{O_2}^{b} \qquad \text{(G5)}$$

with *a* and *b* are equal to -0.28 and 1.07 respectively. In addition, they give L-H single site and dual site models with "single site" indicating that the pathway proceeds through the reactant adsorbed site; i.e. it is an E-R mechanism inferred to be:

$$2Pt \cdot CO + O_2 \xrightarrow{k_{115}} 2CO_2 + 2Pt \qquad (115)$$

They express the single site reaction via the modified Voltz et al. reaction of Eqn. (G2) and the dual site global reaction is:

$$R = \frac{k_r K_{CO} K'_{O_2} \bar{C}_{CO} \bar{C}_{O_2}}{\left(1 + K_{CO}\bar{C}_{CO} + K'_{O_2}\bar{C}_{O_2}\right)^2} \qquad \text{(G6)}$$

A result of their paper is that the L-H dual site model fits the data with the highest accuracy.

The next few years find a number of interesting results. In 1977, Hegedus et al. validate McCarthy et al.'s findings by illustrating that there is a change in reaction rate from positive order in carbon monoxide at low concentration to negative order in high

concentration [92]. In the following year, Dabil et al. determine that the presence of hydrogen in the intake stream promotes the oxidation rate of CO [93]. This illustrates that the global and detailed mechanisms may require adaptation in a future work when the inlet stream includes hydrogen. In this same year, Cant et al. find this transition from positive order to negative order requires two different reaction mechanisms verifying both McCarthy et al. and Hegedus et al.'s efforts [94]. Cant et al. states that the reaction mechanism for CO oxidation occurs first through an E-R mechanism with adsorbed atomic oxygen reacting with gaseous CO; Eqn. (110). The second reaction of importance would be an L-H mechanism with adsorbed molecular oxygen reacting with adsorbed CO as in Eqn. (111). The third important reaction would be of the L-H variety where adsorbed atomic oxygen reacts with adsorbed CO:

$\mathrm{Pt}\cdot\mathrm{O}+\mathrm{Pt}\cdot\mathrm{CO}\xrightarrow{k_{116}}\mathrm{CO}_2+2\mathrm{Pt}$	(116)

It states that at low turnover number, which is the number of moles of substrate that a mole of catalyst can convert before activation, the E-R mechanism takes place and at high turnover number, the L-H mechanism of Eqn. (116) takes place.

In 1979, Cutlip finds that a periodic switching between CO and oxygen increases the average reaction rate as compared to a steady-state reaction rate when the time averaged feed concentration is stoichiometric [95]. Cutlip takes both L-H and E-R mechanisms into consideration but does not make a distinction between the two. This paper presents reactions that take into account the atomic oxygen storage bonding to the surface and the dual site conversion via Eqn. (116). With respect to the atomic oxygen storage on the surface, this occurs via the combination of the two reactions, Eqns. (108) and (109):

$\mathrm{O}_2+2\mathrm{Pt}\underset{k_{-117}}{\overset{k_{117}}{\rightleftharpoons}}2\mathrm{Pt}\cdot\mathrm{O}$	(117)

The adsorption of molecular oxygen and subsequent dissociation are two unique steps; however, he writes it as one complex reaction of a dissociative adsorption of oxygen.

In the same year, Finlayson and Young perform a hysteresis for the oxidation reaction where the steady-state conversion of the reactor depends on the history of operation (mathematical model is taken from Voltz et al. paper) [96]. In particular, they discover different outlet conversions for the same inlet temperature depending on whether the device starts out hot or cold. This is more prevalent when there are high CO levels and low flow rates, which are of large importance to the catalyst modeling community as the conversion between conventional, and LTC combustion will impose this CO level hysteresis. In addition, this is important for dual LNT devices systems that have a reduced flow in the catalyst in order to improve the conversion characteristics [60-63, 97-99].

In the following year, Herz and Samuel find that the L-H dual site mechanism is unable to explain several oxidation studies [100]. As a result, they develop two models that include separate adsorption-desorption and surface reaction rates via a three-step mechanism represented by Eqns. (107), (117) and (116). From these models, they formulate two global rate expressions with the first version represented by Eqn. (G6) and the second form omitting the oxygen dependence from the rate expression:

$$R = \frac{k\bar{C}_{CO}}{\left(1 + K_{CO}\bar{C}_{CO}\right)^2} \qquad \text{(G7)}$$

In the same year, Gland begins to look into the effects of oxygen storage on platinum in order to gain a better understanding of how this diatomic molecule without an electronegative charge bonds to the surface [101]. His surface studies indicate that below 170K, molecular oxygen bonds to the surface. Above 170K, the molecular oxygen starts to desorb from the surface while at the same time dissociating into atomic oxygen. Since atomic

oxygen is a free radical it forms a covalent bond with surface which explains its high energy for desorption. He determines that the activation of energy of dissociation is less than the activation energy of molecular oxygen adsorption meaning that dissociation reaction is very fast, Eqn. (109), as compared to adsorption; hence, the combination of two reactions into one reaction via Eqn. (117). Atomic oxygen does not start desorbing until the temperature is above 600K, which means that at the conditions prevalent in the exhaust of an automobile, oxygen typically bonds to the surface in atomic format.

In 1982, Goodman et al. write a detailed kinetic mechanism consisting of the following four steps in succession: Eqns. (107), (117), (116) and an additional E-R mechanism Eqn. (110) [102]. However, they neglect the E-R mechanism without mention and develop three different L-H models with Model 1 and Model 3 illustrated respectively:

$R = \frac{kK_{CO}p_{CO}K''^{1/2}_{O_2}p^{1/2}_{O_2}}{\left(1+K_{CO}p_{CO}+K''^{1/2}_{O_2}p^{1/2}_{O_2}\right)^2}$	(G8)
$R = \frac{kK^2_{CO}K''_{O_2}p^2_{CO}p_{O_2}}{\left(1+K_{CO}p_{CO}+K''_{O_2}p_{O_2}\right)^3}$	(G9)

where K''_{O_2} utilizes the adsorption heat of dissociated oxygen; e.g. $K''_{O_2} = k_{117}/k_{-117} = Ae^{-\Delta H''_{O_2}/(R_u T)}$. Model 2 is the same as (G6) but using partial pressures instead of concentrations and utilizing the adsorption heats calculated via Eqn. (117). However, while they present three models they do not explain as to which of the three is the preferred option.

In the same year, Barshad finds that the time average oxidation rate for periodic feed switching is much higher than steady-state operation supporting previous efforts like Cutlip [103]. The explanation follows in the L-H reaction written in the paper from Eqns. (107), (117) and (116). High-resolution infrared studies indicated that it is more probable that adsorbed

CO and adsorbed oxygen reacts, which favors this mechanism. In this paper, they also include Eqn. (110) and mention that the E-R pathway through this reaction is also possible. What is interesting is that for the global reaction mechanism, they still use the version of Voltz et al., Eqn. (G2).

In 1988, Winkler et al. find that the dissociation of molecular oxygen on platinum is so efficient; it suppresses the adsorption of molecular oxygen and the reaction pathway proceeds via Eqn. (117) validating earlier papers regarding this interaction [104]. In the next year, Su et al. again find this result with respect to dissociative oxygen adsorption on platinum [105]. They write the CO oxidation reaction via an L-H mechanism for low pressure using Eqn. (116). However, at high pressures, the reaction proceeds via both L-H and E-R pathways. They formulate the high-pressure L-H kinetic model using Eqns. (107), (117) and (116) with addition of the E-R reactions Eqns. (110) and (115). With respect to the E-R reactions, it is mentioned that for Eqn. (115), the reaction rate increases until 400K, but afterwards decreases due to the evaporation of CO from the surface. In contrast, the other E-R reaction rate continues to increase with temperature. When utilizing only the L-H kinetic model to predict the results, they find that variations of the three reactions could not give reasonable predictions. As a result, they state the requirement of the E-R mechanism in conjunction with the L-H mechanism in order for accurate modeling of CO oxidation. This can be easily accomplished using detailed kinetics, but requires care with respect to a global kinetic reaction.

In 1991, Skoglundh et al. mention that the reaction mechanism is of the L-H type following Eqns. (107), (109) and (116) [106]. In the same year, Harold and Garske create five different models to account for the findings that the basic L-H model of Eqns. (107), (117)

and (116) is not sufficient for predicting the behavior of the reaction. The corresponding global reaction model for these detailed reactions, Eqn. (G6), uses pressures instead of concentrations [30]. The second model involved the previous L-H model along with Eqns. (108), (109), (110), (111) and (112) resulting in the following global model:

$$R = \frac{2k_2 p_{O_2}}{\left(1 + K_{CO} p_{CO} - \frac{2k_2}{k_{-1}} p_{O_2}\right)} \qquad \text{(G10)}$$

This version assumes that oxygen can adsorb both molecularly and dissociatively, and at high pressures, the E-R reactions consisting of Eqns. (110) and (112) can dominate the mechanism.

The third model uses an oxygen site exclusion feature keeping only Eqns. (108), (109) and (111) from the second model in addition to the basic L-H model; however, it does not take into consideration CO inhibition. The fourth model uses both CO and oxygen site exclusions where CO and oxygen cannot adsorb on complete platinum sites and can only have maximum coverage fractions of 0.5. The fifth model takes into consideration an irreversible adsorption of oxygen in both molecular and atomic form. The authors do not present these models here because of the specific formulation of the global reactions presented in their paper. They mention that the fifth model is firmly rooted in physical chemistry as compared to the second and third model; however, these models do a better job in predicting the experimental result. They do state that there is no experimental evidence to rule out the E-R mechanism for CO oxidation on platinum.

A few years later, Nibbelke et al. find that the light-off temperature of CO oxidation on a plain Pt catalyst is greater than that of a pre-reduced Pt-Rh catalyst indicating one of two options when it comes to modeling this reaction for a multi-component device [107]:

1. Add other metal detailed reactions to account for the interactions that ensue.
2. Recalibrate the kinetic constants to the new catalyst formulation.

While the first option is inherently more accurate, trying the second option initially because of faster numerical speed warrants a precursory check. The key to this option is if the second (or multiple) metal changes fundamentally the detailed mechanism pathway. If the same processes occur but just with a different frequency, then the models within this paper are still valid and predictive. If the processes change and the RDS is affected, then a different global model is required. The authors leave this exploration of multiple metal effects on the mechanism to future efforts, as the first requirement is a conclusion regarding the CO oxidation mechanism.

In the same year, Nijhuis et al. find that at relatively high temperatures (above 473K), the CO_2 production rate is not inhibited by CO surface coverage possibly indicating the effect of an E-R mechanism [108]. At lower temperatures, CO poisoning of the surface occurs that supports an L-H mechanism. By performing an isotopic study, they find that CO oxidation occurs as per the L-H mechanism with dissociative adsorption of oxygen, Eqn. (117), as the RDS. Their results also support a four-step reaction for CO oxidation with the last step equal to desorption of CO_2 from the surface:

$\mathrm{Pt \cdot CO_2} \xrightarrow{k_{118}} \mathrm{CO_2 + Pt}$	(118)

Continuing the findings of this year, Rinnemo et al. determine that at low concentrations of CO, the oxidation reaction increases rapidly by raising the concentration of CO [109]. This indicates a direct dependence on the concentration of CO with an L-H version mentioned as the mechanism. CO desorbs in the temperature range of 300 to 500K. The activation energy for CO oxidation on the platinum group metals decreases with an increase

in CO coverage for CO oxidation written as: $E_{CO}\theta_{CO} = E_{CO}(0) - A\theta_{CO}$. Tieber et al. find that oxygen adsorbs on platinum in the atomic phase corroborating the previous findings of Gland [110]. Their work does find different temperatures as the threshold point for molecular oxygen adsorption is 150K; above this, it adsorbs atomically until 800K when it desorbs from the surface. At the same time, Kahlich et al. [111] find that this step, Eqn. (117), is the RDS for CO oxidation validating a number of previous researchers.

In 1999, Hoebink and Marin consider both L-H and E-R mechanisms but again do not differentiate with respect to matching experimental data [112]. In addition, they find that while CO can inhibit its own reaction through adsorption, it can adsorb on an oxygen-covered site and then react to produce carbon dioxide. Hence, one platinum site could contain both CO and atomic oxygen:

$\mathrm{Pt \cdot O \cdot CO} \xrightarrow{k_{119}} \mathrm{CO_2 + Pt}$	(119)

They determine this result through a feed change principle as to when carbon dioxide forms it leaves a vacant site. In the initial stage, only oxygen is present in the feed so it adsorbs on the surface. However, when changing the feed to CO they find that it can adsorb on the surface illustrating the dual species adsorption. In the same year, Thormahlen et al. determine that the activation energy of CO changes with surface coverage of CO and depends upon the size distribution of the platinum particles [113]. At low temperatures, CO blocks oxygen from adsorbing inhibiting the low temperature activity of the metal corroborating previous researchers.

In 2000, Wojciechowski and Asprey propose that the rate-controlling step is the reaction between adsorbed carbon monoxide and adsorbed oxygen atoms [114]. They develop two models with the first involving a dual site mechanism involving the dissociative

adsorption of oxygen, Eqn. (G8), and the second instead using molecular adsorption of oxygen:

$$R = \frac{kK_{CO}K'_{O_2}p_{CO}p_{O_2}}{\left(1+K_{CO}p_{CO}+K'_{O_2}p_{O_2}\right)^2}. \quad \text{(G11)}$$

They also propose another model considering both oxygen adsorption pathways, but later dismiss it after documenting that it does not work. They determine that the first model works best for the conditions posed in the literature.

In the following year, Carlsson et al. determine that at low temperatures, the catalytic activity increases by modulating the oxygen on both three-way and platinum-only catalysts [115]. This pulsation causes a disturbance in the adsorbate layer producing more spaces that are open that result in additional oxygen adsorbing on the platinum. As a result, at low oxygen concentrations this pulsed oxygen helps the CO oxidation reaction proceed.

In 2003, Bourane and Bianchi observe that the heat of adsorption of CO linearly decreases with an increase in coverage of CO species [116]. They calculate the heat of adsorption at zero and at one hundred percent coverage while specifying the heat of adsorption for intermediate coverages can be determined using a linear relationship. Furthermore, based on pressure, temperature and the values of initial and final equilibrium constants, the surface coverage of CO can be calculated. Their experiments and simulations show that CO coverage is nearly constant until approximately 600K and decreases linearly with an increase in temperature. As a result, values for the heat of adsorption of CO are independent of platinum dispersion and depend only on the surface coverage. Similar results have been obtained by others on platinum/silica catalysts [117-118].

In the same year, Garcia et al. report that the turnover frequency for the largest metal dispersion is the lowest in the case of platinum supported by silica [119]. They suggest that the

difference in CO oxidation rate does not depend only upon dispersion but also in pretreatment activity. A surface undergoing reducing pretreatment has activity even at low temperatures (like 373K) as compared to oxidative pretreatment that does not demonstrate significant activity even at 403K. They further indicate that the apparent activation energy decreases with a reduction in dispersion (increase in particle size). This is attributed to the fact that highly disperse platinum is easily oxidized as compared to low dispersion of platinum resulting in the loss of activity. They further support the Langmuir Hinshelwood reaction mechanism for CO oxidation. Of importance, CO is not adsorbed on an oxidized platinum surface below 373K; however, with an increase in temperature, oxidized platinum is reduced by CO even in presence of oxygen. The rate per unit mass for CO conversion is the same for high and low dispersion, indicating an increase in turnover frequency with growth in platinum particle size suggesting a decrease in apparent activation energy. However, they further mention that the increase in CO turnover frequency is true for very small platinum particles and as particle size increases, this increase is offset by a reduction in the number of reaction sites.

A year later in 2004, Oran et al. determine that the rate-limiting step is the dissociative adsorption of oxygen and the reaction takes place via an L-H mechanism [120]. When introducing ceria into the support, they find that the mechanism changes because oxygen dissociatively adsorbs on ceria first and then transfers to platinum. Having ceria as the washcoat ($Pt\text{-}CeO_2$) is a better catalyst than the typical alumina washcoat ($Pt\text{-}Al_2O_3$) with a found lower light-off temperature and activation energy. Since most automotive catalysts contain both ceria and alumina, this finding has potential ramifications to future mechanism development. If the RDS remains the same between all potential combinations of platinum,

ceria and alumina, this might allow for one calibrated detailed mechanism. However, if the RDS changes based on the incorporation of these metals, then this interaction and potential additional reactions (like cerium only reactions) require inclusion in the detailed mechanism.

In the same year, Bourane et al. find that platinum dispersion has no significant impact on the CO heat of adsorption illustrating that this component in the model might be constant in mechanism development [121]. Chang et al. determine that CO oxidation on Pd/Rh catalysts occurs through an E-R mechanism and CO oxidation on Pt/Rh occurs by an L-H mechanism indicating potential future revisions of the kinetic model when all three metals are present [122].

Carlsson et al. find in the same year, that CO coverage on platinum is very high for low reactive states and oxygen coverage is very high for high reaction states [123]. A decrease in CO coverage increases the reaction rate and decreases the CO desorption rate while an increase in temperature increases both rates. They determine that the reaction proceeds via an L-H mechanism through a competitive associative adsorption of CO, Eqn. (107), and dissociative adsorption of oxygen, Eqn. (117). In this same year, Arnby et al. find that CO desorbs more easily on larger platinum crystallites [124]. They mention it is better to have larger platinum crystals as the increased CO desorption will leave more space for oxygen to adsorb and increase catalyst light off.

In the following year, Arnby et al. discover that heterogeneously prepared catalysts, where the platinum is locally concentrated on the alumina support, increases the low temperature activity of the reaction due to mass transfer and catalyst structure [125]. Since the oxidation reaction is exothermic, if it is heterogeneously distributed, a manufacturer can strategically modify the local heat production to increase local reaction rates. Their work

indicates the idea of how modeling activities can help minimize precious metal usage saving manufacturer production costs.

In the same year, Uner and Uner claim that the heat of adsorption is closely related to adsorbate-substrate bond [126]. Thus, the differential heat of adsorption depends on the surface coverage of the adsorbate due to a lateral adsorbate-adsorbate interaction supporting the earlier claim of Bourane and Bianchi [116]. They mention that the CO oxidation reaction follows a Langmuir Hinshelwood reaction mechanism and the structure sensitivity of CO oxidation is natural. They report values of the heat of adsorption for both CO and oxygen adsorption, maintaining that the data is still limited. The heat of adsorption of oxygen is nearly constant until the oxygen surface reaches 0.8 times its saturation coverage for the corresponding dispersion; however, data indicates a slight dependence on the structure of the catalyst; i.e. particle size. With respect to CO adsorption, it does not exhibit any such structure sensitivity, but instead largely varies with surface coverage.

In 2006, Koci et al. consider the basic L-H reaction model by studying the porous nature of the washcoat and its effect on platinum distribution [127]. They conclude that the reaction rate expression depends non-linearly on the amount of platinum in the porous washcoat. In the same year, Petersson et al. describe the CO oxidation mechanism via the three-step L-H mechanism of Eqns. (107), (109) and (116) [128]. Oxygen requires two adjacent sites due to the dissociative adsorption of Eqn. (117) and CO adsorption requires only a single site. Instead of competing for the same platinum sites, Bourane and Bianchi suggest that CO and oxygen adsorb on different or neighboring sites [116, 129-130]. They discover that this three-step mechanism accurately models the experimental data.

In the same year, Atalik and Uner support earlier claims that CO oxidation is faster at a higher oxygen to CO ratio; however, selectivity of CO decreases [131]. The reaction rate of CO oxidation per unit amount of catalyst is similar for different dispersions, but the turnover frequency increases with an increase in particle size. This is attributed to a decrease in activation energy with an increase in particle size. They mention that the difference in activation energy as reported in the literature depends on measurement conditions and the experimental temperature range. In addition, the reaction order with respect to oxygen demonstrates a slight variation with a change in particle size, suggesting that the CO oxidation reaction depends less on the oxygen partial pressure for small particles. In addition, both the oxygen and CO adsorption processes are not structure sensitive. They clearly show that as dispersion increases, the light off temperature (temperature at which 50% of CO is converted) decreases.

More recently, Salomons et al. indicate that the typical L-H global rate expression only works well for steady-state operation over a narrow range of operation conditions [132]. As a result, they create four detailed kinetic mechanisms via both L-H and E-R pathways. The E-R mechanism reappears because they discover that introducing CO to an oxygen-covered site will result in the formation of CO_2; however, oxygen introduced to CO covered sites does not cause a reaction. The first model involves the following reversible reactions; Eqns. (107), (116) and (117), revised to utilize (118). The second model uses both L-H and E-R steps via Eqns. (107), (108), (109) and (116), the following reaction

$\mathrm{CO} + \mathrm{Pt}\cdot\mathrm{O} \underset{k_{-120}}{\overset{k_{120}}{\rightleftarrows}} \mathrm{Pt}\cdot\mathrm{O}\cdot\mathrm{CO}$	(120)

and Eqn. (119).

The third model is the same as the L-H mechanism and in the Herz and Marin paper [100]. The fourth model incorporates the fact that an oxygen-covered surface can adsorb a significant amount of CO that compresses the adsorption of oxygen; inferred here as the pushing of oxygen towards Pt making the bond stronger. This finding expands the detailed model as following:

$CO + 2Pt \cdot O \underset{k_{-121}}{\overset{k_{121}}{\rightleftarrows}} Pt \cdot CO + Pt \cdot OO$	(121)
$Pt \cdot CO + Pt \cdot OO \underset{k_{-122}}{\overset{k_{122}}{\rightleftarrows}} CO_2 + Pt \cdot O + Pt$	(122)
$Pt \cdot OO + Pt \underset{k_{-123}}{\overset{k_{123}}{\rightleftarrows}} 2Pt \cdot O$	(123)

In order to determine the model that is most accurate, they compare their use against experimental light-off curves. They find that the first model does better than the second model; however, the first model has an issue with respect to reversible molecular oxygen adsorption, which does not occur. They do not discuss the third model accuracy and the fourth model performs just as well as the first model. This model has the advantage of modeling phenomenon not accounted for in the first model, but additional steps and parameters require consideration before reaching an agreement.

In the year 2008, Yang et al. documents a number of previous models and simplifies the results down to a singular power-law expression [133]:

$R = k\bar{C}_{O_2}^{\alpha}\bar{C}_{CO}^{\beta}$.	(G12)

where α = 0.74 and β = -0.50. They state that the energies proposed by various people are different from what they determine because their inlet compositions and initial conditions of reactor and catalyst differ. They also state that as platinum particle size increases, CO conversion increases indicating that aging might help for CO oxidation. Recently, Salomons et al. support their previous findings by stating that the fourth best describes CO oxidation

[134]. In addition, they state that hydrogen enhances CO oxidation on platinum following previously documented efforts.

3.1.2 HISTORICAL SUMMARY:

During the early 1970s, most researchers assumed that CO oxidation on platinum took place as per an Eley-Rideal mechanism. In this case, gaseous CO reacts with adsorbed oxygen and forms carbon dioxide. Researchers theorized this result because observations at high temperatures found that CO oxidation does not depend on the inlet CO concentration. Hence, the self-poisoning inhibition of CO does not influence the reaction mechanism at these temperatures. Researchers then found at low temperatures, CO oxidation was not occurring due to selective adsorption of CO on platinum. As the temperature increased, CO desorbs from platinum surface and these sites become available for oxygen to adsorb. Further studies revealed that the reaction might actually take place as per a Langmuir-Hinshelwood mechanism. These later 1970s observations determined that adsorption of both CO and oxygen must occur for the reaction to proceed.

In the 1980s, in-depth studies of oxygen adsorption revealed that when oxygen adsorbs on platinum, it dissociates directly into atomic oxygen at normal operating temperatures. This illustrates that for this adsorption to occur; oxygen requires two adjacent sites for both atoms in the oxygen molecule. As a result, the adsorption of oxygen on platinum became the Rate Determining Step in the CO oxidation reaction mechanism. In addition, during this time researchers discovered that at relatively low CO concentrations, the reaction rate increases by adding CO to the inlet mixture. However, after a certain threshold the self-inhibiting effect of carbon monoxide begins to reduce the reaction rate.

In the next decade, researchers moved towards just the L-H mechanism for describing the reaction rate; however, they could not completely disprove an E-R effect. For example, some studies indicate that when CO gas passes over a surface completely covered by oxygen, there is some reactivity. However, the same is not true when oxygen passes over a surface covered by CO. Other studies indicated that CO adsorption on platinum is independent of catalyst activity and further study into the self-inhibition of CO gave an approximate threshold with CO desorbing from the surface at temperatures above 550K.

The most recent decade indicates that the highest likelihood model for the reaction is an L-H dual site dissociative oxygen adsorption version. There are better fitting models taking into consideration both CO and atomic oxygen on platinum at the same time; however, more studies are still needed as to this impact on the overall reaction rate and its implementation into a global reaction expression. In addition, this does not completely disprove an E-R reaction in deference to a dual species adsorbed platinum site. Recent efforts show that bigger platinum particles work better at lower temperatures as they promote CO desorption creating available oxygen adsorption sites. In addition, while the L-H model does predict light off curves well, they have a reduced accuracy when simulating transient studies indicating the possible need for detailed mechanism incorporation.

3.1.3 DETAILED REACTION MECHANISM:

Based on this historical summary, the authors feel that the CO oxidation reaction over platinum occurs via the following steps:

3.1.3.1 CO Adsorption

CO adsorption is the first step of the mechanism because of the low initial sticking coefficient of oxygen on platinum as compared to CO [135]. It is important to understand how

this happens before writing the reaction rate Equation because CO will inhibit its own oxidation due to self-poisoning. Platinum is a transition metal and has a tendency to donate electrons and, as a result, can assume a partial positive charge. Carbon monoxide has an inherent dipole structure because of its bond formation that causes the carbon side to have a partial negative charge. As opposite charges attract, the carbon will bond with platinum via covalent bonding as Yates et al. experimentally discovered [136].

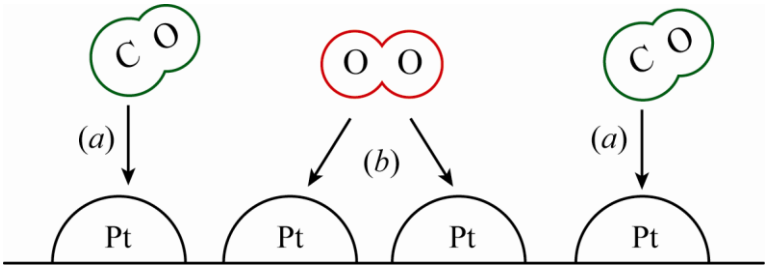

Figure 14: First Two Steps of Detailed Reaction Mechanism.

3.1.3.2 Dissociative Oxygen Adsorption

The second step in this mechanism is the dissociative oxygen adsorption on platinum illustrated in Figure 14. Elg et al. found that molecular oxygen physisorbs on platinum below 30K, but chemisorbs above 45K [137]. Around 130 to 150K, the O – O bond appears to weaken and begins to dissociate the molecule (also seen by Tieber et al. in [110]). Above 150K, the adsorbed molecular oxygen dissociates into its atomic parts, which only starts desorbing at a much higher temperature (800 K) as shown in Figure 15. Oxygen is not present at substrate level with only platinum found, illustrating that this process does not form platinum oxide. Because of the need to find two adjacent platinum sites, some researchers consider this step the Rate Determining Step.

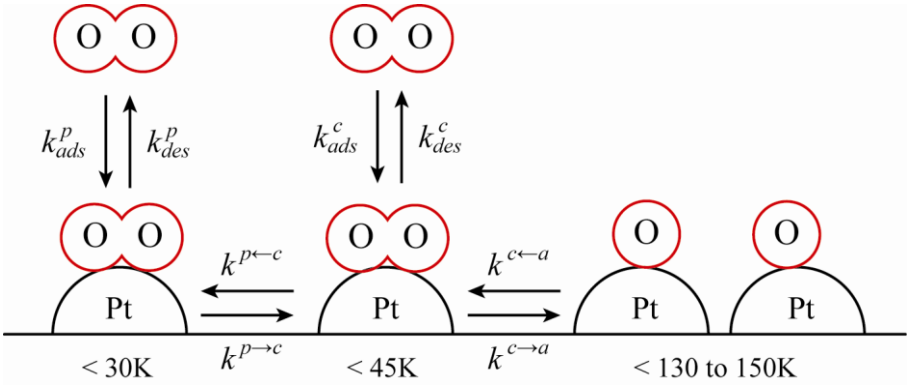

Figure 15: Oxygen Adsorption Mechanism as Described by Temperature. The Letters *a*, *c* and *p* Denote Atomic State, Chemisorbed and Physisorbed Molecular States.

3.1.3.3 Adsorbed CO/O Reaction

The third step in this mechanism is subject to some discussion. Most researchers believe that the most important reaction is that of adsorbed CO with adsorbed atomic oxygen via an L-H mechanism as indicated in Figure 16. However, as the Reaction History section indicates, this may not be the only possible reaction occurring on the surface at this time. It appears to be the most widely assumed prospect, but mechanisms developed using only this conversion reaction does not necessarily predict the most accurate results. The final step would be desorption of CO_2 from platinum that researchers often assume happens instantaneously.

As a result, the detailed mechanism is:

$CO + Pt \underset{k_{-a}}{\overset{k_a}{\rightleftarrows}} Pt \cdot CO$	(a)
$Pt \cdot O_2 + Pt \underset{k_{-b}}{\overset{k_b}{\rightleftarrows}} 2Pt \cdot O$	(*b*)
$Pt \cdot O + Pt \cdot CO \overset{k_c}{\rightarrow} 2Pt + CO_2$	(*c*)

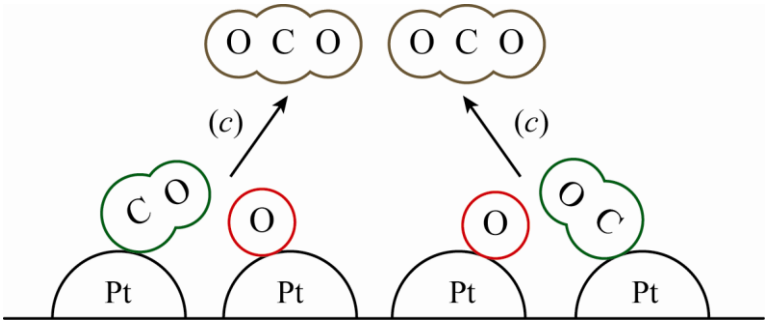

Figure 16: Final Step of the Detailed Reaction Mechanism.

Where the first reaction is considered reversible above 550K and below this temperature, desorption rate is considered negligible. Because of the dissociation of oxygen, the second reaction is typically considered reversible in the realm of automotive usage; desorption of oxygen starts above 800 K and becomes quite significant above 1200K. However, the authors write it so here in order to calculate the global mechanism in the next section. Since the carbon dioxide structure cannot remain bonded to the platinum structure, this instantaneous rejection from the surface causes the third L-H reaction to go to completion without an intermediate. Note that the most likelihood extension of this model to include E-R effects would occur via atomic oxygen on the surface and gaseous CO:

$CO + Pt \cdot O \xrightarrow{k_d} Pt + CO_2$	(*d*)

Over the history of the L-H reaction mechanism, there is still no consensus as to the true RDS. For an E-R mechanism via Eqn. (*d*), the RDS would be Eqn. (*b*). However, a number of researchers indicate that both Eqn. (*b*) and Eqn. (*c*) can be the RDS for the L-H mechanism. For example, Chorkendorff states that the reaction between adsorbed oxygen atom and adsorbed CO is the rate-determining step because researchers have found this reaction step to have an energy barrier of 100 kJ/mol, while other steps have energy barrier of less than 30 kJ/mol [138]. It is quite possible that at lower CO concentrations, Eqn. (*c*) is the RDS and at higher CO concentrations, Eqn. (*b*) becomes the RDS. As a result, the global

reaction mechanism would need either to switch between reaction expressions or incorporate both within a single expression. This is a significant issue when applying the model equally to Low Temperature Combustion, Spark Ignition and Compression Ignition exhaust emissions that all have varying levels of CO concentrations.

3.1.4 GLOBAL REACTION MECHANISM:

In order for completeness, this section presents two global kinetic mechanisms as a function of the potentially different RDS depending on local CO concentrations. For the first reaction, Eqn. (*a*), the forward and reverse reactions are:

$R_a = k_a p_{\mathrm{CO}} \theta_{\mathrm{Pt}}$	(124)
$R_{-a} = k_{-a} \theta_{\mathrm{Pt\cdot CO}}$	(125)

At equilibrium, the forward and backward rate becomes equal:

$k_a p_{\mathrm{CO}} \theta_{\mathrm{Pt}} = k_{-a} \theta_{\mathrm{Pt\cdot CO}}$	(126)

where the equilibrium constant equals:

$K_{\mathrm{CO}} = k_a / k_{-a}$	(127)

For the second reaction, Eqn. (*b*), the forward and reverse reactions are:

$R_b = k_b p_{\mathrm{O_2}} \theta_{\mathrm{Pt}}^2$	(128)
$R_{-b} = k_{-b} \theta_{\mathrm{Pt\cdot O}}^2$	(129)

and at equilibrium,

$k_b p_{\mathrm{O_2}} \theta_{\mathrm{Pt}}^2 = k_{-b} \theta_{\mathrm{Pt\cdot O}}^2$,	(130)

the constant equals:

$K''_{\mathrm{O_2}} = k_b / k_{-b}$	(131)

For the last reaction, the reaction only proceeds in the forward direction:

$R_c = k_c \theta_{\mathrm{Pt\cdot CO}} \theta_{\mathrm{Pt\cdot O}}$	(132)

If this is the RDS, solution of the global mechanism occurs by first utilizing the equilibrium constant of CO in Eqn. (127),

$$\frac{\theta_{\text{Pt·CO}}}{\theta_{\text{Pt}}} = K_{\text{CO}} p_{\text{CO}}, \quad (133)$$

and that of dissociative oxygen adsorption in Eqn. (131)

$$\frac{\theta_{\text{Pt·O}}}{\theta_{\text{Pt}}} = K''^{1/2}_{\text{O}_2} p^{1/2}_{\text{O}_2}. \quad (134)$$

Dividing Eqn. (134) by (133) results in:

$$\theta_{\text{Pt·O}} = \frac{\theta_{\text{Pt·CO}} K''^{1/2}_{\text{O}_2} p^{1/2}_{\text{O}_2}}{K_{\text{CO}} p_{\text{CO}}} \quad (135)$$

Using the fact that $\theta_{\text{Pt}} = \left(1 - \theta_{\text{Pt·CO}} - \theta_{\text{Pt·O}}\right)$ and substituting Eqn. (135) into Eqn. (133) results in the following for surface coverage of CO:

$$\theta_{\text{Pt·CO}} = \frac{K_{\text{CO}} p_{\text{CO}}}{\left(1 + K_{\text{CO}} p_{\text{CO}} + K''^{1/2}_{\text{O}_2} P^{1/2}_{\text{O}_2}\right)} \quad (136)$$

Incorporating this into the RDS step, Eqn. (132) along with Eqn. (135) ends in the following global reaction mechanism:

$$R_{\text{CO}} = \frac{k K_{\text{CO}} K''^{1/2}_{\text{O}_2} p_{\text{CO}} p^{1/2}_{\text{O}_2}}{\left(1 + K_{\text{CO}} p_{\text{CO}} + K''^{1/2}_{\text{O}_2} p^{1/2}_{\text{O}_2}\right)^2} \quad (\text{CO-RDS-}c)$$

which is the same as the global mechanism calculated by Hori and Schmidt in 1975 using molecular oxygen adsorption, Goodman et al. in 1982 for atomic oxygen and shown by Wojciechowski and Asprey to fit data quite well.

If the RDS step is the dissociative adsorption of oxygen, Eqn. (*b*), since the CO concentration is relatively high it is difficult for two adjacent empty sites to be available preventing oxygen from adsorbing. In such a case, since CO is in excess, it is reasonable to assume that the coverage fraction of atomic oxygen is much less than CO: $\theta_{\text{Pt•CO}} >> \theta_{\text{Pt•O}}$. As a result, the amount of free platinum surface sites equals $\theta_{\text{Pt}} \cong \left(1 - \theta_{\text{Pt·CO}}\right)$. Utilizing this assumption in Eqn. (133), results in the following for surface coverage of CO:

$\theta_{Pt\cdot CO} = \frac{K_{CO} p_{CO}}{\left(1 + K_{CO} p_{CO}\right)}$	(137)

Now, incorporating this into the RDS step, Eqn. (128), finds:

$R_{CO} = \frac{k p_{O_2}}{\left(1 + K_{CO} p_{CO}\right)^2}$	(CO-RDS-*b*)

Researchers have suggested that if CO is excess [139], the first global mechanism developed is still valid simply by eliminating the oxygen terms in the denominator; $K_{CO} p_{CO} >> K''^{1/2}_{O_2} p^{1/2}_{O_2}$ and leaving the oxygen dependency on top:

$R_{CO} = \frac{k K''^{1/2}_{O_2} p^{1/2}_{O_2}}{\left(1 + K_{CO} p_{CO}\right)^2}$	(CO-RDS-*b'*)

This is very similar to the global mechanism presented here.

It is important to note, that the CO concentrations where this potential transition between the RDS versions of the global mechanisms is still an unknown as well as the impact of the E-R step of Eqn. (*d*) on the global mechanism. This is what the authors believe future efforts should target in order to define a definitive global expression that works across all concentration and temperature regimes.

The Equation labeled as "CO-RDS" are the global reaction rate expression that should be used while modeling the CO oxidation on platinum and platinum/alumina catalysts. Although the same Equation will be used for different platinum catalysts, the values of pre-exponential factor, activation energy, and enthalpies will change with dispersion, catalyst preparation, particle diameter, etc.

3.2 Review of Detailed and Global Reaction Mechanism for Hydrogen Oxidation on Platinum and Platinum/Alumina Catalysts:

Similar to carbon monoxide, hydrogen is one of the major pollutants from SI engines and causes significant environmental and health problem. In the early history, researchers equated hydrogen oxidation global rate mechanisms to carbon oxidation. Since the hydrogen content in the exhaust gas is important for catalyst modeling activities due to its heat of reaction and demand for O_2, Kuo et al. took the oxidation rate to be the same as that for CO [140]; Young and Finlayson followed suit a few years later [141-142]. In particular, the reaction rate coefficients of CO oxidation found in the seminal modeling efforts of Voltz et al. [143]over platinum catalysts were directly applied to the rate expression defining hydrogen oxidation [46, 144-145]. It is not until Montreuil et al. that the reaction rate expression differs by incorporating hydrogen inhibition in addition to carbon monoxide inhibition as found through their mass spectrometry readings [146]. However, this effort is singular in its nature as most recent models follow the Voltz et al. process by utilizing the same functional form of the reaction rate expression with coefficient values equal or slightly higher [147-149].

3.2.1 REACTION HISTORY:

The research into hydrogen oxidation over platinum started in 1820, when Sir Johann Dobereiner began investigating platinum as a catalytic material. His early experiments illustrate that it remains present during the conversion of alcohol into acetic acid and is therefore an avenue for the mass production of acetic acid. Later in 1823, he exposed powered platinum to hydrogen gas and upon the introduction of air found that all of the hydrogen and oxygen converted into water [150]. Later experiments, based on this work by Faraday, ascribed this conversion to an adsorptive property of platinum. In a review of the work in 1835, Berzelius coined the term “catalysis” for all such types of reaction

phenomenon [151]. Dobereiner later turned his discovery into practical device through the design of a new lighter and lamp but never patented his research.

In 1922, Langmuir wrote a seminal paper in the investigation of the hydrogen oxidation reaction on platinum in which he claims that this reaction rate is much greater than that of CO oxidation [83]. In this paper, he states that hydrogen oxidation happens as per an Eley-Rideal (E-R) mechanism where the hydrogen molecule reacts with an adsorbed oxygen atom as per Eqn. (117) and:

$H_2 + 2Pt \underset{k_{-138}}{\overset{k_{138}}{\rightleftharpoons}} 2Pt \cdot H$	(138)
$Pt \cdot O + H_2 \xrightarrow{k_{139}} Pt + H_2O$	(139)

Hydrogen oxidation did give an erratic result at low temperatures (300 to 600K) and when platinum is inactive the results are similar to those of CO oxidation. The rate is roughly proportional to partial pressure of oxygen and inversely proportional to partial pressure of hydrogen. This analysis led him to believe that the adsorbed hydrogen acts as a "poison" that inhibits the forward reaction rate. At high temperatures (700 to 900K), hydrogen oxidation closely resembles CO oxidation. During this condition, he postulates that every striking hydrogen molecule reacts with adsorbed oxygen atoms. By bringing platinum into a proper condition (not specified), the adsorbed hydrogen atom reacts with oxygen molecule or with the adsorbed oxygen atom in the surrounding structure.

Nearly a decade later in 1931, Tanner and Taylor study the hydrogen oxidation reaction at standard temperature and pressure and additionally at 373K on platinum wires [152]. They find that more oxygen disappears than corresponding water formation indicating the creation of hydrogen peroxide; however, after time oxygen disappears corresponding to water formation. In addition, when oxygen is in excess, it accelerates the reaction at 373K.

They find the reaction rate increases at the same temperature when hydrogen is also present in excess. At much higher pressures, their research indicates that the reaction rate is independent of hydrogen partial pressures.

In 1966, Acres postulates the first detailed kinetic model of the hydrogen oxidation mechanism [153]. In the first step, hydrogen and oxygen adsorb on the platinum surface in atomic form. Then, the adsorbed oxygen reacts with hydrogen molecules and adsorbed hydrogen reacts with oxygen molecules. During this process, they claim that water vapor retards the reaction rate. In addition, oxygen strongly chemisorbs as compared to hydrogen, but oxygen cannot displace pre-adsorbed hydrogen from the surface. As a result, they propose the formation of a hydroxyl group from the reaction of hydrogen atoms with the oxygen molecule or weakly adsorbed oxygen atoms:

$Pt \cdot H + Pt \cdot O \xrightarrow{k_{140}} Pt + Pt \cdot OH$	(140)

and their rate determining step comes from the perceived slow reaction:

$Pt \cdot H + Pt \cdot OH \xrightarrow{k_{141}} Pt + Pt \cdot H_2O$	(141)

It was not until 1969, that surface catalysis research began in depth with Lewis proposing that hydrogen adsorbs through a covalent bond in its atomic state on platinum by transferring an electron from the metal to the atom with the atom sitting above the metal surface [154]. They find that a single hydrogen atom can bond to number of different platinum atoms on the surface. This leads to stronger binding force than through a single substrate atom. This is a precursor to later findings regarding hydrogen adsorption on two or three platinum atoms instead of a single platinum atom. They determine desorption of hydrogen from the platinum surface occurs around 460K.

Five years later, Firth et al. state that the reaction rate of hydrogen oxidation is relatively high above 273K [87]. They propose that the reaction follows an E-R mechanism for hydrogen oxidation where oxide ions of the surface oxide species take part in the reaction. In addition, they assert that water adsorbs on platinum, but alumina removes some of this adsorbed water and its associated hydroxyl group making it available for the reaction to proceed. This is an important result as it justifies use of an alumina washcoat support for this reaction. They claim that hydrogen oxidation of platinum wire is a zero order reaction in the temperature range of 318 to 373K; however, they could not determine its order over a platinum and alumina catalyst. This is because the reaction is quite rapid above the freezing point of water and below that, it forms ice making it difficult to study over this catalyst.

A second publication by the same set of scientists determine that the reaction rate of hydrogen oxidation does not depend on oxygen pressure, i.e. it was found to be of zero order with respect to oxygen [155]. They now suggest a Langmuir Hinshelwood (L-H) reaction mechanism while stating that a competition does not exist between the molecules for vacant sites. A weak adsorbed hydrogen molecule reacts with a strong adsorbed oxygen species on surface:

$H_2 + Pt \xrightarrow{k_{142}} Pt \cdot H_2$	(142)
$Pt \cdot H_2 + Pt \cdot O \xrightarrow{k_{143}} 2Pt + H_2O$	(143)

However, on an oxidized surface, hydrogen weakly adsorbs making it more like an E-R mechanism:

$H_2 + Pt \cdot O \xrightarrow{k_{144}} H_2 \cdot Pt \cdot O$	(144)
$H_2 \cdot Pt \cdot O \xrightarrow{k_{145}} Pt + H_2O$	(145)

In the same year, Nishiyama and Wise publish a paper stating that carbon monoxide exhibits a relatively high sticking probability relative to that of hydrogen and oxygen under ultra high vacuum condition 0.133 kPa [156]. They claim that at 300K and at a low surface coverage area, hydrogen adsorbs in atomic state as per Eqn. (138) and has the lowest surface-sticking coefficient of the three species; H_2, O_2 and CO. In addition, their work indicates that CO can displace the previously adsorbed hydrogen and act as a poison for the hydrogen oxidation reaction.

The following year, Peng et al. state that hydrogen adsorbs in a dissociative manner as either strongly or weakly bound [157]. The strong bonded species are associated with negative surface potential electronegative (H^-) while the weakly bound species are electropositive (H^+). The hydrogen on surface is in equilibrium with hydrogen in gas as the adsorption and desorption rates are equal. At the same time, Weinberg and Merrill determine that this reaction proceeds as per an E-R mechanism where hydrogen gas reacts with the adsorbed oxygen atom on the surface to form water as per Eqn. (139) [158]. They further state that the L-H reaction for hydrogen oxidation is endothermic,

$\mathrm{Pt}\cdot\mathrm{O}+2\mathrm{Pt}\cdot\mathrm{H}\xrightarrow{k_{146}}3\mathrm{Pt}+\mathrm{H_2O}$	(146)

and thus reject its inclusion for hydrogen oxidation.

In 1976, Christmann et al. continue to research the adsorption of hydrogen and find that at 150K hydrogen adsorbs in an dissociative manner with an initial sticking coefficient of 0.1 [159]. They calculate that the adsorption energy is less than 10 kcal per mol at low coverage and the energy decreases with an increase in coverage attributed to a repulsive lateral interaction between adsorbate particles; i.e. hydrogen atoms. In the same year, Pacia and Dumesic suggest that the oxidation reaction happens as per an L-H reaction mechanism

through an adsorbed oxygen atom reacting with an adsorbed hydrogen atom to form water [160]. In their work, they investigate temperatures between 300K and 1700K, with a pressure 1.3157×10^{-8} atm and eliminate the possibility of an E-R mechanism stating that it cannot explain the observation of a maximum in the rate of reaction with varying oxygen pressure at constant temperature. In addition, they postulate that hydrogen desorbs from the surface at a much lower temperature than oxygen and propose the following detailed reaction steps after the adsorption of hydrogen and oxygen via Eqns. (138), (117) and (146):

$\mathrm{Pt\cdot H} \xrightarrow{k_{147}} \mathrm{Pt + H}$	(147)
$\mathrm{Pt\cdot O} \xrightarrow{k_{148}} \mathrm{Pt + O}$	(148)

with these Equations and the reverse reaction, Eqn. (117), only valid at high temperatures (around 1300K in the paper).

For hydrogen to oxygen pressure ratio greater than five, oxides do not form on the surface and they write the reaction rate expression as:

$R = \dfrac{k p_{\mathrm{O_2}}}{p_{\mathrm{H_2}}^{1/2}}$	(G13)

However, when the oxygen to hydrogen pressure ratio is greater than 20, they observe oxide formation and express the reaction rate as:

$R = \dfrac{k_4 K p_{\mathrm{H_2}}}{\left(1 + K_{\mathrm{H_2}}^{1/2} p_{\mathrm{H_2}}^{1/2}\right)^2}$	(G14)

where *k* is an Arrhenius rate expression, $k = Ae^{-E_a/(R_u T)}$, and $K_{\mathrm{H_2}}$ utilizes the absorption heat of H_2; e.g. $K_{\mathrm{H_2}} = k_{136}/k_{-136} = Ae^{-\Delta H_{\mathrm{H_2}}/(R_u T)}$.

In the next year, Boudart et al. compare the oxidation reaction at high pressures (1330 Pa) versus low pressures (10^{-6} Pa) [161]. They determine that the reaction is more likely to occur at lower pressures as compared to higher pressures with an observed difference in

reaction rate of 10^6 times faster. At high pressures, neither the support nor the particle size has an effect on reaction rate expression and they explain this discrepancy as function of the relative surface coverage. At low pressures, adsorbed hydrogen reacts with adsorbed oxygen to form water via an L-H type of reaction mechanism. However, it is not clear in their paper whether they believe that hydrogen adsorbs atomically or molecularly. At high pressures, oxygen largely covers the surface as it has a higher sticking probability as compared to hydrogen and therefore there is minimum space left for hydrogen to adsorb and react. The reaction in this case still proceeds via an L-H mechanism, but takes into account this observation.

Further continuing adsorption studies, Collins et al. show that electrons at the top of the platinum valence band have the most important role in adsorption of hydrogen and oxygen on the surface [162]. In addition, atomic oxygen has a lower sticking probability as compared to CO, but adsorbs at a lower temperature of 300K. Hydrogen has the lowest sticking coefficient among the three, but it adsorbs at an even lower temperature of 200K. They state that since oxygen has a higher sticking coefficient than hydrogen, it inhibits the reaction.

In 1978, Dabil and coworkers find that hydrogen oxidation has distinct kinetic region, between 320 to 360K with activation energy of 80 kJ/mol [144]. Above 360K, the reaction becomes washcoat diffusion limited. They further suggest that the reaction happens as per an E-R mechanism with CO as an inhibiting factor. In the same year, Hanson et al. claim that water vapor, formed as a product, inhibits the rate of reaction for a catalyst supported using either alumina or platinum wire [163]. In addition, findings show the reaction rate has a first order dependence on hydrogen concentration, either when oxygen or hydrogen is in excess.

They determine that the reaction rate decreases when adding excess oxygen at the same temperature and attribute this to the inhibition effect of oxygen on the reaction. However, they do not determine the reaction rate dependence on oxygen concentration in their paper. They support previous findings that this reaction follows an L-H mechanism at both low and high oxygen concentrations. While this paper uses silica as support instead of alumina, earlier findings from Boudart et al. illustrate that the support does not have a large impact on the reaction.

A few years later in 1981, Barteau et al. further examine hydrogen adsorption and suggest it continues to decrease as the temperature increases above 300K [164]. The reverse happens, increasing hydrogen adsorption, if the temperature decreases below 300K. They attribute this result to desorption of weakly bonded hydrogen from the surface at the higher temperatures. In the same year, Harris et al. claim that hydrogen oxidation happens as per the E-R mechanism of Eqn. (139) and reject the L-H reaction mechanism [165]. This is because they find that the rate of hydrogen oxidation increases as oxygen coverage decreases. However, they conclude that as the hydrogen molecule reaches the metal sites, it breaks apart liberating high kinetic energy H atoms. These H atoms collide with O to form OH, and OH reacts with subsequent H atoms to form water respectively, essentially stating that the reaction undergoes an L-H type mechanism.

The next year, Fisher et al. propose that water formation on platinum has low activation energy of 8 kcal/mol [166]. The oxidation reaction begins at 100K and reaches completion by 120K. Hydrogen adsorbs dissociatively below 90K and its maximum desorption rate occurs at 300K, while the desorption temperature of water is 180K. As a result, they postulate that the oxidation reaction happens as per an L-H reaction mechanism

in which adsorbed oxygen reacts with adsorbed hydrogen atom to form an adsorbed hydroxyl group as per Eqn. (140). At 135K, all of the adsorbed oxygen in this hydroxyl group now reacts with additional adsorbed hydrogen to form water.

Gdowski et al. support these low temperature findings by discovering at room temperatures, oxidation does occur [167]. They find that under a constant oxygen flow, the reaction rate continues to increase with temperature. In addition, the reaction rate increases with added hydrogen concentrations. Their work supports earlier findings by determining that oxygen and hydrogen both adsorb dissociatively on platinum. By performing an experiment using a mixture of hydrogen and deuterium (D_2), they observe that water forms as H_2O, D_2O and HDO in various ratios as per the input ratio. They reason that this is only possible via an L-H type of mechanism and, as a result, rule out E-R mechanisms for this reaction. In addition, they neglect oxygen desorption because it starts at relatively high temperatures, out of the scope of their studied range. They suggest that hydrogen desorption from the surface starts at 675K, while the water formation reaction is significant below 500K. Hence, hydrogen on the surface prefers to form water instead of desorbing, indicating the possibility of neglecting the reverse of Eqn. (138). Their findings suggest that the reaction is second order dependant on surface hydrogen atoms at a constant oxygen flux. As a result, they eliminate the reaction between two hydroxyl molecules because such a reaction does not yield a proper answer as indicated in a phase lag study:

$2Pt \cdot OH \xrightarrow{k_{149}} Pt \cdot H_2O + Pt \cdot O$	(149)
$Pt \cdot H_2O \xrightarrow{k_{150}} Pt + H_2O$	(150)

Furthermore, the formation of a hydroxyl group is an endothermic reaction and therefore not favorable thermodynamically. This is why OH has a very short life span over

platinum, as it will dissociate to form oxygen and hydrogen atoms, making it difficult to detect an OH group on the surface.

$Pt \cdot OH + Pt \xrightarrow{k_{151}} Pt \cdot O + Pt \cdot H$	(151)

where this reaction is the reverse of Eqn. (140).

In the same year, Gland and coworkers support the Gdowski et al. efforts by determining that after a hydroxyl group forms on the surface, it reacts quicker with an adsorbed hydrogen atom as compared to the reaction between and adsorbed hydrogen atom and an adsorbed oxygen atom indicating that step (140) is slower than step (141) [168]. Any residual hydrogen atoms left over desorbs between 220 and 290K, whereas residual oxygen atom desorption occurs above 625K. In addition, they rule out E-R mechanisms through a similar deuterium investigation and find that the hydroxyl group is intermittent in the water formation reaction.

They propose a detailed reaction model of Eqns. (138), (117), (140) and (141) while suggesting that oxygen can form islands on the platinum surface. An oxygen atom on the periphery is more reactive than an oxygen atom towards the center of the platinum particle. They create a model indicating that the adsorption rate of hydrogen near the reactive perimeter of oxygen is the Rate Determining Step (RDS). However, this model is out of the scope of this paper and the authors refer the reader to this paper for more investigation. Finally, they mention the following detailed reaction step as a possibility; however, it is not a major step in water formation:

$Pt \cdot H_2 + Pt \cdot O \xrightarrow{k_{152}} Pt \cdot OH + Pt \cdot H$	(152)

Concurrent to these efforts, White and Creighton conclude that the stoichiometry of the disproportional reaction between water and atomic oxygen is 2:1 and suggest that the OH producing reaction is [169]:

$2Pt \cdot H_2O + Pt \cdot O \xrightarrow{k_{153}} 3Pt \cdot OH + Pt \cdot H$	(153)

Future work by Ertl and coworkers support this reaction step in a 1999 paper [170]. In addition, they find the same intermediate at the reaction front; OH and H_2O in equilibrium with each other.

In 1983, Brown et al. conclude that in excess oxygen, the reaction is first order dependent on hydrogen concentration and independent of oxygen concentration and platinum dispersion [171]. In the same year, Nieuwenhuys supports the previous findings that hydrogen adsorbs dissociatively from 100 to 300K [172]. In addition, he states that at low temperatures (80 to 180K), water adsorbs molecularly on the surface. This molecule bonds with an oxygen atom, theorized as through one lone pair of electrons, which subsequently decomposes into a hydroxyl group at 155K; the reverse of Eqn. (149):

$Pt \cdot H_2O + Pt \cdot O \xrightarrow{k_{154}} 2Pt \cdot OH$	(154)

However, as temperature increases, this hydroxyl group decomposes to form water at 200K as per Eqn. (149). He proposes that hydrogen oxidation happens as per an L-H mechanism via Eqn. (140) and (141), with Eqn. (140) the rate determining step of the mechanism.

Ogle et al. report similar ideas the following year by stating that the rate of reaction depends on hydrogen pressure, temperature and initial oxygen coverage but not on the oxygen concentration [173]. They suggest that at temperatures above the desorption temperature of water, i.e. 200K, water formation is first order dependant on hydrogen

concentration with the Gland et al. island model as a possible explanation. However, at temperatures below 200K, the reaction is half-order dependent on hydrogen. In this temperature range, the reaction rate does not vary with oxygen and water coverage. They suggest that at these relatively lower temperatures, dissociative adsorption of water is the RDS. They also propose a new intermediate in water formation instead of OH, since they did not find any OH on the surface:

$Pt \cdot H + Pt \cdot O \xrightarrow{k_{155}} H \cdot Pt \cdot O + Pt$	(155)
$Pt \cdot H + H \cdot Pt \cdot O \xrightarrow{k_{156}} Pt \cdot H_2O + Pt$	(156)

As a result, they theorize a new reaction model based on temperatures below the freezing point and suggest that this model is not feasible for the higher temperature region of automotive exhaust.

In 1986, Akhtar and White formulate an important concept regarding the island formation model involving the oxygen atoms. In particular, both the oxygen atoms at the periphery and intermediate (internal to the island) are equally accessible and reactive [174]. This is different from all of the previous findings, which base their models on an islanding of oxygen. In the same year, Ogle and White state that in reactions above 300K, adsorption of hydrogen is the RDS [175]. Below 135K, a large amount of un-reactive hydrogen is present on the surface. At this lower temperature range, the concentration of surface hydrogen atoms controls the rate. Their detailed mechanism happens via Eqns. (117), (140) and (141) along with the following new reactions:

$Pt \cdot H_r \underset{k_{-157}}{\overset{k_{157}}{\rightleftarrows}} Pt \cdot H_n$	(157)
$2Pt \cdot H_2O + Pt \cdot O \xrightarrow{k_{158}} I$	(158)
$2Pt \cdot H_r + I \xrightarrow{k_{159}} 3Pt \cdot H_2O$	(159)

where H_r is a reactive hydrogen atom, H_n is a non-reactive hydrogen atom and *I* is an intermediate in the process.

They state that the intermediate production step is important to include as it helps reduce water formation in the initial stage until the consumption of adsorbed oxygen atoms. Once the intermediate forms from this process, water production increases significantly. To clarify, in the starting phase, creation of the intermediate occurs through all of the formed water. After the utilization of all oxygen on the surface, additional hydrogen reacts with the intermediate to form water. Since this reaction happens below the desorption temperature (<180K), platinum is first covered by oxygen. All created water on the platinum surface is present as ice; hence, upon starting the process, only the intermediate forms.

In the same year, Zhadnov et al. review the reaction history and write the detailed reaction as a function of Eqns. (138), (117), (140) and (141) [176]. They believe that at high temperatures, reactions (140) and (141) occur relatively fast. In addition, at these temperatures the reaction rate does not depend on hydrogen pressure and is proportional to the oxygen pressure. They propose two different steady state expressions for the adsorption of hydrogen and oxygen in terms of sticking coefficients.

Mitchell et al. continues the work by stating that the kinetics at low temperatures (<200K) are very different from high temperatures (>300K) [177]. At high temperatures, the reaction is first order dependent on hydrogen pressure, while at low temperature, it is half order dependent. Until this work, researchers assume reaction (141) to be much faster than reaction (140). However, at temperatures between 130 and 160K, Mitchell et al. find that the RDS involves hydrogen diffusion. They find that both reactions (140) and (141) proceed at the same rate since both involve this diffusion dependence. In addition, they support Ogle

and White's derivation for hydrogen oxidation involving Eqns. (138), (117), (140), (141), (157), (158) and (159) and propose a structure for the intermediate (I) involving two OH groups cross linked by a water molecule. However, in the following year, these same authors accept OH as reaction intermediate during the reaction [178].

At the end of the 1980s, Ljüngstrom et al. investigate the impact of OH as an intermediate [179]. At temperatures above 900K, they observe OH desorbing from the surface through laser-induced florescence detection and from this, they postulate that OH production occurs through reaction (154). In the temperature range of 900 to 1300K, they believe the reaction mechanism follows Eqns. (138), (117), (140) and (141); however, at low temperatures, Eqn. (149) may replace Eqn. (141) with Eqn. (150) providing the water production in both cases. At sufficiently high temperatures, OH may desorb before reacting:

$Pt \cdot OH \xrightarrow{k_{160}} Pt + OH$	(160)

Nevertheless, this is not significant enough to influence the kinetics of the reaction and they do not consider it in their modeling activities. In addition, they neglect the dissociation of OH into its elementary atoms and desorption of oxygen, as the water formation rate is much faster than these dissociation reactions. They state that the creation of OH is the most significant step in the reaction and they formulate their kinetics as per this reaction step.

Their findings indicate that as hydrogen concentration increases, the poisoning effect of oxygen decreases and OH forms faster as there is a larger supply of hydrogen to react with oxygen. This results in a perceived first order dependence of water production on hydrogen partial pressure. At lower flow rates of hydrogen, the hydroxyl compound on the surface does not receive enough hydrogen to react until completion; hence, as there is not enough

supply of hydrogen, the OH molecules on the surface remain. In addition, they postulate that at higher pressures and low temperatures, the surface coverage of OH increases and, thus, the reaction rate improves.

In 1990, Verheij et al. support the claim that the hydrogen sticking probability is lower on an oxygen covered surface as compared to clean surface in the temperature range of 400 to 550K [180]. Moreover, they find that water production does not depend on the initial oxygen coverage. When the oxygen coverage is low, some of the adsorbed hydrogen can desorb, but as coverage increases, hydrogen tends to react with oxygen to form water and then desorb. Their efforts additionally show that hydrogen sticking probability is constant at 400K, whereas at 550K, it decreases with an increase in oxygen coverage. At the same time, Anton and Cadogan investigate the reaction in temperature range of 373 to 723K [181]. They propose that the reaction mechanism happens through Eqns. (138), (117) and (140) with the final steps involving Eqns. (141) or (149) with Eqn. (150) assumed instantaneous. When hydrogen is in excess as compared to oxygen, Eqn. (141) predicts the reaction effectively. When oxygen is in excess to hydrogen, hydroxyl coverage increases linearly with temperature and the reaction pathway (149) dominates the mechanism. The RDS in their mechanism is either of these hydroxyl consumption reactions.

In the same year, Hellsing at el. analyze these two hydroxyl reactions and state that at high temperatures and moderate hydrogen partial pressures, reaction (141) is dominant [182]. Conversely, at low temperatures and high oxygen concentrations Eqn. (149) is the principal reaction. They propose that hydrogen oxidation happens as per Eqns. (138), (117), (140), (141) and (149) with one additional step via Eqn. (160). At high temperatures, hydrogen oxidation on platinum is a relatively fast reaction. In addition, they mention that oxygen

primarily covers the surface and research indicates that in excess of oxygen, researchers can assume zero hydrogen coverage. The reaction rate of water formation is the same using either reaction Eqns. (141) and (149); however, for the latter Equation, a strong coverage dependence of OH desorption energy is required, which is questionable. For the first reaction method, their work proposes using OH decomposition and water decomposition for the kinetics as these reactions are important. Finally, they support the findings of Anton and Cadogan that the inlet feed stream conditions define which reaction is dominant for water formation.

In 1992, Kwasneiwski et al.'s efforts led to a recommendation of using the reaction mechanism previously proposed with a singular addition [183]. They suggest that hydrogen reacts with oxygen below 180K, but not fully to completion. As a result, the detailed mechanism follows Eqns. (138), (117), (140), (141), (149), (150), (151), (154) and the reverse of Eqn. (141):

$Pt \cdot H_2O + Pt \xrightarrow{k_{161}} Pt \cdot OH + Pt \cdot H$	(161)

In the next year, Fassihi et al. investigate the oxidation reaction at a pressure of one atmosphere [184]. They postulate that the light-off temperature increases by raising the hydrogen pressure. When ratio of hydrogen pressure to total reactant pressure (hydrogen + oxygen pressure: α) goes below 0.1, ignition happens below room temperature with the mechanism following Eqns. (138), (117), (140), (141) or (149). The reaction is faster above this temperature as the activation barrier remains low. Because of this, it does not matter the route, Eqn. (141) or (149), as the water formation occurs independent to these reactions happening. When the temperature and reactant pressure is that of typical exhaust gases, the hydroxyl and oxygen desorption rates are negligible. In this range, the reaction rate of water

formation is faster than the adsorption rate of hydrogen and oxygen. Therefore, under excessive hydrogen regimes, hydrogen covers the surface. Then, all oxygen molecules that adsorb react with this hydrogen to form water and hydrogen either reacts with oxygen to form water or desorb. Conversely, under excessive oxygen regimes, oxygen dominates the surface. During this situation, oxygen desorption is negligible and oxygen coverage is nearly unity. They state that the water production rate in both cases is twice the rate of oxygen adsorption.

Their work proposes that before ignition, hydrogen covers the surface unless it has a low partial pressure. After ignition, reactant diffusion to the surface limits the reaction rate and the ignition temperature depends only on hydrogen adsorption and desorption. Hence, the main reason for light off is desorption rate of hydrogen as temperature increases, creating more sites for the reaction to happen. After light off, oxygen mainly covers the surface and if the hydrogen partial pressure is not sufficiently large, then the reaction will not continue to proceed. This is why as the hydrogen partial pressure increases, the ignition temperature increases.

In the same year, Zhdanov predicts a hysteresis in the reaction rate at low hydrogen partial pressures (oxygen and hydrogen pressure is 0.135 atm) between 300 and 500K [185]. He postulates that the reaction happens via Eqns. (138), (117), (140) and (141) while supporting Fassihi et al.'s findings. The next year finds Warnatz et al. confirming that the ignition temperature of hydrogen oxidation depends on the rate of hydrogen dissociation on platinum, which in turn depends on the hydrogen partial pressure in the mixture [186]. In 1995, Verheij and Hugenschmidt perform hydrogen oxidation experiments in the temperature range of 300 to 600K [187]. They find that hydrogen adsorption is the RDS for water formation when

oxygen coverage is greater than 10% of its saturation coverage. In this case, the hydrogen-sticking probability is equal to the water formation rate per incident molecule. This means that every incident hydrogen molecule will form water by reacting with an adjacent oxygen atom.

A couple years later, Eisert and Rosen confirm that in the range of 300 to 700K and pressures varying from 10^{-5} to 10^{-3} mbar, hydrogen oxidation happens as per Eqns. (138), (117), (140), (141) or (149) [188]. They state that above 400K, when α is greater than 0.25, oxygen coverage rapidly decreases below detection levels. They attempt to determine whether reaction Eqns. (141) or (149) is responsible for the water formation, but they end up concluding that both reactions are in good agreement with the experimental data. Thus, they are unable to draw a supposition and leave this investigation to future efforts.

In the year 1998, Verheij and Hugenschmidt reference their previous papers and state that only a few special platinum sites are reactive with the reaction possibly proceeding non-homogenously on the surface [189]. They propose that water forms over the active sites along with the following reaction responsible for transport of hydrogen atom to these sites:

$\mathrm{Pt \cdot H_2O + Pt \cdot OH \xrightarrow{k_{162}} Pt \cdot OH + Pt \cdot H_2O}$	(162)

This Equation describes a proton transfer happening at the reaction front below the desorption temperature; i.e. the proton transfer from the surface of a water island to the internal part of the island and again forming reacting OH on the surface. It occurs below 220K, when water is still adsorbed on the platinum sites; however, above this temperature, water begins to desorb and the reaction ceases. They postulate that a new reaction begins at temperatures above 300K when oxygen atoms become mobile but they do not explain how

this happens. This contradicts previous findings that the oxygen atom is immobile on the surface.

They claim that the hydrogen oxidation reaction proceeds non-homogenously on the surface and oxygen diffusion is the RDS with hydrogen not being involved, which again contradicts previous findings by other researchers. For a homogeneous surface, they state that the water formation reaction is first order with respect to oxygen and zero order with respect to hydrogen below 400K. It is second order with respect to oxygen and first order in hydrogen between 400 and 600K. Regarding a non-homogenous surface between temperatures of 300 to 600K, the measured signals were the same as that of homogenous surface. Hence, below 400K, the reaction does not depend on hydrogen with a reduced alliance on oxygen in comparison to the ideal surface. Above 400K, the dependence on oxygen is non-linear and for the reaction to continue, it requires at least two oxygen atoms. They conclude that the reaction happens non-homogenously on a stepped platinum surface.

They postulate a detailed mechanism based starting with Eqns. (138), (117), (140), (141), (149) and then as follows:

$\mathrm{Pt\cdot O} \underset{k_{-163}}{\overset{k_{163}}{\rightleftarrows}} \mathrm{Pt\cdot O}_{rs}$	(163)
$\mathrm{Pt\cdot OH}_{rs} \underset{k_{-164}}{\overset{k_{164}}{\rightleftarrows}} \mathrm{Pt\cdot OH}$	(164)

where the above reactions happen as a function of diffusion and the subscript *rs* indicates the reactive site in the reaction. For reaction (149), they propose an intermediate species (H_2O_2) in the mechanism:

$\mathrm{Pt\cdot OH}_{rs} + \mathrm{Pt\cdot O}^{*} + \mathrm{Pt\cdot H} \xrightarrow{k_{165}} \mathrm{Pt\cdot H_2O_{2rs}}$	(165)
$\mathrm{Pt\cdot OH}_{rs} + \mathrm{Pt\cdot OH}^{*} \underset{k_{-166}}{\overset{k_{166}}{\rightleftarrows}} \mathrm{Pt\cdot H_2O_{2rs}}$	(166)
$\mathrm{Pt\cdot H_2O_{2rs}} \xrightarrow{k_{167}} \mathrm{Pt\cdot H_2O_2}$	(167)

$Pt \cdot H_2O_2 \underset{k_{-168}}{\overset{k_{168}}{\rightleftarrows}} Pt \cdot O + Pt \cdot H_2O$	(168)

with the superscript * denoting the site near the reactive site. They state that between 400 and 500K, hydrogen oxidation involves two oxygen atoms and thus the second path, the disproportionate reaction of two OH to form water, is dominant. Finally, they conclude the paper by stating that the reaction is independent of hydrogen and first order dependent on oxygen below 800K for the non-homogeneous surface.

Volkening et al. state in the following year, that simple hydrogen addition to OH is the incorrect mechanism for the reaction [190]. They claim that oxygen atoms, water and OH are the only intermediates that cover the platinum surface as determined from their experiments in an ultra high vacuum at low temperatures. They discuss that at temperatures below 170K, reaction (149) and reaction (154) form an autocatalytic reaction. This is where one water molecule breaks down into two OH groups and then hydrogen atoms react with these OH molecules to form two water molecules. However, above the desorption temperature, water desorbs immediately after formation and there is not any water available for reaction (154). Hence, the reaction continues via Eqns. (140) and (141). They propose that reaction (140) is the RDS at high temperatures. However, at even higher temperatures, there may be other complex mechanisms occurring to explain the perceived increase in activation energy.

In the same year, Young et al. assume that hydrogen oxidation happens on platinum as per the reversible reactions given by Eqns. (138), (117), (140), (141), (147), (148), (149), (150), (151), (154), (160), (161) and the following [191]:

$OH + Pt \xrightarrow{k_{169}} Pt \cdot OH$	(169)
$Pt + H_2O \xrightarrow{k_{170}} Pt \cdot H_2O$	(170)

$Pt + H \xrightarrow{k_{171}} Pt \cdot H$	(171)
$Pt + O \xrightarrow{k_{172}} Pt \cdot O$	(172)

that are the reverse reactions of Eqns. (160), (150), (147) and (148) respectively. They propose a different method of modeling the reaction, which takes into account a consideration of the change in activation energy via the possible different reaction pathways.

The next year finds Forsth and co-worker describing that the adsorption and desorption reactions are the RDS instead of the surface reactions [192]. Their work indicates that hydrogen adsorption is the dominant path when hydrogen is in excess to that of oxygen. In comparison, the hydroxyl disproportion path, Eqn. (149), is dominant when oxygen is in excess of hydrogen. At 1300K and a total pressure less than 1 Torr, this behavior is best modeled using a low sticking coefficient for hydrogen adsorption when hydrogen is in excess. A high sticking coefficient is evident when the hydroxyl disproportional reaction dominates. However, there is some ambiguity with respect to their overall conclusions.

In 2001, Michaelides and Hu investigate OH adsorption and find that it binds strongly to platinum surface [193]. They conclude that this hydroxyl component diffuses very easily on the surface and tends to form clusters at low surface coverage. At high coverage, there is an H bonding interaction between neighboring OH groups that leads to an increase in the activation energy of OH bonding with platinum. In the same year, these authors publish another paper that examines the various adsorption and reaction pathways of the intermediates species [194]. They support the results that the reaction progresses through Eqns. (140) and (141), while at temperatures below 180K water remains bonded to the surface. Then, the reaction continues through fronts as per Eqn. (154). They postulate that reaction (140) is slightly exothermic and once OH is formed, it will cluster and create an island or

domain of OH on the surface. The presence of another H_2O molecule improves the energy of formation of OH in this domain. Here, one of the two water molecules remains intact, but in order for the reaction to continue, it does not require both of them to be present.

They state that the reaction between adsorbed hydrogen and adsorbed oxygen is endothermic, but the reaction between OH and adsorbed hydrogen is exothermic. Furthermore, water desorption energy is lower than its dissociation energy. Hence, when heated, water will desorb rather than dissociate. (Below 180 K, adsorbed oxygen will not react with adsorbed hydrogen, as this is an endothermic reaction and the required activation energy is not present; hence, OH does not readily form. However, the addition of a hydrogen atom to the OH group on the surface is achievable at this temperature; therefore, once OH forms it quickly converts into water. Since, hydroxyl formation by addition of H to O is not favored at this temperature, the disproportionate reaction occurs and the water molecule converts into OH. They further explain that the disproportionate reaction is not a single step reaction, like Eqn. (153), instead it occurs through reaction (154) and then as follows:

$\mathrm{Pt}\cdot\mathrm{H_2O} + 2\mathrm{Pt}\cdot\mathrm{OH} \xrightarrow{k_{173}} 3\mathrm{Pt}\cdot\mathrm{OH} + \mathrm{Pt}\cdot\mathrm{H}$	(173)

Reaction (173) has a relatively high energy barrier; therefore it is not possible to convert all of the water to OH species. In addition, hydroxyl formation stops at Eqn. (154), but even this reaction requires support from other water molecules to form OH. Thus, after this happens the surface will consist of species in the ratio of two OH radicals to one water molecule.

In the next year, Forsth uses the past history to describe the reactions occurring on the surface via Eqns. (138), (117), (140), (141), (143), (144), (147), (148), (149), (150), (158), (159), (170), (171), (172) and (173)[195]. For dissociative hydrogen adsorption on the surface

represented by Eqn. (138), he determines the sticking coefficient to have a linear dependence on coverage. To note, the history of this reaction illustrates that the sticking coefficient for the reactants varies widely reported by the researchers. Of additional interest, this work includes a study of gas phase, homogeneous hydrogen oxidation in combination with surface reactions in order to determine the relative impact of both during the conversion process.

In 2003, Nagasaka et al. support the findings of the autocatalytic reaction of water formation below the desorption temperature through reactions (138), (117), (140), (141) and (153)[196]. The reaction rate of water decreases drastically above this desorption temperature as the autocatalytic reaction stops. They discuss that water forms in three steps starting with an induction phase, followed by a fast reaction period of increasing OH and water coverage through consuming O and finally a slow reaction period of converting OH into water without utilizing atomic oxygen. They include a kinetic study of the water formation along with a modeling study; however, their simulation results do not match experimental observations.

In 2005, Kharlamov V.F. and Kharlamov F.V. propose the participation of molecular hydrogen in the RDS of the reaction [197]. They claim that the presence of water vapor has no effect on the rate of reaction and the reaction progresses via Eqns. (138), (117), (140), (142), (143) and the following:

$Pt \cdot H_2 + Pt \xrightarrow{k_{174}} 2Pt \cdot H$	(174)
$Pt \cdot H_2 + 2Pt \cdot OH \xrightarrow{k_{175}} 3Pt + 2H_2O$	(175)
$H_2 + 2Pt \cdot O \xrightarrow{k_{176}} 2Pt \cdot OH$	(176)
$O_2 + 2Pt \cdot H \xrightarrow{k_{177}} O_2 \cdot 2Pt \cdot H$	(177)
$O_2 \cdot 2Pt \cdot H \xrightarrow{k_{178}} 2Pt + 2H_2O$	(178)

In the same year, Nagasaka et al. continue their earlier work in investigating the oxidation reaction below the desorption temperature [198]. They confirm their earlier results that the reaction progresses through Eqns. (138), (117), (140), (141) and (153). With respect to this mechanism, since reaction (140) is slow at low temperatures (< 180K), after the initiation of the autocatalytic cycle, they believe it does not contribute to the reaction. This paper also explores the adsorption of hydrogen, oxygen, OH and water in detail and finds that hydrogen adsorption reduces when oxygen is present. They explain this by stating that hydrogen requires two neighboring vacant sites for adsorption, and since oxygen has a greater affinity towards platinum, when oxygen is present hydrogen will not adsorb.

In addition, hydrogen adsorption does not occur if OH or water occupies a site between two vacant hollow sites. As hydrogen adsorbs, it distributes randomly because of its high mobility and low interaction energy. In this temperature range, oxygen atoms and OH molecules are immobile. Their investigation of the processes at the reaction front indicates that the OH to H_2O coverage ratio is 1:1 at this location. If proton transfer between H_2O and OH does not occur, then OH species stay at boundary and form the barrier between O and H_2O. This will slow down the reaction process and, thus, proton transfer may play a significant role in the reaction process.

In the next year, Salomons et al. conclude that hydrogen converts fully to water at room temperature [199]. In their work, they document the reaction steps as following Eqns. (138), (117), (140), (141), (149) and (150). When the temperature is above the desorption temperature, the activation energy of hydrogen oxidation increases nearly four times as compared to activation energy below desorption temperature. They use this finding to explain why the reaction rate decreases to some extent at room temperature. However, as the

temperature increases further, so does the reaction rate. They also demonstrate that when CO is present, hydrogen and CO light off simultaneously. This may be a reason why modelers often utilize the CO reaction rate expression for simulating hydrogen oxidation. In the same year, Younis model this reaction and propose values for the activation energy and pre-exponential factor according to the following rate expression [200]:

$$R = AC_{H_2}C_{O_2}^{0.5}\exp\left(-\frac{E_a}{R_uT}\right) \quad \text{(G15)}$$

In 2007, Schiros et al. refer to earlier papers and state that H_2O and OH molecules on the surface form a nearly flat layer [201]. The OH bonds are parallel to platinum surface, while the water molecule bonds to platinum through the oxygen and lies flat on surface. As the temperature increases from 120 to 155K, hydroxyl formation starts from the reaction of water and oxygen. From 155 to 185K, OH coexists with water and the water-hydroxyl phase is stable. Above 185K, the hydroxyl disproportion reaction begins and the water formed immediately desorbs from the surface. However, if cooling occurs below 185K, then the water hydroxyl layer remains stable.

In the next year, Nagasaka et al. investigate the proton transfer impact on platinum [202]. They consider this an important facet in the water formation reaction below the desorption temperature (180K). This investigation occurs in two ways; one method was the direct transfer of proton from water molecule to OH and other is through a H_3O^+ mediated molecule. They determine that the time for proton transfer through H_3O^+ is high as compared to direct transfer.

In the recent year, Salomons et al. continue their work investigating both hydrogen and CO oxidation simultaneously [203]. The presence of hydrogen improves CO oxidation, while CO inhibits the hydrogen oxidation reaction. They utilize the same process for

hydrogen oxidation as in their 2006 paper and provide detailed reaction rate expressions for each step. Their experimental efforts confirm that when CO is present, hydrogen converts concurrently. In addition, when both CO and hydrogen are present, CO oxidizes first and when conversion reaches 50%, hydrogen begins rapidly converting. This again illustrates that using the CO oxidation model for simulating hydrogen oxidation in presence of CO might be a valid methodology.

3.2.2 HISTORICAL SUMMARY:

From the time Sir Dobereiner discovered the use of platinum for hydrogen oxidation, scientists have been working to determine the correct mechanism and global reaction rate expression for this reaction. In his famous paper, Langmuir gives a detailed analysis of hydrogen oxidation and proposes an Eley-Rideal mechanism. However, his work does not rule out the possibility of a Langmuir-Hinshelwood version. After more than one and half centuries, scientists are still endeavoring to formulate the correct reaction mechanism.

It is not until the decade of the 1970s when research on hydrogen oxidation increases significantly. The literature around this time demonstrates a significant amount of confusion with respect to the reaction mechanism. Until the mid 1970s, scientists were still proposing E-R versions; however, soon thereafter, theorized L-H versions began to be more prevalent. The literature illustrates that persons proposing one mechanism were strongly refuting other mechanism based on various studies and experimental data; however, researchers do not reach a common consensus.

During the next decade, investigators finally conclude that the reaction mechanism happens as per an L-H method. It is clear that both hydrogen and oxygen adsorb via dissociation on the platinum surface, well below the freezing temperature. The atomic

species then react to form water through the subsequent addition of a hydrogen atom to oxygen. However, the main issue in this mechanism now lies in the proper description of intermediate formation. Many researchers propose that OH is the intermediate; however, they are not able to discover it through experimental observation as it they perceive it to be short lived on the surface. As a result, scientists propose many other different intermediates, but are not positive about their presence. While it is clear that the reaction does follow an L-H type of mechanism and all experiments prove this conclusion, the elusive intermediate process becomes the main question. In order to help determine the proper pathway, scientists began studying the reaction below the desorption temperature of 180K. This leads to a new interpretation of the mechanism of hydrogen oxidation.

In the 1990s, researchers confirm that OH is the intermediate for the hydrogen oxidation reaction. However, two different reaction mechanisms began to take shape with one mechanism describing the process below the desorption temperature and the other mechanism for above this temperature. As a result, the focus of this decade involves investigating the reactions below the desorption temperature along with the interaction of adsorbed water and intermediate OH molecules. Researchers find that the reaction proceeds along the surface through reaction fronts on the platinum surface. Investigations include the detailed structure of these fronts along with the orientation of OH and water molecules with respect to the surface and each other. One result of this work is the discovery of hydrogen transfer at this reaction front between OH and water molecules.

The current decade finds hydrogen oxidation investigated concurrently with CO oxidation and their resultant impact on each other's oxidation rate. Scientists find that CO inhibits hydrogen oxidation while hydrogen promotes CO oxidation. When CO and

hydrogen are both present in the stream, they oxidize at the same temperature; i.e., each species light off nearly at the same time. Further description of the reaction expressions below desorption temperature continues and investigators find that the orientation of hydroxyl group and water is important in this process. Results show that from 120 to 185K, unless all oxygen converts into an intermediate, water formation is very low. Once all the oxygen converts, the reaction suddenly increases and water formation takes place.

3.2.3 DETAILED REACTION MECHANISM:

Based on this historical summary, the authors feel that the hydrogen oxidation reaction over platinum occurs via the following steps:

3.2.3.1 Dissociative Oxygen Adsorption:

The first step in the mechanism is dissociative oxygen adsorption on platinum. This is because oxygen has a larger sticking coefficient as compared to hydrogen:

$O_2 + 2Pt \underset{k_{-a}}{\overset{k_a}{\rightleftarrows}} 2Pt \cdot O$	(*a*)

Researchers have found that if the oxygen concentration is significantly large in comparison to hydrogen, it will act to inhibit the reaction. In addition, history indicates the OH formed due to this excess oxygen will also inhibit hydrogen adsorption. This is because the OH created will not immediately convert into water due to lack of sufficient hydrogen and it will remain on the surface blocking the reaction from proceeding.

With respect to oxygen adsorption, Elg et al. found that molecular oxygen physisorbs on platinum below 30K, but chemisorbs above 45K as shown in Figure 15 [137]. Around 130 to 150K, the O–O bond appears to weaken and begins to dissociate the molecule (also seen by Tieber et al. in [110]). Above 150K, the adsorbed molecular oxygen dissociates into its atomic parts, which only starts desorbing at a much higher temperature (800K). Oxygen is

not present at substrate level with only platinum found, illustrating that this process does not form platinum oxide. Although, the methodology of oxygen adsorption is same as described in section 3.1.3.2, its description has been repeated here in order to better elucidate to the reader the formulation of a global reaction mechanism for hydrogen oxidation.

3.2.3.2 Dissociative Hydrogen Adsorption:

The second step in the hydrogen oxidation reaction is dissociative hydrogen adsorption on platinum around a temperature of 90K [159, 166, 172]:

$H_2 + 2Pt \underset{k_{-b}}{\overset{k_b}{\rightleftarrows}} 2Pt \cdot H$	(*b*)

through the formation of a covalent bond. As discussed in the previous section, when oxygen is in excess this is the RDS as oxygen inhibits its adsorption [168, 175, 187]. Hydrogen begins to desorb from the surface around 300K and as temperature increases, hydrogen coverage decreases.

3.2.3.3 Reaction Between Adsorbed O and H:

Both oxygen and hydrogen atoms react with each other on the surface to form a hydroxyl group:

$Pt \cdot H + Pt \cdot O \xrightarrow{k_c} Pt + Pt \cdot OH$	(*c*)

The group formed is unstable and it further reacts with hydrogen atom to form water or dissociate into parent atoms. In the temperature range of typical engine exhaust (300 to 700K), sequential addition is preferred over dissociation. Many researchers believe this is the RDS for hydrogen oxidation [172, 190], while also proposing that this is the RDS when hydrogen is in excess as compared to oxygen. Subsequent reactions in the hydrogen oxidation process may occur in three different ways as per the temperature range and concentration of the reactants.

3.2.3.4 Temperature Lower than Desorption Temperature:

In this temperature range, hydrogen oxidation proceeds in a different manner. Since water does not desorb from the surface, after time the reaction stops and ice covers the entire surface. In order to investigate the reactions at these temperatures, researchers pre-adsorb oxygen on the platinum surface and then flow hydrogen into the system. In this case, reactions (*a*), (*b*) and (*c*) occur followed by a small amount of OH reacting with a hydrogen atom to form water:

$Pt \cdot H + Pt \cdot OH \xrightarrow{k_d} Pt + Pt \cdot H_2O$	(*d*)

This small amount of water then reacts with an adjacent oxygen atom to re-form OH:

$2Pt \cdot H_2O + Pt \cdot O \xrightarrow{k_e} 3Pt \cdot OH + Pt \cdot H$	(*e*)

This OH again reacts with a hydrogen atom and forms water, which again converts to OH by reacting with oxygen atom. Thus, at these temperatures the system undergoes an autocatalytic reaction that continues until conversion of all of the oxygen atoms into OH groups. A reaction front develops and continues outwards engulfing surrounding oxygen atoms. During this time, little water forms until consuming all oxygen that then frees up the water on the surface to release and water production suddenly increases.

3.2.3.5 Temperature Greater than Desorption Temperature and Hydrogen Excess:

When the temperature is above the desorption range, and hydrogen is in excess or in one is to one ratio with oxygen, then the reaction proceeds as per Eqns. (*a*), (*b*) and (*c*). The OH formed immediately reacts with adjacent hydrogen atom to form a water molecule:

$Pt \cdot H + Pt \cdot OH \xrightarrow{k_f} 2Pt + H_2O$	(*f*)

This water molecule immediately desorbs from the surface and the reaction is complete. This is the simplest reaction mechanism and typically the chosen path for hydrogen oxidation.

3.2.3.6 Temperature Greater than Desorption Temperature and Oxygen Excess:

When the temperature is above the desorption temperature, and oxygen is in excess, the reaction proceeds as per Eqns. (*a*), (*b*) and (*c*) followed by the hydroxyl disproportionate reaction [183]:

$2\mathrm{Pt}\cdot\mathrm{OH}\xrightarrow{k_g}\mathrm{Pt}+\mathrm{Pt}\cdot\mathrm{O}+\mathrm{H_2O}$	(*g*)

Since oxygen is in excess of hydrogen, sufficient hydrogen atoms are not available to convert each oxygen atom to water. As a result, as OH forms it does not have enough hydrogen in the nearby vicinity, but another OH molecule is present to convert. These two OH molecules then react to form water, which then desorbs from the surface.

3.2.4 GLOBAL REACTION MECHANISM:

In the exhaust of an internal combustion engine, the temperature is significantly greater than 180K. As a result, this section will ignore the reactions that occur below this value. In addition, in order to determine the RDS, it is necessary to understand the conditions of the exhaust as a function of engine type. In a spark ignition or gasoline engine, oxygen and hydrogen will be at similar concentration levels since these engines run around stoichiometric conditions. As a result, the case involving hydrogen excess will resemble the closest comparison.

In this situation, dissociative oxygen adsorption on platinum is the first step with the forward and reverse rates expressed as:

$R_a = k_a p_{\mathrm{O_2}} \theta_{\mathrm{Pt}}^2$	(179)

$$R_{-a} = k_{-a}\theta_{\mathrm{Pt\cdot O}}^2 \quad (180)$$

At equilibrium, the forward and backward rate becomes equal, hence

$$k_a p_{\mathrm{O_2}} \theta_{\mathrm{Pt}}^2 = k_{-a}\theta_{\mathrm{Pt\cdot O}}^2, \quad (181)$$

where the equilibrium constant equals:

$$K_{\mathrm{O_2}} = k_a / k_{-a} \quad (182)$$

At the same time, dissociative hydrogen adsorption is also occurring with the forward and reverse rates equal to:

$$R_b = k_b p_{\mathrm{H_2}} \theta_{\mathrm{Pt}}^2 \quad (183)$$

$$R_{-b} = k_{-b}\theta_{\mathrm{Pt\cdot H}}^2 \quad (184)$$

and at equilibrium,

$$k_b p_{\mathrm{H_2}} \theta_{\mathrm{Pt}}^2 = k_{-b}\theta_{\mathrm{Pt\cdot H}}^2, \quad (185)$$

where the equilibrium constant equals:

$$K_{\mathrm{H_2}} = k_b / k_{-b} \quad (186)$$

As the ratio of hydrogen to oxygen concentration in a gasoline engine would not be small, oxygen adsorption does not inhibit hydrogen adsorption. From the reaction history, when oxygen does not inhibit the hydrogen adsorption on the surface, then hydroxyl formation reaction is the RDS [172, 190]. Researchers consider the subsequent hydrogen addition and formation of water fast and may neglect it from the overall expression [168, 172, 176, 190]. In addition, in the temperature range under study (300 to 550K), water desorption is very fast to an extent that any water formed will immediately desorb from the surface. As a result, the authors will ignore inhibition due to water on the surface. Hence, in this case, the surface reaction between the adsorbed oxygen atom and adsorbed hydrogen atom will be the RDS.

$$R_c = k_c \theta_{\mathrm{Pt\cdot O}} \theta_{\mathrm{Pt\cdot H}} \quad (187)$$

If this is the RDS, derivation of the global reaction rate expression occurs through the surface coverage fractions:

$\frac{\theta_{\mathrm{Pt\cdot O}}}{\theta_{\mathrm{Pt}}} = K_{\mathrm{O_2}}^{1/2} p_{\mathrm{O_2}}^{1/2}$	(188)
$\frac{\theta_{\mathrm{Pt\cdot H}}}{\theta_{\mathrm{Pt}}} = K_{\mathrm{H_2}}^{1/2} p_{\mathrm{H_2}}^{1/2}$	(189)

Using the fact that $\theta_{\mathrm{Pt}} = \left(1 - \theta_{\mathrm{Pt\cdot H}} - \theta_{\mathrm{Pt\cdot O}}\right)$ and the above surface coverage fractions results in the following expression:

$\theta_{\mathrm{Pt}} = \frac{1}{\left(1 + K_{\mathrm{H_2}}^{1/2} p_{\mathrm{H_2}}^{1/2} + K_{\mathrm{O_2}}^{1/2} p_{\mathrm{O_2}}^{1/2}\right)}$	(190)

Substituting this into Eqn. (188) and (189), and then utilizing Eqn. (187) results in:

$R_{\mathrm{H_2}} = \frac{k_c K_{\mathrm{H_2}}^{1/2} K_{\mathrm{O_2}}^{1/2} p_{\mathrm{H_2}}^{1/2} p_{\mathrm{O_2}}^{1/2}}{\left(1 + K_{\mathrm{H_2}}^{1/2} p_{\mathrm{H_2}}^{1/2} + K_{\mathrm{O_2}}^{1/2} p_{\mathrm{O_2}}^{1/2}\right)^2}$	(Hy-RDS-*c*)

This is the global reaction rate expression when hydrogen oxidation happens as per subsequent hydrogen addition to oxygen.

However, when oxygen is present in excess, it inhibits hydrogen adsorption. In addition, since oxygen does not desorb from the surface below 800K, oxygen completely covers the surface. This condition is possible in a compression ignition or diesel engine and hence, modeling oxidation catalysts for these engines requires creating global expression involving this phenomenon. History shows us that, when oxygen is in excess for hydrogen oxidation, water forms as per hydroxyl disproportionate reaction.

It will follow the same step of dissociative oxygen adsorption and desorption from the surface. However, there will not be any hydrogen on the surface. This is because every hydrogen molecule that encounters the surface will react immediately with atomic oxygen to form water with the high diffusivity of the hydrogen atom promoting this interaction. In addition, since any water formed in the considered temperature range immediately desorbs, the surface will not contain any water or hydroxyl compound. As a result, the only species available on the surface will be oxygen that acts to inhibit the adsorption process.

In this case, the surface coverage expression is simpler, $\theta_{Pt} = \left(1 - \theta_{Pt\cdot O}\right)$, by substituting Eqns. (181) and (182) into this expression, the following results:

$\theta_{Pt} = \dfrac{1}{1 + K_{O_2}^{1/2} p_{O_2}^{1/2}}$	(191)

The RDS will now be hydrogen adsorption on the surface via Eqn. (183), resulting in the following global rate expression:

$R_{H_2} = \dfrac{k_b p_{H_2}}{\left(1 + K_{O_2}^{1/2} p_{O_2}^{1/2}\right)^2}$	(Hy-RDS-*b*)

At lower temperatures before light off, either global mechanism is valid depending upon the hydrogen concentration. However, after light off occurs, mass transfer to the surface becomes the rate determining step and, as a result, hydrogen adsorption becomes the RDS. This is because oxygen mass transfer is not an issue since it has a relatively high desorption temperature (> 900K) and a low adsorption temperatures (> 90K).

Research indicates that hydrogen oxidation follows a slightly different trend as that of CO oxidation [204]. When CO is in excess, it inhibits oxygen adsorption on the surface and thus oxygen adsorption becomes the RDS. However, for hydrogen oxidation, oxygen has higher sticking coefficient than hydrogen and oxygen acts as the inhibitor rather than hydrogen. Therefore, when oxygen is in excess hydrogen adsorption then becomes the RDS. When neither is in excess, the L-H step for conversion is the RDS for both hydrogen and CO oxidation. Therefore, hydrogen oxidation closely resembles CO oxidation and that is a reason why past researchers use the same reaction rate expressions for both.

The Equation labeled as "Hy-RDS" are the global reaction rate expression that should be used while modeling the hydrogen oxidation on platinum and platinum/alumina catalysts. Although the same Equation will be used for different platinum catalysts, the values of pre-

exponential factor, activation energy, enthalpies will change with dispersion, catalyst preparation, particle diameter, etc.

3.3 Review of Detailed and Global Reaction Mechanism for NO Oxidation on Platinum and Platinum/Alumina Catalysts:

Current and future emission regulations for nitrogen oxide (NO_x) emissions are particularly challenging for Compression Ignition (CI) or diesel engines. For a Spark Ignition (SI) engine, carbon monoxide (CO), hydrogen (H_2) and hydrocarbons (HC) exist in sufficient quantity to reduce NO_x emissions from the engine over a Platinum Group Metal (PGM) catalyst. However, the exhaust of CI engines contains mainly oxygen (O_2) and nitrogen monoxide (NO) without any other species in adequate amounts to act as a reductant. Since NO_x decomposition catalysts are not readily available, a continual conversion of NO_x over a catalytic aftertreatment device is not possible. As a result, the commercial vehicle industry is investigating a different device, the Lean NO_x Trap (LNT), to handle NO_x conversion.

There are two distinct phases of LNT operation: lean and rich. In the lean phase, the engine out NO_x is stored on an alkali or alkali earth metal. After a certain amount of storage time, a periodic rich charge approximating SI exhaust is sent to the catalyst to chemically release the NO_x. This rich charge, along with the released NO_x, is then reduced by PGM on the catalyst in a manner similar to a Three-Way Catalyst (TWC) for SI engines. One possible method for producing this rich mixture is by using a late injection timing in-cylinder while the exhaust valve is open. Another common method for achieving this rich charge is by injecting fuel directly into the exhaust downstream of the engine cylinder; i.e. post-cylinder fuel injection.

Since the majority of NO_x emitted from lean-burning engines is in the form of NO, this presents a problem for LNT operation as they prefer NO_2 for storage. Typically, only 10-30% of the nitrogen oxides emitted by a CI engine are the chemical species NO_2 [205]. To compensate, LNTs typically include a PGM to promote the oxidation of NO to NO_2. As a result, any LNT modeling activities must include an accurate reaction rate expression for NO oxidation in order to simulate the lean storage phase.

3.3.1 REACTION HISTORY FOR NO OXIDATION OVER PLATINUM/ALUMINA:

In 1989, Cooper and Thoss are among the first to investigate NO oxidation on a platinum catalyst [206]. They claim that platinum converts 70% of the NO to nitrogen dioxide through oxidation at 573K when the inlet mixture includes NO, oxygen, water and nitrogen. Above this temperature, NO oxidation is thermodynamically limited and they observe a conversion close to the equilibrium limit. The addition of other exhaust gas constituents like carbon monoxide, carbon dioxide and sulphur dioxide does reduce the maximum conversion to 58% at 623K. From their research, they propose the following NO oxidation global reaction:

$NO + 0.5O_2 \underset{k_{-192}}{\overset{k_{192}}{\rightleftharpoons}} NO_2$	(192)

In order to obtain this result, they postulate a Langmuir Hinshelwood (L-H) reaction mechanism through Eqn. (117) and the following steps:

$NO + Pt \underset{k_{-193}}{\overset{k_{193}}{\rightleftharpoons}} Pt \cdot NO$	(193)
$Pt \cdot NO + Pt \cdot O \xrightarrow{k_{194}} Pt \cdot NO_2 + Pt$	(194)

The reaction rate order for NO is determined equal to 0.5 and that with respect to oxygen is 0.22. They postulate that the Rate Determining Step (RDS) for NO oxidation is the reaction between adsorbed oxygen and adsorbed NO via Eqn. (194). In the presence of other

reactants like CO, CO_2 and SO_2, they ascertain the reaction order of NO to be greater than one, which implies that a side reaction can occur as follows:

$2\mathrm{Pt}\cdot\mathrm{NO}\xrightarrow{k_{195}}\mathrm{Pt}\cdot\mathrm{NO}_2+\frac{1}{2}\mathrm{N}_2$	(195)

This reaction happens because CO reacts with adsorbed oxygen, freeing a Pt site allowing two NO molecules to adsorb in the vicinity and react. Based on their efforts, they formulate a global reaction rate Equation:

$R=k_4 C_{\mathrm{NO}}^{0.5} C_{\mathrm{O}_2}^{0.22}$	(G16)

In 1993, Ambs and McClure claim that oxidation catalysts (OC) increase nitrogen dioxide in automotive exhaust through the oxidation of NO on the surface [207]. They observe a maximum NO conversion on a monometallic oxidation catalyst around 648K, while above 550K the concentration of nitrogen dioxide leaving the catalyst is greater than the inflow. However, they find in modern bimetallic catalysts, the conversion of NO to nitrogen dioxide only occurs above 648K. Below this temperature, nitrogen dioxide instead reduces to NO. They observe that the conversion of NO to NO_2 on the oxidation catalyst does not yield a one to one molar ratio. Instead, they see the consumption of more NO than the amount of NO_2 formed. They provide no explanation and instead conclude simply that the reaction follows a more complex route than Eqn. (192). In addition, when the residence time increases, additional NO conversion occurs.

In the same year, Loof et al. investigate catalyst sintering in various oxidizing and reducing atmospheres in the temperature range of 473 to 973K for Pt/alumina catalysts [208]. They find that the sintering influence of NO is much higher than that of oxygen with NO triggering sintering even at 473K. This in turn decreases the dispersion of platinum with its effect more pronounced as the temperature increases. They postulate that molecular NO

adsorption on oxidized platinum particles is responsible for the sintering effect with its influence larger for pre-oxidized catalysts as compared to pre-reduced catalysts.

In 1995, Majewski et al. claim that precious metal catalysts act to convert NO to NO_2 [209]. They state that the importance of NO_2 deserves special attention as it exhibits high chemical activity in NO_x catalysis. Their experiments involve two different catalytic materials, platinum and palladium, in the temperature range of 423 to 773K. Their results indicate that platinum catalysts promote the oxidation of nitric oxide to nitrogen dioxide as per Eqn. (192). In particular, NO oxidation begins at 523K and reaches a maximum between 633 and 653K. They find that NO oxidation is thermodynamically limited and after 653K it reaches equilibrium where NO_2 production becomes stable. This means that the computation of product concentrations follows the equilibrium constant, which is only dependent on the temperature. They perform various calculations via Eqn. (192) in order to determine the equilibrium constant in the temperature range of 423 to 773K. At temperatures below 473K, the equilibrium concentration of NO is nearly zero and therefore all NO can convert to nitrogen dioxide. As the temperature increases, the equilibrium concentration of NO increases and conversion decreases. They observe that below 523K, the outlet concentration of NO is greater than its inlet concentration, although the difference is small. Hence, the outlet values of nitrogen dioxide are less than its inlet concentration indicating that a reduction reaction is happening over the catalyst. Thus, below 523K, platinum actually reduces nitrogen dioxide and the nitrogen oxides on the surface follow other reactions in deference to NO oxidation.

The global reaction for NO oxidation illustrates that one mole of NO should convert into one mole of nitrogen dioxide. However, Majewski et al. do not observe this to be the

case for a platinum catalyst. Between 623 and 673K, about seven moles of NO disappear for the generation of each mole of nitrogen dioxide. This dictates that the platinum catalyst is net NO_x remover above 523K with maximum conversion at 653K. At temperatures below 523K, platinum has a reverse tendency of converting nitrogen dioxide to NO. Furthermore, they discuss that nitrous oxide (N_2O) and ammonia (NH_3) are also present, but in low concentrations and therefore they neglect these formation reactions. They show that NO and nitrogen dioxide reacts with hydrocarbons and carbon monoxide to form nitrogen gas. Moreover, they calculate the equilibrium constant of various reactions and find that the formation of NO from nitrogen and oxygen molecules is not possible in the exhaust temperature range (assumed less than 800K). The decomposition of NO into nitrogen and oxygen is nearly zero below 973K and, therefore, NO is a stable compound in the automotive exhaust gas temperature range. However, the disproportion reaction regarding the conversion of NO to nitrogen dioxide via Eqn. (195) has a large thermodynamic possibility and is therefore possible. This itself cannot explain the seven times decrease in NO for formation of nitrogen dioxide. It is important to understand that their efforts include hydrocarbon in inlet gases along with NO and oxygen, which is not directly applicable to the review. Future efforts including the influence of other gases will consider this finding.

They find that there is large reduction in NO concentration when forming nitrogen dioxide. They postulate that this may be due to subsequent reaction of nitrogen dioxide with hydrocarbons and CO to form nitrogen. Their efforts illustrate that NO_2 has a larger oxidative power than NO and formation of NO_2 is pre-cursor step in NO_x reduction catalysts. However, they do not specify the path of NO formation from nitrogen dioxide at low

temperatures, since the amount of NO generated was higher than the amount of nitrogen dioxide consumed.

In 1996, Hepburn et al. propose that the NO oxidation reaction follows an L-H kinetic mechanism while providing the following rate expressions for the forward and reverse reactions of Eqn. (192) [210].

$R_f = \frac{k_1 K_{NO} K_{O_2}^{0.5} S_{Pt}^2 C_{NO} C_{O_2}^{0.5}}{\left(1 + K_{NO} C_{NO} + K_{O_2}^{0.5} C_{O_2}^{0.5} + K_{NO_2} C_{NO_2}\right)^2}$	(G17)
$R_r = \frac{k_{-1} K_{NO_2} S_{Pt}^2 C_{NO_2}}{\left(1 + K_{NO} C_{NO} + K_{O_2}^{0.5} C_{O_2}^{0.5} + K_{NO_2} C_{NO_2}\right)^2}$	(G18)

In a LNT, alkali or alkaline earth metals are present along with the platinum or other oxidation catalytic material. The NO_2 generated after NO oxidation reacts with this material in order to form a nitrate species. This lowers the NO_2 concentration and promotes the oxidation reaction in forward direction with a subsequent increase of NO conversion into nitrogen dioxide. They find that a high platinum loading on the surface increases the rate of NO oxidation. Furthermore, they suggest an inhibition influence of sulfur present in the fuel on NO oxidation and storage.

In the same year, Xue et al. summarize the importance of the metal support on the NO oxidation reaction [211]. They find that Pt/SiO_2 has the highest conversion capability of NO and reaches equilibrium at 673K. A Pt/Al_2O_3 catalyst is slightly less active and platinum containing catalysts show a much higher activity as compared to those just containing the corresponding support material further implying that platinum is the active phase for the reactions. As platinum loading increases on a platinum/alumina catalyst, the reaction rate of NO oxidation also increases. In addition, the turnover frequency of NO increases slightly as the size of the platinum particle increases.

Furthermore, they study NO desorption on both Pt/Al_2O_3 and Al_2O_3 only catalysts and find that desorption of NO is rather complicated. Their experiments show multiple desorption peaks over the entire temperature range of 273 to 773K. The platinum containing catalysts indicate desorption at similar temperatures, but with a slightly lower intensity as compared to alumina support alone. Investigation on nitrogen dioxide gives a similar trend of desorption for each catalyst. This demonstrates that the alumina support governs the desorption characteristic even for the platinum loaded samples. Moreover, the adsorption of NO and NO_2 is stronger on alumina as compared to the SiO_2 support. In the case of platinum/alumina catalysts, the influence of support on the reaction rate is larger as they state that NO most likely adsorbs primarily on the support and then migrates to the platinum sites.

In next year, Burch and Watling propose an Eley Rideal (E-R) reaction mechanism for conversion of NO with hydrocarbons [212]. They assume that nitrogen dioxide pre-adsorbs on the platinum surface and then reacts with hydrocarbons through a gas-phase reaction:

$Pt \cdot O + NO \xrightarrow{k_{196}} Pt \cdot NO_2$	(196)
$Pt \cdot NO_2 \xrightarrow{k_{197}} Pt \cdot O + NO$	(197)

These reactions are much faster than any other reaction of NO or NO_2 in order to create nitrogen or N_2O. They also propose that NO can dissociate on vacant platinum site as follows:

$Pt \cdot NO + Pt \xrightarrow{k_{198}} Pt \cdot O + Pt \cdot N$	(198)

They suggest that this reaction is not preferred on the metal surface. Moreover, as the concentration of oxygen increases resulting in a high surface coverage of oxygen, the lack of available platinum sites inhibits NO dissociation. This reaction is preferred at high temperatures while at low temperatures, NO is molecularly adsorbed on platinum.

In the same year, Fritz and Pitchon indicate that the rate of NO dissociation is temperature dependent [213]. At lower temperatures, NO adsorbs molecularly and only a fraction of it dissociates on the surface. NO can recombine with a nitrogen atom to form N_2O via the following reaction:

$Pt \cdot NO + Pt \cdot N \xrightarrow{k_{199}} Pt \cdot N_2O$	(199)

However, as the temperature increases, NO dissociation increases and N_2O formation is no longer a preferred reaction as reported by Burch et al. [212]. Instead, two adsorbed nitrogen atoms will react to form nitrogen gas, but the selectivity of this happening on platinum/alumina is low in presence of oxygen:

$Pt \cdot N + Pt \cdot N \xrightarrow{k_{200}} Pt \cdot N_2$	(200)

In 1998, Burch et al. suggest that the rate of NO oxidation is large enough that a pseudo-equilibrium is established between NO and nitrogen dioxide [214]. They find that the oxidation of NO to NO_2 increases with NO concentration and that conversion starts around 413K and improves with temperature. In addition, their experiments demonstrate that an increase in oxygen concentration also acts to increase NO oxidation reaching a peak at 613K supporting Majewski et al.'s earlier finding. They reinforce their previous claim [212] that NO oxidation happens as per an E-R Mechanism through Eqns. (117) and (196) with NO_2 decomposition occurring via Eqn. (197). Moreover, they state that a high oxygen concentration inhibits NO dissociation, while low concentrations lead to NO dissociation supporting earlier declarations [212-213]. Further continuing their work in the same year, Burch et al. assert that NO adsorption over platinum increases in the presence of oxygen while validating their previous efforts [215].

In the same year, Wang and Yeh look into the formation of platinum oxide in the presence of oxygen over a platinum/alumina catalyst [216]. Oxygen adsorbs atomically at temperatures above 160K and desorbs at temperatures above 650K. Moreover, oxygen adsorption on platinum is structure sensitive and its adsorption increases with an increase in dispersion. With respect to surface platinum oxides, they form above 300K with a further penetration inside the platinum structure occurring above 800K. Below this temperature, a protective surface layer of platinum oxide materializes that inhibits surface penetration of atomic oxygen. As dispersion decreases, desorption temperature for oxygen decreases as the adhesive interaction bond strength between oxygen and platinum decreases. They prove this statement by determining that the evolved heat of adsorption increases as dispersion increases.

Concurrently, Fridell et al. confirm that maximum NO oxidation happens at 648K [217]. They propose that NO oxidation transpires as per an L-H reaction mechanism via Eqns. (193), (117) and (194). In the temperature range of 523 to 673K, NO and NO_2 are in a quasi-equilibrium state. Their efforts demonstrate that the desorption temperature of NO and NO_2 is 673K on an oxidized surface and above this temperature there is no storage of nitrogen compounds on the catalyst. This dictates that the binding of NO is weaker on an oxygen-covered surface. However, on pre-reduced surface, NO mostly desorbs as N_2 and N_2O following Eqns. (199) and (200). In the said temperature range, when stopping the oxygen flow metal sites become open for dissociation of NO which gives rise to these species. Following this effort, Lee and Kung claim that NO oxidation is higher at low platinum dispersions (4.4%) and low on high platinum dispersions (82%) [218]. In addition, the oxidation rate of NO is relatively high at low temperatures. They indicate that the rate of desorption of

NO may be structure sensitive and there is strong influence of platinum dispersion on NO oxidation. They indicate that the reduction of NO to nitrous oxide and nitrogen does not depend on oxidation of NO and is not a necessary step in the mechanism. Moreover, the reduction of NO is not structure sensitive but instead depends on other gas constituents.

In the year 1999, Mahzoul et al. find that NO adsorption on a pre-reduced catalyst is twice that of normal catalyst [219]. They describe the presence of two types of platinum sites; one near a barium particle and other a distance away. They claim that on the platinum sites away from BaO sites for an LNT, adsorbed NO and adsorbed oxygen atom react to form nitrogen dioxide. Thus, they propose an L-H reaction mechanism for NO oxidation as per reaction Eqns. (193), (117) and (194). Platinum sites near BaO directly convert adsorbed NO and adsorbed oxygen atoms into a nitrate chemisorbed on barium. In addition, a higher Ba content and/or platinum amount increases the storage capacity of the catalysts. They further support earlier findings that maximum NO conversion happens at 623K and at temperatures higher than this, the conversion becomes equilibrium limited.

Further continuing the study, Olsson et al. investigate NO oxidation in the temperature range of 523 to 723K at atmospheric pressure [148]. They consider the alumina support inert in said temperature range, which differs from previous observations [211]. They postulate the kinetic model for NO oxidation through Eqns. (193), (117), (196) and (197) while including two additional reactions:

$NO_2 + Pt \underset{k_{-201}}{\overset{k_{201}}{\rightleftarrows}} Pt \cdot NO_2$	(201)
$Pt \cdot NO_2 + Pt \xrightarrow{k_{202}} Pt \cdot NO + Pt \cdot O$	(202)

This mechanism assumes that NO oxidation follows both L-H and E-R mechanistic steps. However, since NO oxidation does not self-poison via high oxygen coverage, the E-R

mechanism is favored. This reaction becomes the RDS for NO oxidation in both the kinetic and thermodynamic limiting regions with 623K being the set point between the two. In addition, they state that the activation energy for NO_2 adsorption is equal to zero as NO_2 adsorbs easily at low temperatures. Their efforts include an investigation into oxygen adsorption and desorption through Temperature Programmed Desorption (TPD) with oxygen beginning to desorb from the surface around 573K. For their mechanism, they provide reaction rate coefficients for all of the detailed reactions.

In the same year, Schneider et al. supported Loof et al.'s research by indicating that NO causes considerable sintering of pre-reduced platinum catalysts above 473K, whereas the effect is not significant on pre-oxidized catalysts [220]. NO decomposition occurs only above 573K on reduced catalysts, while it remains molecularly adsorbed on oxidized platinum catalysts. In addition, oxygen atoms produced during decomposition further inhibit continued decomposition. This is important in this review as it reduces the mechanistic possibility through Eqns. (199) and (200).

In 2000, Denton et al. support the claim of Lee and Kung [218] in illustrating that NO oxidation increases as dispersion decreases from 80% to 4% on a meso-alumina support [221]. In addition, they find that NO dissociation increases with larger particle sizes while also determining that the nature of the support material does not significantly influence the reaction rate. Below 508K, reduction of NO into nitrogen and nitrous oxide occurs at a conversion rate of 25% and 47% respectively. Above this temperature, their data demonstrates a preference for NO oxidation. It is important to note that their experiments contain propene gas as a reactant. Hence, this review references these important results but cannot conclude significantly based on their findings.

In the same year, Seker and Gulari suggest that NO is oxidized to NO_2 at significant rates above 423K and reaches equilibrium around 573K [222]. On the high temperature side, reduced oxygen concentrations promote NO oxidation to NO_2 and the rate of oxygen adsorption increases faster than rate of NO adsorption with an increase in temperature. At lower temperatures, the availability of the metallic surface sites limits the rate of NO decomposition. In addition, they support earlier efforts by stating that as the surface coverage of oxygen increases, NO dissociation decreases and is structure sensitive. Similar to the work of Denton et al., Seker and Gulari add propene to the reactants along with NO, oxygen, nitrogen dioxide and water. Moreover, they use δ-alumina as the support; therefore, for completeness this review references this paper without drawing any definitive conclusions.

In the next year, Bourane et al. explore the adsorption of NO in the temperature range of 300 to 600K [223]. They claim that NO dissociates above 400K and the oxidation reaction happens as per an E-R mechanism through Eqns. (117) and (196). As a result, if any NO dissociates, adsorbed oxygen formed in NO dissociation can react with NO in order to form nitrogen dioxide. They conclude that this is the reason why pre-adsorbed oxygen does not influence the amount of NO adsorbed on the surface.

Further continuing their work in 2001, Olsson et al. propose a model for NO oxidation and NO_x storage on Pt/Al_2O_3 and $Pt/BaO/Al_2O_3$ [224]. They indicate that dissociative oxygen adsorption is the first step for NO oxidation as per Eqn. (117). Following Eqns. (193), (117), (196) and (197), three different kinetic models are proposed (L-H, E-R and a combination approach) with parameters obtained from calibration with experimental data. They determine that both NO (0.9) and NO_2 (0.97) have relatively high sticking coefficients

and neglect the activation energy of adsorption for both of these species. Findings indicate that the activation energy of NO_2 adsorption decreases if absorbed oxygen is already present on the surface. In addition, the activation energy of adsorption for both NO and nitrogen dioxide can be neglected and taken as zero since they calculate it to be less than 2 kcal/mol. All three models have the same standard deviation and therefore they do not reach a consensus as to the preferred option. However, since NO_2 decomposition requires two platinum sites, they choose the L-H mechanism over the other models contradicting their previous paper in 1999 [148], which specifies an E-R mechanism for NO oxidation.

Their findings indicate that at low temperatures (<550 K), NO_2 decomposition is slower than NO oxidation and they propose two mechanisms in order to explain this low decomposition capacity. The first mechanism assumes that when nitrogen dioxide decomposes, it leaves oxygen on the surface leading to oxygen poisoning. Since nitrogen dioxide requires two adjacent vacant sites for dissociation [225], oxygen poisoning decreases reduction of nitrogen dioxide. The second mechanism presumes that both nitrogen dioxide and oxygen atom block the surface. When NO_2 dissociates, it leaves adsorbed atomic oxygen on the surface, leading to an oxygen poisoning effect. The second mechanism proposed results in a low activation energy and low pre-exponential factor. However, the change in entropy is unrealistic for this model and this is why they choose the first mechanism. For an experiment performed in the range of 523 to 723K, the L-H model predicts a high oxygen coverage and relatively slow nitrogen dioxide decomposition. Oxygen adsorption does not occur in the temperature range of 313 to 473K, but above 573K it starts to become active. Therefore, above this temperature the surface coverage of oxygen increases as it possesses enough energy to overcome the activation energy barrier for

adsorption. The RDS in the L-H mechanism for NO_2 reduction to NO is oxygen desorption. In addition, the capacity of reducing nitrogen dioxide to NO is low and attributed to oxygen poisoning of the surface.

In the same year, Prinetto et al. report the weak adsorption of NO over the surface [226]. However, if oxygen accompanies NO in the feed stream, adsorption significantly increases. They find that NO_2 has the highest adsorption value among the three options: NO, NO+O_2 and NO_2. Concurrently, Westerberg and Fridell report the interaction of NO+O_2 and NO_2+O_2 with alumina and Pt/alumina in the temperature range of 373 to 673K [30]. They confirm that NO oxidizes to NO_2 above 423K while also finding that alumina is an important storage site at temperatures below 573 K.

In 2002, Olsson and Fridell confirm that the platinum particle size influences the NO oxidation rate [227]. Their efforts illustrate that when dispersion decreases, the platinum particle size increases enhancing the oxidation mechanism. In addition, the dissociation of nitrogen dioxide decreases with time between the 573 and 673K temperature range due to adsorbed oxygen on the surface and particle size promoted NO oxidation. However, at low temperatures, the dissociation of nitrogen dioxide is slow as there is a low amount of oxygen desorbing from the surface which supports their earlier effort [224]. At temperatures higher than 673K, the thermodynamic impact of equilibrium influences the reaction and there is an additional decrease in activity due to loss in the number of active sites at higher temperatures. They find that conversion of NO_2 to NO is low for high dispersion catalysts and as dispersion decreases, a corresponding increase in conversion is found. In addition, their efforts demonstrate an increase in NO oxidation when dispersion decreases. Hence, as a catalyst sinters, NO oxidation increases. Moreover, NO oxidation follows a kinetic path at low

temperature. Both of these findings lead to a higher conversion of NO at low temperatures on a lower dispersed platinum catalyst. However, the deactivation of the platinum surface is relatively fast at low temperatures as compared to high temperatures. They find that along with NO_2, oxygen additionally acts to deactivate the platinum surface and as its concentration increases, it adsorbs more readily on the surface. Experiments show that oxygen desorption begins at 573K and reaches a peak at 723K and they attribute any decrease in platinum activity during this time to the formation of platinum oxide ($Pt{\cdot}O$ and $Pt{\cdot}O_2$) on the surface which is less active then metallic platinum. They attribute the effect of dispersion to particle size as smaller particles form more platinum oxide, which is less active and results in a lower oxidation rate of NO or dissociation of nitrogen dioxide.

In 2004, Crocoll and Weisweiler model NO oxidation through an E-R mechanism as per Eqns. (193), (117), (196), (197) and (201) [228]. Concurrently, in Epling et al.'s review paper they confirm that NO oxidation is thermodynamically limited at high temperatures and kinetically limited at low temperatures with the maximum NO conversion occurring in the range of 583 to 635K [229]. They find that at a temperature of 623K, equilibrium has still yet to happen along the catalyst length. Even at 673K, their efforts show that the first two thirds of the catalyst length are kinetically limited and equilibrium only takes place in the last one-third. In addition, they confirm that NO oxidation depends on platinum particle size and dispersion. The higher the dispersion value, the smaller the platinum particle size and the lower the conversion. Sintering impacts this condition by decreasing dispersion, this subsequently increases NO oxidation. They support the efforts of Olsson et al. [227] in stating that NO oxidation occurs per a L-H reaction mechanism with the RDS equal to the oxygen desorption from the surface. However, they maintain that there still is not a conclusive result

as both the E-R and L-H reaction models work equally well for NO oxidation. Since adsorbed oxygen is also present on the surface due to dissociation of nitrogen dioxide, it inhibits the reaction mechanism. In addition, the amount of platinum, dispersion and choice of support material is important for NO oxidation. NO oxidation only happens in the presence of platinum and without this metal; the support alone cannot provide any conversion capacity. They conclude that enhanced platinum oxidation occurs with an increase in particle size; thus, when platinum sinters, NO oxidation initially increases before reaching a maximum and then decreases due to a subsequent loss of available sites. One possible reason for low oxidation at high dispersion is through the easier formation of platinum oxide on the smaller sized platinum particles. As described previously, platinum oxides are less effective at oxidation as compared to free platinum metal sites. They conclude that the reaction is first order with respect to NO and oxygen. In the same year, Kabin et al. indicate an enhanced NO oxidation with an increase in residence time (e.g. low space velocity) while demonstrating that conversion approaches the equilibrium limit at 648K [230].

In 2005, Mulla et al. claim that nitrogen dioxide inhibits its own formation from NO oxidation and therefore it needs to be included in the kinetic model for NO oxidation [231]. Their efforts result in the following reaction rate expression in power rate law form:

$R = k_f [\mathrm{NO}]^a [\mathrm{O_2}]^b [\mathrm{NO_2}]^c (1-\eta)$	(G19)

where k_f is the forward rate constant, a, b and c are the reaction orders and η is the approach to equilibrium given by:

$\eta = \dfrac{[\mathrm{NO_2}]}{K_{eq}[\mathrm{NO}][\mathrm{O_2}]^{1/2}}$	

with K_{eq} equal to the equilibrium constant and values of η in the experiment conducted were in the range of 0.02 to 0.14, which indicates that the reaction is carried far from equilibrium.

They determine that the rate of NO oxidation is nearly first order with respect to NO and O_2 and negative first order with respect to NO_2. Hence, we can predict the values of *a*, *b* and *c* as 1, 1 and -1 respectively. In addition, they describe the forward reaction rate as:

$$R_f = A\exp\left(\frac{-E_a}{R_u T}\right)\frac{[NO][O_2]}{[NO_2]} \quad \text{(G20)}$$

When NO_2 is not present, the activation energy in this expression is half the value of the associated value when NO_2 is present. In addition, similar to past researchers, they find that larger platinum particle sizes exhibit a higher activity than smaller particles. Therefore, they state that the activation energy may change with particle size while also claiming that such an observation has not been reported in literature to date. They attribute nitrogen dioxide inhibition to the fact that it adsorbs preferentially on platinum as compared to NO. Hence, it maintains surface oxidation preventing conversion of the NO species. Thus, they reason that a large extent of the surface, oxidation comes from nitrogen dioxide decomposition reaction rather than from the dissociative adsorption of oxygen. They additionally support that NO oxidation happens as per an L-H reaction mechanism via Eqns. (193), (194), and (202) but include (108) and (109). They assume step (108) is the RDS, resulting in the following reaction rate expression:

$$R = \frac{k_{14}[L][O_2]}{1+\frac{K_{13}[NO_2]}{K_9[NO]}} \quad \text{(G21)}$$

where [*L*] denotes the total surface concentration of metal sites and $K_9 = k_{199}/k_{201}$.

In the same year, Benard et al. confirm a number of trends found by past researchers [232]. In particular, NO oxidation increases with temperature, reaches a peak and then decreases due to thermodynamic limitations. They further support that NO oxidation increases with a decrease in platinum dispersion and subsequent increase in platinum particle size. They find that as platinum particle size increases, NO oxidation begins at a lower temperature. Additionally, this larger particle size has a strong Pt·NO bond favoring NO dissociation. This large particle size leads to lower desorption temperatures for oxygen due to weak Pt·O bonds. Apart from particle size, high BET area of the support favors NO oxidation. They explain a high platinum activity for large particle sizes by a relatively low amount of platinum oxide formation. These results cause Bernard et al. to conclude that NO oxidation happens via an L-H mechanism. Their efforts also illustrate that the alumina supports plays an important role. NO adsorbs on alumina and then migrates towards platinum in order to react with oxygen. This is important for oxidation as adsorption of NO on platinum is presence of oxygen is very low. Hence, the support provides a second avenue for NO adsorption and facilitation of the reaction.

Concurrently, Crocoll et al. investigate the NO oxidation reaction under oxygen rich conditions [233]. They observe that the conversion of NO increases across all temperatures investigated (423 to 773K) as the concentration of oxygen increases up to certain point, confirming previous results. They find that NO adsorbs at room temperature and begins to desorb at 473K, while nitrogen dioxide shows no tendency to adsorb at room temperature. They state that the NO oxidation reaction follows Eqns. (193), (117), (196), (197) and (201) in an E-R manner. While proposing a detailed kinetic model, they neglect the activation energy for adsorption of all gaseous species, which follows a common literature postulation.

At the same time, Olsson et al. suggest a model for NO oxidation while simulating LNT devices [234]. They propose that NO oxidation is the RDS with the following rate expression given:

$$R_f = k_4 C_{NO} C_{O_2}^{1/2} - \frac{k_4}{K_4} C_{NO_2} \quad \text{(G22)}$$

where $K_4 = k_4/k_{12}$.

In 2006, Mulla et al. develop a new rate expression for the reaction [235].

$$R_f = A \exp\left(\frac{-E_a}{R_u T}\right) [NO]^{\alpha} [O_2]^{\delta} [NO_2]^{\gamma} \quad \text{(G23)}$$

where α, δ and γ are the reaction orders. They express a first order dependence for NO and O_2 and negative first order dependence on NO_2. Their efforts involve an investigation into NO oxidation on two types of catalysts, one sintered by pre-treatment and the other fresh. They illustrate that the impact of different species on NO oxidation does not change with temperature and remains consistent over the entire temperature range for both catalysts. In addition, they find that NO oxidation has same dependency on its products and reactants over sintered catalysts with nitrogen dioxide inhibiting the oxidation reaction. They do find that the power with respect to oxygen decreases to around 0.7 on the sintered catalyst; however, the there is no significant change to the activation energy. Moreover, NO oxidation has a significant turnover ratio on the sintered catalyst because of the larger platinum particle sizes. This further confirms that platinum particle size influences NO oxidation and its rate increases with particle size.

Their efforts demonstrate the deactivation for both fresh and sintered catalysts with a reduced oxidation activity. Deactivation is independent of reaction temperature and concentration of species; however, it is completely reversible in a reducing atmosphere demonstrating that it may be due to the oxidation of the platinum surface. One significant

difference indicated here with respect to previous reports is that deactivation does not occur while the catalyst is in its working phase. Instead, deactivation proceeds when the catalyst cools after normal operation. This work supports their previous claim that NO oxidation transpires as per an L-H reaction method with Eqn. (108) as the RDS. In addition, they support Eqn. (G22) as the global reaction rate Equation for NO oxidation. Moreover, this validates their previous result of the impact of platinum particle size on NO oxidation, as the turnover rate for NO oxidation is higher for a sintered catalyst as compared to a fresh catalyst. This is because a larger platinum particle is more difficult to oxidize. Moreover, they support the idea that nitrogen dioxide dissociation results in the oxidation of platinum particles further deactivating the catalyst. Based on XPS and CO titration, they verify that platinum oxide formation is the main reason for a decrease in NO oxidation over highly dispersed platinum surfaces.

In the same year, Schmitz et al. support earlier claims that NO oxidation is structure sensitive [236]. They find a significant increase in reaction rate as the platinum particle size increases, whether it supported by alumina or silica. As a result, they propose a pseudo-first order reaction rate in NO, given by:

$$-\nu \frac{\mathrm{d}C_{\mathrm{NO}}}{\mathrm{dV}} = k_f C_{\mathrm{NO}} \left(1 - \frac{C_{\mathrm{NO_2}}}{K_1 C_{\mathrm{NO}} C_{\mathrm{O_2}}^{1/2}} \right) \qquad \text{(G24)}$$

where ν indicates the total volumetric flow rate of the NO oxidation reaction. However, their efforts differ from previous work of Mulla et al [235] in that the activation energy of NO oxidation for different platinum loadings does not vary significantly. They verify that nitrogen dioxide does inhibit NO oxidation and its reaction rate is structure sensitive; e.g., it increases with a growth in particle size. Nevertheless, they maintain that no one has yet discovered a definitive explanation for the structure sensitivity. Through statistical analysis,

they conclude the strength of influence in NO oxidation first by support, then by pretreatment and subsequently through loading.

In next year, Hauptmann et al. compare various global reaction models proposed by Marques, Olsson and Mulla et al. [237]. To note, the Marques efforts on NO oxidation were on platinum but with a support other than alumina [238]. At low temperatures, the Marques model fits the experimental model best (368K), but at high temperatures it results in complete NO conversion, which is not possible due to thermodynamic limitations. Olsson's model, Eqn. (G22), fits the experimental result at high temperatures (596K); however, Mulla's model of Eqn. (G19) has a better accuracy for entire range of temperature conditions (368 to 596K). This model still has some discrepancies, as it does not consider catalyst deactivation. The result of this effort is a new reaction rate expression considering all models:

$$R = kC_{NO}^{\alpha} C_{O_2}^{\beta} C_{NO_2}^{\gamma} \left(1 - \frac{C_{NO_2}}{C_{NO} C_{O_2}^{1/2} K_{eq}}\right)^{\delta} \qquad \text{(G25)}$$

Hauptmann et al. were not able to justify whether the reaction follows an L-H or an E-R pathway; hence, no suffix is available for *k*. They base the inhibition effect of nitrogen dioxide on the amount of this species and the current oxidation state. However, they express that the oxidation state of platinum cannot only be a function of the amount of nitrogen dioxide and therefore set γ equal to zero. Furthermore, they fix δ equal to one and the reaction orders of NO and oxygen equal to 0.28 and 0.49 respectively. Their model is able to predict NO oxidation over the complete temperature range, but there still exists some deviation in accuracy between 425 and 450K. This deviation is due to the deactivation of catalyst that global reaction rate models cannot simulate. Instead, simulating this phenomenon is only possible via detailed modeling of the reaction surface. Nevertheless,

they still support global modeling because of its advantage of fewer parameters and reduced computational time.

In the same year, Takahashi et al. report a high NO oxidation activity for platinum as compared to palladium and rhodium [239]. They confirm previous findings of increasing NO oxidation activity with ageing catalysts and a higher rate of conversion for platinum/silica as compared to platinum/alumina. Moreover, they write the reaction rate for NO oxidation:

$$R = kC_{\mathrm{NO}}^{m} C_{\mathrm{O_2}}^{n} \exp\left(-E_a / R_u T\right) \quad \text{(G26)}$$

where *m* and *n* are the reaction orders of NO and oxygen respectively. Over a fresh catalyst, the reaction order for NO is 0.4; whereas, over an aged catalyst it is equal to 0.6 demonstrating the higher affinity towards NO as particle size increases. For oxygen, the reaction order is equal to 1.4 for both catalyst conditions.

In 2008, Kromer et al. study NO oxidation and storage while proposing a reaction expression based 1D catalyst modeling [240]. They support Mulla et al.'s [231] model of the L-H reaction mechanism for NO oxidation and assume Eqn. (108) to be the RDS with atomic oxygen the dominant surface species. This results in the development of the following reaction rate expression:

$$R = k_{13}\left(\frac{C_{\mathrm{NO}} C_{\mathrm{O_2}}}{C_{\mathrm{NO_2}}}\right) \quad \text{(G27)}$$

This result has same apparent reaction orders for NO, oxygen and nitrogen dioxide as that of Mulla et al.; e.g., one, one and -1 respectively. However, this model is only valid for the forward reaction of NO oxidation as the model deviates from equilibrium in case of NO_x storage over alkali metals. In addition, this model is valid only under the condition that the reaction is not mass transfer limited.

In 2009, Weiss and Iglesia support Eqn. (G20) as the global reaction rate expression with the rate proportional to NO and oxygen while inversely proportional to nitrogen dioxide [241]. Their detailed mechanism follows Eqns. (108) and (109) while additionally including:

$\mathrm{Pt}\cdot\mathrm{O}_2 + \mathrm{Pt}\cdot\mathrm{NO} \xrightarrow{k_{203}} \mathrm{Pt}\cdot\mathrm{O} + \mathrm{Pt} + \mathrm{NO}_2$	(203)
$\mathrm{Pt}\cdot\mathrm{O} + \mathrm{NO} \underset{k_{-204}}{\overset{k_{204}}{\rightleftharpoons}} \mathrm{Pt} + \mathrm{NO}_2$	(204)

Reaction Eqn. (204) is not an elementary step in NO oxidation, but instead a reflection of a sequence of combining quasi-equilibrium elementary steps. If adsorbed oxygen is the most abundant species on the surface, then Eqn. (108) becomes the RDS of NO oxidation and the global reaction rate is:

$R = \left(\frac{k_{14} C_{\mathrm{O}_2}}{1 + K_{19} C_{\mathrm{NO}}^{-1} C_{\mathrm{NO}_2}} \right) (1 - \mu)$	(G28)
$\mu = K_{eq}^{-1} \left[\mathrm{NO}_2\right]^2 \left[\mathrm{O}_2\right]^{-1} \left[\mathrm{NO}\right]^{-2}$	

where μ is approach to equilibrium. The surface coverage of adsorbed oxygen atoms depends on the NO_2/NO ratio instead of oxygen pressure. Moreover, they compare the forward and reverse reaction rates using an oxygen isotopic exchange rate experiment. They mention that Eqn. (203) is not required in simulating NO conversion as oxygen dissociation proceeds at a much faster rate than this reaction. In addition, oxygen dissociation does not require any other reactant like NO or CO to be present in the reactant feed as it is proceeds rapidly on platinum surface. Their efforts illustrate that the NO oxidation rate increases with cluster size due to a decrease in binding energy of adsorbed oxygen atoms in the large cluster resulting in an increase in available sites for NO oxidation. Finally, they state that nitrogen dioxide inhibits NO oxidation and researchers can minimize this effect by introducing NO_2 adsorption materials (like BaO) in the material formulation.

Meanwhile, Bhatia et al. assert that NO oxidation never reaches steady state as they find a decreasing reaction rate with time [242]. This is due to the inhibition effect of nitrogen dioxide that causes deactivation of the catalyst. Moreover, their results back earlier findings that NO oxidation increases with particle size. Tests performed with a reductive pretreatment of the catalyst demonstrate a higher conversion rate as compared to an oxidative pretreatment with NO_2. They mention that this is the result of inhibition by adsorbed nitrogen dioxide and not a function of platinum oxide formation as others have described. In addition, as inlet NO_2 concentration increases, NO conversion decreases, further suggesting the importance of nitrogen dioxide inhibition. Their L-H reaction mechanism follows Eqn. (193), (194), (201), (202), (108) and (109). At low temperatures (< 423K), adsorbed NO predominantly covers the surface, but at high temperatures, adsorbed atomic oxygen is the dominant species. While they state that NO_2 is the main inhibitor, they mention that its surface coverage is low as compared to other adsorbed species. In their mechanism, while molecular oxygen adsorption is an independent step, they do not observe any molecular oxygen on platinum sites. By performing a parametric sensitivity analysis on all the four Equations, they conclude that oxygen adsorption and desorption has the largest influence on the NO oxidation rate; hence, Eqn. (108) becomes the RDS. The other reactions are in equilibrium and they obtain the following reaction rate:

$$R = k_{13} C_{O_2} \left[1 - \frac{1}{C_{O_2} K_{13} K_{14}} \left(\frac{K_{11} C_{NO_2}}{K_4 K_2 C_{NO}} \right)^2 \right] \theta_v \qquad \text{(G29)}$$

where

$$\theta_v = \frac{1}{1 + K_2 C_{NO} + K_{11} C_{NO_2} + \frac{K_{11} C_{NO_2}}{K_4 K_2 C_{NO}} + \frac{1}{K_{14}} \left(\frac{K_{11} C_{NO_2}}{K_4 K_2 C_{NO}} \right)^2} \qquad \text{(205)}$$

and $K_4 = k_4 / k_{12}$. They further neglect the surface coverage of adsorbed nitrogen dioxide and adsorbed oxygen as it is negligible as compared to atomic oxygen and NO. Through this assumption, they find

$$\theta_v = \frac{1}{1 + K_2 C_{NO} + \frac{K_{11} C_{NO_2}}{K_4 K_2 C_{NO}}} \quad (206)$$

Their paper contains further derivation of global kinetics model based on different RDS, but they reject all other possibilities citing differences between experimental and simulated results.

In the same year, Hauptmann et al. investigate NO oxidation in both upward and downward temperature ramps at the rate of 5 degree Celsius per minute [243]. They conclude that conversion is higher during positive ramps then during negative ramps, which is different from other oxidation reactions (like CO oxidation) in which conversion is higher during the downward experiment. By repeating the cycle without any pretreatment of the catalyst, the conversion during this second ramp closely follows the conversion during first ramp in both positive and negative directions. They mention that there are several reasons for the hysteresis of the oxidation reaction on the catalyst. The first reason involves the thermal inertia of the catalyst. During heat up, the average catalyst temperature is behind inlet temperature, while during cooling, average catalyst temperature is ahead of inlet temperatures. In addition, in the case of exothermic reactions, the heat given off sustains the reaction even at inlet temperatures below the ignition or light-off point. Although this works in favor of CO oxidation, it cannot explain the found NO oxidation hysteresis.

One potential explanation for the inverse hysteresis is through platinum oxide formation. Higher temperatures promote the oxidation of platinum by nitrogen dioxide and

oxygen in order to form a less active platinum oxide surface. However, at lower temperatures, reduction of platinum occurs back into its native metal state. They explain that although the presence of nitrogen dioxide decreases the activity of the catalyst, NO can actually increase the platinum activity by reducing the platinum oxide on the surface. This can offset the deactivation of the catalyst by nitrogen dioxide, but this cannot reverse the impact completely as nitrogen dioxide has strong oxidation potential as compared to NO reduction. They support their claim that platinum oxide formation is the reason for inverse hysteresis, by performing partial cooling and reheating ramps. In this experiment, conversion follows the same pathway as with the initial heating ramp. However, during the cooling ramp, they do not allow the catalyst to cool back to the starting temperature before reheating. They find a considerable reduction in NO conversion during the second heating as complete reduction of platinum oxides sites does not occur. The catalyst activity is still higher than the original experiments, which supports partial regeneration.

Their results suggest that deactivation occurs at a timescale comparable to the timescale of temperature change. In their experiment, they heat and cool their catalyst in 25 degree Celsius steps with 30 minutes of steady state operation at each temperature. Compared to transient temperature ramps, these experiments demonstrate a significant decrease in the inverse hysteresis effect. The conversion during heating is lower than the transient temperatures ramps, while conversion during cooling is highly enhanced as the catalyst has more time for reactivation. The conversion during cooling is still less than the heating ramps, although not as significant as during the transient ramps. This small hysteresis may be because 30 minutes may not be long enough to reach the steady state activity rate.

They support NO oxidation via an L-H mechanism following steps (193), (117), (194) and an additional step in order to include the hysteresis:

$Pt \cdot NO_2 \underset{k_{-207}}{\overset{k_{207}}{\rightleftarrows}} Pt \cdot O_x + NO$	(207)

Their model is able to predict the inverse hysteresis using the above reaction steps, but this cannot be taken as proof that oxide formation is the reason for the inverse hysteresis finding.

The following section separates out the history of the NO oxidation reaction according to individual platinum metals tested. This is done for completeness and in order to help understand the correct formulation of the reaction rate Equation. It is through a combination of individual metals and complete surfaces that a full understanding of the reactions happening on the surface may occur.

3.3.2 REACTION HISTORY FOR NO OXIDATION OVER PLATINUM METAL:

This section illustrates that NO oxidation is highly structure sensitive and the study of NO oxidation over platinum metals without support may not reflect the exact mechanism of the same with alumina support. However, this review provides insight into the adsorption and desorption mechanisms of NO, oxygen and nitrogen dioxide on platinum. This is useful in deriving the global reaction rate expression and understanding the reaction mechanism. While studies on NO, oxygen and nitrogen dioxide adsorption and desorption exists from the past four decades, the authors summarize literature sources that support the focus of the paper. In other words, the goal is to determine the best reaction mechanism that describes NO oxidation.

In 1980, Gland studies oxygen adsorption on Pt_{111} and Pt(S)-12(111)×(111) surfaces using various mechanisms [244]. His results demonstrate that oxygen adsorbs molecularly at

100K. Heating the surface to between 150 and 170K results in partial dissociation and desorption. Above this temperature, a complete dissociation of adsorbed molecular oxygen occurs. Hence, at room temperature, oxygen never adsorbs molecularly on the surface. It is important to note that the adsorption of oxygen in its atomic state does proceed through an adsorbed molecular precursor state with small activation energy. At high temperatures, atomic oxygen recombines and desorbs from the surface. This is important in understanding the role of oxygen adsorption and desorption for NO oxidation.

In 1981, Gorte and Schmidt investigate the decomposition of NO over Pt_{111}, Pt_{110} and Pt_{100} materials [245]. They find that NO adsorbs molecularly on Pt_{111} in the temperature range of 100 to 600K. During these conditions, less than 2% of the NO decomposes on the surface, even when carbon monoxide (CO) or oxygen is present illustrating that NO does not tend to decompose on the Pt_{111} surface. However, on Pt_{100} significant dissociation during NO adsorption and desorption is found. This subsequently leads to the release of nitrogen and oxygen gas from the surface. A small amount of N_2O also desorbs around 500K, but they find that this is less than 2% of the total nitrogen desorption. Hence, they postulate that NO is dissociatively adsorbed in the 390 to 510K temperature range. In addition, they determine that at room temperatures, NO adsorption happens molecularly on Pt_{100}. As a result, the dissociation reaction occurs in-between 300 and 390K. Moreover, if oxygen is present in the feed, it significantly inhibits NO oxidation. On Pt_{110}, they find marginal NO decomposition (about 15%) at temperatures above 450K. Their results illustrate that Pt_{100} binds NO more strongly as compared to Pt_{111} and Pt_{110} surfaces. This clearly shows that NO decomposition on surface is structure sensitive; however, if oxygen is present, it will inhibit NO dissociation on any surface type.

In 1987, Bartram et al. study the adsorption of nitrogen dioxide on Pt_{111} [225]. They find that it adsorbs molecularly at 120K and completely dissociates by 240K. Their investigation discovers that NO_2 bonds to the surface in bridge format with the nitrogen atom bonding to one platinum site and one of the oxygen atoms bonding to a neighboring platinum site. At high nitrogen dioxide coverage, this species decomposes at temperatures as low as 100K forming an adsorbed NO and adsorbed oxygen atom. However, desorption becomes competitive with dissociation at high coverage. At 285K, all of the NO_2 dissociates and around 500K all NO on the surface desorbs. The adsorption of nitrogen dioxide destroys the bond equivalence of the two N and O bonds. In a nitrogen dioxide molecule, there are two N-O bonds. The covalent sharing of two electrons from each nitrogen and oxygen form one bond with the other bond a coordinate bond created through the donation of a loan pair of electrons from nitrogen to oxygen. However, observations show that both bonds have same length and energy (phenomenon is called resonance). When nitrogen dioxide adsorbs on the surface, a disruption in this equivalence in bond length and energy occurs as one bond becomes weaker. As a result, the length of the N and O bond parallel to surface increases leading to its eventual dissociation. This demonstrates that nitrogen dioxide rarely adsorbs molecularly on the surface and modelers can neglect any surface concentration for nitrogen dioxide in the studied temperature range of 300 to 800K.

In 1989, Gohndrone and Masel further investigate NO decomposition on platinum [246]. Their results show that Pt_{111} and Pt_{110} are inactive for NO decomposition, but Pt_{411} is active at 110K and Pt_{100} and Pt_{211} are active above 400K. They support the earlier efforts of Gorte and Schmidt with respect to the Pt_{100} catalyst findings and determine that 66% of the NO adsorbed decomposes on this surface resulting in nitrogen gas. They find nearly the same

result for the Pt_{411} catalyst with 70% of NO adsorbed decomposing to form nitrogen and oxygen gas. In addition, 66% of the adsorbed NO decomposes on Pt_{211}. This again proves that NO decomposition is structure sensitive while also depending on surrounding atmosphere.

A few years later, Agrawal and Trenary study NO adsorption on defect sites of Pt_{111} [247]. Defect sites are those where there is a step in the adsorbed platinum layer, the sites are at the side/edge of the catalyst or where there is a discontinuity of the platinum surface. Their efforts illustrate that NO chemisorbs molecularly on these sites. Any adsorbed oxygen acts to block NO adsorption on platinum, further inhibiting NO dissociation. Although NO adsorbs molecularly, some dissociation is observed in the temperature range of 300 to 500K. They postulate that decomposition products such as N_2 and N_2O likely form in such a case, but they did not observe any of these species in the outflow. Their results indicate that NO adsorbs on the surface with the nitrogen atom bonding to the surface platinum site with the molecule in linear orientation. Furthermore, in 1997, Kinnersley et al. propose that NO adsorption on Pt_{111} is non-activated and adsorbs molecularly [248]. They state that NO bonds to the surface through the nitrogen atom end.

In 2003, Zhu et al. study NO adsorption and find that below 300K, NO adsorbs molecularly with nitrogen pointing towards platinum surface on Pt_{111} [249]. However, further discussion in the paper relates to temperatures below 300K, out of the scope of the studied range for automotive exhaust catalysis. The following year, Mei et al. build on these results through their investigation of NO decomposition on platinum (Pt_{100}) and rhodium sites (Rh_{100}) [250]. They show that NO dissociation can proceed through a direct decomposition to form adsorbed nitrogen and oxygen atoms or by coupling two NO molecules to form nitrous

oxide. At a higher coverage, this coupling reaction may be as equally important as the NO decomposition reaction. First, the NO molecule adsorbs molecularly on the platinum surface as per Eqn. (193) followed by dissociation as per Eqn. (198). This adsorbed molecule can then react with either an adsorbed oxygen atom to form nitrogen dioxide as per Eqn. (194) or it can react with adsorbed nitrogen from dissociation to form nitrous oxide as per Eqn. (199). In addition, two atomic oxygen or atomic nitrogen atoms can combine to form oxygen or nitrogen gas respectively.

Their efforts demonstrate that NO dissociation begins at 350K and its maximum level occurs within the 400 to 425K range. At a high NO coverage (< 0.4 ML), NO decomposition is not possible due to the lack of empty sites; however, the coupling reaction between two NO molecules to form N_2O is possible. In addition, as the initial coverage of NO increases, more N_2O forms instead of nitrogen. At a lower coverage, NO desorption occurs at 300K. At this temperature, the dissociation ratio, which is percentage of initial amount of NO on the surface that dissociates, is equal to 62%. As the temperature increases, NO_2 formation decreases due to the thermodynamic limit; however, N_2 increases as additional dissociation happens. At low temperatures, oxygen bonds strongly to surface and inhibits both the oxidation and dissociation reactions of NO. However, at temperatures higher than 700K, oxygen inhibition decreases as it begins to desorb giving rise to vacant sites. These sites are now available for NO decomposition or NO adsorption.

In the subsequent year, Ovesson et al. maintain that NO bonds to Pt_{111} through the nitrogen atom [251]. NO oxidation happens as per an L-H reaction mechanism, but they claim that NO oxidation is endothermic and platinum does not readily support NO oxidation. As oxygen coverage increases, a strong repulsive force between two adsorbed oxygen atoms

changes the flow of energy of the NO oxidation reaction. In addition, both adsorbed NO and oxygen atoms diffuse to form nitrogen dioxide confirming the L-H reaction pathway. However, activation of this reaction at low temperatures (below 300K) does not occur. In the same year, Ford et al. determine that the binding strength of atomic oxygen is larger than CO, which is in turn greater than NO [252].

In 2006, Disselkamp et al. support past researchers by proposing an L-H reaction mechanism via Eqn. (193), (117), (194) and (201) on Pt_{100} [253]. However, they consider the L-H reaction step as the RDS, which is quite different from the findings of NO oxidation in the previous section. The next year finds Getman and Schneider investigating NO oxidation on the atomic level over Pt_{111} [254]. They propose that the reaction proceeds via an L-H mechanism with the NO adsorbed on platinum either dissociating or oxidizing with an adsorbed oxygen atom to form NO_2. Since NO_2 has a significantly large adsorption energy, it will not adsorb at low temperatures. In addition, any excess oxygen on the surface will promote NO oxidation because it weakens the bond of both Pt·NO and Pt·O due to a lateral interaction resulting in the breaking of the Pt·O bond and subsequent formation of O·NO. The resulting nitrogen dioxide formed will desorb from the surface due to the high surface adsorption energy and lateral hindrance caused by surrounding atoms. This hindrance is due to an interaction that will repel nitrogen dioxide more as it requires two sites to bond on the surface and, therefore, it desorbs more quickly after formation. From this finding, it is possible to combine Eqns. (194), (201) and (202) in the determination of the global reaction rate expression.

A couple years later, Smeltz et al. support the L-H reaction mechanism for NO oxidation with the adsorption of oxygen on the Pt_{111} as the RDS [255]. They find that the order

of reaction for NO is 1.3, oxygen is 1 and nitrogen dioxide is -2. They postulate that this deviation in order dependence, in comparison to previous efforts, is because of repeatable deactivation or through the contamination of the surface due to impurities. At temperatures above 400K, nitrogen dioxide controls the oxygen coverage on the surface rather than the reactant oxygen. They predict this as the reason for nitrogen dioxide inhibition on platinum surfaces. When nitrogen dioxide adsorbs on the surface depositing a large amount of oxygen, it inhibits molecular oxygen adsorption. Since NO oxidation is endothermic, at a low coverage NO prefers to dissociate instead of oxidize. At a high coverage, NO and oxygen co-adsorbed near the same vacant sites combine to form an OONO complex. This intermediate binds to platinum through an oxygen atom and then further decomposes to form nitrogen dioxide as follows:

$Pt \cdot O_2 + Pt \cdot NO \xrightarrow{k_{208}} Pt \cdot OONO$	(208)
$Pt \cdot OONO \xrightarrow{k_{209}} Pt \cdot O + NO_2$	(209)

At low oxygen coverages, NO oxidation follows an L-H reaction mechanism through Eqns. (193), (117) and (194). However, at high oxygen coverage, it follows Eqn. (208) and (209). They state that both pathways are possible for NO oxidation depending on reaction conditions.

Concurrently, other efforts by Mudiyanselage et al. claim that NO adsorbs and desorbs molecularly from an O-free platinum surface Pt_{111} at 200K; i.e., it does not dissociate to form adsorbed nitrogen and adsorbed oxygen atoms [256]. Adsorbed oxygen atoms inhibit NO oxidation, which results in a weakly bound NO molecule on the platinum surface. At around 250K and low oxygen coverage (0.25 ML), NO does not react with adsorbed oxygen atoms. However, at a high oxygen coverage (0.75 ML), they observe the oxidation reaction

occurring. At these coverage levels, the reaction between NO and O begins without further external assistance at a temperature as low as 200K. They do find that NO cannot completely remove oxygen from platinum surface at these temperatures. They postulate that high oxygen coverage supports NO oxidation, but NO does not dissociate and is instead weakly adsorbed. They obtain oxygen coverage up to 0.25 ML through chemisorption of the oxygen on the platinum surface. Larger oxygen coverages (above 0.25 ML) require nitrogen dioxide dissociation as the chemisorption of oxygen is not sufficient. They determine that nitrogen dioxide dissociates on a clean platinum surface around 400K. However, if nitrogen dioxide forms through NO oxidation at this temperature, it tends to desorb rather than dissociate. This illustrates that NO oxidation follows an L-H reaction mechanism and in the temperature range of 300 to 500K, nitrogen dioxide formed tends to desorb rather than dissociate under ultra high vacuum conditions.

Recently in 2010, Getman and Schneider study NO oxidation over Pt_{111} and find that its rate is associated with the relative surface coverage of oxygen [257]. They state that oxygen bonded strongly to the surface promotes oxygen dissociation; however, when it binds weakly it promotes an O-NO bond instead. Moreover, highly dispersed platinum surfaces favor strong bonds and oxygen dissociation. However, at high coverage of atomic oxygen, their result shows that the Pt-O bond energy decreases resulting in the production of O-NO bonds. This proves that a high amount of surface oxygen is favorable for nitrogen dioxide formation. From a modeling perspective, they state that the adsorption energy and reaction pathway changes with surface coverage and infer that dissociative oxygen adsorption is the RDS. In addition, the L-H step is in quasi-equilibrium for NO oxidation.

With respect to NO and NO_2 bonding, NO adsorbs strongly on an oxygen covered surface, whereas NO_2 demonstrates a different bonding pattern. At a low coverage of oxygen, nitrogen dioxide bonds along one NO bond as a bridge between two platinum atoms. However, as oxygen coverage increases, it bonds on top of the platinum site with nitrogen bonded to the surface. This bonding is weak in nature and under NO oxidation conditions, the nitrogen dioxide coverage is negligible. An oxygen molecule bond is the weakest of all of the considered species and, therefore, it has a negligible presence on the surface of the catalyst. They further summarize that the L-H step changes with surface coverage. At low coverage of adsorbed species (i.e. both oxygen and NO), the adsorbed NO binds with an adsorbed oxygen atom in order to form a similar structure like that of nitrogen dioxide at low oxygen coverage. At a higher coverage, the bond strength with the adsorbed oxygen atom decreases as compared to an O-NO bond. This results in desorption of nitrogen dioxide from the surface. They also demonstrate that dissociative oxygen adsorption on platinum decreases with increasing oxygen coverage. Moreover, they discover low bond energy of adsorbed oxygen favoring NO oxidation. Thus, it is clear that at a low oxygen coverage, NO oxidation is endothermic and activated, whereas, oxygen adsorption is facile. At a high coverage, NO oxidation is facile, while oxygen adsorption is activated thus making it the RDS. While earlier researchers separate oxygen adsorption and dissociation of oxygen on surface as two independent steps with the prior being the RDS, the paper of Getman and Schneider combines both steps into the RDS.

Finally, they make an interesting statement regarding the dissociation of oxygen, stating that it can occur via Eqn. (208) and (209). However, they rule out this arrangement mentioning that at low oxygen coverage, direct dissociation of oxygen is more favorable.

Under high oxygen coverage, there is not enough NO on surface for the reaction to happen. However, at very high NO to oxygen pressure ratios, this Equation might be the path for oxygen dissociation.

Furthermore in the same year, Smeltz et al. probe NO oxidation on Pt_{111} and Pt_{321} and compare the results with supported NO oxidation [258]. They assume oxygen adsorption Eqn. (108) is the RDS and find that the activation energy over Pt_{321} is larger as compared to the value for Pt_{111}. This demonstrates that for different surfaces the activation energy is structure dependent. Moreover, as the ratio of nitrogen dioxide to NO increases, the order of reaction with respect to oxygen increases from one-half to one. Similarly, the order of reaction with respect to NO increases from one to two and nitrogen dioxide decreases from -1 to -2 (Order of reaction is the values of *a*, *b* and *c* in Eqn. G19). Atomic oxygen is the abundant species on the surface with temperature and oxygen pressure having virtually no effect on its presence. They consider both E-R and L-H mechanisms, and state that the choice of mechanism will not influence the reaction rate expression if the RDS is oxygen adsorption. This type of behavior was also reported by Olsson et al in their 2001 paper, as both L-H, E-R and a combination of the two mechanisms provide the same results [224]. They assume that atomic oxygen and free sites are the abundant surface species, with negligible presence of nitrogen containing molecules. Based on this assumption, they derive the global reaction rate expression as Eqn. (G28). At temperatures above 400K, atomic oxygen dominates the surface and the level of NO is insignificant. In the presence of nitrogen dioxide, the surface concentration of atomic oxygen increases. This is because nitrogen dioxide adsorbs on the surface and dissociates in order to form NO and atomic oxygen. Adsorbed NO further desorbs leaving only atomic oxygen, which is consistent with earlier studies.

One interesting point of their study is whether oxygen adsorbs molecularly or dissociatively. They point out that oxygen adsorbs molecularly when the surface concentration of the oxygen is more than 0.6 ML; whereas, for the NO oxidation regime, it lies in-between 0.3 to 0.6 ML. However, this may only be applicable to platinum metals as compared to supported platinum as there is low atomic oxygen coverage on crystal surfaces. With the two catalysts, kinetic parameters like activation energy and reaction order of oxygen and NO increases with the said ratio while reaction order of nitrogen dioxide decreases with the same increase. At lower ratios, NO adsorption can be the RDS; whereas at higher ratios, it switches to oxygen adsorption.

3.3.3 SUPPORT FOR REACTION HISTORY FOR NO OXIDATION OVER PLATINUM/ALUMINA:

Although, this review is intended for NO oxidation on Pt/alumina, NO oxidation on Pt/silica has been shown to follow the same mechanism path with a slightly higher activity [211, 259-260]. Hence, the authors postulate that the same reaction mechanism developed for Pt/alumina may be valid for Pt/silica. This will require changing the values of activation energy, pre-exponential factors and heats of adsorption. Moreover, information from the Pt/silica literature may help shed some light on the pathway of the reaction mechanism over alumina.

In 1993, Xue et al. studied NO oxidation on platinum/silica catalysts in the presence and absence of sulphur dioxide [261]. In absence of sulphur dioxide, NO oxidation reaches equilibrium at 623K; however, sulphur dioxide largely suppresses NO oxidation. Their efforts support earlier work of NO oxidation over platinum with respect to the fact that NO oxidation is equilibrium limited. Moreover, they find a deactivation of the catalysts over

subsequent runs. By reducing the deactivated catalyst, they are able to recover some activity similar to NO oxidation over platinum/alumina catalysts [235-236].

In the year 1996, Jayat et al. study NO_x reduction in lean burn conditions over platinum/silica catalysts in the range of 373 to 773K [262]. Although this review focuses on platinum/alumina, the Jayat et al. efforts demonstrate a guideline for NO oxidation on platinum catalysts. In particular, the light-off temperature of NO oxidation increases with greater platinum particle sizes. However, the maximum conversion of NO is independent of particle size. Therefore, as the particle size increases, the light-off temperature of the reaction increases with the conversion percentage of NO decreasing due to the previously discussed thermodynamic limitation. They find that more than 60% conversion is achieved around 573K on the same catalysts.

Eight years later, Despres et al. examine NO oxidation over Pt/SiO_2 helping to understand some of the concepts involved for alumina catalysts [259]. Similar to previous findings, as the concentration of oxygen increases, oxidation of NO increases and reaches a maximum at 573K. Above this temperature, it becomes thermodynamically limited and conversion starts decreasing. They determine that there is a threshold in oxygen concentration as beyond a certain level it will not augment NO conversion as the catalyst is saturated with oxygen. However, even in the thermodynamically limited region, conversion can increase with a rising oxygen concentration before this limit. In addition, increasing NO concentration causes conversion of NO to NO_2 to decrease until the equilibrium constraints occurs. Above this limit, conversion becomes constant irrespective of the NO concentration. This is only possible when NO oxidation follows an L-H reaction mechanism. The high concentration of any one reactant should saturate adsorption sites, which will result in a

competition between NO and oxygen for adsorption sites, further inhibiting the reaction. In the case of an E-R mechanism, NO oxidation would be independent of NO concentration. Moreover, they find an increase in the temperature of maximum conversion with a boost in NO concentration. Finally, they state that the addition of small quantity of NO_2 significantly inhibits NO oxidation. Nitrogen dioxide causes the deactivation of platinum catalysts that they attribute to platinum oxide formation because of the strong oxidizing nature of nitrogen dioxide.

In 2006, Ji et al. studied NO oxidation on platinum/silica [263]. They determine the reaction order for NO and oxygen as 0.46 and 0.52 respectively. Their efforts support earlier findings that NO oxidation increases with an increase in particle size (decrease in dispersion). Moreover, they support the L-H reaction mechanism, in which NO adsorbed on silica migrates towards platinum and reacts with adsorbed atomic oxygen on platinum.

3.3.4 HISTORICAL SUMMARY:

Although the adsorption and desorption of NO, NO_2 and oxygen has been under consideration for nearly four decades, only relatively recently has there been an increase in the study of NO oxidation on a platinum catalyst. The early adsorption and desorption investigations were mainly accomplished in order to investigate NO_x reactions with other species like CO, hydrogen and hydrocarbons. However, they do provide some insight into the process of NO oxidation on a platinum/alumina surface.

The 1990s saw many advances in understanding the NO oxidation reaction, but the information still remained incomplete in order to predict the reaction accurately. Before this decade, it was clear that NO decomposition is structure and concentration sensitive. If oxygen is present in the inlet stream, researchers find that its adsorption competes with NO

on the surface and can inhibit its dissociation. In specific, oxygen adsorption and dissociation begins at a relatively low temperature and remains stable on the surface until a relatively high temperature (800K). Research indicates that NO adsorbs molecularly until 300K, and then it tends to dissociate on the irregular structure of the surface. They determined that the nitric oxide molecule does not dissociate due to lack of active sites and will remain in molecular form in the presence of oxygen. Moreover, at these high temperatures, nitrogen dioxide forms that also adsorbs on available platinum sites further inhibiting the decomposition reaction of NO.

At this point, there was not a clear distinction whether the reaction proceeds via a Langmuir Hinshelwood or Eley Rideal pathway as the evaluation of both types of kinetic mechanisms gave out satisfactory results. In addition, it became clear that NO oxidation is thermodynamically limited at high temperatures (above 573K) and kinetically limited at low temperatures. Hence, they find that 100% conversion of NO to nitrogen dioxide is not possible. They observe that that NO oxidation reaction occurs in the temperature range of 473 to 773K with maximum conversion obtained around the range of 613 to 633K. Above this range, the conversion decreases due to thermodynamic limitations. Research indicates that NO can easily adsorb on both platinum as well as alumina sites and it does not inhibit its own oxidation reaction. However, the adsorption bond between NO and alumina is much stronger than the bond between NO and platinum. As a result, NO adsorbed on alumina does not take part in the reaction, as it requires a relatively high energy to break the bond. This adsorbed alumina NO must diffuse to a platinum site in order to react. In addition, observations find a decreasing rate of NO oxidation corresponding to an increase in dispersion of platinum on the surface. Moreover, NO oxidation contributes to the sintering

of the catalyst, which decreases dispersion resulting in an increase in NO oxidation. However, no reason is stated in regards to the dispersion effect.

In recent years, findings show that the reaction is endothermic in nature and not a preferred mechanism for oxidation. However, as the surface temperature increases along with subsequent oxygen coverage, this increases the lateral repulsion of adsorbed reactants. Adsorbed oxygen atoms repel both adsorbed oxygen and nitric oxide resulting in the reaction of NO and adsorbed oxygen as their bond strength with platinum decreases. This is why relatively high temperatures are required to overcome this activation barrier. Researchers begin to report that nitrogen dioxide inhibits its own formation. Nitrogen dioxide adsorbs at low temperatures, dissociates on the platinum surface to give NO, and adsorbed oxygen. This dissociation is more favorable at high temperatures then desorption. The resultant adsorbed oxygen blocks the site for NO adsorption, which results in the inhibition of the NO oxidation reaction.

Other important results illustrate that platinum dispersion, and in turn platinum particle size, has a significant influence on the NO oxidation rate. The larger the dispersion, the smaller the platinum particle size and a decreased oxidation rate is found. Larger platinum particles will increase the NO oxidation rate along with shifting the peak of maximum conversion to a lower temperature. Researchers attribute this to a weak Pt·O bond on these platinum particles. However, for a high dispersion, platinum oxide formation deactivates the sites for NO oxidation resulting in a low NO conversion. This is helpful in understanding the NO impact as a relatively strong sintering agent. In the temperature range of NO oxidation, NO sinters the platinum surface and hence platinum particle size increases resulting in an enhanced in NO conversion. Thus, NO oxidation on sintered platinum

catalysts is greater than fresh catalysts. However, both fresh and sintered catalyst deactivate with time for the NO oxidation reaction. With respect to global reaction rates, the literature illustrates that NO oxidation is directly proportional to NO and oxygen concentration and inversely proportional to nitrogen dioxide concentration. The order of the reaction varies, but it is commonly assumed that it is one for NO and oxygen and negative one for nitrogen dioxide.

By this time, it is clear that either the L-H or E-R mechanism yields the same result for NO oxidation as the RDS is oxygen adsorption. Hence, the variation in the final step does not influence the reaction strongly. However, the historical review indicates that the mechanism follows the L-H reaction pathway. This is because for the reaction to proceed, it has to overcome a relatively high activation energy before final conversion to nitrogen dioxide. The reaction is endothermic at low temperatures and coverage with a relatively large surface coverage required in order for the reaction to proceed. Nitrogen dioxide strongly inhibits the conversion, such that the activation energy for NO oxidation in presence of nitrogen dioxide is nearly double as compared to the value in its absence. During the course of the reaction, the surface is mostly covered by NO and atomic oxygen with the coverage of molecular oxygen and nitrogen dioxide negligible. While oxygen adsorbs molecularly on the surface, it quickly dissociates to atomic oxygen with the molecular adsorption acting only as a precursor. The surface does tend to deactivate during longer NO oxidation experiments; however, it can be partially regenerated by cooling the catalyst. Complete regeneration is not possible because of a relatively large amount of platinum oxide formation due to the oxidizing effect of nitrogen dioxide.

3.3.5 DETAILED REACTION MECHANISM:

Nitrogen oxides are formed by the high temperature dissociation reaction of nitrogen and oxygen molecules in the combustion chamber of an internal combustion engine. It is stable below 900K and cannot be converted back into these species without catalytic means. In a gasoline engine operating around stoichiometry, there are enough partial combustion products (CO, H_2, HC) to react with this species on a PGM catalyst in order to convert it back into nitrogen gas. However, in lean burning engines, very little of these species exist. As a result, other methods of catalytic reduction are needed which often require the creation of NO_2 from this NO in order to enhance their operation. In this section, the authors describe the detailed mechanism of this NO oxidation reaction in order to aid modeling of exhaust aftertreatment devices for these engines.

3.3.5.1 Nitric Oxide Adsorption and Desorption

The first step in the mechanism is the adsorption and desorption of nitric oxide:

$NO + Pt \underset{k_{-a}}{\overset{k_a}{\rightleftarrows}} Pt \cdot NO$	(*a*)

The dissociation of NO is inhibited by adsorbed oxygen (present in a later detailed step). As a result, one can neglect Eqns. (198), (199) and (200) in the reaction mechanism because of the ample amount of oxygen present in the exhaust. Moreover, NO adsorption is the first step as it has a higher sticking coefficient as compared to oxygen on a platinum surface [243, 264]. NO adsorption and dissociation is structure sensitive with the molecule bonding N-atom downwards forming a Pt·NO bond. NO tends to desorb from the surface around 500K and it adsorbs on the top site of platinum in presence of oxygen since oxygen covers most of the surface as illustrated in Figure 17. At low temperatures, NO is

preferentially adsorbed as compared to oxygen; however, as the temperature increases, NO desorbs leaving spaces for oxygen adsorption.

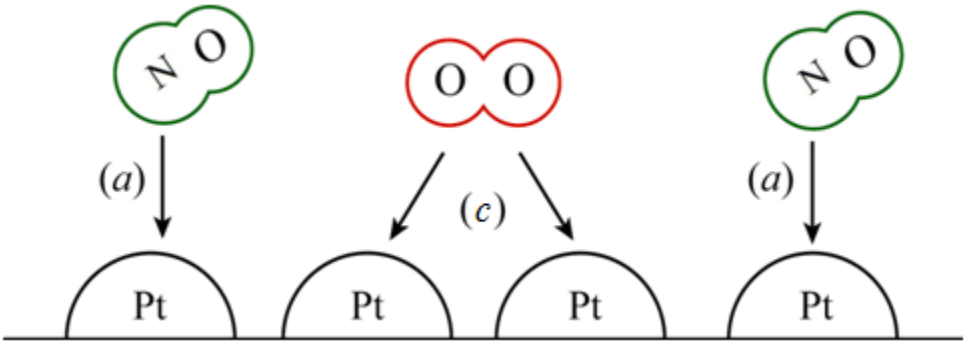

Figure 17: Nitric Oxide and Oxygen Adsorption Steps.

3.3.5.2 Langmuir Hinshelwood Oxidation and Dissociative Adsorption of Nitrogen Dioxide

The exhaust gas leaving the engine does contain some nitrogen dioxide along with nitric oxide. Initially, at low surface coverage and low temperature, nitrogen dioxide adsorbs on the surface in bridge format as a bond forms between two platinum atoms [257]. The bond soon breaks forming adsorbed NO and adsorbed atomic oxygen on the surface. Although this may be written as a two step process, it is combined in one step as both adsorption and dissociation of nitrogen dioxide are fast:

$Pt \cdot NO + Pt \cdot O \underset{k_{-b}}{\overset{k_b}{\rightleftharpoons}} NO_2 + 2Pt$	(*b*)

It is clear that at low temperature and low surface coverage, the backward reaction is predominant and the probability of the forward reaction is negligible. As the surface coverage of NO and O increases along with temperature, the forward reaction will become significant in the kinetic limited range with equilibrium limitation starting to occur around 633 to 655K.

Before light off, negligible nitrogen dioxide is formed by NO oxidation and the backward reaction consumes nitrogen dioxide from engine exhaust. However, once the

reaction progresses in the forward direction, the nitrogen dioxide formed desorbs from the surface in the kinetic range and dissociatively adsorbs in the equilibrium range. In fact, high atomic oxygen coverage is achieved by nitrogen dioxide dissociation as oxygen adsorption itself cannot yield a similar coverage as that obtained by nitrogen dioxide [265]. Hence, at low temperatures desorption of nitrogen dioxide is favorable leading to negligible NO_2 coverage. As the temperature increases, dissociation into NO and O becomes considerable while desorption decreases. This again prevents any significant NO_2 coverage on the surface. Above the thermodynamic limit, desorption is very low as a large amount of nitrogen dioxide formed converts back to nitric oxide and atomic oxygen as shown in Figure 18. Hence, at any temperature, the surface coverage of nitrogen dioxide is negligible.

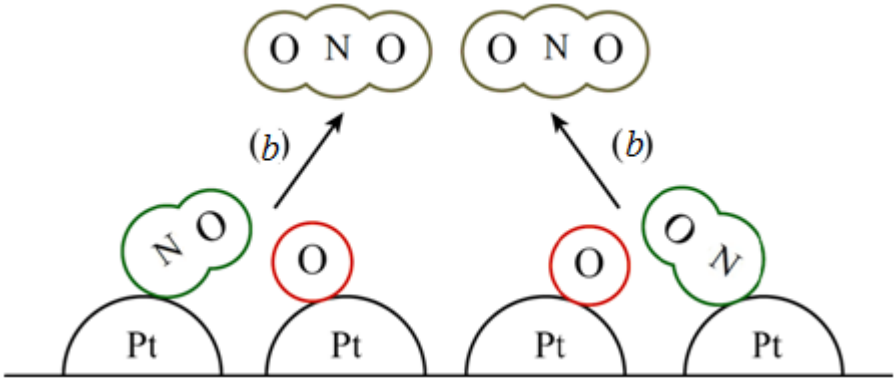

Figure 18: Langmuir Hinshelwood Oxidation and Dissociative Adsorption of Nitrogen Dioxide.

3.3.5.3 Molecular Oxygen Adsorption and Dissociation

The final step in the mechanism is molecular oxygen adsorption on platinum and its subsequent dissociation:

$O_2 + Pt \underset{k_{-c}}{\overset{k_c}{\rightleftarrows}} Pt \cdot O_2$	(*c*)
$Pt \cdot O_2 + Pt \underset{k_{-d}}{\overset{k_d}{\rightleftarrows}} 2Pt \cdot O$	(*d*)

With respect to oxygen adsorption, Elg et al. found that molecular oxygen physisorbs on platinum below 30K, but chemisorbs above 45K [137]. Around 130 to 150K, the O·O bond appears to weaken and begins to dissociate the molecule (also seen by Tieber et al. in [110]). Gland proposed that oxygen has two desorption peaks [244]. At low temperatures (below 100K), oxygen adsorbs and desorbs molecularly. Above 150K, the adsorbed molecular oxygen dissociates into its atomic parts, which only starts desorbing at a much higher temperature (800K).

At standard exhaust conditions, Gland indicates that molecular oxygen would quickly dissociate into atomic oxygen bonded on platinum. Hence, the first thought is to combine the two steps into a singular step for use within the model similar to CO oxidation over platinum. However, the presence of NO and NO_2 species changes the mechanism of oxygen adsorption. As indicated in the previous section, nitrogen dioxide dissociates while adsorbing on platinum leading to adsorbed atomic oxygen [225]. In addition, adsorbed NO on top of the platinum site promotes oxygen dissociation. This increases the overall amount of atomic oxygen on the surface leading to the activation of oxygen adsorption. The lateral repulsion between oxygen atoms will inhibit its further adsorption resulting in Eqn (*c*) as the RDS.

Therefore, initially at low surface coverage and temperature, molecular oxygen adsorption and its dissociation will be fast and deactivated. During this time, there is little NO oxidation occurring. However, once the surface coverage and temperature increases, oxygen adsorption will become active and oxygen will have to overcome the barrier for adsorption on the surface. Although, oxygen is adsorbed molecularly, it just acts as a precursor for further dissociation of oxygen [244]. Hence, molecular oxygen coverage is

negligible on the platinum surface because of this dissociation. As a result, while step (*d*) is fast, it is important to make the molecular adsorption of oxygen and its dissociation distinct in case of NO oxidation.

One of the determining features in the reaction is oxygen desorption from the platinum surface. For adsorbed NO to interact with adsorbed oxygen, high surface coverage is required to lose the Pt·O bond for interacting with adsorbed NO. Hence, NO oxidation increases as oxygen coverage increases. Therefore, if oxygen desorption increases, it will actually inhibit the oxidation reaction; hence, oxygen adsorption is the RDS. The global reaction rate expression determined in the next section uses this assumption.

3.3.6 GLOBAL REACTION MECHANISM:

For the global reaction mechanism, NO adsorption and desorption is occurring with the forward and reverse rates equal to:

$R_a = k_a p_{\mathrm{NO}} \theta_{\mathrm{Pt}}$	(210)
$R_{-a} = k_{-a} \theta_{\mathrm{Pt\cdot NO}}$	(211)

At equilibrium, the forward and backward rate becomes equal, hence

$k_a p_{\mathrm{NO}} \theta_{\mathrm{Pt}} = k_{-a} \theta_{\mathrm{Pt\cdot NO}},$	(212)

where the equilibrium constant equals:

$K_{\mathrm{NO}} = k_a / k_{-a}$	(213)

In presence of nitrogen dioxide, second step of the reaction is the L-H oxidation reaction and desorption of nitrogen dioxide from the surface:

$R_b = k_b \theta_{\mathrm{Pt\cdot NO}} \theta_{\mathrm{Pt\cdot O}}$	(214)
$R_{-b} = k_{-b} p_{\mathrm{NO_2}} \theta_{\mathrm{Pt}}^2$	(215)

and at equilibrium,

$k_b \theta_{\mathrm{Pt\cdot NO}} \theta_{\mathrm{Pt\cdot O}} = k_{-b} p_{\mathrm{NO_2}} \theta_{\mathrm{Pt}}^2$	(216)

where the equilibrium constant equals:

$K_{NO_2} = k_b / k_{-b}$	(217)

Substituting Eqn. (212) and Eqn. (217) in Eqn. (216),

$K_{NO_2} p_{NO} K_{NO} \theta_{Pt\cdot O} = p_{NO_2} \theta_{Pt}$	(218)

At the same time, molecular oxygen adsorption and desorption on platinum with the forward and reverse rates expressed as:

$R_c = k_c p_{O_2} \theta_{Pt}$	(219)
$R_{-c} = k_{-c} \theta_{Pt\cdot O_2}$	(220)

From the previous section discussion, the authors assume that this step in the reaction is RDS,

$R_{NO} = k_c p_{O_2} \theta_{Pt}$	(221)

The next step is dissociation of adsorbed molecular oxygen into atomic oxygen, with forward and backward step as:

$R_d = k_d \theta_{Pt} \theta_{Pt\cdot O_2}$	(222)
$R_{-d} = k_{-d} \theta_{Pt\cdot O}^2$	(223)

At equilibrium,

$k_d \theta_{Pt} \theta_{Pt\cdot O_2} = k_{-d} \theta_{Pt\cdot O}^2$,	(224)

and the equilibrium constant given by,

$K_{O_2} = k_d / k_{-d}$	(225)

Using the fact that $\theta_{Pt} = (1 - \theta_{Pt\cdot NO} - \theta_{Pt\cdot O})$, with NO_2 and O_2 levels on the surface assumed negligible, and Eqns. (212) and (218) results in the following expression:

$\theta_{Pt} = \dfrac{1}{\left(1 + \dfrac{p_{NO_2}}{K_{NO_2} p_{NO} K_{NO}} + p_{NO} K_{NO}\right)}$	(226)

Using Eqn (224) and (218),

$\theta_{Pt\cdot O_2} = \left(\dfrac{p_{NO_2}}{K_{NO_2} p_{NO} K_{NO}}\right)^2 \dfrac{1}{K_{O_2}} \theta_{Pt}$	(227)

Substituting Eqn. (227) into (221) results in:

$R_{NO} = \left[k_b p_{O_2} - \frac{k_{-b}}{K_{O_2}} \left(\frac{p_{NO_2}}{K_{NO_2} p_{NO} K_{NO}} \right)^2 \right] \theta_{Pt}$	(NO-RDS)

where θ_{Pt} is given by Eqn. (226). This is the global reaction rate expression for NO oxidation with molecular adsorption of oxygen as the Rate Determining Step.

The Equation labeled as "NO-RDS" are the global reaction rate expression that should be used while modeling the NO oxidation on platinum and platinum/alumina catalysts. Although the same Equation will be used for different platinum catalysts, the values of pre-exponential factor, activation energy, and enthalpies will change with dispersion, catalyst preparation, particle diameter, etc.

3.4 CONCLUSION:

This chapter provides a historical review of the oxidation of carbon monoxide, hydrogen and nitrogen oxide species and the effects of dispersion, concentrations and surface structures on the descriptions of the individual reactions. This effort helps to determine fundamentally correct reaction mechanisms, which will be used in modeling each respective reaction. Of importance, each reaction is investigated independently, without taking into consideration the influence of other species on its reaction rate. This is important to understand, as different species may alter the reaction pathway through facilitation of a faster reaction or inhibition of the rate. However, efforts within the KU laboratories through collaboration with the Chemical and Petroleum Engineering Department are geared towards improving modeling capabilities through writing the kinetic expressions in an adaptive manner. In specific, incorporating metal parameters (like weight and dispersion) into the reaction expressions will help create more predictive mechanisms. Combined with better models, as presented in the previous chapter, will help optimize precious metal loading and

minimize the cost, while maximizing the effectiveness of aftertreatment devices. Therefore, each reaction is investigated individually in order to minimize the complexity of the modeling and experimental efforts.

The next chapter describes the simulation of CO oxidation using the reaction rate expression determined in this chapter while comparing the modified 1D model to the classical 1D model. CO oxidation was chosen because it is the most widely referenced reaction rate with data available in the literature that can be used for validation of the models. In addition, this is a precursor to current data gathering efforts in the KU laboratories for NO oxidation utilizing adaptive kinetics. H_2 oxidation is planned as future work. As a result, the next chapter describes Computational Fluid Dynamic (CFD) techniques combined with the CO oxidation reaction rate expression in the simulation of a platinum/alumina catalyst.

Chapter 4: CFD Modeling

The newly developed 1D model of a catalytic converter must be able to model both low flow and high flow conditions with the same accuracy. As a result, it is necessary to validate the modified 1D model over typical high flow situations and then demonstrate its use under low flow conditions. In order to accomplish this, the classical 1D model for catalytic converters is simulated initially for CO oxidation in order to determine the parameters needed for the reaction rate expression. Then, using the same parameters and reaction rate expression, the modified 1D model will be compared against the classical version. Moreover, by reducing the flow velocity methodically, this will determine the velocities at which bulk gas conduction and diffusion become important. However, before any simulation study can be completed, this chapter presents the finite different modeling techniques in order to compute the solutions for both the classical and modified models.

4.1 Finite Difference Modeling of Classical 1D Model of Catalytic Converter:

Classical 1D catalyst modeling includes four equations; namely, the bulk gas phase temperature equation, bulk gas phase species equation, surface phase temperature equation and surface species equation. Using these equations, CO oxidation experiments described in an Arnby et al. paper published in 2004 will be simulated [124]. In order to check the author's model for correctness, the code generated in this thesis will be compared to the classical catalyst model of the author's advisor. This work will use MATLAB as the programming framework because of its ability to post-process the results graphically aiding the fast development of code. Subsequent efforts may involve porting the code to a more traditional programming language (FORTRAN, C++) for faster computational times.

The differential equations of the model will be simulated using finite difference discretization techniques. For this technique, parameter values are determined at specific grid points pre-determined by the modeler [32]. This method does have disadvantages in the form of truncation errors. However, these errors can be reduced by using the proper stability conditions. In the following sections, the four discretized equations are derived along with their boundary conditions.

4.1.1 BULK PHASE TEMPERATURE EQUATION:

The classical bulk gas phase temperature equation is given by Eqn. (8) in chapter 1 as:

$$\rho c_p u \frac{\partial T}{\partial x} = \frac{h_c G_a}{\varepsilon}\left(T_m - T\right) \tag{8}$$

This can be rewritten in finite difference format using an Euler Implicit method as follows:

$$\frac{T_i - T_{i-1}}{\Delta x} = \frac{h_c G_a}{\rho c_p u \varepsilon}\left(T_{m,i} - T_i\right) \tag{228}$$

Solving for the temperature of interest (T_i) finds:

$$T_i = \left(T_{i-1} + \frac{\Delta x h_c G_a}{\rho c_p u \varepsilon} T_{m,i}\right) \Bigg/ \left(1 + \frac{\Delta x h_c G_a}{\rho c_p u \varepsilon}\right) \tag{229}$$

In this equation, the heat transfer coefficient is computed as Eqns. (90) and (91) in Chapter 2 [31, 266-267].

Therefore, using Eqns. (229), (90) and (91), the bulk gas phase temperature equation can be computed along the length of the catalyst. Since this is a first-order differential equation, only one boundary condition is required to make the solution unique for this application.

4.1.1.1 Boundary Condition

In a catalytic converter, the inlet condition of the bulk gas phase temperature equation is often measured by the experimentalist; hence, it is used as the boundary condition for this effort [29]:

$T_1 = \text{Specified}$	(230)

For the experimental CO oxidation conversion efforts of Arnby et al., the temperature is increased at the rate of 5 degrees Kelvin per minute from 373 K to 523 K. Hence, this information provides the inlet conditions for the bulk gas phase temperature equation.

4.1.2 BULK PHASE SPECIES EQUATION:

The bulk gas phase species equation is given by Eqn. (7) in Chapter 1 as:

$u\frac{\partial \overline{C}_j}{\partial x} = \frac{\kappa_j G_a}{\varepsilon}\left(\overline{C}_{s,j} - \overline{C}_j\right)$	(7)

Using the same discretization technique as the temperature equation, in finite difference form this equation becomes:

$\frac{\overline{C}_{j,i} - \overline{C}_{j,i-1}}{\Delta x} = \frac{\kappa_j G_a}{u\varepsilon}\left(\overline{C}_{s,j,i} - \overline{C}_{j,i}\right)$	(231)

with solution for the species of interest as:

$\overline{C}_{j,i} = \left(\overline{C}_{j,i-1} + \frac{\Delta x \kappa_j G_a}{u\varepsilon}\overline{C}_{s,j,i}\right) \Big/ \left(1 + \frac{\Delta x \kappa_j G_a}{u\varepsilon}\right)$	(232)

The mass transfer coefficients that describe flow between the bulk gas and the surface are given in Chapter 2 as Eqns. (93) and (94) [31, 266-267].

Therefore, from Eqns. (232), (93) and (94), the bulk gas phase species equation can be computed along the length of the catalyst. Since this is also a first-order derivative similar to the temperature equation, only one boundary condition is required.

4.1.2.1 Boundary Condition

For a catalytic converter, the inlet condition of the bulk gas phase species equation is often measured by the experimentalist; hence, it is used as boundary condition here:

$\overline{C}_{j,1} = \text{Specified}$	(233)

For the experimental CO oxidation conversion efforts of Arnby et al., they use 0.01% or 0.1% CO in 10% oxygen with remaining fraction as the inert gas nitrogen. Hence, this information provides the inlet conditions for the bulk gas species equation for this effort.

4.1.3 SURFACE PHASE TEMPERATURE EQUATION:

From Chapter 1, the surface temperature equation is:

$\rho_m c_m \frac{\partial T_m}{\partial t} = \lambda_m \frac{\partial^2 T_m}{\partial x^2} + \frac{h_c G_a}{1-\varepsilon}\left(T - T_m\right) + \frac{G_{ca}}{1-\varepsilon}\sum_{j=1}^{NM} R_j h_j$	(10)

The discretization method chosen by the author is the forward difference for time and central difference for space (FTCS) method. Although conditionally stable, the FTCS method yields a direct result from the previous time step values. Whereas, the unconditionally stable implicit method, generates a system of equations which need to be solved simultaneously [268]. This can be computationally intensive, depending upon the equations. While the implicit method does not have a theoretical time step limit, the truncation error associated with its discretization depends on this time step. Hence, the accuracy of the solution is a function of the time step chosen. Therefore, the author prefers the FTCS method to implicit methods. Moreover, the author's advisor utilizes this discretization method in his efforts; therefore, a direct check for accuracy between codes is possible.

Written in explicit finite difference form, the FTCS description of the surface temperature equation equals:

$$\rho_m c_m \frac{T_{m,i}^{n+1} - T_{m,i}^{n}}{\Delta t} = \lambda_m \frac{T_{m,i+1}^{n} - 2T_{m,i}^{n} + T_{m,i-1}^{n}}{\Delta x^2} + \frac{h_c G_a}{1-\varepsilon}\left(T_i^n - T_{m,i}^n\right) + \frac{G_{ca}}{1-\varepsilon}\sum_{j=1}^{NM} R_j h_j \quad (234)$$

Since this differential equation is second order in space and first order in time, it requires two boundary conditions and one initial condition to satisfy the analysis.

4.1.3.1 Boundary and Initial Condition:

One of the assumptions for 1D catalytic converter modeling is that catalytic converter is treated as an adiabatic device. Using this assumption, the boundary conditions are defined at the inlet and outlet of the catalytic converter as [29, 32]:

$$\frac{dT_{m,1}^{n}}{dx} = 0, \frac{dT_{m,L}^{n}}{dx} = 0, \quad (235)$$

When converting these equations into a finite difference format, a first-order differential cannot be utilized (like the bulk gas species and temperature equations). This is because the FTCS method is discretized according to second-order in space; hence, the solution of the boundary conditions and the main method would be mismatched. As a result, a second-order central differentiation for space is used for the boundary conditions:

$$\frac{dT_{m,1}^{n}}{dx} = \frac{T_{m,2}^{n} - T_{m,0}^{n}}{2\Delta x} = 0 \text{ and } \frac{dT_{m,L}^{n}}{dx} = \frac{T_{m,L-1}^{n} - T_{m,L+1}^{n}}{2\Delta x} = 0 \quad (236)$$

From this information, the nodes that are on the exterior of the catalyst can be computed:

$$T_{m,0}^{n} = T_{m,2}^{n} \text{ and } T_{m,L+1}^{n} = T_{m,L-1}^{n} \quad (237)$$

Substituting these results into the main FTCS methodology provides the governing finite difference equations at the inlet and outlet of the catalytic converter:

$$\rho_m c_m \frac{T_{m,1}^{n+1} - T_{m,1}^{n}}{\Delta t} = 2\lambda_m \frac{T_{m,2}^{n} - T_{m,1}^{n}}{\Delta x^2} + \frac{h_c G_a}{1-\varepsilon}\left(T_1^n - T_{m,1}^n\right) + \frac{G_{ca}}{1-\varepsilon}\sum_{j=1}^{NM} R_j h_j \quad (238)$$

$$\rho_m c_m \frac{T_{m,L}^{n+1} - T_{m,L}^{n}}{\Delta t} = 2\lambda_m \frac{-T_{m,L}^{n} + T_{m,L-1}^{n}}{\Delta x^2} + \frac{h_c G_a}{1-\varepsilon}\left(T_L^n - T_{m,L}^n\right) + \frac{G_{ca}}{1-\varepsilon}\sum_{j=1}^{NM} R_j h_j \quad (239)$$

Since the FTCS is first order in time, an initial condition is required to begin the computational effort. Therefore, at zero time, the temperature across the catalytic converter is either specified or taken equal to the ambient temperature:

$$T_{m,i}^{0} = \text{Specified} \tag{240}$$

4.1.3.2 Stability Analysis

Since the surface temperature phase equation involves a time dependency, it is necessary to perform a stability analysis in order to determine the maximum time step allowed by the method. Traditionally, a Von Neumann or Fourier analysis is accomplished in order to determine the criterion [32]. In this analysis, *D* represents the exact solution for the equation while *N* represents the numerical solution with a finite accuracy. From this, the error in the solution is given by *E = N-D*. Since the numerical solution must satisfy the differential equation:

$$\rho_m c_m \frac{D_{m,i}^{n+1} + E_{m,i}^{n+1} - D_{m,i}^{n} - E_{m,i}^{n}}{\Delta t} = \left\{ \begin{array}{l} \lambda_m \dfrac{D_{m,i+1}^{n} + E_{m,i+1}^{n} - 2\left(D_{m,i}^{n} + E_{m,i}^{n}\right) + D_{m,i-1}^{n} + E_{m,i-1}^{n}}{\Delta x^2} \\ + \dfrac{h_c G_a}{1-\varepsilon}\left(T_i^n - D_{m,i}^{n} - E_{m,i}^{n}\right) + \dfrac{G_{ca}}{1-\varepsilon}\displaystyle\sum_{j=1}^{NM} R_j h_j \end{array} \right\} \tag{241}$$

Moreover, since *D* is the exact solution, it will also satisfy the differential equation:

$$\rho_m c_m \frac{D_{m,i}^{n+1} - D_{m,i}^{n}}{\Delta t} = \left\{ \lambda_m \frac{D_{m,i+1}^{n} - 2\left(D_{m,i}^{n}\right) + D_{m,i-1}^{n}}{\Delta x^2} + \frac{h_c G_a}{1-\varepsilon}\left(T_i^n - D_{m,i}^{n}\right) + \frac{G_{ca}}{1-\varepsilon}\sum_{j=1}^{NM} R_j h_j \right\} \tag{242}$$

Subtracting Eqn. (242) from (241), results in:

$$\rho_m c_m \frac{E_{m,i}^{n+1} - E_{m,i}^{n}}{\Delta t} = \left\{ \lambda_m \frac{E_{m,i+1}^{n} - 2\left(E_{m,i}^{n}\right) + E_{m,i-1}^{n}}{\Delta x^2} + \underbrace{\frac{h_c G_a}{1-\varepsilon}\left(-E_{m,i}^{n}\right)}_{A} \right\} \tag{243}$$

Thus, the error in the solution also satisfies the differential equation.

This error can be expressed using Fourier series in terms of exponentials as [32, 269]:

$$E_{m,i}^{n} = e^{at} e^{ik_m x} \tag{244}$$

Substituting Eqn. (244) in Eqn. (243),

$$\frac{e^{a(t+\Delta t)}e^{ik_m x}-e^{at}e^{ik_m x}}{\Delta t}=\left\{\lambda_m\frac{e^{at}e^{ik_m(x+\Delta x)}-2\left(e^{at}e^{ik_m x}\right)+e^{at}e^{ik_m(x-\Delta x)}}{\rho_m c_m\Delta x^2}-\frac{A\left(e^{at}e^{ik_m x}\right)}{\rho_m c_m}\right\} \quad (245)$$

and dividing by $e^{at}e^{ik_m x}$ recovers:

$$\rho_m c_m\frac{e^{a(\Delta t)}-1}{\Delta t}=\left\{\lambda_m\frac{e^{ik_m\Delta x}-2+e^{ik_m-\Delta x}}{\Delta x^2}-A\right\} \quad (246)$$

Through modifying Eqn. (246),

$$e^{a(\Delta t)}=1+\frac{\lambda_m\Delta t}{\rho_m c_m\Delta x^2}\left(e^{ik_m\Delta x}-2+e^{ik_m-\Delta x}\right)-A\frac{\Delta t}{\rho_m c_m}, \quad (247)$$

and using a property of trigonometry determines:

$$\left(e^{ik_m\Delta x}-2+e^{ik_m-\Delta x}\right)=-4\sin^2\left(\frac{k_m}{2}\right) \quad (248)$$

Substituting Eqn. (248) back into Eqn. (247):

$$e^{a(\Delta t)}=1-\frac{\lambda_m\Delta t}{\rho_m c_m\Delta x^2}4\sin^2\left(\frac{k_m}{2}\right)-A\frac{\Delta t}{\rho_m c_m} \quad (249)$$

Now, the Von Neumann method states that the solution of Eqn. (234) will be stable if the error in time step *n*+1 will be equal or less than the error in time step *n*. In mathematical form, this is represented as:

$$\left|\frac{E_j^{n+1}}{E_j^n}\right|\le 1 \quad (250)$$

Then, by substituting Eqn. (244) in Eqn. (250),

$$\left|\frac{e^{a(t+\Delta t)}e^{ik_m x}}{e^{at}e^{ik_m x}}\right|\le 1, \quad (251)$$

and incorporating Eqn. (249) in Eqn. (251),

$$\left|e^{a(\Delta t)}\right|=\left|1-\frac{\lambda_m\Delta t}{\rho_m c_m\Delta x^2}4\sin^2\left(\frac{k_m}{2}\right)-A\frac{\Delta t}{\rho_m c_m}\right|\le 1 \quad (252)$$

The method is left with two possible solutions for a stable time-step. The first solution details that:

$$1-\frac{\lambda_m \Delta t}{\rho_m c_m \Delta x^2} 4\sin^2\left(\frac{k_m}{2}\right) - A\frac{\Delta t}{\rho_m c_m} \le 1 \quad (253)$$

which can be further simplified as:

$$\frac{\lambda_m \Delta t}{\rho_m c_m \Delta x^2} 4\sin^2\left(\frac{k_m}{2}\right) + A\frac{\Delta t}{\rho_m c_m} \ge 0 \quad (254)$$

Since the left hand side is always positive, Eqn. (254) always holds and the time-step is not defined by this criterion.

For the second solution, one starts with:

$$1-\frac{\lambda_m \Delta t}{\rho_m c_m \Delta x^2} 4\sin^2\left(\frac{k_m}{2}\right) - A\frac{\Delta t}{\rho_m c_m} \ge -1 \quad (255)$$

By simplifying this result, we obtain:

$$\frac{\lambda_m \Delta t}{\rho_m c_m \Delta x^2} 4\sin^2\left(\frac{k_m}{2}\right) + A\frac{\Delta t}{\rho_m c_m} \le 2 \quad (256)$$

Since the maximum value of the square of the sine value will always be one, by substituting back the value of *A*, the solution of the finite difference equation for the surface temperature equation will be stable given the following time-step:

$$\Delta t \le \frac{2\rho_m c_m}{\frac{4\lambda_m}{\Delta x^2} + \frac{h_c G_a}{1-\varepsilon}} \quad (257)$$

Therefore, only if this condition is satisfied, Eqn. (234) will yield stable solution.

4.1.4 SURFACE PHASE SPECIES EQUATION:

From Chapter 1, the surface species equation is written as:

$$\frac{d\overline{C}_{s,j}}{dt} = \frac{\kappa_j G_a}{1-\varepsilon}\left(\overline{C}_j - \overline{C}_{s,j}\right) - \frac{G_{ca}\overline{R}_j}{1-\varepsilon} \quad (9)$$

It is important to note that the left hand side of this equation represents the storage of gas on the catalyst, which is negligible and most researchers omit it from their description. However, it is written here in this manner in order to aid in the computational development of the model. Without this term, the model becomes a numerically stiff algebraic equation

involving exponentially dependent reaction rate expressions that is difficult to compute. Writing the equation in this manner allows use of Matlab ODE solvers. In particular, the left hand side is iterated using updated values of the surface gas species until the change between successive iterations is zero; effectively providing the same result an algebraic solver would accomplish. Although this equation is written as an ordinary differential equation in time, since it is solved until steady-state using the initial value from the previous time-step, it does not require a boundary condition. While not numerically elegant, this methodology has proven to be quite effective at reducing numerical stiffness.

The above finite difference equations and respective boundary conditions provide the solution of the classical catalytic converter model. In the following section, the modified 1D model bulk gas phase and species equations are expressed in finite difference format.

4.2 Finite Difference Modeling of Modified 1D Model of Catalytic Converter:

For the modified 1D model, the surface phase equations and respective boundary conditions are the same; hence, they can be used as indicated for the classical 1D model. However, the bulk phase equations need to be redefined with new sets of boundary conditions.

4.2.1 BULK PHASE TEMPERATURE EQUATION:

The modified bulk gas phase temperature equation is given by Eqn. (95) in Chapter 2 as:

$$\rho c_p u \frac{\partial T}{\partial x} = \lambda \frac{\partial^2 T}{\partial x^2} + \frac{h_c G_a}{\varepsilon}\left(T_m - T\right) \qquad (95)$$

This is an advection diffusion equation and is now written incorporating a second-order differential for both components as:

$$\frac{T_{i+1}-T_{i-1}}{2\Delta x}=\frac{\lambda}{\rho c_p u}\frac{T_{i+1}-2T_i+T_{i-1}}{\Delta x^2}+\frac{h_c G_a}{\rho c_p u\varepsilon}\left(T_{m,i}-T_i\right) \quad (258)$$

This ensures second order accuracy and consistency of the finite difference equation, ensuring convergent solution of the equation [268, 270]. This equation can further solved using either of two methods.

4.2.1.1: Iterative Solution:

From Eqn. (258), the solution at the desired point of computation is determined as:

$$T_i=\frac{\left(-1+\frac{2\lambda}{\rho c_p u\Delta x}\right)T_{i+1}+\left(1+\frac{2\lambda}{\rho c_p u\Delta x}\right)T_{i-1}+\frac{2\Delta x h_c G_a}{\rho c_p u\varepsilon}T_{m,i}}{\left(\frac{4\lambda}{\rho c_p u\Delta x}+\frac{2\Delta x h_c G_a}{\rho c_p u\varepsilon}\right)} \quad (259)$$

4.2.1.2: Matrix Method and Thomas Algorithm:

Eqn. (258) can be further expanded as

$$\left(\frac{1}{2\Delta x}+\frac{\lambda}{\rho c_p u\Delta x^2}\right)\left(-T_{i-1}\right)+\left(\frac{2\lambda}{\rho c_p u\Delta x^2}+\frac{h_c G_a}{\rho c_p u\varepsilon}\right)T_i+\left(\frac{1}{2\Delta x}-\frac{\lambda}{\rho c_p u\Delta x^2}\right)T_{i+1}=\frac{h_c G_a}{\rho c_p u\varepsilon}\left(T_{m,i}\right) \quad (260)$$

Applying Eqn. (260) at each point in the discrete finite difference grid results in tri-diagonal system of FDE's that is solved using Thomas algorithm. The structure of the matrix and solution of Thomas algorithm is available in various books on computational fluid dynamics and hence not presented here [268, 271].

In either case, since Eqn. (95) involves a second-order derivative, two boundary conditions are now required.

4.2.1.3 Boundary Condition

The first boundary condition is used as-is from the classical method,

$$T_1=\text{Specified} \quad (230)$$

while the second boundary condition is developed from adiabatic nature of the model. Using this assumption, the boundary condition at the outlet of the catalytic converter is [29, 32]:

$$\frac{dT_L}{dx} = 0, \tag{261}$$

Similar to the discussion involving the surface temperature equation, a central difference method is required for this boundary condition in order to remain consistent with the main differential equation. Therefore, using central differentiation for space on this boundary condition provides:

$$\frac{dT_L}{dx} = \frac{T_{L-1} - T_{L+1}}{2\Delta x} = 0 \tag{262}$$

which results in the computation of the node outside of the domain:

$$T_{L+1} = T_{L-1} \tag{263}$$

Substituting equation (263) into the governing equation (258), the last node in modeling the catalytic converter is:

$$\frac{T_{L+1} - T_{L-1}}{2\Delta x} = \frac{2\lambda}{\rho c_p u}\left(\frac{T_{L-1} - T_L}{\Delta x^2}\right) + \frac{h_c G_a}{\rho c_p u \varepsilon}\left(T_{m,L} - T_L\right) \tag{264}$$

From this, the temperature of importance is equal to:

$$T_L = \frac{\left(\frac{2\lambda}{\rho c_p u \Delta x^2}\right) T_{L-1} + \frac{h_c G_a}{\rho c_p u \varepsilon} T_{m,L}}{\left(\frac{2\lambda}{\rho c_p u \Delta x^2} + \frac{h_c G_a}{\rho c_p u \varepsilon}\right)} \tag{265}$$

whereas for the Thomas algorithm Eqn. (264), it is written as

$$\left(\frac{2\lambda}{\rho c_p u \Delta x^2} + \frac{h_c G_a}{\rho c_p u \varepsilon}\right) T_L + \left(\frac{2\lambda}{\rho c_p u \Delta x^2}\right)\left(-T_{L-1}\right) = \frac{h_c G_a}{\rho c_p u \varepsilon}\left(T_{m,L}\right) \tag{266}$$

4.2.2. BULK PHASE SPECIES EQUATION:

The modified bulk phase species equation is given by equation (96) in Chapter 2:

$u\frac{\partial \overline{C}_i}{\partial x}-\delta_{im}\frac{\partial^2 \overline{C}_i}{\partial x^2}=\frac{\kappa_i G_a}{\varepsilon}\left(\overline{C}_{s,i}-\overline{C}_i\right)$	(96)

Using a similar discretization technique as the modified temperature equation, this becomes:

$\frac{\overline{C}_{j,i+1}-\overline{C}_{j,i-1}}{2\Delta x}-\frac{\delta_{im}}{u}\left(\frac{\overline{C}_{j,i+1}-2\overline{C}_{j,i}+\overline{C}_{j,i-1}}{\Delta x^2}\right)=\frac{\kappa_j G_a}{u\varepsilon}\left(\overline{C}_{s,j,i}-\overline{C}_{j,i}\right)$	(267)

Similar to bulk phase temperature equation, species equation can be solved in either of two methods.

4.2.2.1: Iterative Solution:

From Eqn. (267), the solution at the desired point of computation is determined as:

$\overline{C}_{j,i}=\frac{\left(-1+\frac{2\delta_{im}}{\Delta x u}\right)\overline{C}_{j,i+1}+\left(1+\frac{2\delta_{im}}{\Delta x u}\right)\overline{C}_{j,i-1}+\frac{2\Delta x\kappa_j G_a}{u\varepsilon}\overline{C}_{s,j,i}}{\left(\frac{4\delta_{im}}{\Delta x u}+\frac{2\Delta x\kappa_j G_a}{u\varepsilon}\right)}$	(268)

4.2.1.2: Matrix Method and Thomas Algorithm:

Eqn. (267) can be further expanded as

$\left(\frac{-1}{2\Delta x}-\frac{\delta_{im}}{u\Delta x^2}\right)\overline{C}_{j,i-1}+\left(\frac{2\delta_{im}}{u\Delta x^2}+\frac{\kappa_j G_a}{u\varepsilon}\right)\overline{C}_{j,i}+\left(\frac{1}{2\Delta x}-\frac{\delta_{im}}{u\Delta x^2}\right)\overline{C}_{j,i+1}=\frac{\kappa_j G_a}{u\varepsilon}\left(\overline{C}_{s,j,i}\right)$	(269)

Applying Eqn. (269), at each point in the discrete finite difference grid results in tri-diagonal system of FDE's that is solved using Thomas algorithm [268, 271].

Similar to the modified temperature equation, two boundary conditions are required for the modified species equation.

4.2.2.3 Boundary Condition

The first boundary condition is used as-is from the classical method,

$\overline{C}_{j,1}=\text{Specified}$	(233)

while at the outlet, it is assumed that the concentration of the species does not change once it leaves the catalytic converter; e.g., it remains constant in the *x*-direction. This is represented as:

$$\frac{d\overline{C}_{j,L}}{dx} = 0, \tag{270}$$

Again, similar to the modified bulk temperature equation, a central difference method is applied to the boundary resulting in the following expression:

$$\frac{\overline{C}_{j,L+1} - \overline{C}_{j,L-1}}{2\Delta x} - \frac{2\delta_{im}}{u}\frac{\overline{C}_{j,L-1} - \overline{C}_{j,L}}{\Delta x^2} = \frac{\kappa_j G_a}{u\varepsilon}\left(\overline{C}_{s,j,L} - \overline{C}_{j,L}\right) \tag{271}$$

From this, the last node for the bulk gas species equals:

$$\overline{C}_{j,L} = \frac{\left(\frac{2\delta_{im}}{u\Delta x^2}\right)\overline{C}_{j,L-1} + \frac{\kappa_j G_a}{u\varepsilon}\overline{C}_{s,j,L}}{\left(\frac{2\delta_{im}}{u\Delta x^2} + \frac{\kappa_j G_a}{u\varepsilon}\right)} \tag{272}$$

and for the Thomas algorithm Eqn. (271), is written as

$$\left(-\frac{2\delta_{im}}{u\Delta x^2}\right)\overline{C}_{j,L-1} + \left(\frac{2\delta_{im}}{u\Delta x^2} + \frac{\kappa_j G_a}{u\varepsilon}\right)\overline{C}_{j,L} = \frac{\kappa_j G_a}{u\varepsilon}\left(\overline{C}_{s,j,L}\right) \tag{273}$$

While modeling the catalytic converter, value of monolith temperature at next time step is calculated as per Eqn. (234) from values of previous time step. But bulk phase species and temperature equation and surface phase species equation do not have time dependant differentiation and hence, they need to be solved simultaneously for any given time step. Also, these three equations are dependant on each other and as no solution is available for any of the equation at given time step, they are to be iterated to reach a stable solution.

If bulk phase temperature equation or bulk phase species equation were to be solved independently of each other, the matrix method (Thomas algorithm) would be the best choice as it only takes one step in order to find the solution. However, the coefficients of the

dependant variable are not directly available. In such a case, application of matrix method for every iteration will be time consuming and computationally intensive. Instead, the iterative method will yield better computational efficiency as the three equations will be solved simultaneously.

For the iterative method, it is necessary to provide a final round off error in order to stop infinite iteration; e.g., the solution becomes stable below the round off error. This value is derived numerically for ten nodes. A higher number of nodes will have a higher accuracy and will satisfy the round off error generated from this lower number of nodes. This is done for both classical and modified model and the light-off temperature is compared to experimental value.

4.3 Data for Modeling:

In order to validate the model, the author employs experimental data from Arnby et al. with parameters indicated in Table 1. Moreover, references from other researchers provide needed values, such as monolith density, that were not indicated by Arnby et al.. Finally, the author refers the reader to Appendix IV in order to find the information needed for diffusion calculations in the model equations.

Table 1. Parameters Utilized in Modeling of Arnby et al. CO Oxidation Experiments.

Sr. No.	Description	Symbol	Value	Units	Ref:
1.	Thermal conductivity of gas (constant)	λ	0.0338	W/mK	[50]
2.	Space velocity		17000	hr^{-1}	[31, 124]
3.	Length of catalyst	L	23	mm	[124]
4.	Diameter of catalyst		13	mm	[124]
5.	Velocity	u	0.108611	m/s	*
6.	Channel per square inch of the catalyst		400	CPSI	[124]
7.	Length of side of the channel	d	1	mm	[124]
8.	Density of the monolith	ρ_m	1800	kg/m^3	[31, 272]
9.	Specific heat capacity of the monolith	c_m	1020	J/kg·K	[31, 272]
10.	Thermal conductivity of the monolith	λ_m	1.5	W/m·K	[31, 272]
11.	Number of channels		82		[124]

* calculated from the space velocity and catalyst length

4.4 Conclusion:

This chapter presents the discretized versions of both classical and modified 1D catalyst models. In the derivation of these models, the stability criterion with respect to the maximum limit on the time step is given in order to simulate the experimental data. Moreover, all boundary conditions and other values necessary in order to run the simulations are given. The next chapter describes the results of modeling within the MATLAB framework using the discretized models. Furthermore, Appendix I and Appendix II provide the written code of the model within MATLAB for the classical and modified 1D simulations respectively.

Chapter 5: Results and Conclusion

The goal of this thesis is to improve the modeling of catalytic converters in order to solve two issues: Cold start emissions and low flow catalyst conditions represented here as the regenerative leg of LNT devices. To achieve this objective, the author presents a modified 1D catalyst model while reformulating the chemical kinetics from first principles by reviewing each respective reaction history. The modified 1D model is applicable mainly under low flow situations; whereas, the chemical kinetics formulated are applicable for every catalytic converter model. Therefore, this chapter is divided into two parts; the first section explains the results of improved chemical kinetics and second part describes the influence of the modified 1D model.

5.1 Improved Chemical Kinetics

The study of chemical kinetics was undertaken for the three oxidation reactions of CO, H_2, and NO in order to create global reaction rate expressions valid under typical operating conditions (with respect to temperature, pressure and catalyst properties) of a catalytic converter. This resulted in two outcomes; the first being reduced cold start emissions through better prediction of species light off temperatures while the second is a reduction in the cost of these devices through better placement of platinum group metals. The reduction in cold start emissions results from a more fundamentally correct global mechanism based on a thorough literature review as described in the previous chapter. One such mechanism will be employed in the next section when describing a CO oxidation light off experiment. The second outcome is worth exploring in some detail here.

This review of chemical kinetics reveals that, apart from partial pressure and temperature, the reaction rate depends on the physical structure of the catalytic surface.

Surface properties like BET, dispersion and particle diameter influence the reaction rate for each species. For example, if dispersion increases, the level of CO oxidation decreases. Similarly for NO oxidation, as dispersion decreases, oxidation rate increases. At the same time, as BET increases, the surface area available for each reaction goes up, increasing the number of sites for reaction. While other researchers are familiar with these concepts in the chemical engineering field, they are not common knowledge in the automotive modeling realm and have not been incorporated in the global reaction rate expressions utilized in 1D modeling.

Researchers typically model experimental data by curve fitting to different reaction rate expressions, either based on mathematical formulation of chemical laws or by using a power rate expression [19]. While this curve fit works well for their own particular data, it may not agree and in some cases fails to predict experimental data of the same catalyst formulation, but different values for dispersion or particle diameter [91, 114, 273]. Sometimes the values used to curve fit the data can even lead to unscientific outcomes or a disagreement with results from other papers [114, 274-276 100, 112]. This leads to confusion within the modeling community as to the proper kinetic parameters to utilize. Because of the non-linearity of the kinetic expressions, researchers have been known to use the same reaction rate formulation, but different values in order to model to their experimental data [102, 114]. Even the earlier efforts at KU within Dr. Depcik's laboratory used to follow the same technique.

However, after analyzing the history of the individual reactions, a better methodology exists how to simulate the chemical reactions on the surface for multiple sets of data using a single global reaction rate expression. To understand this in detail, consider the global reaction rate expression of CO oxidation as given in Chapter 3:

$R_{CO} = \frac{k K_{CO} K''^{1/2}_{O_2} p_{CO} p^{1/2}_{O_2}}{\left(1 + K_{CO} p_{CO} + K''^{1/2}_{O_2} p^{1/2}_{O_2}\right)^2}$	(CO-RDS-*c*)

where the adsorption equilibrium constants are:

$K_{CO} = \frac{k_a}{k_{-a}} = A_{CO} \exp\left(-\frac{\Delta H_{CO}}{R_u T_m}\right)$	(274)
$K_{O_2} = \frac{k_b}{k_{-b}} = A_{O_2} \exp\left(-\frac{\Delta H_{O_2}}{R_u T_m}\right)$	(275)

with *k* given by the Arrhenius expression:

$k = A \exp\left(-\frac{E_a}{R_u T_m}\right)$	(276)

It is common practice to adjust the heats of adsorption, activation energy, and pre-exponential factors in order to fit a simulation to the data. However, history dictates that oxygen and CO adsorption are not structure sensitive; e.g., there is insignificant variation in the enthalpies of adsorption and desorption for CO and oxygen. In addition, the values of heat of adsorption can be found experimentally and, therefore, do not need to be predicted or assumed. Similarly, the values of the pre-exponential factors (A_{CO} and A_{O_2}) can be calculated using kinetic gas theory [277]. Finally, experimental data illustrates that the activation energy decreases with increasing dispersion. As a result, the reaction rate expression can be determined through a systematic experimental study of CO conversion curves over platinum/alumina surfaces using different dispersion values while maintaining the same BET characteristics. Moreover, the pre-exponential factor in the CO-RDS will increase in value with respect to dispersion, as it leads to more sites for the reaction to occur. All these findings, when collectively applied will result in a model that can predict a different conversion over the same catalyst through dissimilar dispersion values, thus making the model truly global and independent. In addition, the literature dictates that as the catalyst

ages, its dispersion decreases due to a sintering effect of temperature and species. This new adaptive model will have the capability to predict this change without adjusting values or re-calibration. This will enhance the models, as the reaction kinetics will now work for the lifetime of the catalyst.

As a result, other work by the author, his advisor and a colleague in the lab have published an initial paper based on this adaptive kinetics framework [31]. This effort proved to be a good learning experience and the derivation of a more fundamental kinetics model is occurring utilizing the help of collaborators within the chemical engineering department. This merging of chemical and mechanical engineering will result in unique efforts of KU researchers and is a direct result of the research of the author in this thesis. Since model formulation is still occurring, it is too preliminary to add this effort to this thesis; however, the historical background presented in Chapter 3 provides the framework of understanding.

5.2 Modified 1D Model:

As discussed in the previous chapters, the modified 1D model should simulate both low and high flow conditions; whereas, because of the assumptions utilized in its formulation, the classical model may not be suited for low flow conditions. In this chapter, the modified 1D model is first tested under traditional moderate to high flow conditions, as it should produce the same result as the classical 1D model. Then, the influence of conduction and diffusion will be explored through parametric studies involving low flow conditions.

In order to perform a realistic test of the model, the experimental CO oxidation light-off curves from Arnby et al. [124] are utilized. Values of various parameters required for modeling are given in Table 1; however, other components like the pre-exponential factor and heat of adsorption (as previously discussed in section 5.1) are required. As mentioned

earlier, the author has already collaborated on a published CO oxidation adaptive kinetics paper. As a result, the values for the different parameters in the reaction rate expression are obtained from this paper and provided in Table 2 [31]. This will validate the model developed by the author and allow for comparison between the classical and modified 1D model.

Table 2. Calibrated Parameters for Arnby et al. 2004 data [31]

Parameters	Units	Values
k	[mol m^{-2} s^{-1}]	6.861×10^{16}
E_a	[kJ mol^{-1}]	119.01
A_{CO}	[atm^{-1}]	67.40
ΔH_{CO}	[kJ mol^{-1}]	-27.98
A_{O_2}	[atm^{-1}]	4.436×10^{-6}
ΔH_{O_2}	[kJ mol^{-1}]	-19.36

However, before simulating the flow condition, it is necessary to determine the limit on the round off error so as to produce consistent results. The simulation was performed for both classical and modified model on both the CO concentration of 0.1% and 0.01%. The result of the simulations are displayed in the Table 3.

Table 3. Error in Simulation for Various Error Limits

CO Conc.	Round off error limit	T_{50} Exp (K)	T_{50} Class (K)	T_{50} Mod (K)	% Error Class	% Error Mod
0.01%	10^{-5}	398.65	404.47	403.25	1.46	1.15
	10^{-6}		403.51	402.44	1.22	0.90
	10^{-7}		403.14	402.45	1.12	0.90
	10^{-8}		403.14	402.45	1.11	0.90
0.1%	10^{-5}	455.97	449.05	447.45	1.51	1.86
	10^{-6}		448.48	447.15	1.64	1.93
	10^{-7}		448.47	447.15	1.63	1.93
	10^{-8}		448.47	447.15	1.63	1.93

From the above table it is clear that the simulation yields stable result for limit of 10^{-7} for 0.01% CO and 10^{-6} for 0.1% CO. Although the difference in error is small, it is important to choose proper limit for reproduction of results. In addition, in case of 0.1% CO, the error

appears to be increasing with decrease in error limit; however, it is more important to yield a stable result as compared to an inconsistent result. The results may be little bit inaccurate as same values are used for different parameters in reaction rate expression for both 0.01% CO and 0.1% CO.

Utilizing the information provided, conversion curves for 0.01% CO and 0.1% CO in 10% oxygen and balance nitrogen are modeled as shown in Figure 19. The figure illustrates that the modified 1D model provides the same result as classical model. This is demonstrated by the fact that for the 0.01% CO oxidation experiment, the light off temperature (50% conversion) of the modified model is 402.4K and for classical model, it is 402.9K. This is because Peclet number for diffusion of heat in these cases is 64, while Peclet number for diffusion of the species is about 115. Hence, as discussed earlier in Chapter 1, neither conduction nor diffusion will have significant impact on the catalyst model, resulting in the same result from both classical and modified 1D models.

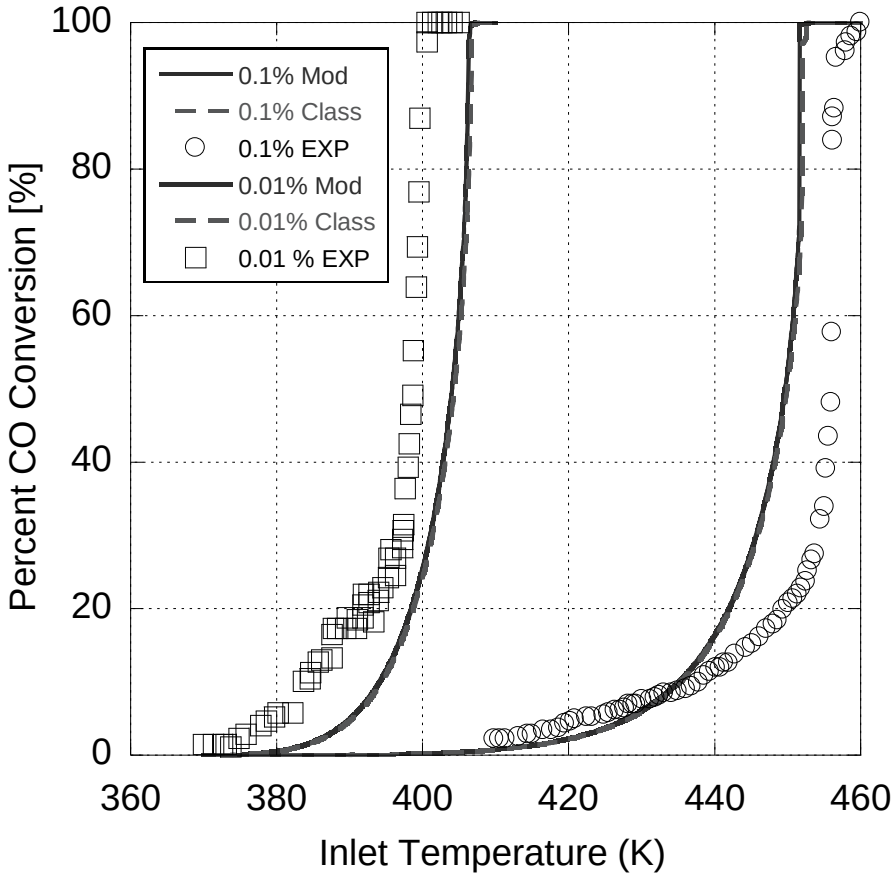

Figure 19: Comparison of Classical and Modified 1D Model Conversion Curves for CO Oxidation

It is important to note that the slight variation between the experimental data and simulation results is due to the use of adaptive kinetics rather than calibrating the expression to each set of data. Since, the kinetic parameters are not fit to each data set; a deviation is inevitable in the simulation studies. Efforts are underway at reducing this difference under a wide variation of catalyst metal parameters as discussed.

In order to explore the modified model under low flow conditions, it would be pertinent to have experimental data for this situation. However, the author could not find and does not have access to such data; hence, the same experiment from before is simulated for low flow conditions by performing a parametric study on velocity. In Figure 19, the flow

velocity of the experiment is 17000 hr^{-1} (0.1086 m/s). The parametric study involves decreasing the flow velocity to values of 0.05, 0.02, 0.01, and 0.005 m/s for the same experimental inlet conditions of pressure, temperature and species. Furthermore, this effort is accomplished for both the 0.01% and 0.1% CO conditions in order to investigate the effect of decreasing velocity on both conversion curves.

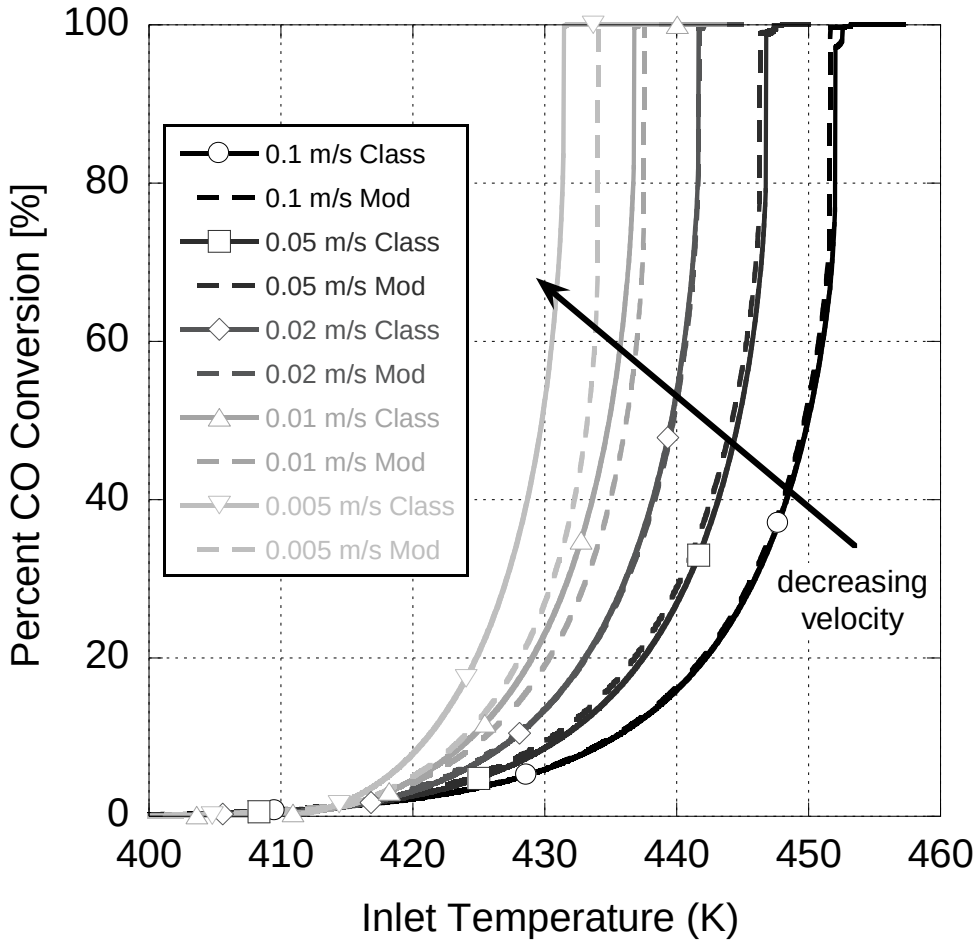

Figure 20: Simulation of 0.1% CO Conversion at Various Velocities.

From Figure 20, simulating 0.1% CO conversion using the modified model at low flow velocities around 10% and 5% of the original flow indicates a light off temperature of 436.18K and 433.22K; however, the classical models at the same velocities yield 434.90K and 429.73K respectively, which is a significant difference. This reduction in velocity is within the limit of the LNT dual leg system that is 5-10% of the actual flow value. Hence,

this indicates that the modified model must be used instead of classical model at low flow conditions.

Figure 21 shows simulation results for 0.01% CO conversion at different flow velocities. Light off temperatures at 10% and 5% of the original velocities simulated by modified model are 399.35K and 397.93K respectively; whereas, at the same reduced speeds the classical model yields 397.85K and 394.27K. This further indicates that modified model must be used for one dimensional model in simulating regeneration leg of LNT. Since, experimental data at low flow rates for CO oxidation is not available, this conclusion cannot be verified directly through experiments.

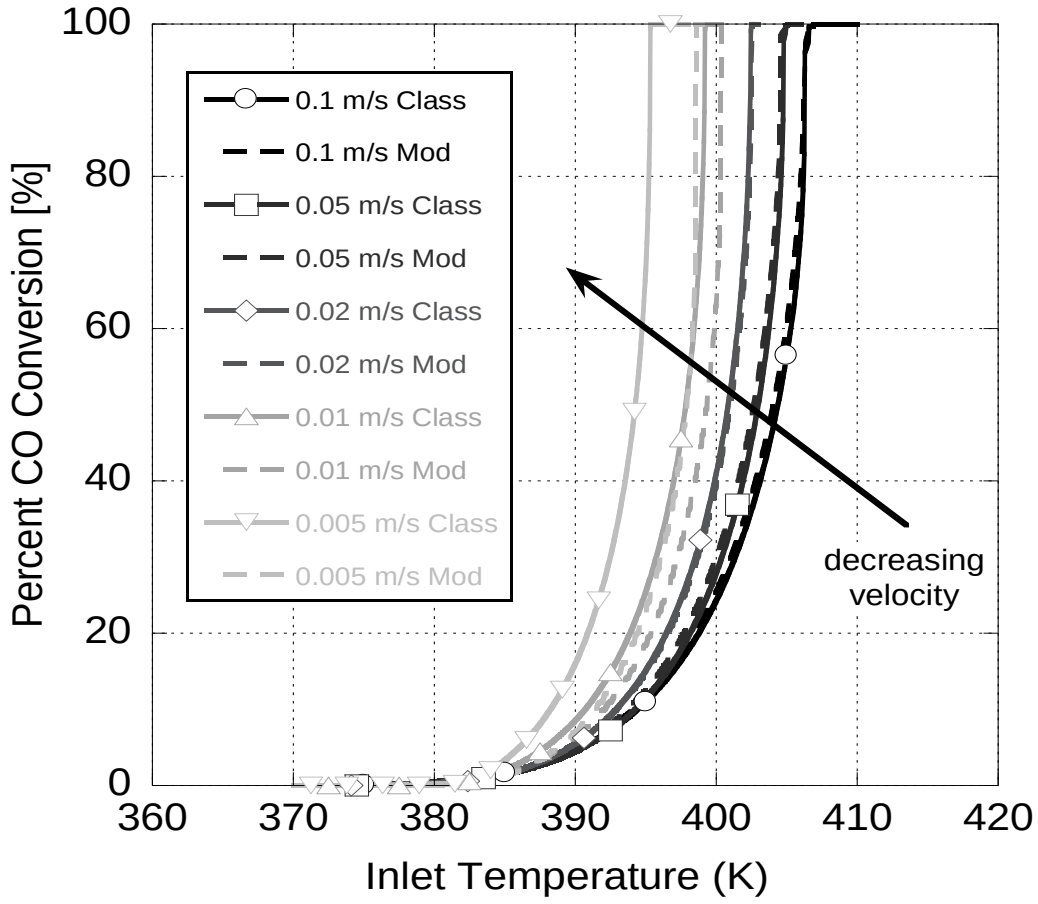

Figure 21: Simulation of 0.01% CO Conversion at Various Velocities.

This increase in accuracy does come with a drawback as the modified 1D model consumes more computational resources as compared to the classical 1D model. Figure 22 illustrates that as the number of computational nodes increases, the run time of the modified model increases more significantly than that of the classical model. Both classical and modified models use an iterative method in order to solve for the bulk temperature and species equations. Since the classical model involves only a first order derivative, individual nodes are iterated; however, the modified method involves a second order derivative resulting in the necessity to iterate over all the nodes simultaneously. Hence, as number of nodes increases, the modified model will consume more time and resources as compared to classical model. In this comparison, the computer architecture involved an Intel Core i7 – 2600 processor with 3.4 GHz clock speed, 4GB RAM (3.24 usable) and the operating system was 32-bit Windows 7. Twenty experiments were run for each data point and the standard deviation in run time is indicated on the graph.

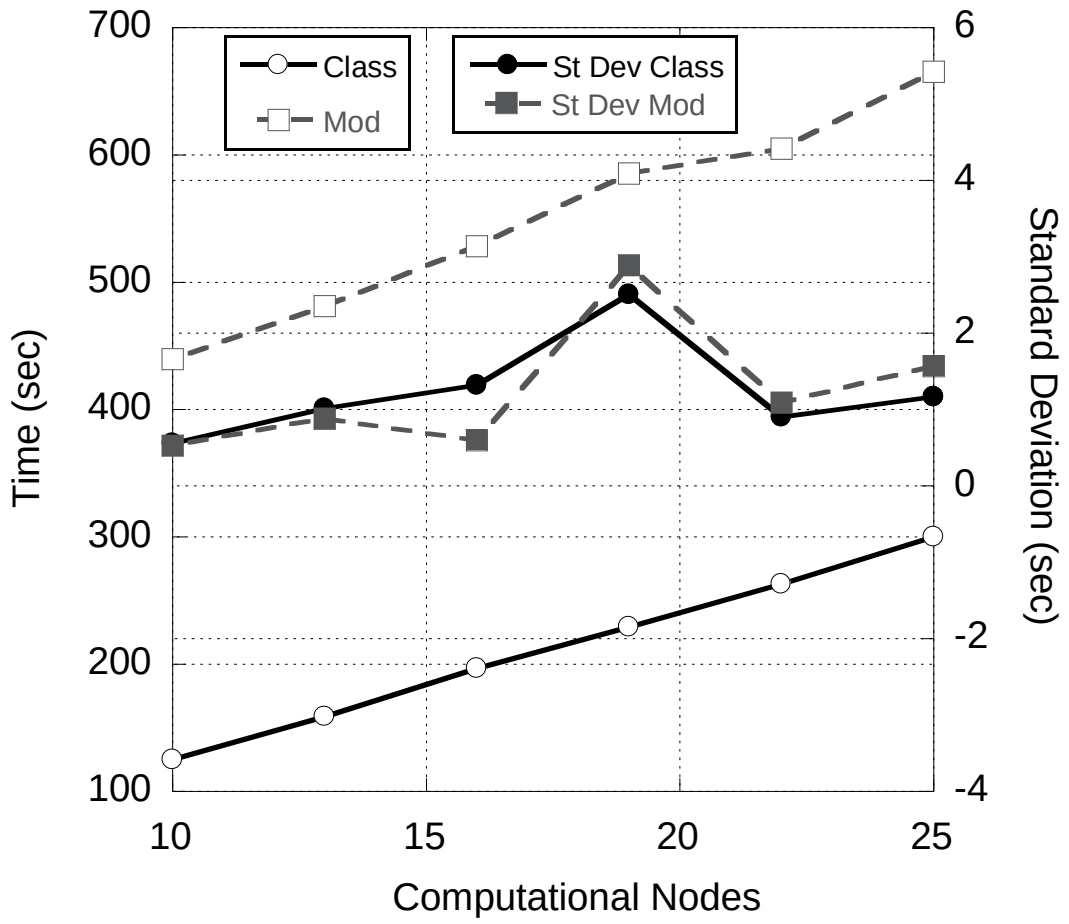

Figure 22: Computational Time for Both of the Models for Different Nodes in 0.01% CO Oxidation Simulation.

At this point in the analysis, it is clear that using the modified model comes at a cost of time and computational resources. Because one of the focuses of the author includes a better understanding of the catalytic surface in order to minimize costs (relating back to Chapter 1), running the modified model will help determine the proper loading of the metal catalyst on the washcoat.

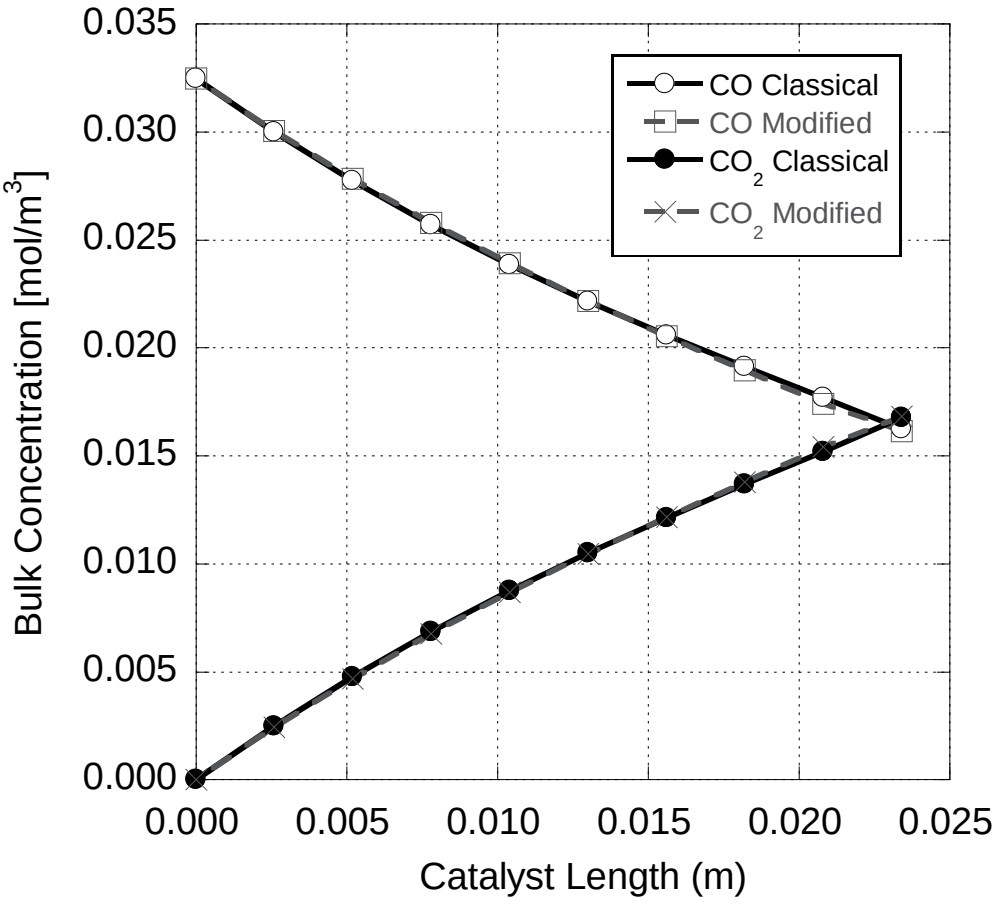

Figure 23: Bulk Concentration of Gases across the Catalyst at 50% Conversion for 0.108 m/s.

For example, in Figure 23 under the original flow rate conditions, the modified and classical models predict nearly the same concentration level across the length of the catalyst as shown at the light off temperature point. This point is a significantly important parameter in catalyst operation as it determines the temperature at which converter goes from a non-functional state (i.e., near zero conversion and kinetically limited) to a functional state (i.e., near 100% conversion and mass transfer limited).

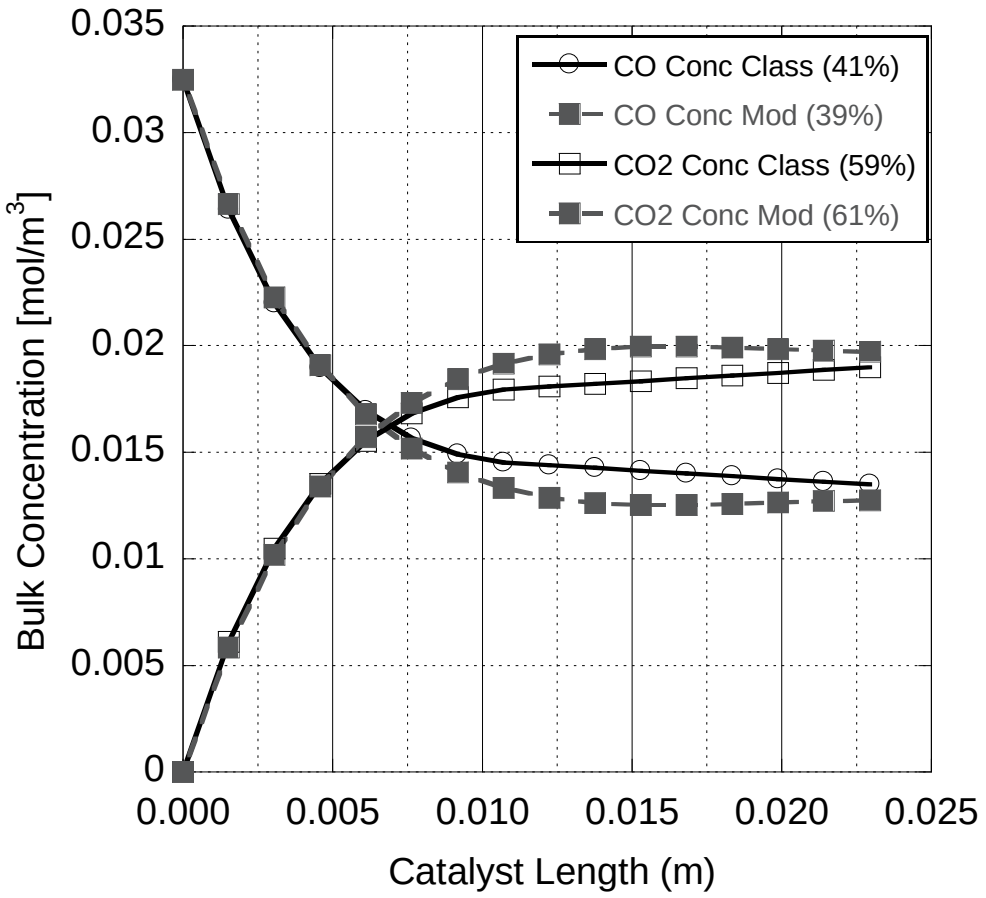

Figure 24: Bulk Concentration of Gases across the Catalyst at 50% Conversion for 0.01 m/s

However, when the velocity is reduced to 10% of the original flow rate (similar to a situation involving LNT regeneration in a dual leg), the modified model predicts a dissimilar conversion profile as indicated in Figure 24. This indicates at low flow velocities, the conversion of toxic gas increases and light off can occur at reduced temperatures.

5.3 Conclusion:

To date, the classical 1D model effectively simulates a wide range of catalytic converters. However, with the advent of new catalytic washcoat formulations and low velocity regenerative operations, the bulk gas phase equations need to be modified in order to take into consideration the phenomena of diffusion and conduction. This thesis describes the

existing model, the assumptions made in its development along with its associated drawbacks. From this analysis, a modified version of the model including diffusion and conduction is presented from a first principles basis. When developing this model, the author addresses various issues such as the energy equation paradox under dynamic incompressible flow and the formulation of a predictive diffusion coefficient.

For both models, of significant importance is the inclusion of an accurate reaction rate expression that can simulate the surface. To this end, the reaction rate expressions for CO, H_2 and NO oxidation are formulated from first principles for inclusion. While this is accomplished in the absence of other gases present in engine exhaust that influence converter efficiency, the goal was first to obtain knowledge in this chemical engineering realm. This stepwise approach will combine with efforts of other students working with Dr. Depcik, both in Mechanical and Chemical Engineering, in order to build a fundamental chemical reaction mechanism. It has already led to a better understanding of the influence of catalyst properties on the reaction rate and a publication illustrating an adaptive kinetics approach, unique to the literature in this area. Hence, future efforts will continue to build model complexity through combining the reactions while including an adaptive modeling component.

To illustrate the differences between the classical and modified 1D models, they were tested under both low and high flow conditions. The author began this work with the initial assumption that the classical model will fail for low flow conditions, results demonstrate that this is in fact true in the LNT flow velocity regimes. In addition, when understanding catalyst material placement on the surface, the modified 1D model will improve the predictive capabilities and help improve the low temperature performance of the catalyst.

Finally, this thesis will help Dr Depcik's efforts in this field and can be utilized as a starting point for future students in the area of catalyst modeling. The report is intended to introduce a student to the various aspects involved in catalyst modeling; fluid mechanics, source terms and chemical species. It is applicable for both TWC and LNT devices and can aid in catalytic material placement and modeling for dual leg LNT systems. The only issue is that while the diffusion calculation in the model is subject to some inaccuracies, research demonstrates that the methodology employed by the authors will be within an error range of eight percent [74].

Appendix I: MATLAB Code

Classical 1D Model:

```
% Classical 1D Modeling of Catalytic Converter

% Assigning Numbers to Species
% 1:CO
% 2:CO2
% 3:H2O
% 4:O2
% 5:Nitrogen

clc;            % Clear Screen
close all;      % Close All Windows
clear all,      % Clear All Data

tic;            % Start of Time

% Defining Global Variables
global AC
global Eps
global ShSurf
global DiffMix
global d
global Concbulk
global Tm
global i
global R
global Pres
global RR
global EffDia
global EffMol
global EffKBEp
global U

% Values of Coefficients from Chemkin for Calculation of Specific Heat and
Enthalpy of Gases (300 to 1000 K)

a11=3.262451;   a12=0.0015119409;   a13=-0.000003881755;
a14=0.000000005581944;  a15=-0.000000000002474951;  a16=-14310.539;     %
Coefficients of CO
a21=2.275724;   a22=0.009922072;    a23=-0.000010409113;
a24=0.000000006866686;  a25=-0.00000000000211728;   a26=-48373.14;      %
Coefficients of CO2
a31=3.386842;   a32=0.003474982;    a33=-0.000006354696;
a34=0.000000006968581;  a35=-0.000000000002506588;  a36=-30208.11;      %
Coefficients of H2O
a41=3.212936;   a42=0.0011274864;   a43=-0.000000575615;
a44=0.00000000013138773; a45=-0.0000000000008768554; a46=-1005.249;      %
Coefficients of O2
a51=3.298677;   a52=0.0014082404;   a53=-0.000003963222;
a54=0.000000005641515;  a55=-0.000000000005641515;  a56=-1020.8999;     %
Coefficients of Nitrogen
```

```
% Properties of Gas from Fundamentals of Heat and Mass Transfer by Frank
Incorpera
K=0.0338;       % Constant Thermal Conductivity for Gases (W/mK)
R=8.314;        % Universal Gas Constant (J/K/Mol)

% Properties of Monolith from IMECE Paper
Rhom=1800;      % Constant Density for Monolith (kg/m^3)
Km=1.5;         % Constant Thermal Conductivity for Monolith (W/mk)
Cpm=1020;       % Constant Specific Heat for Monolith at Constant Pressure
(J/KgK)

% For Calculating Diffusion from Diffusion Mass Transfer in Fluid System
by Cussler
Dia(1)=3.69;                % Diameter of CO
Dia(2)=3.941;               % Diameter of CO2
Dia(3)=2.641;               % Diameter of H2O
Dia(4)=3.467;               % Diameter of O2
Dia(5)=3.798;               % Diameter of Nitrogen
EpKB(1)=91.7;               % Epsilon by Kb for Carbon Monoxide
EpKB(2)=195.2;              % Epsilon by Kb for Carbon Dioxide
EpKB(3)=809.1;              % Epsilon by KB for H2O
EpKB(4)=106.7;              % Epsilon by Kb for Oxygen
EpKB(5)=71.4;               % Epsilon by Kb for Nitrogen

% Standard Properties
Mol(1)=28.0101;             % Molecular Weight of CO (Kg/Kmol)
Mol(2)=44.0095;             % Molecular Weight of CO2 (Kg/kmol)
Mol(3)=18.01528;            % Molecular Weight of H2O (Kg/Kmol)
Mol(4)=32;                  % Molecular Weight of O2 (Kg/Kmol)
Mol(5)=28.01348;            % Molecular Weight of Nitrogen (Kg/Kmol)

% Experimental Values from Arnby et al. 2004
U=0.16;                                         % Inlet Velocity for the
Monolith (m/s)
L=0.023;                                            % Length of Catalytic
Converter for Discretization (m)
D=0.013;                                            % Catalytic Converter
Diameter (m)
CPSI=400/0.00064516;                                % Channels per Square
Meter
d=0.001;                                            % Side of Square
Channel (m)
N=82;                                               % Number of Channels
h=input('Enter the Discretization number: ');       % Number of
Discretization
Pres=101325;                                        % Pressure at Which
Diffusion is to be Calculated (pas)

% Geometrical Constants
Eps=(N*d*d*4)/(pi*D*D);                             % Value of Epsilon
Ga=4*Eps/d;                                         % Geometric Surface
Area per Unit Volume (/m)
AC=Ga/(1-Eps);                                      % Area Constant (Ga/1-
Epsilon) (/m)
```

```
options=odeset('RelTol',1e-6,'Stats','on');          % Option for ODE
Solver

% Discretization Values of Model
delx=L/(h-1);                                        % Discretization
Length
x=1:1:h;                                             % Length Array

% Initial Condition
Conc(1)=0;          % Inlet CO Concentration (Mole Fraction)
Conc(2)=0;          % Inlet CO2 Concentration (Mole Fraction)
Conc(3)=0;          % Inlet H2O Concentration (Mole Fraction)
Conc(4)=0;          % Inlet O2 Concentration (Mole Fraction)
Conc(5)=1;          % Inlet Nitrogen Concentration (Mole Fraction)

% Initial Calculations for Species Modeling
MolMassMix=0;                                                    %
Initilization
for j=1:5
    for k=1:5
        EffDia(j,k)=0.5*(Dia(j)+Dia(k));                         %
Calculation of Effective Collision Diameter
        EffMol(j,k)=((Mol(j)+Mol(k))/(Mol(j)*Mol(k)))^0.5;       %
Calculation of Effective Molecular Weight
        if j~=k
        EffKBEp(j,k)=(1/((EpKB(j)*EpKB(k))^0.5));                %
Effective Energy Calculation
        end
    end
    MolMass(j)=Conc(j)*Mol(j);                                   %
Molecular Mass of Individual Species in 1 Kmol of Mixture (Kg/Kmol)
    MolMassMix=MolMassMix+MolMass(j);                            %
Calculation of Molecular Mass of Mixture (Kg/Kmol)
end
Rmass=(R*1000)/MolMassMix;                                       % Gas
Constant of Mixture (J/Kg/K)
Tin=370;                                                         % Initial
Temperature across the catalyst
Rho=Pres/(Rmass*Tin);                                            % Density
(Kg/m^3)
for j=1:5
    Cin(j)=(Rho/MolMassMix)*Conc(j)*1000;                        % Inlet
Concentration of Individual Species (mol/m^3)
end

% Geometrical Calculation of the Catalytic Converter
Nu=2.98;                                                         %
Nusselt's Number for Heat Transfer Coefficient
Hc=Nu*K/d;                                                       % Heat
Transfer Coefficient (W/m^2/K)
delt=((2*Rhom*Cpm)/(((4*Km)/(delx*delx))+(Hc*AC)));              % Defining
the Time Difference for Monolith Temperature Modeling
a=1;                                                             % Defining
the Initial Value for Time
S=1;
```

```
% Checking for Stability
TimeStep=0.5;                                                    % Defining
the Time Step as Per Temperature Ramp
if TimeStep<delt
    dt=TimeStep;
else
    exit;
end

% Initilization of Various Parameters
for i=1:h
    Tia(i)=300;                          % Initial Temperature Values
Across the Bulk
    Tm(i)=300;                           % Initial Monolith Temperatures
    RR(i)=0;                             % Initialization of Reaction Rate
at Various Nodes
    for j=1:5
        Concbulk(i,j)=Cin(j);            % Initial Concentration of Each
Species
        Csurf(i,j)=Cin(j);               % Initial Concentration of Each
Species at Surface
    end
end


% Starting Caluclation for New Time step

for Tin=370:0.0416665:420
    Tia(1)=Tin;                          % Input Temperature at the Given
Time Step
    Toa(1)=Tin;

    % Input Concentrations
    Conc(1)=0.0001;                      % Inlet CO Concentration (% Vol)
    Conc(2)=0;                           % Inlet CO2 Concentration (% Vol)
    Conc(3)=0;                           % Inlet H2O Concentration (% Vol)
    Conc(4)=0.1;                         % Inlet O2 Concentration (% Vol)
    Conc(5)=0.8999;                      % Inlet Nitrogen Concentration (%
Vol)

    % Initial Calculations for Species Modeling
    MolMassMix=0;                                                %
Initialization
    for j=1:5
        MolMass(j)=Conc(j)*Mol(j);                               %
Molecular Mass of Individual Species in 1 Kmol of Mixture (Kg/Kmol)
        MolMassMix=MolMassMix+MolMass(j);                        %
Calculation of Molecular Mass of Mixture (Kg/Kmol)
    end

    for j=1:5
        Y(1,j)=(Conc(j)*Mol(j))/MolMassMix;                      % Mass
Fraction of Individual Species
        X(1,j)=Conc(j);                                          % Mole
Fraction
```

```
        Concbulk(1,j)=(Rho/MolMassMix)*Conc(j)*1000;                % 
Inlet Concentration of Individual Species (mol/m^3)
    end

% Calculation of Monolith Temperature at Next Time Step.
    for i=1:h
        % Calculations of Enthalpy at Node 1

Hp(i,1)=R*Tm(i)*(a11+(a12*Tm(i)/2)+(a13*Tm(i)*Tm(i)/3)+(a14*Tm(i)*Tm(i)*Tm
(i)/4)+(a15*Tm(i)*Tm(i)*Tm(i)*Tm(i)/5)+(a16/Tm(i)));      % Calculation of
Enthalpy for CO

Hp(i,2)=R*Tm(i)*(a21+(a22*Tm(i)/2)+(a23*Tm(i)*Tm(i)/3)+(a24*Tm(i)*Tm(i)*Tm
(i)/4)+(a25*Tm(i)*Tm(i)*Tm(i)*Tm(i)/5)+(a26/Tm(i)));      % Calculation of
Enthalpy for CO2

Hp(i,3)=R*Tm(i)*(a31+(a32*Tm(i)/2)+(a33*Tm(i)*Tm(i)/3)+(a34*Tm(i)*Tm(i)*Tm
(i)/4)+(a35*Tm(i)*Tm(i)*Tm(i)*Tm(i)/5)+(a36/Tm(i)));      % Calculation of
Enthalpy for H2O

Hp(i,4)=R*Tm(i)*(a41+(a42*Tm(i)/2)+(a43*Tm(i)*Tm(i)/3)+(a44*Tm(i)*Tm(i)*Tm
(i)/4)+(a45*Tm(i)*Tm(i)*Tm(i)*Tm(i)/5)+(a46/Tm(i)));      % Calculation of
Enthalpy for O2

Hp(i,5)=R*Tm(i)*(a51+(a52*Tm(i)/2)+(a53*Tm(i)*Tm(i)/3)+(a54*Tm(i)*Tm(i)*Tm
(i)/4)+(a55*Tm(i)*Tm(i)*Tm(i)*Tm(i)/5)+(a56/Tm(i)));      % Calculation of
Enthalpy for Nitrogen

        % Total Heat Released from Reactions
        THR(i)=((-Hp(i,1)*RR(i))+(Hp(i,2)*RR(i))-(Hp(i,4)*RR(i)*0.5));

        if i==1
            Qcond(i)=(((Km*dt*2)/(Rhom*Cpm*delx*delx))*(Tm(i+1)-Tm(i)));
% Heat From Conduction
            Qconv(i)=(((Hc*AC*dt)/(Rhom*Cpm))*(Tia(i)-Tm(i)));
% Heat From Convection
            Tmf(i)=Tm(i)+Qcond(i)+Qconv(i)-(((dt)/(Rhom*Cpm*(1-
Eps)))*THR(i));    % End Boundary Condition for Monolith at the Start
        elseif i<h
            Qcond(i)=(((Km*dt)/(Rhom*Cpm*delx*delx))*(Tm(i+1)-
2*Tm(i)+Tm(i-1)));  % Heat From Conduction
            Qconv(i)=(((Hc*AC*dt)/(Rhom*Cpm))*(Tia(i)-Tm(i)));
% Heat From Convection
            Tmf(i)=Tm(i)+Qcond(i)+Qconv(i)-(((dt)/(Rhom*Cpm*(1-
Eps)))*THR(i));    % Calculations of Monolith Temperature at New Node
        else
            Qcond(i)=(((Km*dt*2)/(Rhom*Cpm*delx*delx))*(Tm(i-1)-Tm(i)));
% Heat From Conduction
            Qconv(i)=(((Hc*AC*dt)/(Rhom*Cpm))*(Tia(i)-Tm(i)));
% Heat From Convection
            Tmf(i)=Tm(i)+Qcond(i)+Qconv(i)-(((dt)/(Rhom*Cpm*(1-
Eps)))*THR(i));    % End Boundary Condition for Monolith at the End
        end
    end
    for i=1:h
        Tm(i)=Tmf(i);
```

```
    end

    % Calculation for Node 1-------------------------------------------
-
    i=1;

    % Diffusion of Species in mixture
    [DiffMix, ShSurf]=DiffusionCalculator(Toa,X,Y);
% Calling Diffusion Calculator at the Node

    % Species Modeling at Node 1 on Monolith
    delb=1;
% Initialization of Error for Surface Concentrations
    while delb>0.000001
        [t,Z]=ode15s(@SpeciesODECO, [0 dt], Csurf(i,:),options);
% Calling ODE Solver for Initial Node
        [m,n]=size(Z);
        Csurfo(1,1)=Z(m,1);
% Putting the Values back in Designated Species
        Csurfo(1,2)=Z(m,2);
% Putting the Values back in Designated Species
        Csurfo(1,3)=Z(m,3);
% Putting the Values back in Designated Species
        Csurfo(1,4)=Z(m,4);
% Putting the Values back in Designated Species
        Csurfo(1,5)=Z(m,5);
% Putting the Values back in Designated Species
        for j=1:5
            B(j)=abs(Csurfo(i,j)-Csurf(i,j));
% Calculation of Error
            Csurf(i,j)=Csurfo(i,j);
% Putting Values Back for Further Calculations
        end
        delb=max(B);
% Calculating Maximum Error
    end

    % End of Calculation for Node 1

    % Calculations for Internal Nodes-----------------------------------
-
    for i=2:h

        delc=1;
        while delc>0.000001

            % Calculation of Mass Fraction at Individual Point
            ConcTot=0;
% Initialization of Total Concentration
            for j=1:5
                ConcTot=ConcTot+Concbulk(i,j);
% Total Concentration at New Node
            end
            for j=1:5
```

```
                X(i,j)=((Concbulk(i,j)/ConcTot));
% Mole Fraction of Individual Species
            end
            Na=isnan(X(i,:));
            for j=1:5
               if Na(j)==1
                  X(i,j)=0;
               end
            end

            MolMassMix=0;
% Initialization of Molecular Mass
            for j=1:5
                MolMass(j)=X(i,j)*Mol(j);
% Molecular Mass of Individual Species in 1 Kmol of Mixture (Kg/Kmol)
                MolMassMix=MolMassMix+MolMass(j);
% Calculation of Molecular Mass of Mixture (Kg/Kmol)
            end
            for j=1:5
                Y(i,j)=(X(i,j)*Mol(j))/MolMassMix;
% Mass Fraction of Individual Species
            end

            Na=isnan(Y(i,:));
            for j=1:5
               if Na(j)==1
                  Y(i,j)=0;
               end
            end

            % Modeling Bulk Temperature

            % Calculations of Specific Heat

Cp(i,1)=R*(a11+a12*Tia(i)+a13*Tia(i)*Tia(i)+a14*Tia(i)*Tia(i)*Tia(i)+a15*T
ia(i)*Tia(i)*Tia(i)*Tia(i));

Cp(i,2)=R*(a21+a22*Tia(i)+a23*Tia(i)*Tia(i)+a24*Tia(i)*Tia(i)*Tia(i)+a25*T
ia(i)*Tia(i)*Tia(i)*Tia(i));

Cp(i,3)=R*(a31+a32*Tia(i)+a33*Tia(i)*Tia(i)+a34*Tia(i)*Tia(i)*Tia(i)+a35*T
ia(i)*Tia(i)*Tia(i)*Tia(i));

Cp(i,4)=R*(a41+a42*Tia(i)+a43*Tia(i)*Tia(i)+a44*Tia(i)*Tia(i)*Tia(i)+a45*T
ia(i)*Tia(i)*Tia(i)*Tia(i));

Cp(i,5)=R*(a51+a52*Tia(i)+a53*Tia(i)*Tia(i)+a54*Tia(i)*Tia(i)*Tia(i)+a55*T
ia(i)*Tia(i)*Tia(i)*Tia(i));

            Cpmix=0;
            for j=1:5
                Cpmix=Cpmix+Cp(i,j)*X(i,j);
% Calculation of Constant Pressure Specific Heat mol Basis (J/mol/K)
            end
```

```
            Cpmixmass=Cpmix*1000/MolMassMix;
% Calculation of Constant Pressure Specific Heat kg Basis (J/Kg/K)
            Na=isnan(Cpmixmass);
            if Na==1
              Cpmixmass=0;
            end

            Toa(i)=(Tia(i-
1)+((delx*4*Hc)/(d*Rho*Cpmixmass*U))*(Tm(i)))/(1+((delx*4*Hc)/(d*Rho*Cpmix
mass*U)));  % Calculation of Bulk Temperatures

            % Diffusion of Species in Mixture
            [DiffMix, ShSurf]=DiffusionCalculator(Toa,X,Y);
% Calling Diffusion Calculator at the Node

            % Calculation of Bulk Concentration using Gauss Jordon Method
            for j=1:5
                Concbulko(i,j)=(Concbulk(i-
1,j)+((delx*4*ShSurf(j)*DiffMix(j))/(U*d*d))*(Csurf(i,j)))/(1+(delx*4*ShSu
rf(j)*DiffMix(j))/(U*d*d));       % Calculation of Species Concentration
at Various Points
                C(j)=abs(Concbulko(i,j)-Concbulk(i,j));
                Concbulk(i,j)=Concbulko(i,j);
            end

            % Calculation of New Diffusion Coefficients for the Bulk
Concentrations
            ConcTot=0;
% Initialization of Total Concentration
            for j=1:5
                ConcTot=ConcTot+Concbulk(i,j);
% Total Concentration at the New Node
            end
            for j=1:5
                X(i,j)=((Concbulk(i,j)/ConcTot));
% Mole Fraction of Individual Species
            end

            MolMassMix=0;
% Initialization of Molecular Mass
            for j=1:5
                MolMass(j)=X(i,j)*Mol(j);
% Molecular Mass of Individual Species in 1 Kmol of Mixture (Kg/Kmol)
                MolMassMix=MolMassMix+MolMass(j);
% Calculation of Molecular Mass of Mixture (Kg/Kmol)
            end
            for j=1:5
                Y(i,j)=(X(i,j)*Mol(j))/MolMassMix;
% Mass Fraction of Individual Species
            end

            [DiffMix, ShSurf]=DiffusionCalculator(Toa,X,Y);
% Calling Diffusion Calculator at the Node

            % Calculations for Surface Concentrations
```

```
            delb=1;
% Initialization of Error for Surface Concentrations
            while delb>0.0000001
                [t,Z]=ode15s(@SpeciesODECO, [0 dt], Csurf(i,:),options);
% Calling ODE Solver for Initial Node
                [m,n]=size(Z);
            Csurfo(i,1)=Z(m,1);
% Putting the Values back in Designated Species
            Csurfo(i,2)=Z(m,2);
% Putting the Values back in Designated Species
            Csurfo(i,3)=Z(m,3);
% Putting the Values back in Designated Species
            Csurfo(i,4)=Z(m,4);
% Putting the Values back in Designated Species
            Csurfo(i,5)=Z(m,5);
% Putting the Values back in Designated Species
                for j=1:5
                    B(j)=abs(Csurfo(i,j)-Csurf(i,j));
% Calculation of Error (Infinity Norm)
                    Csurf(i,j)=Csurfo(i,j);
% Putting Values Back for Further Calculations
                end
            delb=max(B);
% Calculating Maximum Error
            end

             C(6)=abs(Toa(i)-Tia(i));    % Arbitrary Array for Calculating
Error
             Tia(i)=Toa(i);              % Putting Value Back
             delc=max(C);

        end
    end
    % End of Calculations for Intermediate Nodes-------------------------
------

    ResultTemp(a)=Tin;
    Conv(a,1)=((Concbulk(1,1)-Concbulk(h,1))/Concbulk(1,1))*100;      %
Conversion Percentage

    % Detrmining the Concentration of bulk species across the length of
the catalyst at 50% Conversion
    if Conv(a,1)>50 && S==1
        Conc50(:,:)=Concbulk(:,:);
        S=2;
    end

    a=a+1;
end

    % Plot for Conversion Vs Inlet Temperature
    figure;
    plot(ResultTemp,Conv(:,1))
    xlabel('Inlet Temperature (K)')
    ylabel('Conversion (%)')
    legend('Conversion Curve')
```

```
    title(['Conversion Curve for CO Oxidation at inlet CO concentration of
',num2str(Conc(1)*100),'%'])

    timespan=toc;           % End of time

% End of Program
```

Modified 1D Model:

```
% Modified 1D Modeling of Catalytic Converter

% Assigning Numbers to Species
% 1:CO
% 2:CO2
% 3:H2O
% 4:O2
% 5:Nitrogen

clc;            % Clear Screen
close all;      % Close All Windows
clear all;      % Clear All Data

tic;            % Start of Time

% Defining Global Variables
global AC
global Eps
global ShSurf
global DiffMix
global d
global Concbulk
global Tm
global i
global R
global Pres
global RR
global EffDia
global EffMol
global EffKBEp
global U
global L

% Values of Coefficients from Chemkin for Calculation of CP and Enthalpy
from (300 to 1000 K)

a11=3.262451;   a12=0.0015119409;   a13=-0.000003881755;
a14=0.000000005581944;  a15=-0.000000000002474951;  a16=-14310.539;     %
Coefficients of CO
a21=2.275724;   a22=0.009922072;    a23=-0.000010409113;
a24=0.000000006866686;  a25=-0.00000000000211728;   a26=-48373.14;      %
Coefficients of CO2
```

```
a31=3.386842;   a32=0.003474982;    a33=-0.000006354696;
a34=0.000000006968581;  a35=-0.000000000002506588;  a36=-30208.11;      %
Coefficients of H2O
a41=3.212936;   a42=0.0011274864;   a43=-0.000000575615;
a44=0.0000000013138773; a45=-0.0000000000008768554; a46=-1005.249;      %
Coefficients of O2
a51=3.298677;   a52=0.0014082404;   a53=-0.000003963222;
a54=0.000000005641515;  a55=-0.000000000005641515;  a56=-1020.8999;     %
Coefficients of Nitrogen

% From Fundamentals of Heat and Mass Transfer by Frank Incorpera
K=0.0338;       % Constant Thermal Conductivity for Gases (W/mK)
R=8.314;        % Universal Gas Constant (J/K/Mol)

% From IMECE Paper
Rhom=1800;      % Constant Density for Monolith (kg/m^3)
Km=1.5;         % Constant Thermal Conductivity for Monolith (W/mk)
Cpm=1020;       % Constant Specific Heat for Monolith at Constant Pressure
(J/KgK)

% From Diffusion Mass Transfer in Fluid System by Cussler
Dia(1)=3.69;                % Diameter of CO
Dia(2)=3.941;               % Diameter of CO2
Dia(3)=2.641;               % Diameter of H2O
Dia(4)=3.467;               % Diameter of O2
Dia(5)=3.798;               % Diameter of Nitrogen
EpKB(1)=91.7;               % Epsilon by Kb for Carbon Monoxide
EpKB(2)=195.2;              % Epsilon by Kb for Carbon Dioxide
EpKB(3)=809.1;              % Epsilon by KB for H2O
EpKB(4)=106.7;              % Epsilon by Kb for Oxygen
EpKB(5)=71.4;               % Epsilon by Kb for Nitrogen

% From Internet
Mol(1)=28.0101;             % Molecular Weight of CO (Kg/Kmol)
Mol(2)=44.0095;             % Molecular Weight of CO2 (Kg/kmol)
Mol(3)=18.01528;            % Molecular Weight of H2O (Kg/Kmol)
Mol(4)=32;                  % Molecular Weight of O2 (Kg/Kmol)
Mol(5)=28.01348;            % Molecular Weight of Nitrogen (Kg/Kmol)

% Values From User
U=0.16;                                     % Inlet Velocity for the
Monolith (m/s)
L=0.023;                                        % Length of Catalytic
Converter for Discretization (m)
D=0.013;                                        % Catalytic Converter
Diameter (m)
CPSI=400/0.00064516;                            % Channels per Square
Meter
d=0.001;                                        % Side of Square Channel
(m)
N=82;                                           % Number of Channels
h=input('Enter the Discretization number: ');   % Inlet Velocity for the
Monolith
Pres=101325;                                    % Pressure at Which
Diffusion is to be Calculated (pas)
```

```
% Geometrical Constants
Eps=(N*d*d*4)/(pi*D*D);                                          % Value of
Epsilon
Ga=4*Eps/d;                                                      %
Geometric Surface area per unit volume (/m)
AC=Ga/(1-Eps);                                                   % Area
Constant (Ga/1-Epsilon) (/m)
options=odeset('RelTol',1e-6,'Stats','on');                      % Option
for ODE Solver

% Discretization Values of Model
delx=L/(h-1);                                                    %
Discritization Length
x=1:1:h;                                                         % Length
Array

% Initial Condition
Conc(1)=0;          % Inlet CO Concentration (Mole Fraction)
Conc(2)=0;          % Inlet CO2 Concentration (Mole Fraction)
Conc(3)=0;          % Inlet H2O Concentration (Mole Fraction)
Conc(4)=0;          % Inlet O2 Concentration (Mole Fraction)
Conc(5)=1;          % Inlet Nitrogen Concentration (Mole Fraction)

% Initial Calculations for Species Modeling
MolMassMix=0;                                                    %
Initialization of Molecular Mass
for j=1:5
    for k=1:5
        EffDia(j,k)=0.5*(Dia(j)+Dia(k));                         %
Calculation of Effective Collision Diameter
        EffMol(j,k)=((Mol(j)+Mol(k))/(Mol(j)*Mol(k)))^0.5;       %
Calculation of Effective Molecular Weight
        if j~=k
        EffKBEp(j,k)=(1/((EpKB(j)*EpKB(k))^0.5));                %
Effective Energy Calculation
        end
    end
    MolMass(j)=Conc(j)*Mol(j);                                   %
Molecular Mass of Individual Species in 1 Kmol of Mixture (Kg/Kmol)
    MolMassMix=MolMassMix+MolMass(j);                            %
Calculation of Molecular Mass of Mixture (Kg/Kmol)
end
Rmass=(R*1000)/MolMassMix;                                       % Gas
Constant of Mixture (J/Kg/K)
Tin=370;                                                         % Initial
Temperature across the catalyst
Rho=Pres/(Rmass*Tin);                                            % Density
(Kg/m^3)
for j=1:5
    Cin(j)=(Rho/MolMassMix)*Conc(j)*1000;                        % Inlet
Concentration of Individual Species (mol/m^3)
end

% Geometrical Calculation of the Catalytic Converter
Nu=2.98;                                                         %
Nusselt's Number for Heat Transfer Coefficient
```

```
Hc=Nu*K/d;                                                          % Heat
Transfer Coefficient (W/m^2/K)
delt=((2*Rhom*Cpm)/(((4*Km)/(delx*delx))+(Hc*AC)));                 % Defining
the Time Difference for Monolith Temperature Modeling
a=1;                                                                % Defining
the Initial Value for Time
S=1;

% Checking for Stability
TimeStep=0.5;                                                       % Defining
the Time Step as Per Input File
if TimeStep<delt
    dt=TimeStep;
else
    exit;
end

% Initialization of Various Parameters
for i=1:h
    Tia(i)=300;                          % Initial Temperature Values
Across the Bulk
    Tiaf(i)=300;
    Tm(i)=300;                           % Initial Monolith Temperatures
    RR(i)=0;                             % Initialization of Reaction Rate
at Various Nodes
    for j=1:5
        Concbulk(i,j)=Cin(j);            % Initial Concentration of each
Species
        ConcbulkF(i,j)=Cin(j);
        Csurf(i,j)=Cin(j);               % Initial Concentration of each
Species at Surface
    end
end


% Starting Calculation for New Time step

for Tin=370:0.0416665:408
    Tia(1)=Tin;                          % Input Temperature at the given
Time Step
    Toa(1)=Tin;

    % Input Concentrations
    Conc(1)=0.0001;     % Inlet CO Concentration (% Vol)
    Conc(2)=0;          % Inlet CO2 Concentration (% Vol)
    Conc(3)=0;          % Inlet H2O Concentration (% Vol)
    Conc(4)=0.1;        % Inlet O2 Concentration (% Vol)
    Conc(5)=0.8999;     % Inlet Nitrogen Concentration (% Vol)

    % Initial Calculations for Species Modeling
    MolMassMix=0;                                                   %
Initialization of Molecular Mass
    for j=1:5
        MolMass(j)=Conc(j)*Mol(j);                                  %
Molecular Mass of Individual Species in 1 Kmol of Mixture (Kg/Kmol)
```

```
        MolMassMix=MolMassMix+MolMass(j);                                   %
Calculation of Molecular Mass of Mixture (Kg/Kmol)
    end

    for j=1:5
        Y(1,j)=(Conc(j)*Mol(j))/MolMassMix;                                 % Mass
Fraction of Individual Species
        X(1,j)=Conc(j);                                                     % Mole
Fraction
        Concbulk(1,j)=(Rho/MolMassMix)*Conc(j)*1000;                        %
Inlet Concentration of Individual Species (mol/m^3)
    end

% Calculation of Monolith Temperature at Next Time Step.
    for i=1:h
        % Calculations of Enthalpy at Node 1

Hp(i,1)=R*Tm(i)*(a11+(a12*Tm(i)/2)+(a13*Tm(i)*Tm(i)/3)+(a14*Tm(i)*Tm(i)*Tm
(i)/4)+(a15*Tm(i)*Tm(i)*Tm(i)*Tm(i)/5)+(a16/Tm(i)));      % Calculation of
Enthalpy for CO

Hp(i,2)=R*Tm(i)*(a21+(a22*Tm(i)/2)+(a23*Tm(i)*Tm(i)/3)+(a24*Tm(i)*Tm(i)*Tm
(i)/4)+(a25*Tm(i)*Tm(i)*Tm(i)*Tm(i)/5)+(a26/Tm(i)));      % Calculation of
Enthalpy for CO2

Hp(i,3)=R*Tm(i)*(a31+(a32*Tm(i)/2)+(a33*Tm(i)*Tm(i)/3)+(a34*Tm(i)*Tm(i)*Tm
(i)/4)+(a35*Tm(i)*Tm(i)*Tm(i)*Tm(i)/5)+(a36/Tm(i)));      % Calculation of
Enthalpy for H2O

Hp(i,4)=R*Tm(i)*(a41+(a42*Tm(i)/2)+(a43*Tm(i)*Tm(i)/3)+(a44*Tm(i)*Tm(i)*Tm
(i)/4)+(a45*Tm(i)*Tm(i)*Tm(i)*Tm(i)/5)+(a46/Tm(i)));      % Calculation of
Enthalpy for O2

Hp(i,5)=R*Tm(i)*(a51+(a52*Tm(i)/2)+(a53*Tm(i)*Tm(i)/3)+(a54*Tm(i)*Tm(i)*Tm
(i)/4)+(a55*Tm(i)*Tm(i)*Tm(i)*Tm(i)/5)+(a56/Tm(i)));      % Calculation of
Enthalpy for Nitrogen

        % Total Heat Released from Reactions
        THR(i)=((-Hp(i,1)*RR(i))+(Hp(i,2)*RR(i))-(Hp(i,4)*RR(i)*0.5));

        if i==1
            Qcond(i)=(((Km*dt*2)/(Rhom*Cpm*delx*delx))*(Tm(i+1)-Tm(i)));
% Heat From Conduction
            Qconv(i)=(((Hc*AC*dt)/(Rhom*Cpm))*(Tia(i)-Tm(i)));
% Heat From Convection
            Tmf(i)=Tm(i)+Qcond(i)+Qconv(i)-(((dt)/(Rhom*Cpm*(1-
Eps)))*THR(i));    % End Boundary Condition for Monolith at the Start
        elseif i<h
            Qcond(i)=(((Km*dt)/(Rhom*Cpm*delx*delx))*(Tm(i+1)-
2*Tm(i)+Tm(i-1)));  % Heat From Conduction
            Qconv(i)=(((Hc*AC*dt)/(Rhom*Cpm))*(Tia(i)-Tm(i)));
% Heat From Convection
            Tmf(i)=Tm(i)+Qcond(i)+Qconv(i)-(((dt)/(Rhom*Cpm*(1-
Eps)))*THR(i));    % Calculations of Monolith Temperature at new node
        else
```

```
            Qcond(i)=(((Km*dt*2)/(Rhom*Cpm*delx*delx))*(Tm(i-1)-Tm(i)));
% Heat From Conduction
            Qconv(i)=(((Hc*AC*dt)/(Rhom*Cpm))*(Tia(i)-Tm(i)));
% Heat From Convection
            Tmf(i)=Tm(i)+Qcond(i)+Qconv(i)-(((dt)/(Rhom*Cpm*(1-
Eps)))*THR(i));    % End Boundary Condition for Monolith at the End
        end
    end
    for i=1:h
        Tm(i)=Tmf(i);
    end

    % Calculation for Node 1-------------------------------------------
-
    i=1;

    % Diffusion of Species in mixture
    [DiffMix, ShSurf]=DiffusionCalculator(Toa,X,Y);
% Calling Diffusion Calculator at the Node

    % Species Modeling at Node 1 on Monolith
    delb=1;
% Initialization of Error for Surface Concentrations
    while delb>0.000001
        [t,Z]=ode15s(@SpeciesODECO, [0 dt], Csurf(i,:),options);
% Calling ODE Solver for Initial Node
        [m,n]=size(Z);
        Csurfo(1,1)=Z(m,1);
% Putting the Values back in designated species
        Csurfo(1,2)=Z(m,2);
% Putting the Values back in designated species
        Csurfo(1,3)=Z(m,3);
% Putting the Values back in designated species
        Csurfo(1,4)=Z(m,4);
% Putting the Values back in designated species
        Csurfo(1,5)=Z(m,5);
% Putting the Values back in designated species
        for j=1:5
            B(j)=abs(Csurfo(i,j)-Csurf(i,j));
% Calculation of error
            Csurf(i,j)=Csurfo(i,j);
% Putting Values Back for Further Calculations
        end
        delb=max(B);
% Calculating Maximum error
    end

    % End of Calculation for Node 1

    % Calculations for Internal Nodes----------------------------------
-
    deld=1;             % Error for Complete Length of Catalyst
    while deld>0.000001;

        for i=2:h
```

```
            % Calculation of Mass Fraction at Individual Point
                ConcTot=0;
% Initialization of Total Concentration
                for j=1:5
                    ConcTot=ConcTot+Concbulk(i,j);
% Total Concentration at the new Node
                end
                for j=1:5
                    X(i,j)=((Concbulk(i,j)/ConcTot));
% Mole Fraction of Individual Species
                end
                Na=isnan(X(i,:));
                for j=1:5
                   if Na(j)==1
                      X(i,j)=0;
                   end
                end

                MolMassMix=0;
% Initialization
                for j=1:5
                    MolMass(j)=X(i,j)*Mol(j);
% Molecular Mass of Individual Species in 1 Kmol of Mixture (Kg/Kmol)
                    MolMassMix=MolMassMix+MolMass(j);
% Calculation of Molecular Mass of Mixture (Kg/Kmol)
                end
                for j=1:5
                    Y(i,j)=(X(i,j)*Mol(j))/MolMassMix;
% Mass Fraction of Individual Species
                end

                Na=isnan(Y(i,:));
                for j=1:5
                   if Na(j)==1
                      Y(i,j)=0;
                   end
                end

                % Calculation of Bulk Temperatures
                % Calculations Of Specific Heat

Cp(i,1)=R*(a11+a12*Tia(i)+a13*Tia(i)*Tia(i)+a14*Tia(i)*Tia(i)*Tia(i)+a15*T
ia(i)*Tia(i)*Tia(i)*Tia(i));

Cp(i,2)=R*(a21+a22*Tia(i)+a23*Tia(i)*Tia(i)+a24*Tia(i)*Tia(i)*Tia(i)+a25*T
ia(i)*Tia(i)*Tia(i)*Tia(i));

Cp(i,3)=R*(a31+a32*Tia(i)+a33*Tia(i)*Tia(i)+a34*Tia(i)*Tia(i)*Tia(i)+a35*T
ia(i)*Tia(i)*Tia(i)*Tia(i));

Cp(i,4)=R*(a41+a42*Tia(i)+a43*Tia(i)*Tia(i)+a44*Tia(i)*Tia(i)*Tia(i)+a45*T
ia(i)*Tia(i)*Tia(i)*Tia(i));

Cp(i,5)=R*(a51+a52*Tia(i)+a53*Tia(i)*Tia(i)+a54*Tia(i)*Tia(i)*Tia(i)+a55*T
ia(i)*Tia(i)*Tia(i)*Tia(i));
```

```
                Cpmix=0;
                for j=1:5
                    Cpmix=Cpmix+Cp(i,j)*X(i,j);
% Calculation of Constant Pressure Specific Heat mol basis (J/mol/K)
                end

                Cpmixmass=Cpmix*1000/MolMassMix;
% Calculation of Constant Pressure Specific Heat kg basis (J/Kg/K)
                Na=isnan(Cpmixmass);
                if Na==1
                  Cpmixmass=0;
                end

                % Temperature Modeling for Middle Nodes
                if i<h
                    Toa(i)=(Tia(i-1)-
Tia(i+1)+(((2*K)/(Rho*U*delx*Cpmixmass))*(Tia(i+1)+Tia(i-
1)))+((Hc*8*delx*Tm(i))/(d*Rho*U*Cpmixmass)))/(((4*K)/(Rho*U*delx*Cpmixmas
s))+((Hc*8*delx)/(d*Rho*U*Cpmixmass)));  % Calculation of Temperatures
                else
                    Toa(i)=((((2*K)/(Rho*U*delx*delx*Cpmixmass))*(Tia(i-
1)))+((Hc*4*Tm(i))/(d*Rho*U*Cpmixmass)))/(((2*K)/(Rho*U*delx*delx*Cpmixmas
s))+((Hc*4)/(d*Rho*U*Cpmixmass)));  % Calculation of Temperatures
                end

                % Diffusion of Species in mixture
                [DiffMix, ShSurf]=DiffusionCalculator(Toa,X,Y);
% Calling Diffusion Calculator at the Node

                % Calculation of Bulk Concentration using Gauss Jordon
Method
                for j=1:5
                    if i<h
                       %
Concbulko(i,j)=(((U*delx+2*DiffMix(j))/(delx*U))*Concbulk(i-1,j)+(-
1+(2*DiffMix(j))/(delx*U))*Concbulk(i+1,j)+((ShSurf(j)*DiffMix(j)*8*delx)/
(d*d*U))*Csurf(i,j))/(((4*DiffMix(j))/(delx*U))+((ShSurf(j)*DiffMix(j)*8*d
elx)/(d*d*U)));      % Calculation of Species Concentration at Various
Points
                          Concbulko(i,j)=((2*DiffMix(j)/delx)*(Concbulk(i-
1,j)+Concbulk(i+1,j))+U*(Concbulk(i-1,j)-
Concbulk(i+1,j))+((ShSurf(j)*DiffMix(j)*8*delx)/(d*d))*Csurf(i,j))/((4*Dif
fMix(j)/delx)+(ShSurf(j)*DiffMix(j)*8*delx)/(d*d));
                    else
                        Concbulko(i,j)=((2/(delx*delx))*Concbulk(i-
1,j)+((ShSurf(j)*4)/(d*d))*Csurf(i,j))/((2/(delx*delx))+((ShSurf(j)*4)/(d*
d)));      % Calculation of Species Concentration at Various Points
                    end
                    Concbulk(i,j)=Concbulko(i,j);
                end

                % Calculation of New Diffusion Coefficients for the Bulk
Concentrations
                ConcTot=0;
% Initialization of Total Concentration
```

```
                for j=1:5
                    ConcTot=ConcTot+Concbulk(i,j);
% Total Concentration at the new Node
                end
                for j=1:5
                    X(i,j)=((Concbulk(i,j)/ConcTot));
% Mole Fraction of Individual Species
                end

                MolMassMix=0;
% Initialization
                for j=1:5
                    MolMass(j)=X(i,j)*Mol(j);
% Molecular Mass of Individual Species in 1 Kmol of Mixture (Kg/Kmol)
                    MolMassMix=MolMassMix+MolMass(j);
% Calculation of Molecular Mass of Mixture (Kg/Kmol)
                end
                for j=1:5
                    Y(i,j)=(X(i,j)*Mol(j))/MolMassMix;
% Mass Fraction of Individual Species
                end

                [DiffMix, ShSurf]=DiffusionCalculator(Toa,X,Y);
% Calling Diffusion Calculator at the Node

                % Calculations for Surface Concentrations
                delb=1;
% Initialization of Error for Surface Concentrations
                while delb>0.000001
                    [t,Z]=ode15s(@SpeciesODECO, [0 dt],
Csurf(i,:),options);            % Calling ODE Solver for Initial Node
                    [m,n]=size(Z);
                Csurfo(i,1)=Z(m,1);
% Putting the Values back in designated species
                Csurfo(i,2)=Z(m,2);
% Putting the Values back in designated species
                Csurfo(i,3)=Z(m,3);
% Putting the Values back in designated species
                Csurfo(i,4)=Z(m,4);
% Putting the Values back in designated species
                Csurfo(i,5)=Z(m,5);
% Putting the Values back in designated species
                    for j=1:5
                        B(j)=abs(Csurfo(i,j)-Csurf(i,j));
% Calculation of Error (Infinity Norm)
                        Csurf(i,j)=Csurfo(i,j);
% Putting Values Back for Further Calculations
                    end
                delb=max(B);
% Calculating Maximum Error
                end

                 Tia(i)=Toa(i);              % Putting Value Back
        end

        for i=2:h
```

```
            for j=1:5
                D(i-1,j)=abs(ConcbulkF(i,j)-Concbulk(i,j));
                ConcbulkF(i,j)=Concbulk(i,j);
            end
            D(i-1,6)=abs(Tiaf(i)-Tia(i));
            Tiaf(i)=Tia(i);
        end

        del=max(D);
        deld=max(del);
    end

    % End of Calculations for Intermediate Nodes-------------------------
------

    ResultTemp(a)=Tin;
    Conv(a,1)=((Concbulk(1,1)-Concbulk(h,1))/Concbulk(1,1))*100;      %
Conversion Percentage

    % Bulk Concentration of Species Across the Length of catalyst At 50%
Conversion

    if Conv(a,1)>50 && S==1
        Conc50(:,:)=Concbulk(:,:);
        S=2;
    end

    a=a+1;

end

    % Plot for Conversion Vs Inlet Temperature
    figure;
    plot(ResultTemp,Conv(:,1))
    xlabel('Inlet Temperature (K)')
    ylabel('Conversion (%)')
    legend('Conversion Curve')
    title(['Conversion Curve for CO Oxidation at inlet CO concentration of
',num2str(Conc(1)*100),'%'])

    timespan=toc;           % End of time

% End of Program
```

Subroutine 1: ODE Solver for Species Concentration on Surface

```
function dZdt = SpeciesODECO(t,Z)

% Defining Global Variables
global AC
global Eps
global ShSurf
global DiffMix
global d
global Concbulk
global Tm
global i
global R
global Pres
global RR

% Getting the Initial Values from array
Cs(1)=Z(1);
Cs(2)=Z(2);
Cs(3)=Z(3);
Cs(4)=Z(4);
Cs(5)=Z(5);

% Values from IMECE paper:
PreExp=6.861*10^16;             % Pre Exponential Factor
Ea=119010;                      % Activation Energy
Aco=67.40;                      % Per Atmosphere
Hco=-27980;                     % Enthalpy of Carbon Monoxide
Kco=Aco*exp(((-1)*Hco)/(R*Tm(i)));
Ao2=4.436*10^-6;                % Per Atmosphere
Ho2=-19360;                     % Enthalpy of Oxygen
Ko2=Ao2*exp(((-1)*Ho2)/(R*Tm(i)));

% Getting Partial Pressures
SurfConcTotal=0;
for j=1:5
   SurfConcTotal=SurfConcTotal+Cs(j);
end
for j=1:5
   P(j)=(9.86923*(10^-6)*Pres)*((Cs(j))/SurfConcTotal);     % Getting
Individual Partial Pressure (atm)
   if P(j)<0
      P(j)=0;
   end
end
Na=isnan(P);
for j=1:5
   if Na(j)==1
      P(j)=0;
   end
end
```

```
% Reaction Rate Expression Calculations
RR(i)=((PreExp*exp(-
Ea/(R*Tm(i)))*Kco*P(1)*((Ko2*P(4))^0.5))/((1+(Kco*P(1))+(Ko2*P(4))^0.5)^2)
);

% Calculation of New Concentration

dZdt(1) = (((ShSurf(1)*DiffMix(1)*AC)/d)*(Concbulk(i,1)-Cs(1)))-RR(i)/((1-
Eps));
dZdt(2) = (((ShSurf(2)*DiffMix(2)*AC)/d)*(Concbulk(i,2)-Cs(2)))+RR(i)/((1-
Eps));
dZdt(3) = (((ShSurf(3)*DiffMix(3)*AC)/d)*(Concbulk(i,3)-Cs(3)));
dZdt(4) = (((ShSurf(4)*DiffMix(4)*AC)/d)*(Concbulk(i,4)-Cs(4)))-
((0.5)*RR(i))/(1-Eps);
dZdt(5) = (((ShSurf(5)*DiffMix(5)*AC)/d)*(Concbulk(i,5)-Cs(5)));
dZdt=dZdt';
```

Subroutine 2: Diffusion Calculator

```
% Diffusion Calculator for CO oxidation

function [DiffMix, ShSurf]=DiffusionCalculator(Toa,X,Y)
global i
global Pres
global EffDia
global EffMol
global EffKBEp
global U
global d

% Individual Diffusion of Species in Binary State
for j=1:5
    for k=1:5
        KBTEp(j,k)=(EffKBEp(j,k)*Toa(i));           % Inverse Energies
        if KBTEp(j,k)<5                             % Calculation of Omega
            Ohm(j,k)=1.4803*(KBTEp(j,k)^-0.397);    % Equation from Curve
Fitting in Excel
        else
            Ohm(j,k)=1.0765*(KBTEp(j,k)^-0.16);     % Equation from Curve
Fitting in Excel
        end
        Diff(j,k)=(0.000000186*Toa(i)^1.5*EffMol(j,k))/(Pres*(9.87*10^-
6)*EffDia(j,k)^2*Ohm(j,k));       % Calculation of Individual Diffusion
(m^2/sec)
        if Diff(j,k)==inf
            Diff(j,k)=0;
        end
    end
end

% Diffusion of Species in mixture
 for j=1:5
     DiffMix(j)=0;                                          %
Initialization
     for k=1:5
         if j~=k
```

```
            DiffMix(j)=DiffMix(j)+(X(i,k)/Diff(j,k));      % Diffusion in
Mixture
        end
    end
    DiffMix(j)=((1-Y(i,j))/DiffMix(j));
    if DiffMix(j)==inf
        DiffMix(j)=0;
    end
    Na=isnan(DiffMix(j));
    if Na==1
        DiffMix(j)=0;
    end

 end

 for j=1:5
    ShSurf(j)=2.98*((1+(0.095*d*U/DiffMix(j)))^0.45);  % Calculation for
Sherwood Number
    if ShSurf(j)==inf
        ShSurf(j)=0;
    end

 end
```

Appendix II: Various Terms

App 2.1 Vector Calculus:

The vector operator provides a simplification of expression of the governing equations:

$$\nabla = i\left(\frac{\partial}{\partial x}\right) + j\left(\frac{\partial}{\partial y}\right) + k\left(\frac{\partial}{\partial z}\right) \tag{277}$$

When velocity is to the right of dot product

$$\nabla \cdot V = \left\{ i\left(\frac{\partial}{\partial x}\right) + j\left(\frac{\partial}{\partial y}\right) + k\left(\frac{\partial}{\partial z}\right) \right\} \cdot \{ui + vj + wk\} = \left(\frac{\partial u}{\partial x} + \frac{\partial v}{\partial y} + \frac{\partial w}{\partial z}\right) \tag{278}$$

When velocity is to the left of dot product

$$V \cdot \nabla = \{ui + vj + wk\} \cdot \left\{ i\left(\frac{\partial}{\partial x}\right) + j\left(\frac{\partial}{\partial y}\right) + k\left(\frac{\partial}{\partial z}\right) \right\} = u\left(\frac{\partial}{\partial x}\right) + v\left(\frac{\partial}{\partial y}\right) + w\left(\frac{\partial}{\partial z}\right) \tag{279}$$

Vector operator follows the principle of derivatives as:

$$\begin{aligned} &\nabla \cdot (\rho V) = \rho(\nabla \cdot V) + V(\nabla \cdot \rho) \\ &\nabla \cdot (u + v) = \nabla \cdot u + \nabla \cdot v \\ &\nabla \cdot \nabla V = \nabla^2 V = \left\{ \frac{\partial^2}{\partial x^2} + \frac{\partial^2}{\partial y^2} + \frac{\partial^2}{\partial z^2} \right\} V \end{aligned} \tag{280}$$

App 2.2 Substantial Derivative:

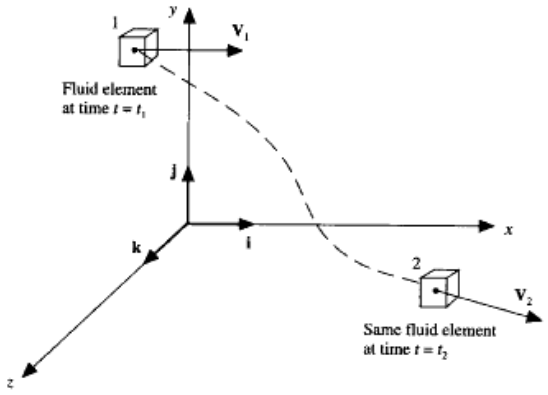

Figure 25: Motion of Fluid From Position (1) to Position (2) [32]

Consider an infinitesimally small control volume as shown in Figure 25 moving with velocity V given by $V = ui+vj+wk$ where u, v and w are the x, y and z component of velocity given by $u=u(x,y,z,t)$, $v=v(x,y,z,t)$ and $w=w(x,y,z,t)$. The properties of a fluid changes with time as well as space and can be represented by the substantial derivative as:

$$\frac{D}{Dt}=\left(\frac{\partial}{\partial t}\right)+\left\{u\left(\frac{\partial}{\partial x}\right)+v\left(\frac{\partial}{\partial y}\right)+w\left(\frac{\partial}{\partial z}\right)\right\} \quad (281)$$

where the first term indicates the local derivative or change with respect to time at position (1) and the second term represents the change with respect to space and is called the advective derivative. In vector form, the substantial derivative is given as:

$$\frac{D}{Dt}=\left(\frac{\partial}{\partial t}\right)+(V\cdot\nabla) \quad (282)$$

App 2.3 Coefficient of Thermal Expansion:

A substance will expand with an increase in energy (heating) and contract with a decrease (cooling). This dimensional response is expressed as the coefficient of thermal expansion. When expressed as a function of volume it is called the volumetric coefficient of thermal expansion that is a thermodynamic property of the substance:

$$\beta=\frac{1}{\cancel{V}}\left(\frac{\partial \cancel{V}}{\partial T}\right)_P=-\frac{1}{\rho}\left(\frac{\partial \rho}{\partial T}\right)_P \quad (283)$$

For an ideal gas, it is given as:

$$\beta\approx\frac{1}{T} \quad (284)$$

App 2.4 Isothermal Compressibility:

The isothermal compressibility of a substance is the measure of rate of change of volume of fluid or solid as a response to a change in pressure at constant temperature. It is a thermodynamic property given as:

$$\alpha = -\frac{1}{\forall}\left(\frac{\partial \forall}{\partial p}\right)_T = \frac{1}{\rho}\left(\frac{\partial \rho}{\partial p}\right)_T \quad (285)$$

For an ideal gas, it is expressed as:

$$\alpha \approx \frac{1}{p} \quad (286)$$

App 2.5 Divergence of Velocity:

The divergence of the velocity is physically the time rate of change of the volume of a moving fluid element, per unit volume. In addition, it represents the volumetric dilation of the fluid element and is given by:

$$(\nabla \cdot V) = \frac{1}{\delta \forall}\frac{D(\delta \forall)}{Dt} \quad (287)$$

App 2.6 CONSERVATIVE and non CONSERVATIVE form:

Consider a general flow field with a control volume $\forall$, defined by a closed surface *S*. The control volume may be fixed in space as shown in Figure 26, with the fluid moving through it. When the fundamental physical principles are applied to this control volume, the resultant equations obtained from this method are called conservative. However, if the control volume is moving with the fluid at the same velocity as that of fluid, as shown in Figure 27, then the equations obtained by applying fundamental physical laws to this volume are called non-conservative.

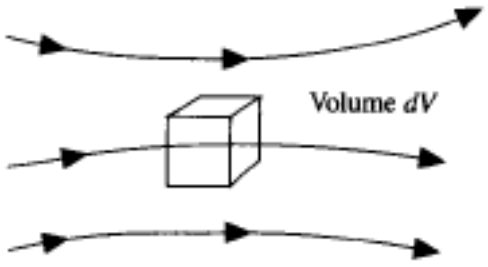

Figure 26: Infinitesimal Small Element Fixed in Space with the Fluid Moving Through it [32].

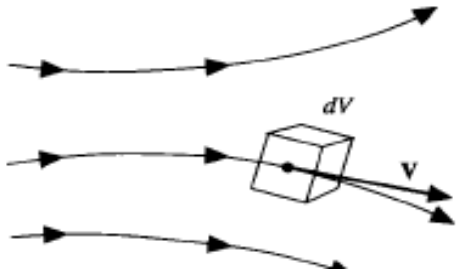

Figure 27: Infinitesimal Fluid Element Moving Along with Streamline with the Velocity V equal to Local Fluid Velocity [32].

App 2.7 Void Fraction:

The void fraction provides the relative ratio of gaseous volume to total catalyst volume.

$\varepsilon = \frac{\not{V}}{\not{V}_{cat}}$ and $1-\varepsilon = \frac{\not{V}_m}{\not{V}_{cat}}$	(288)

where $\not{V}$ is the total gaseous volume in the catalyst, $\not{V}_{cat}$ is the total catalyst volume and $\not{V}_m$ is the monolith volume [30].

App 2.8 Geometric Surface Area per Unit Volume:

The geometric surface area per unit volume indicated in Figure 28 is a convenient simplification that helps the modeler simulate different channel geometries using the same governing equations.

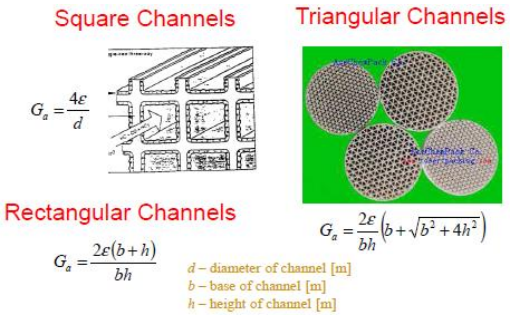

Figure 28: Geometric Surface Area of Various Channel Types [30]

App 2.9 Nusselt Number:

In heat transfer at a boundary within a fluid, ratio of convective to conductive heat transfer normal to boundary is given by Nusselt number. It is dimensionless number Nusselt number is function of Reynolds number and Prandtl number and depends on spatial variable *x*. But for fully developed flow Nusselt number is constant and becomes independent of spatial variable *x*.

App 2.10 Sherwood Number:

Ratio of convective to diffusive mass transport is given by Sherwood number. It is dimensionless number analogous to Nusselt number in heat transfer. It depends on Reynolds number and Schmidt number and similar to Nusselt number depends on *x*. But for fully developed flow it is constant similar to Nusselt number.

Appendix III: Chemkin Data

APP 3.1 POLYNOMIAL COEFFICIENTS REPRESNTING THERMODYNAMIC PROPERTIES FROM 300 TO 1000 K FOR CO [278-280]:

A11=3.262451; A12=0.0015119409; A13=-0.000003881755;
A14=0.000000005581944;
A15=-0.000000000002474951; A16=-14310.539;

APP 3.2 POLYNOMIAL COEFFICIENTS REPRESNTING THERMODYNAMIC PROPERTIES FROM 300 TO 1000 K FOR CO_2 [278-280]:

A21=2.275724; A22=0.009922072; A23=-0.000010409113; A24=0.000000006866686;
A25=-0.00000000000211728; A26=-48373.14;

APP 3.3 POLYNOMIAL COEFFICIENTS REPRESNTING THERMODYNAMIC PROPERTIES FROM 300 TO 1000 K FOR H_2O [278-280]:

A31=3.386842; A32=0.003474982; A33=-0.000006354696; A34=0.000000006968581;
A35=-0.000000000002506588; A36=-30208.11;

APP 3.4 POLYNOMIAL COEFFICIENTS REPRESNTING THERMODYNAMIC PROPERTIES FROM 300 TO 1000 K FOR O_2 [278-280]:

A41=3.212936; A42=0.0011274864; A43=-0.000000575615;
A44=0.0000000013138773; A45=-0.00000000000008768554; A46=-1005.249;

APP 3.5 POLYNOMIAL COEFFICIENTS REPRESNTING THERMODYNAMIC PROPERTIES FROM 300 TO 1000 K FOR N_2 [278-280]:

A51=3.298677; A52=0.0014082404; A53=-0.000003963222;
A54=0.000000005641515;
A55=-0.000000000005641515; A56=-1020.8999;

Appendix IV: Data for Calculating Diffusion Coefficient

APP 4.1 COLLISION INTEGRAL [74]:

k_BT/ε	Ω	k_BT/ε	Ω	k_BT/ε	Ω
0.30	2.662	1.65	1.153	4.0	0.8836
0.35	2.476	1.70	1.140	4.1	0.8788
0.40	2.318	1.75	1.128	4.2	0.8740
0.45	2.184	1.80	1.116	4.3	0.8694
0.50	2.066	1.85	1.105	4.4	0.8652
0.55	1.966	1.90	1.094	4.5	0.8610
0.60	1.877	1.95	1.084	4.6	0.8568
0.65	1.798	2.00	1.075	4.7	0.8530
0.70	1.729	2.1	1.057	4.8	0.8492
0.75	1.667	2.2	1.041	4.9	0.8456
0.80	1.612	2.3	1.026	5.0	0.8422
0.85	1.562	2.4	1.012	6	0.8124
0.90	1.517	2.5	0.9996	7	0.7896
0.95	1.476	2.6	0.9878	8	0.7712
1.00	1.439	2.7	0.9770	9	0.7556
1.05	1.406	2.8	0.9672	10	0.7424
1.10	1.375	2.9	0.9576	20	0.6640
1.15	1.346	3.0	0.9490	30	0.6232
1.20	1.320	3.1	0.9406	40	0.5960
1.25	1.296	3.2	0.9328	50	0.5756
1.30	1.273	3.3	0.9256	60	0.5596
1.35	1.253	3.4	0.9186	70	0.5464
1.40	1.233	3.5	0.9120	80	0.5352
1.45	1.215	3.6	0.9058	90	0.5256
1.50	1.198	3.7	0.8998	100	0.5130
1.55	1.182	3.8	0.8942	200	0.4644
1.60	1.167	3.9	0.8888	300	0.4360

Source: Data from Hirschfelder et al. (1954).

APP 4.2 COLLISION DIAMETERS AND ENERGY OF INTERACTION [74]:

Substance		σ(Å)	ε/k_B(°K
Ar	Argon	3.542	93.3
He	Helium	2.551	10.22
Kr	Krypton	3.655	178.9
Ne	Neon	2.820	32.8
Xe	Xenon	4.047	231.0
Air	Air	3.711	78.6
Br_2	Bromine	4.296	507.9
CCl_4	Carbon tetrachloride	5.947	322.7
CF_4	Carbon tetrafluoride	4.662	134.0
$CHCl_3$	Chloroform	5.389	340.2
CH_2Cl_2	Methylene chloride	4.898	356.3
CH_3Br	Methyl bromide	4.118	449.2
CH_3Cl	Methyl chloride	4.182	350
CH_3OH	Methanol	3.626	481.8
CH_4	Methane	3.758	148.6
CO	Carbon monoxide	3.690	91.7
CO_2	Carbon dioxide	3.941	195.2
CS_2	Carbon disulfide	4.483	467
C_2H_2	Acetylene	4.033	231.8
C_2H_4	Ethylene	4.163	224.7
C_2H_6	Ethane	4.443	215.7
C_2H_5Cl	Ethyl chloride	4.898	300
C_2H_5OH	Ethanol	4.530	362.6
CH_3OCH_3	Methyl ether	4.307	395.0
CH_2CHCH_3	Propylene	4.678	298.9
CH_3CCH	Methylacetylene	4.761	251.8
C_3H_6	Cyclopropane	4.807	248.9
C_3H_8	Propane	5.118	237.1
n-C_3H_7OH	n-Propyl alcohol	4.549	576.7
CH_3COCH_3	Acetone	4.600	560.2
CH_3COOCH_3	Methyl acetate	4.936	469.8
n-C_4H_{10}	n-Butane	4.687	531.4
iso-C_4H_{10}	Isobutane	5.278	330.1
$C_2H_5OC_2H_5$	Ethyl ether	5.678	313.8
$CH_3COOC_2H_5$	Ethyl acetate	5.205	521.3
n-C_5H_{12}	n-Pentane	5.784	341.1
$C(CH_3)_4$	2,2-Dimethylpropane	6.464	193.4
C_6H_6	Benzene	5.349	412.3
C_6H_{12}	Cyclohexane	6.182	297.1
n-C_6H_{14}	n-Hexane	5.949	399.3
Cl_2	Chlorine	4.217	316.0
F_2	Fluorine	3.357	112.6
HBr	Hydrogen bromide	3.353	449
HCN	Hydrogen cyanide	3.630	569.1
HCl	Hydrogen chloride	3.339	344.7
HF	Hydrogen fluoride	3.148	330
HI	Hydrogen iodide	4.211	288.7
H_2	Hydrogen	2.827	59.7
H_2O	Water	2.641	809.1
H_2O_2	Hydrogen peroxide	4.196	289.3
H_2S	Hydrogen sulfide	3.623	301.1
Hg	Mercury	2.969	750
I_2	Iodine	5.160	474.2
NH_3	Ammonia	2.900	558.3
NO	Nitric oxide	3.492	116.7
N_2	Nitrogen	3.798	71.4
N_2O	Nitrous oxide	3.828	232.4
O_2	Oxygen	3.467	106.7
PH_3	Phosphine	3.981	251.5
SO_2	Sulfur dioxide	4.112	335.4
UF_6	Uranium hexafluoride	5.967	236.8

Note: Data from Hirschfelder et al. (1954).

Nomenclature

α	Isothermal compressibility	[atm^{-1}]
a	Acceleration	[$m\ s^{-2}$]
Bi	Biot number	[-]
β	Thermal expansion	[K^{-1}]
c_m	Solid specific heat	[$J\ kg^{-1}\ K^{-1}$]
c_p	Constant pressure specific heat	[$J\ kg^{-1}\ K^{-1}$]
c_v	Constant Volume specific heat	[$J\ kg^{-1}\ K^{-1}$]
$\bar{C}$	Molar species concentration	[$mol\ m^{-3}$]
$\bar{C}_s$	Molar species concentration on surface	[$mol\ m^{-3}$]
d	Channel diameter	[m]
δ	Diffusion coefficient	[$m^2\ s^{-1}$]
D_{cat}	Overall catalyst diameter	[m]
ε	Void fraction or emissivity	[-]
e	Internal energy	[J]
E_a	Activation energy	[$J\ mol^{-1}$]
F	Force	[N]
G_a	Geometric surface area per unit volume	[$m^2\ m^{-3}$]
G_{ca}	Catalytic surface area per unit volume	[$m^2\ m^{-3}$]
g	Acceleration due to gravity	[$m\ s^{-2}$]
h	Specific enthalpy	[$J\ kg^{-1}$]
ΔH	Heat of adsorption	[$J\ mol^{-1}$]
h_c	Heat transfer coefficient	[$W\ m^{-2}\ K^{-1}$]
h_∞	Ambient heat transfer coefficient	[$W\ m^{-2}\ K^{-1}$]
∞	Ambient	[-]
j	Species index number	[-]
κ	Mass transfer coefficient	[$m\ s^{-1}$]
k	Kinetic pre-exponent	[varies]
K	Adsorption equilibrium	[m^2/N]
λ	Thermal conductivity of gas	[$W\ m^{-1}\ K^{-1}$]
λ_v	Lame Viscosity	[$kg\ m^{-1}\ s^{-1}$]
λ_m	Thermal conductivity of monolith	[$W\ m^{-1}\ K^{-1}$]
μ	Dynamic viscosity	[$N\ s\ m^{-2}$]
m	Mass	[kg]
MW	Molecular Weight	[$kg\ kmol^{-1}$]
ν	Kinematic viscosity	[$m^2\ s^{-1}$]
v_A	Velocity of individual species	[$m\ s^{-1}$]
Nu	Nusselt number	[-]
Ω	Dimension less energy integral	[-]
$\dot{\omega}$	Mass based gas reaction rate per unit volume	[$kg\ m^{-3}\ s^{-1}$]
p	Pressure	[atm]
ρ	Density	[$kg\ m^{-3}$]

ρ_m	Density of monolith	[kg m^{-3}]
σ	Stefan-Boltzmann radiation constant	[W m^{-2} K^{-4}]
σ	Collision Diameter in diffusion equation	[m]
$\dot{q}$	Volumetric heat generation	[W m^{-3}]
R	Gas Constant	[J kg^{-1} K^{-1}]
$\bar{R}$	Molar gaseous reaction rate	[mol m^{-2} s^{-1}]
Re	Reynolds number	[-]
Sh	Sherwood number	[-]
t	Time	[s]
T	Gas temperature	[K]
T_m	Monolith temperature	[K]
τ	Shear Stress	[N m^{-2}]
θ	Surface coverage fraction	[-]
u	Velocity in x- direction	[m s^{-1}]
v	Velocity in y- direction	[m s^{-1}]
v_A	Velocity of individual species	[m s^{-1}]
w	Velocity in z- direction	[m s^{-1}]
V	Overall velocity ($ui + vj + wk$)	[m s^{-1}]
~~V~~	Volume	[m^3]
~~v~~	Specific volume	[m^3 kg^{-1}]
x	Channel (axial) distance	[m]
X	Mole fraction	[-]
Y	Mass fraction	[-]

References:

(1) Faiz, A.; Weaver, C.; Walsh, M., Air Pollution from Motor Vehicles. The World Bank: Washington D.C., 1996. http://books.google.com/books?id=Hqsyv_KD0lgC&printsec=frontcover#v=onepage&q&f=false.

(2) Administration, E. I., International Energy Outlook. Energy, U. S. D. o., Ed. Energy Information Admisitration: Washington D.C., 2009; p 284.

(3) Draft Automotive Mission Plan. Enterprises, M. o. H. I. a. P., Ed. Ministry of Heavy Industries and Public Enterprises: 2006; pp 1-46.

(4) Agency, E. P. Automobile Emission: An Overview 1994.

(5) group, W. H. O. W. *Health Aspects of Air Pollution with PM, Ozone and Nitrogen Dioxide*; World Health Organization (WHO): Bonn, Germany, 2003; p 98.

(6) Agency, U. S. E. P., NOx : How Nitrogen Oxides Affect the Way We Live and Breathe. Standards, O. o. A. Q. P. a., Ed. EPA: Washington D.C., 1998; p 6.

(7) Agency, C. E. P. Health Effects of Air Pollution. http://www.arb.ca.gov/research/health/health.htm.

(8) Agency, U. S. E. P. Milestones in Auto Emission Control 1994, p. 3.

(9) Chorkendorff, I.; Niemantsverdriet, J. W., Concepts of Modern Catalysis and Kinetics. 2nd edition ed.; Wiley-VCH 2007. http://books.google.com/books?id=jdoye_XAeU4C&lpg=PA397&dq=heck%20automotive%20air%20pollution&pg=PP1#v=onepage&q=&f=false.

(10) Agency, U. S. E. P. When and How was the EPA Created? http://www.epa.gov/history/topics/epa/15c.htm.

(11) DieselNet Emission Standards: USA - Cars and Light Duty Trucks. http://www.dieselnet.com/standards/us/ld.php.

(12) Heywood, J., *Internal Combustion Engine Fundamentals*. McGraw-Hill, Inc.: New York, 1998.

(13) Scientist, U. o. C. Diesel Passenger Vehicles and Environment 2008. http://www.ucsusa.org/assets/documents/clean_vehicles/acfosdcrt.pdf.

(14) Morriss, A.; Yandle, B.; Dorchak, A., Regulating by Litigation: The EPA's Regulation of Heavy-Duty Diesel Engines. *Administrative Law Review* **2004,** *56* (2), 403-518.

(15) Koltsakis, G.; Stamatelos, A., Catalytic Automotive Exhaust Aftertreatment. *Progress in Energy and Combustion Science* **1997,** *23* (1), 1-39.

(16) Depik, C., Catalyst Modeling: Aftertreatment Devices. In *Catalyst Modeling*, Lawrence, Kansas, 2008; Vol. 1.

(17) Farrauto, R. In *Automotive Emission Control: Past, Present and Future*, Philadelphia Catalysis Society Spring Symposium, North American Catalysis Society: 2008; pp 1-18.

(18) Heck, R.; Farrauto, R.; Gulati, S., *Catalytic Air Pollution Control: Commercial Technology* 3rd ed.; Wiley & Sons: 2009.

(19) Olsson, L.; Andersson, B., Kinetic Modeling in Automotive Catalysis. *Topics in Catalysis* **2004,** *28* (1-4), 89-98.

(20) Catalysts, U. A. Catalysts for Gasoline Engines. http://www.automotivecatalysts.umicore.com/en/autoCatsWebProduct/autoCatsWebGasolineCatalyts/.

(21) Bosch, H.; Janssen, F. J., Formation and Control of Nitrogen Oxides *Catalysis Today* **1988,** *2* (4), 369-379.

(22) Lambert, C.; Hammerle, R.; McGill, R.; Khair, M., Technical Advantages of Urea SCR for Light-Duty and Heavy-Duty Diesel Vehicle Applications. *Society of Automotive Engineers* **2004,** *2004-01-1292*.

(23) Lambert, C.; Vanderslice, J.; Hammerle, R.; Belaire, R., Application of Urea SCR to Light-Duty Diesel Vehicles. *Society of Automotive Engineers* **2001,** *2001-01-3623*.

(24) Sean, B., *Medium/Heavy Duty Truck Engines, Fuel and Computerized Management Systems*. Delmar Publishers: Albany, NY, 1999; p 736.

(25) Schmeißer, V.; Tuttlies, U.; Eigenberger, G., Towards a Realistic Simulation Model for NOx Storage Catalyst Dynamics. *Topics in Catalysis* **2007,** *42-43* (1-4), 77-81.

(26) Depcik, C.; Assanis, D.; Bevan, K., A One-Dimensional Lean NOx Trap Model with a Global Kinetic Mechanism that Includes NH3 and N2O. *International Journal of Engine Research* **2008,** *9* (1), 57-78.

(27) Schenk, C.; McDonald, J.; Olson, B., High-Efficiency NOx and PM Exhaust Emission Control for Heavy-Duty On-Highway Diesel Engines. *Society of Automotive Engineers* **2001,** *2001-01-1351*.

(28) Salasc, S.; Barrieu, E.; Leroy, V., Impact of Manifold Design on Flow Distribution of a Close-Coupled Catalytic Converter. *Society of Automotive Engineers* **2005,** *2005-01-1626*.

(29) Depcik, C.; Assanis, D., One-Dimensional Automotive Catalyst Modeling *Progress in Energy and Combustion Science* **2005,** *31*, 308-369.

(30) Depcik, C., Catalyst Modeling: ME 790. Lawrene, 2008.

(31) Depcik, C.; Loya, S.; Srinivasan, A., Adaptive Carbon Monoxide Kinetics for Exhaust Aftertreatment Modeling. In *ASME International Mechanical Engineering Congress and Exposition (IMECE)*, Lake Buena Vista, Florida, USA, 2009; Vol. IMECE2009-11173.

(32) Anderson, J. J., *Computational Fluid Dynaimcs: The basic With Applications*. McGraw Hill INc.: Singapore, 1995.

(33) Fox, R.; McDonald, A.; Pritchard, P., *Introduction to Fluid Mechanics*. 6th Edition ed.; John Wiley & Sons Inc. : New Jersey, 2003.

(34) White, f., *Fluid Mechanics*. 5th edition ed.; McGraw Hill Inc.: New York, 2003.

(35) Panton, R., *Incompressible Flow*. 3re Edition ed.; John Wiley & Sons Inc.: New Jersey, 2005.

(36) Almgren, A. S.; Bell, J. B.; RendLeman, C. A.; Zingale, M., Low Mach Number Modeling of type Ia Supernovae . I. Hydrodynamics. *The Astrophysical Journal* **2006,** *637*, 922-936.

(37) Byrne, H.; Norbury, J., Mathematical Modeling of Catalytic Converters. *Mathematical Engineering in Industry* **1993,** *4* (1), 27-48.

(38) Graetzel, M.; Infelta, P., *The bases of Chemical Thermodynamics*. universal Publishers: 2002; Vol. 1.

(39) Lawson, D.; Schubert, G., *Geodynamics*. 2nd Edition ed.; Cambridge University Press: New york, 2001.

(40) Morgon, C. R.; Carlson, D. W.; Voltz, S. E., Thermal Response and Emission Breakthrough of Platinum Monolithic Catalytic Converters. *Society of Automotive Engineers* **1973,** *730569*.

(41) Chen, D.; Oh, S.; Bisset, E.; Van Ostrom, D., A Three Diemnsional Model for the Analysis of Transient Thermal and Conversion Characteristics of Monolithic Catalytic Converters. *Society of Automotive Engineers* **1988,** *880282*.

(42) Lee, S.; Aris, R., On the Effects of Radiative Heat Transfer in Monolith. *Chemical Engineering Science* **1977,** *32*, 827-837.

(43) Knudsen, J.; Katz, D., *Fluid Dynamics and Heat Transfer*. McGraw-Hill Publications: 1958; p 576.

(44) Kuo, J. C.; Morgon, C. R.; Lassen, H. G., Mathematical Modeling of CO and HC Catalytic Converter Systems. *SAE* **1989,** *710289*.

(45) Harned, J., Analytical Evaluation of a Catalytic Converter System. *Society of Automotive Engineers* **1972,** *720520*.

(46) Oh, S.; Cavendish, J., Transients of Monolithic Catalytic Converters: Response to Step Changes in Feedstream Temperatures as Related to Controlling Automobile Emissions. *Industrial Engineering Chemical Res* **1982,** *21*, 29-37.

(47) Young, L.; Finlayson, B., Mathematical Modeling of the Monolith Converter. *Adv Chem Sr* **1974,** *133*, 629-643.

(48) Fleming, D. P.; Sparrow, E. M., Flow in the Hydrodynamics Entrance Region of Ducts of Arbitary Cross Section. *Journal of Heat Transfer* **1969,** *91*, 345-354.

(49) Manohar, R., Analysis of Laminar Flow Heat Transfer in the Entrance Region of Circular Tubes. *International journal of Heat and Mass Transfer* **1969,** *12* (1), 15-22.

(50) Incorpera, F.; De Witt, D., *Fundamentals of Heat and Mass Transfer*. 3rd Edition ed.; John Wiley and Sons, Inc: 1990.

(51) Stuwe, K., *Geodynamics of the Lithosphere: an Introduction*. Springer: 2007; p 493.

(52) Albright, L.; Albright, L. F., *Albright's Chemical Engineering Handbook*. CRC Press: 2008; p 1912.

(53) Nielaba, P.; Mareschal, M.; Ciccotti, G., *Bridging Time Scales: Molecular Simulations for the Next Decade*. Springer: 2002; Vol. 605, p 500.

(54) Shi, Z. H.; Gong, M. C.; Chen, Y. Q., Pd Close Coupled Catalyst. *Chinese Chemical Letters* **2006,** *17* (9), 1271-1274.

(55) Mubmann, L.; Lox, E.; Lindner, D.; Kreuzer, T.; Muller, W. O., K.; Waltner, A.; Loose, G.; Hirschmann, A., Development of Close-Coupled Catalyst Systems for European Driving Conditions. *Society of Automotive Engineers* **1998,** *980663*.

(56) Silver, R.; Sawyer, J.; Summers, J., *Catalytic Control of Air Pollution: Mobile and Stationary Sources*. American Chemical Society: New York, 1992.

(57) G.W., N.; Park, J.; Lee, J.; Yeo, G., The Effect of and external Fuel Injection on the Control of LNT System; the Diesel NOx Reductive System. *SAE* **2007,** *2007-01-1242*.

(58) Webb, C.; Weber, P.; Thornton, M., Achieving Tier 2 Bin 5 Emission Levels with a Medium Duty Diesel Pick-Up and a NOX Adsorber, Diesel Particulate Filter Emissions System-Exhaust Gas Temperature Management. *SAE* **2004,** *2004-01-0584*.

(59) Whitacre, S.; Adelman, B.; May-Ricardo, M., Systems Approach to Meeting EPA 2010 Heavy-Duty Emission Standards Using a NOx Adsorber Catalyst and Diesel Particle Filter on a 15L Engine. *SAE* **2004,** *2004-01-0587*.

(60) Crane, S.; Iverson, R. J.; Goldschmidt, S.; Greathouse, M. W.; Khadiya, N., Recent Advances in Utilizing the Plasma Fuel Reformer for Nox Trap Regeneration. *SAE Paper 2005-01-3547* **2005**.

(61) Laroo, C. A.; Schenk, C. R., NOx Adsorber Aging on a Heavy-Duty On-Highway Diesel Engine: Part Two. *SAE Paper 2007-01-0468* **2007**.

(62) Kong, Y.; Huffmeyer, C. R.; Johnson, R. J.; Taylor, W.; Crawley, W.; Hayworth, G., Applications of An Active Diesel Particulate Filter Regeneration System. *SAE Paper 2004-01-2660* **2004**.

(63) Johnson, T. V., Diesel Emission Control in Review. *SAE Paper 2007-01-0233* **2007**.

(64) White, f., *Viscous Fluid Flow*. 3rd Edition ed.; McGraw Hill Inc.: New York, 2006.

(65) Schlichting, H.; Gersten, K., *Boundary Layer Theory*. 8th Edition ed.; Berlin, 2000.

(66) Sankar, L. N. Low Speed Aerodynamics. http://soliton.ae.gatech.edu/people/lsankar/AE2020/.

(67) Kee, R.; Coltrin, M.; Glarborg, P., *Chemically Reacting Flow: Theory & Practice*. John Wiley and Sons: New Jersey, 2003.

(68) Kundu, P.; Cohen, I., *Fluid Mechanics*. 4th Edition ed.; Academic Press: 2008; Vol. 10.

(69) Kreith, F.; Manglik, R. M.; Bohn, M. S., *Principles of Heat Transfer*. 7th ed.; Cengage Learning: 2010.

(70) Roy, S. K., *Thermal Physics and Statistical Mechanics* New Age International: 2001; p 432.

(71) Honerkamp, J., *Statistical Physics: An Advanced Approach with Applications*. 2nd ed.; Springer: 2002; p 515.

(72) Depcik, C.; Kobiera, A.; Assanis, D., Influence of Density Variation on One-Dimensional Modeling of Exhaust Assisted Catalytic Fuel Reforming. *Heat Transfer Engineering* **2009**.

(73) Kuo, K., *Principles of Combustion*. 2nd Edition ed.; John Wiley & Sons Inc.: New Jersey, 2005.

(74) Cussler, E. L., *Diffusion: Mass Transfer in Fluid Systems*. 2nd Edition ed.; Cambridge University Press: Cambridge, 1997.

(75) Perry, R.; Green, D., *Perry's Chemical Engineering Handbook*. 6th Edition ed.; McGraw Hill Inc.: 1984.

(76) Design, R. *Transport Core Utility Manual*; 2003.

(77) Wilke, C. R., Diffusional Properties of Multicomponent Gases. *Chemical Engineering Science* **1950,** *46* (2), 95-104.

(78) Groppi, G.; Belloli, A.; Tronconi, E.; Forzatti, P., A Comparison of Lumped and Distributed Models of monolith Catalytic Combusters. *Chemical Engineering Science* **1995,** *50* (17), 2705-2715.

(79) Hayes, R. E.; Kolaczkowski, S. T., Mass and Heat Trasnfer Effects in Catalytic Monolith Reactors. *Chemical Engineering Science* **1994,** *49* (21), 3587-3599.

(80) Burmeister, L., *Convective Heat Transfer* 2ed.; Wiley-Interscience Publisher: 1993.

(81) Lindeburg, M., *Mechanical Engineering Reference Manual for the PE Exam*. 12 ed.; Professional Publications, Inc.: Belmont, CA, 2006.

(82) Kockmann, N., *Transport Phenomenon in Micro Process Engineering*. Springer: Berlin, 2007.

(83) Langmuir, I., The Mechansim of the Catalytic Action of Platinum in the Reactions 2CO + O2 = 2CO2 and 2H2 + O2 = 2H2O. *Trans Faraday Society* **1922,** *17*, 621-654.

(84) Sklyarov, *Physical Chemistry* **1969,** *189*, 829.

(85) Bonzel, H.; Ku, R., Carbon Monoxide Oxidation on Pt(110). *Journal of vacuum science and technology* **1972,** *9* (2), 663-667.

(86) Voltz, S.; Morgan, C.; Liederman, D.; Jacob, S., Kinetic study of CO and Propylene Oxidation on Platinum Catalysts. *Ind Eng Chem* **1973,** *12* (4), 294-301.

(87) Firth, J.; Gentry, S.; Jones, A., Oxidation Reaction on Platinum Catalysts. *Journal Of catalysis* **1974,** *34*, 159-161.

(88) Shishu, R. C.; Kowalczyk, L. S., *Platinum Met. Rev.* **1974,** *18*, 58.

(89) Hori, G.; Schmidt, L., Transient Kinetics in CO oxidation on Platinum. *journal of Catalysis* **1975,** *38*, 335-350.

(90) Mccarthy, E.; Zahradnik, J.; Kuczynski, G.; Carberry, J., Some Unique Aspects of CO oxidation on Supported Platinum. *journal of Catalysis* **1975,** *39*, 29-35.

(91) Nicholas, D. M.; Shah, Y. T., CO oxidation over platinum fiber glass supported catalyst. *Ind Eng Chem* **1976,** *15* (1), 35-40.

(92) hegedus, L.; Oh, S.; Baron, K., Multiple Steady States in an Isothermal, Integral Reactor: The Catalytic Oxidation of CO over Pt/alumina. *AIChE* **1977,** *23* (5), 632-641.

(93) Dabill, D.; Gentry, S.; Holland, B.; Jones, A., Oxidation of Hydrogen and carbon monoxide mixture over platinum. *journal of Catalysis* **1978,** *53*, 164-167.

(94) Cant, N.; Hicks, P.; Lennon, B., Steady State Oxidation of Carbon Monoxide over Supported Noble Metals with Particular Reference to Platinum. *journal of Catalysis* **1978,** *54*, 372-383.

(95) Cutlip, M. B., Concentration Forcing of Catalytic Surface Rate Process. *AIChE* **1979,** *25*, 502-509.

(96) Finlayson, B.; Young, L., Mathematical Models of the Monolithic Catalytic Converter: Hysteresis in Carbon Monoxide Reactor. *Aiche* **1979,** *25* (1), 192-196.

(97) Schenk, C. R.; McDonald, J. F.; Olson, B. A., High-Efficiency Nox and Pm Exhaust Emission Control for Heavy-Duty On-Highway Diesel Engines. *SAE Paper 2001-01-1351* **2001**.

(98) Papadakis, K.; Odenbrand, C. U. I.; Sjöblom, J.; Creaser, D., Development of a dosing strategy for a heavy-duty diesel exhaust cleaning system based on NOX storage and reduction technology by Design of Experiments. *Applied Catalysis B: Environmental* **2007,** *70* (1-4), 215-225.

(99) Dementhon, J. B.; Colliou, T.; Martin, B.; Bouchez, M.; Guyon, M.; Messaoudi, I.; Noirot, R.; Michon, S.; Gérentet, C.; Pierron, L., Application of NOx Adsorber to Diesel Depollution: Performances and Durability. *Oil & Gas Science and Technology* **2003,** *58* (1), 129-149.

(100) Herz, R.; Samuel, M., Surface Chemistry Model of Carbon Monoxide Oxidation on Supported Platinum catalysts. *journal of Catalysis* **1980,** *65*, 281-296.

(101) Gland, J., Molecular and Atomic Adsorption of Oxygen on Platinum and Pt(s) - 12(111)X(111) Surfaces. *Surface Science* **1980,** *93*, 487-514.

(102) Goodman, M.; Cutlip, M. B.; Kenney, C.; Morton, W.; Mukesh, D., Transient Studies of Carbon Monoxide over Platinum Catalyst. *Surface Science* **1982,** *120*, 453-460.

(103) Barshad, Y., Dynamic study of CO oxidation on supported platinum. *AIChE* **1985,** *31* (4), 649-658.

(104) Winkler, A.; Guo, X.; Siddiqui, H.; Hagans, P.; J., Y., Kinetics and Energetics of Oxygen Adsorption on Platinum(111) and Pt(112) - A Comparison of Flat and Stepped Surfaces *Surface Science* **1988,** *201*, 419-443.

(105) Su, E.; Rothschild, W. G.; Yao, H., CO oxidation over Platinum/Alumina under High Pressure. *journal of Catalysis* **1989,** *118*, 111-124.

(106) Skoglundh, M.; Lowendahl, L.; J., O., Combonation of Platinum and Palladium on Alumina Supports as Oxidation Catalysts. *Applied catalysis* **1991,** *77*, 9-20.

(107) Nibbelke, R.; Campman, M.; Hoebink, J. H.; Marin, G., Kinetic Study of CO Oxidation over Pt/Alumina and Pt/Rh/CeO2/Alumina in the Presence of CO2 and H2O. *journal of Catalysis* **1997,** *171*, 358-373.

(108) Nijhuis, T.; Makkee, M.; Langeveld, A.; Moulijn, J., New insight in platinum catalyzed CO oxidation kinetic mechanism by using an advanced TAP reactor system. *Applied catalysis* **1997,** (4), 237-249.

(109) Rinnemo, M.; Kulginov, D.; Johansson, S.; Wong, K. L.; Zhadnov, V.; Kasemo, B., Catalytic ignition in CO-O2 Reaction on Platinum: experiments and simulations *Surface Science* **1997,** *376*, 297-3009.

(110) Tieber, W.; Athenstaedt, W.; Leisch, M., 3D - Atom Probe Study of oxygen Adsorption on Stepped Platinum Surfaces. *Fresenius Journal of Analytical Chemistry* **1997,** *358*, 116-118.

(111) Kahlich, M.; Gasteiger, H.; Behm, R., Kinetics of Selective CO Oxidation in Hydrogen rich Gas on Pt/Al2O3. *journal of Catalysis* **1997,** *171*, 93-105.

(112) Hoebink, J. H. B. J.; Nievergeld, A. J. L.; Marin, G., CO oxidation in fixed bed reactor with high frequency cycling of the feed. *Chemical Engineering Sciences* **1999,** *54*, 4459-4468.

(113) Thormahlen, P.; Skoglundh, M.; Fridell, E.; Andersson, B., Low Temperature CO Oxidation on Platinum and Cobalt Oxide Catalysts. *journal of Catalysis* **1999,** *188*, 300-310.

(114) Wojciechowski, B.; Asprey, S., Kinetic studies using temperature-scanning: The oxidation of carbon monoxide. *Applied catalysis* **2000,** *190*, 1-24.

(115) Carlsson, P.; Thormahlen, P.; Skoglundh, M.; Persson, H.; Fridell, E.; Jobson, E.; Andersson, B., Periodic control for improved low temperature catalytic activity. *Topics in Catalysis* **2001,** *16/17*, 343-347.

(116) Bourane, A.; Bianchi, D., Heats of Adsorption of the Linear CO Species on Pt/Alumina Using Infrared Spectroscopy: Impact of the Platinum Dispersion. *journal of Catalysis* **2003,** *218*, 447-452.

(117) Sen, B.; Vannice, M. A., The Influence of Platinum Crystallite Size on Hydrogen and CO Heats of Adsorption and CO Hydrogenation *Journal of Catalysis* **1991,** *130* (1), 9-20.

(118) Sharma, S. B.; Miller, M. T.; Dumesic, J. A., Microcalorimetric Study of Silica and Zeolite Supported Platinum Catalysts. *Journal of Catalysis* **1994,** *148* (1), 198-204.

(119) Gracia, F. J.; Bollmann, L.; Wolf, E. E.; Miller, J. T.; Kropf, A. J., In Situ FTIR, EXAFS and Activity Studies of the Effect of Crystallite Size on Silica-Supported Platinum Oxidation Catalysts. *Journal of Catalysis* **2003,** *220*, 382-391.

(120) Oran, U.; Uner, D., Mechanism of CO oxidation reaction and effect of Chlorine ions on CO oxidation reaction over Pt/CeO2 and Pt/CeO2/Alumina catalysts. *Applied catalysis* **2004,** *54* (3), 183-191.

(121) Bourane, A.; Bianchi, D.; Derrouiche, S., Impact of Platinum dispersion on elemetary step of CO oxidation by oxygen on Platinum/Alumina catalysts. . *journal of Catalysis* **2004,** *228*, 288-297.

(122) Chang, C.; Lin, T. S., Pt/Rh and Pd/Rh catalysts use for Ozone Decomposition and Simultaneous Elimination of Ozone and Carbon Monoxide. *reaction kinetics catalysts letter* **2004,** *86* (1), 91-98.

(123) Carlsson, P.; Skoglundh, M.; Thormahlen, P.; Andersson, B., Low-Temperature CO oxidation over a Platinum/Alumina monolith catalysts investigated by step response experiments and simulations. *Topics in Catalysis* **2004,** *30/31*, 375-381.

(124) Arnby, k.; Torncrona, A.; Andersson, B.; Skoglundh, M., Investigations of Pt/Alumina Catalysts with locally High Platinum concentration for oxidation of CO at low temperature. *journal of Catalysis* **2004,** *221*, 252-261.

(125) Arnby, k., Effect of Platinum distribution on oxidation of CO and Hydrocarbons. *journal of Catalysis* **2005,** *233*, 176-185.

(126) Uner, D.; Uner, M., Adsorption Calorimetry in Supported Catalyst Characterization: Adsorption Structure Sensitivity on Platinum/Alumina. *Thermochimica Acta* **2005,** *434* (1), 107-112.

(127) Koci, P.; Stepanek, F.; Kubicek, M.; Marek, M., Meso scale modelling of CO oxidation in digitally reconsructed porous Pt/Alumina Catalyst. *Chemical Engineering Sciences* **2006,** *61*, 3240-3249.

(128) Petersson, M., Ozone promoted carbon monoxide oxidation on Pt/Alumina catalysts. *journal of Catalysis* **2006,** *238*, 321-329.

(129) Bourane, A.; Bianchi, D., *journal of Catalysis* **2001,** *202*, 34.

(130) Bourane, A.; Bianchi, D., *Journal of Catalysis* **2002,** *209*, 114.

(131) Atalik, B.; Uner, D., Structure Sensitivity of Selective CO Oxidation Over Pt/Alumina. *Journal of Catalysis* **2006,** *241*, 268-275.

(132) Salomons, S.; Hayes, R.; Votsmeier, M.; Drochner, A.; Vogel, H.; Malmberg, S.; Gieshoff, J., Mechanistic CO oxidation models with platinum monolith. *Applied catalysis* **2007,** *70*, 305-313.

(133) Yang, J.; Tschamber, V.; Habermacher, D.; Garin, F.; Gilot, P., Effect of sintering on the catalytic activity of Platinum for CO oxidation: Experiments and Modelling. *Applied catalysis B* **2008,** *83*, 229-239.

(134) Salomons, S.; Hayes, R.; Votsmeier, M., The promotion of carbon monoxide oxidation by hydrogen on supported platinum catalyst. *Applied catalysis A* **2009,** *352*, 27-34.

(135) Kneringer, G.; Netzer, F., Adsorption Studies of Oxygen and Carbon Monoxide on Platinum(100) Surface. *Surface Science* **1975,** *49*, 125-142.

(136) Yates, J., Surface Chemistry at metallic step defect sites. *Journal of Vaccumn Science Technology* **1995,** *13* (3), 1359-1367.

(137) Elg, A.-p.; Eisert, F.; Rosen, A., Temperature dependance of the initial sticking probability of oxygen on PT(111) probed with scond harmonic generation. *Surface Science* **1997,** *382*, 57-66.

(138) Chorkendorff, I.; Niemantsverdriet, J., *Concepts of Modern Catalysis and Kinetics*. 2 ed.; Wiley-VCH: 2007; Vol. 1.

(139) Farrauto, R.; Heck, R.; Gulati, S., *Catalytic Air Pollution Control: Commercial Technology*. John Willey & Sons, Inc: 2009.

(140) Kuo, J. C.; Morgan, C. R.; Lassen, H. G., Mathematical Modeling of CO and HC Catalytic Converter Systems. *SAE Paper 710289* **1971**.

(141) Young, L. C.; Finlayson, B. A., Mathematical Models of the Monolithic Catalytic Converter: Part I. Development of Model and Application to Orthogonal Collocation. *A.I.Ch.E. Journal* **1976,** *22* (2), 331-342.

(142) Young, L. C.; Finlayson, B. A., Mathematical Models of the Monolithic Catalytic Converter: Part II. Application to Automobile Exhaust. *A.I.Ch.E. Journal* **1976,** *22* (2), 343-353.

(143) Voltz, S. E.; Morgan, C. R.; Liederman, D.; Jacob, S. M., Kinetic Study of Carbon Monoxide and Propylene Oxidation on Platinum Catalysts. *Industrial and Engineering Chemistry Product Research and Development* **1973,** *12* (4), 294-301.

(144) Dabill, D.; Gentry, S.; Holland, B.; Jones, A., The Oxidation of Hydrogen and Carbon Monoxide Mixtures Over Platinum. *Journal Of catalysis* **1978,** *53* (1), 164-167.

(145) Stetter, J. R.; Blurton, K. F., Catalytic Oxidation of CO and Hydrogen Mixtures in Air. *Industrial and Engineering Chemistry Product Research and Development* **1980,** *19* (2), 214.

(146) Montreuil, C. N.; Williams, S. C.; Adamczyk, A. A., Modeling Current Generation Catalytic Converters: Laboratory Experiments and Kinetic Parameter Optimization - Steady State Kinetics. *Society of Automotive Engineers* **1992,** *920096*.

(147) Koltsakis, G. C.; Konstantinidis, P. A.; Stamatelos, A. M., Development and Application Range of Mathematical Models for 3-Way Catalytic Converters. *Applied Catalysis B: Environmental* **1997,** *12* (2-3), 161-191.

(148) Olsson, L.; Westerberg, B.; Persson, H.; Fridell, E.; Skoglundh, M.; Andersson, B., A Kinetic study of Oxygen adsorpion/desorption and NO oxidation over Pt/Alumina catalysts. *J. Physical Chemistry* **1999,** *103*, 10433-10439.

(149) Tsinoglou, D. N.; Koltsakis, G. C.; Peyton, J., J.C., Oxygen Storage Modeling in Three-Way Catalytic Converters. *Industrial and Engineering Chemistry Research* **2002,** *41* (5), 1152-1165.

(150) Dobereiner, J. W., *Ann. Phys. (Gilbert)* **1823,** *74*, 269-273.

(151) Collins, P. M. D., The Pivotal Role of Platinum in the Discovery of Catalysis. *Platinum Metals Revision* **1986,** *30* (3), 141-146.

(152) Tanner, H.; Taylor, G., Reactions of Hydrogen and Oxygen on Platinum Wires at Low Temperatures and Pressures. *Journal of the American Chemical Society* **1931,** *53* (4), 1289-1296.

(153) Acres, G. J., The Reaction Between Hydrogen and Oxygen on Platinum. Progress in Establishing Kinetics and Mechanisms. *Platinum Metals Revision* **1966,** *10* (2), 60-64.

(154) Lewis, R.; Gomer, R., Adsorption of Hydrogen on Platinum. *Surface Science* **1969,** *17*, 333-345.

(155) Gentry, S.; Firth, J.; Jones, A., Catalytic Oxidation of Hydrogen over Platinum. *Journal of the Chemical Society. Faraday Transaction 1* **1974,** *70* (3), 600-604.

(156) Nishiyama, Y.; Wise, H., Surface Interactions between Chemisorbed Species on Platinum: Carbon Monoxide, Hydrogen, Oxygen and Methanol. *Journal Of catalysis* **1974,** *32*, 50-62.

(157) Peng, Y. K.; Dawson, P. T., The Adsorption, Desorption, and Exchange Reactions of Oxygen, Hydrogen, and Water on Platinum Surfaces. II. Hydrogen Adsorption, Exchange, and Equilibrium *Canadian Journal of Chemistry* **1975,** *53* (2), 298-306.

(158) Weinberg, W. H.; Merrill, R. P., Journal of catalysis: Crystal field surface orbital-bond energy bond order (CFSO-BEBO) calculations for surface reactions I. The reactions CO + O2, NO + CO and H2 + O2 on a platinum (111) surface. *Journal Of catalysis* **1975,** *40* (2), 268-280.

(159) Christmann, K.; Ertl, G.; Pignet, T., Adsorption of Hydrogen on a Pt(111) Surface. *Surface Science* **1976,** *54*, 365-392.

(160) Pacia, N.; Dumesic, J. A., Oxidation of hydrogen on polycrystalline platinum studied by molecular beam reactive scattering. *Journal Of catalysis* **1976,** *41* (1), 155-167.

(161) Boudart, M.; Collins, D. M.; Hanson, F. V.; Spicer, W. E., Reactions between Hydrogen and Oxygen on Pt at low and pressures: A comparison. *Journal of Vacuum Science and Technology* **1977,** *14* (1), 441-443.

(162) Collins, D. M.; Spicer, W. E., The Adsorption of CO, Oxygen and Hydrogen on Pt. Ultraviolet Spectroscopy study. *Surface Science* **1977,** *69* (1), 114-132.

(163) Hanson, F. V.; Boudart, M., The Reaction between Hydrogen and Oxygen over Supported platinum Catalysts. *Journal Of catalysis* **1978,** *53* (1), 56-67.

(164) Barteau, M. A.; Ko, E. I.; Madix, R. J., The Adsorption of CO, Hydrogen and Oxygen on Pt(100). *Surface Science* **1981,** *102* (1), 99-117.

(165) Harris, J.; Kasemo, B.; Tornqvist, E., The Water Reaction on Platinum: An Example of a Precursor Mechanism? . *Surface Science* **1981,** *105*, L288-L296.

(166) Fisher, G. B.; Gland, J. L.; Schmeig, S. J., The Spectroscopic Observation of Water Formation. *Journal of Vacuum Science and Technology* **1982,** *20* (3), 518-521.

(167) Gdowski, G. E.; Madix, R. J., The Kinetics and Mechainsm of the Hydrogen-Oxygen Reactions on Pt(s) - [9(111)X(100)]. *Surface Science* **1982,** *119* (2-3), 184-206.

(168) Gland, J. L.; Fisher, G. B.; Kollin, E. B., The Hydrogen-Oxygen Reaction over the Pt(111) Surface: Transient Titration of Adsorbed Oxygen with Hydrogen. *Journal Of catalysis* **1982,** *77* (1), 263-278.

(169) Creighton, J. R.; White, J. M., *Surface Science* **1982,** *122*, L648.

(170) Bedurftig, K.; Volkening, S.; Wang, Y.; Wintterlin, J.; Jacobi, K.; Ertl, G., *Journal of Physical Chemistry B* **1999,** *103*, 1084.

(171) Brown, N. J.; Schefer, R. W.; Robben, F., High Tempearture Oxidation of H2 on a Platinum Catalyst. *Combustion and Flame* **1983,** *51* (3), 263-277.

(172) Nieuwenhuys, B. E., Adsorption and Reactions of CO, NO, Hydrogen and Oxygen on group VIII Metal Surfaces. *Surface Science* **1983,** *126* (1-3), 307-336.

(173) Ogle, K. M.; White, J. M., The Low Tempertaure Water Formation reaction on Pt(111): A Static SIMS and TDS Study. *Surface Science* **1984,** *139* (1), 43-62.

(174) Akhter, S.; White, J. M., The effect of Oxygen Islanding on CO and H2 Oxidation on Pt(111). *Surface Science* **1986,** *171* (3), 527-542.

(175) Ogle, K. M.; White, J. M., Isotope Effects in the Water Formation on Pt(111). *Surface Science* **1986,** *169* (2-3), 425-437.

(176) Zhdanov, V. P., Some Aspects of the Kinetics of the Hydrogen-Oxygen Reaction over the Pt(111) Surface. *Surface Science* **1986,** *169* (1), 1-13.

(177) Mitchell, G.; Akhter, S.; White, J. M., Water Formation on Pt(111): Reaction of an Intermediate with Hydrogen. *Surface Science* **1986,** *166* (2-3), 283-300.

(178) Mitchell, G.; White, J. M., Identification of the Intermediate in the Water Formation Reaction on Pt(111). *Chemical Physics Letters* **1987,** *135* (1-2), 84-88.

(179) Ljungstrom, S.; Kasemo, B.; Rosen, A.; Wahnstrom, T.; Fridell, E., An Experimental Study of the Kinetics of OH and H2O Formation on Pt in the Hydrogen + Oxygen Reaction. *Surface Science* **1989,** *216* (1-2), 63-93.

(180) Verheij, L.; Hugenschmidt, M.; Poelsema, B.; Comsa, G., The Hydrogen-Oxygen Reactions on the Pt(111) Surface, Influence of Adsorbed Oxygen on the Sticking of Hydrogen. *Surface Science* **1990,** *233* (3), 209-222.

(181) Anton, A. B.; Cadogan, D. C., Kinetics of water formation on Pt(111). *Journal of Vacuum Science and Technology. A: Vacuum, Surface and Films* **1991,** *9* (3), 1890-1897.

(182) Hellsing, B.; Kasemo, B.; Zhdanov, V. P., Kinetics of the Hydrogen-Oxygen Reaction on Platinum. *Journal Of catalysis* **1991,** *132* (1), 210-228.

(183) Kwasniewski, V. J.; Schmidt, L. D., Steps in the reaction Hydrogen+Oxygen.dblharw.Water on Platinum(111):laser-induced thermal desorption at low termperature. *Journal of Physical Chemistry* **1992,** *96* (14), 5931-5938.

(184) Fassihi, M.; Zhdanov, V. P.; Rinnemo, M.; Keck, K. E.; Kasemo, B., A Theoretical and Experimental Study of Catalytic Ignition in the Hydrogen-Oxygen Reaction on Platinum *Journal Of catalysis* **1993,** *141* (2), 438-452.

(185) Zhadnov, V. P., Kinetic Model of the Hydrogen-Oxygen Reaction on Platinum: Bistability, Chemical Waves and Oscillations. *Surface Science* **1993,** *296* (2), 261-273.

(186) Warnatz, J.; Allendore, M.; Kee, R.; Coltrin, M., A Model of Elementary Chemistry and Fluid Mechanics in the Combustion of Hydrogen on Platinum Surfaces. *Combustion and Flame* **1994,** *96* (4), 393-406.

(187) Verheij, L.; Hugenschmidt, M., Hydrogen Adsorption on Oxygen Covered Pt(111). *Surface Science* **1995,** *324* (2-3), 185-201.

(188) Eisert, F.; Rosen, A., In Situ Study of the Catalytic Reaction of H2+O2->H2O on Pt(111) with Second Harmonic Generation. *Surface Science* **1997,** *377* (1-3), 759-764.

(189) Verheij, L.; Hugenschmidt, M., On the Mechainsm of the Hydrogen-Oxygen Reaction on Pt(111). *Surface Science* **1998,** *416* (1), 37-58.

(190) Volkening, S.; Bedurftig, K.; Wintterlin, J.; Ertl, G., Dual-Path Mechanism for Catalytic Oxidation of Hydrogen on Platinum Surface. *Physical Review Letters* **1999,** *83* (13), 2672-2675.

(191) Park, Y.; Aghalayam, P.; Vlachos, D., A Generalized Approach for Predicting Coverage-Dependant reaction Parameters of Complex Surface Reactions: Application to H Oxidation over Platinum. *The Journal of Physical Chemistry A* **1999,** *103*, 8101-8107.

(192) Forsth, M.; Eisert, F.; Gudmundson, F.; Persson, J.; Rosen, A., Analysis of the Kinetics for the H2+O2=H2O Reaction on a hot Pt Surface in the Pressure range of 0.10 to 10 Torr. *Catalysis Letters* **2000,** *66*, 63-69.

(193) Michaelides, A.; Hu, P., A Density Functional Theory Study of Hydroxyl and the Intermediate in the Water Formation Reaction on Pt. *Journal of Chemical Physics* **2001,** *114* (1), 513-519.

(194) Michaelides, A.; Hu, P., Catalytic Water Formation on Platinum: A First-Principle Study. *Journal of the American Chemical Society* **2001,** *123* (18), 4235-4242.

(195) Forsth, M., Sensitivity Analysis of the Reaction Mechanism for Gas-phase Chemistry of Hydrogen and Oxygen Mixtures induced by a Hot Platinum Surface. *Combustion and Flame* **2002,** *130* (3), 241-260.

(196) Nagasaka, M.; Kondoh, H.; Amemiya, K.; Nambu, A.; Nakai, I.; Shimada, T.; Ohta, T., Water formation reaction on Pt(111): Near edge x-ray absorption fine structure experiments and kinetic Monte Carlo simulations. *Journal of Chemical Physics* **2003,** *119* (17), 9233-9241.

(197) Kharlamov, V. F.; Kharlamov, F. V., Model of the Catalytic Reaction 2H2=O2->H2O with the Participation of Molecules in a Precursor State. *Kinetics and Catalysis* **2005,** *48* (3), 430-438.

(198) Nagasaka, M.; Kondoh, H.; Ohta, T., Water formation reaction on Pt(111): Role of proton transfer. *The Journal of Chemical Physics* **2005,** *122*, 204704-1 - 204704-6.

(199) Salomons, S.; Votsmeier, M.; Hayes, R.; Drochner, A.; Vogel, H.; Gieshof, J., CO and Hydrogen Oxidation on a Platinum Monolith Diesel Oxidation Catalyst. *Catalysis Today* **2006,** *117*, 491-497.

(200) Younis, L., Modeling of Hydrogen Oxidation Within Catalytic Packed Bed Reactor. *Journal of the Institute of Energy* **2006,** *79* (4), 222-227.

(201) Schiros, T.; Nslund, L.; Andersson, K.; Gyllenpalm, J.; Karlberg, G. S.; Odelius, M.; Ogasawara, H.; Petterson, L. G. M.; Nilsson, A., Structure and Bonding of the Water-Hydroxyl Mixed Phase on Pt(111). *The Journal of Physical Chemistry* **2007,** *111*, 15003-15012.

(202) Nagasaka, M.; Kondoh, H.; Amemiya, K.; Ohta, T.; Iwasawa, Y., Proton Transfer in a Two-Dimensional Hydrogen-Bonding Network: Water and Hydroxyl on a Pt(111) Surface. *Physical Review Letters* **2008,** *100*, 106101-1-101601-4.

(203) Salomons, S.; Hayes, R.; Votsmeier, M., The Promotion of Carbon Monoxide Oxidation by Hydrogen on Supported Platinum Catalyst. *Applied Catalysis A: General* **2009,** *352* (1), 27-34.

(204) Loya, S.; Depcik, C., Review of Detailed and Global Reaction Mechanisms for CO Oxidation on Platinum. Lawrence, 2009.

(205) Heywood, J. B., *Internal Combustion Engine Fundamentals*. McGraw-Hill, Inc.: New York, 1988.

(206) Cooper, B.; Thoss, J., Role of NO in Diesel Particulate Emission Control. *Society of Automotive engineers* **1989,** (890404), 171-183.

(207) Ambs, J.; McClure, T., The Influence of Oxidation Catalysts on Nitrogen Dioxide in Diesel Exhaust. *Society of Automotive engineers* **1993,** *932494*, 1-7.

(208) Loof, P.; Stenbom, B.; Norden, H.; Kasemo, B., Rapid Sintering in NO of Nanometre-Sized Pt Particles on Alumina Observed by CO Temperature-Programmed Desorption and Transmission Electron Microscopy. *Journal of Catalysis* **1993,** *144* (1), 60-76.

(209) W. Majewski, J. A., Kenneth Bickel, Nitrogen oxides reactions in diesel oxidation catalysts. *Society of Automotive engineers* **1995,** *950374*, 147-154.

(210) Jeffrey Hepburn, E. T., Douglas Dobson, Wiliam Watkins, Experimental and Modeling Investigation of NOx Trap performance. *Society of Automotive engineers* **1996,** *962051*, 1-23.

(211) E. Xue, K. S., J. Ross, Roles of support, Pt loading and Pt dispersion in the oxidation of NO to NO2 and of SO to SO2. *Applied Catalysis B* **1996,** *11*, 65-79.

(212) R. Burch, T. W., Kinetics and Mechanism of the reduction of NO by propane over Pt/Alumina under lean burn condition. *Journal of Catalysis* **1997,** *169*, 45-54.

(213) Fritz, A.; Pitchon, V., The current state of research on automotive lean NOx catalysis *Applied Catalysis B* **1997,** *13* (1), 1-25.

(214) Burch, R.; Fornasiero, P.; Watling, T. C., Kinetic and Mechanism of the reduction of NO by n-octane over Pt/Alumina under lean burn condition. . *Journal of Catalysis* **1998,** *176* (1), 204-214.

(215) Burch. R; Watling. T; J, S., Mechanistic consideration for the reduction of NO over Pt/Alumina catalysts under lean burn condition. *Catalysis Today* **1998,** *42*, 13-23.

(216) Wang, C.-B.; Yeh, C.-T., Effects of Particle Size on the Progressive Oxidation of Nanometer Platinum by Dioxygen. *Journal of Catalysis* **1998,** *178* (2), 450-456.

(217) Fridell, E.; Skoglundh, M.; Johansson, S.; Westerberg, B.; Torncrona, A.; Smedler, G., Investigations of NOx storage Catalysts. *Studies in Surface Science and Catalysis* **1998,** *116*, 537-547.

(218) Lee, J.-H.; Kung, H., Effect of Pt dispersion on the reduction of NO by propene over alumina-supported Pt catalysts under lean-burn conditions. . *Catalysis Letters* **1998,** *51* (1), 1-4.

(219) H. Mahzoul, J. B., P. Gilot, Experimental and mechanistic study of NOx adsorption over NOx trap catalysts. *Applied Catalysis B* **1999,** *20*, 47-55.

(220) S. Schneider, D. B., F. Garin, G. Maire, M. Capelle, G. Meunier, R. Noirot, NO reaction over nanometer scale platinum clusters deposited on alumina: an XAS study. *Applied Catalysis A* **1999,** *189*, 139-145.

(221) Denton, P.; Giroir-Fendler, A.; Praliaud, H.; Primet, M., Role of the Nature of the Support (Alumina or Silica), of the Support Porosity, and of the Pt Dispersion in the Selective Reduction of NO by Propene under Lean-Burn Conditions *Journal of Catalysis* **2000,** *189*, 410-420.

(222) Seker, E.; Gulari, E., Activity and Nitrogen Selectivity of Sol-Gel Prepared Pt/Alumina Catalysts for Selective NOx Reduction. *Journal of Catalysis* **2000,** *194* (1), 4-13.

(223) Bourane, A.; Dulaurent, O.; Salasc, S.; Sarda, C.; Bouly, C.; Bianchi, D., Heats of Adsorption of Linear NO Species on a Pt/Alumina Catalyst Using in Situ Infrared Spectroscopy under Adsorption Equilibrium *Journal of Catalysis* **2001,** *204* (1), 77-88.

(224) Olsson, L.; Persson, H.; Fridell, E.; Skoglundh, M.; Andersson, B., A Kinetic Study of NO Oxidation and NOx Storage on Pt/Alumina and Pt/BaO/Alumina. *J. Physical Chemistry* **2001,** *105*, 6895-6906.

(225) Bartram, M.; Windham, R.; Koel, B., The Molecular Adsorption of Nitrogen Dioxide on Platinum Studied by TPD and Vibrational Spectroscopy. *Surface Science* **1987,** *184* (1), 57-74.

(226) Prinetto, F.; Ghiotti, G.; Nova, I.; Lietti, L.; Tronconi, E.; Forzatti, P., FT-IR and TPD Investigations of the NOx Storage Properties of BaO/Alumina and Pt-BaO/Alumina Catalysts. *Journal of Physical Chemistry B* **2001,** *105*, 12732-12745.

(227) Olsson, L.; Fridell, E., The Influence of Pt Oxide Formation and Pt Dispersion on the Reactions of NO2<-> NO +1/2 Oxygen over Pt/Alumina and Pt/ BaO/Alumina *Journal of Catalysis* **2002,** *210*, 340-353.

(228) Crocoll, M.; Weisweiler, W., Kinetische Untersuchungen Zur Pt-Katalysierten Oxidation von NO: Modellierung und Simulation. *Chemie Ingenieur Technik* **2004,** *76* (10), 1490-1494.

(229) Epling, W.; Campbell, L.; Yezerets, A.; Currier, N.; Parks, j., Overview of the Fundamental Reactions and Degradation Mechanism of NOx Storage/Reduction Catalysts. *Catalysis Reviews* **2004,** *46* (2), 163-245.

(230) Kabin, K.; Muncrief, R.; Harold, M.; Li, y., Dynamics of Storage and Reaction in a Monolith reactor: Lean NOx Reduction. *Chemical Engineering Science* **2004,** *59*, 5319-5327.

(231) Mulla, S. S.; Chen, N.; Delgass, W. N.; Epling, W.; Ribeiro, F. H., NO2 Inhibits the Catalytic Reaction of NO and Oxygen over Pt. *Catalysis Letters* **2005,** *100* (3-4), 267-270.

(232) Benard, S.; Retailleau, L.; Gaillard, F.; Vernoux, P.; Giroir-Fendler, A., Supported Platinum Catalysts for NO Oxidation Sensors. *Applied Catalysis B* **2005,** *55* (1), 11-21.

(233) Crocoll, M.; Kureti, S.; Weisweiler, W., Mean Field Modelling of NO Oxidation Over Pt/Alumina Catalyst Under Oxygen Rich Conditions. *Journal of Catalysis* **2005,** *229*, 480-489.

(234) Olsson, L.; Blint, R.; Fridell, E., Global Kinetic Model for Lean NO Traps. *Industrial and Engineering Chemistry Research* **2005,** *44* (9), 3021-3032.

(235) Mulla, S.; Chen, N.; Cumaranatunge, L.; Blu, G.; Zemlyanov, D.; Delgass, W.; Epling, W.; Ribeiro, F. H., Reaction of NO and Oxygen to Nitrogen Dioxide on Pt: Kinetics and Catalysts Deactivation. *Journal of Catalysis* **2006,** *241*, 389-399.

(236) Schmitz, P. J.; Kudla, R. J.; Drews, A. R.; Chen, A. E.; Lowe-Ma, C. K.; McCabe, R. W.; Schneider, W. F.; Goralski Jr., C. T., NO Oxidation over Supported Pt: Impact of Precursor, Support, Laoding and Processing Conditions Evaluated via High Throughput Experimentation. *Applied Catalysis B* **2006,** *67*, 246-256.

(237) Hauptmann, W.; Drochner, A.; Vogel, H.; Votsmeier, M.; Gieshoff, J., Global Kinetic Models for the Oxidation of NO on Platinum under Lean Conditions. *Topics in Catalysis* **2007,** *42-43*, 157-160.

(238) Marques, R.; Darcy, P.; Costa, P. D.; Mellottee, H.; Trichard, J.-M.; Djega-Mariadassou, G., Kinetics and Mechanisms of Steady-State Catalytic NO+O2 Reactions on Pt/SiO2 and Pt/CeZrO2. *Journal of Molecular Catalysis A: Chemical* **2004,** *221*, 127-136.

(239) Takahashi, N.; Dohmae, K.; Sobukawa, H.; Shinioh, H., Influence of Support Materials and Aging on NO Oxidation Performance of Pt Catalysts Under an Oxidative Atmosphere at Low Temperature. *Journal of Chemical Engineering of Japan* **2007,** *40* (9), 741-748.

(240) Kromer, B.; Cao, L.; Cumaranatunge, L.; Mulla, S.; Ratts, J.; Yezerets, A.; Currier, N.; Ribeiro, F. H.; Delgass, W.; Caruthers, J., Modeling of NO Oxidation and NOx Storage on Pt/BaO/Alumina NOx Traps. *Catalysis Today* **2008,** *136* (1), 93-103.

(241) Weiss, B.; Iglesia, E., NO Oxidation Catalysis on Pt Clusters: Elementary Steps, Structural Requirements and Synergistic Effects of Nitrogen Dioxide Adsorption Sites. *Journal of Physical Chemistry C* **2009,** *113*, 13331-13340.

(242) Bhatia, D.; McCabe, R. W.; Harold, M.; Balakotaiah, V., Experimental and Kinetic Study of NO oxidation on model Pt Catalysts. *Journal of Catalysis* **2009,** *266* (1), 106-119.

(243) Hauptmann, W.; Votsmeier, M.; Gieshoff, J.; Drochner, A.; Vogel, H., Inverse Hysteresis During the NO Oxidation on Pt Under Lean Conditions. *Applied Catalysis B* **2009,** *93* (1), 22-29.

(244) Gland, J., Molecular and Atomic Adsorption of Oxygen on the Pt(111) and Pt(S)-12(111)x(111) Surfaces. *Surface Science* **1980,** *93*, 487-514.

(245) Gorte, R. J.; Schmidt, L. D., Binding States and Decomposition of NO on Single Crystal Planes of Pt. *Surface Science* **1981,** *109* (2), 367-380.

(246) Gohndrone, J.; Masel, R. I., A TPD Study of Nitric Oxide Decomposition on Pt(100), Pt(411) and Pt(211). *Surface Science* **1989,** *209* (1-2), 44-56.

(247) Agrawal, V.; Trenary, M., An Infrared Study of NO Adsorption at Defect Sites on Pt(111). *Surface Science* **1991,** *259* (1-2), 116-128.

(248) Kinnersley, A. D.; Darling, G. R.; Holloway, S., Effect of Initial Rotations on the Sticking of NO on Pt(111). *Surface Science* **1997,** *377-379*, 567-571.

(249) Zhu, J.; Kinne, M.; Fuhrmann, T.; Denecke, R.; Steinruck, H., In Situ High Resolution XPS Studies on Adsorption of NO on Pt. *Surface Science* **2003,** *529*, 384-396.

(250) Mei, D.; Ge, Q.; Neurock, M.; Kieken, L.; Lerou, J., First-Principles-based Kinetic Monte Carlo Simulation of Nitric Oxide Decomposition Over Platinum and Rhodium Surfaces Under Lean-Burn Conditions *Molecular Physics* **2004,** *102* (4), 361-369.

(251) Ovesson, S.; Lundqvist, B.; Schneider, W.; Bogicevic, A., NO Oxidation Properties of Pt(111) revealed by AB INITIO kinetic Simulations. *Physical Review B* **2005,** *71*, 115406-115410.

(252) Ford, D.; Xu, Y.; Mavrikakis, M., Atomic and Molecular Adsorption on Pt(111). *Surface Science* **2005,** *587*, 159-174.

(253) Disselkamp, R. S.; Tonkyn, R. G.; Chin, Y.-H.; Peden, C. H., Developing Multiple - Site kinetic Models in Catalysis Simulations: A Case Study of O2+2NO<-> 2NO2 Oxidation-Reduction Chemistry on Pt(100) Catalyst Crystals Facets. *Journal of Catalysis* **2006,** *238* (1), 1-5.

(254) Getman, R.; Schneider, W., DFT-Based Characterization of the Multiple Adsorption Modes of Nitrogen Oxides on Pt(111). *Journal of Physical Chemistry C* **2007,** *111*, 389-397.

(255) Smeltz, A. D.; Getman, R.; Schneider, W.; Ribeiro, F. H., Coupled Theoretical and Experimental Analysis of Surface Coverage Effects in Pt-Catalyzed NO and Oxygen Reaction to NO2 on Pt(111). *Catalysis Today* **2008,** *136* (1-2), 84-92.

(256) Mudiyanselage, K.; Yi, C.-W.; Szanyi, J., Oxygen Coverage Dependence of NO Oxidation on Pt(111). *Journal of Physical Chemistry C* **2009,** *113*, 5766-5776.

(257) Getman, R.; Schneider, W., DFT-Based Coverage -Dependent Model of Pt-Catalyzed NO Oxidation. *CHEMCATCHEM* **2010,** *2* (11), 1450-1460.

(258) Smeltz, A. D.; Delgass, W.; Ribeiro, F. H., Oxidation of NO with Oxygen on Pt(111) and Pt(321) Large Single Crystals *Langmuir* **2010,** *26* (21), 16578-16588.

(259) Despress, J.; Elsener, M.; Koebel, M.; Krocher, O.; Schnyder, B.; Wokaun, A., Catalytic Oxidation of Nitrogen Monoxide Over Pt/Silica. *Applied Catalysis B* **2004,** *50*, 73-82.

(260) Oi-Uchisawa, J.; Obuchi, A.; Enomoto, R.; Liu, S.; Nanba, T.; Kushiyama, S., Catalytic Performance of Pt Supported on Various Metal Oxides in the Oxidation of Carbon Black. *Applied Catalysis b* **2000,** *26* (1), 17-24.

(261) Xue, E.; Seshan, K.; Ommen, J. G.; Ross, J. R. H., Catalytic Control of Diesel Engine Particulate Emission: Studies on Model Reactions Over a EuroPt-1 (Pt/SiO2) Catalyst. *Applied Catalysis B* **1993,** *2* (2-3), 183-197.

(262) Jayat, F.; Lembacher, C.; Schubert, U.; Martens, J. A., Catalytic NOx reduction in lean burn exhaust over Pt/silica catalysts with controlled Pt particle size. *Applied Catalysis B* **1999,** *21*, 221-226.

(263) Ji, Y.; Toops, T.; Graham, U.; Jacobs, G.; Crocker, M., A Kinetic and DRIFTS Study of Supported Pt Catalysts for NO Oxidation. *Catalysis Letters* **2006,** *110* (1-2), 29-37.

(264) Rankovic, N.; Nicolle, A.; Berthout, D.; Da Costa, P., Extension of a Kinetic Model for NO oxidation and NOx Storage to fixed-Bed Pt/Ba/Alumina Catalysts. *Catalysis Communications* **2010,** *12* (1), 54-57.

(265) Parker, D. H.; Bartram, M.; Koel, B., Study if High Coverages of Atomic Oxygen on the Pt(111) Surface. *Surface Science* **1989,** *217* (3), 489-510.

(266) Groppi, G.; Belloli, A.; Tronconi, E.; Forzatti, P., A comparison of lumped and distributed models of monolith catalytic combustors. *Chemical Engineering Science* **1995,** *50* (17), 2705-2715.

(267) Hayes, R. E.; Kolaczkowski, S. T., Mass and heat transfer effects in catalytic monolith reactors. *Chemical Engineering Science* **1994,** *49* (21), 3587-3599.

(268) Hoffman, J. D., *Numerical Methods for Engineers and Scientists*. McGraw-Hill, Inc.: New York, 1992.

(269) Tannehill, J.; Anderson, D.; Pletcher, R., *Computational Fluid Mechanics and Heat Transfer*. 2nd ed.; Taylor & Francis: 1997.

(270) Hirsch, C., *Numerical Computation of Internal and External Flows*. John Wiley & Sons Limited: New York, 1991; Vol. 1.

(271) Morton, K. W.; Mayers, D. F., *Numerical Solution of Partial Differential Equations: An Introduction*. Second ed.; Cambridge University Press: Cambridge, 2005; p 278.

(272) Koltsakis, G. C.; Konstantinidis, P. A.; Stamatelos, A. A., Development and Application Range of Mathematical Models for 3-Way Catalytic Converters. *Applied Catalysis B: Environmental* **1997,** *12* (2-3), 161-191.

(273) Konstantas, G.; Stamatelos, A. M., Modelling Three-Way Catalytic Converters: An Effort to Predict The Effect of Precious Metal Loading *Journal of Automobile Engineering* **2007,** *221*, 355-373.

(274) Herskowitz, M.; Kenney, C., CO Oxidation on Pt Supported Catalysts - Kinetics and Multiple Study-States. *Canadian Journal of Chemical Engineering* **1983,** *61* (2), 194-199.

(275) Campbell, C. T.; Ertl, G.; Kuipers, H.; Segner, J., A Molecular Beam Study of the Adsorption and Desorption of Oxygen from a Pt(111) Surface. *Surface Science* **1981,** *107* (1), 220-236.

(276) Yeo, Y. Y.; Vattuone, L.; King, D. A., Calorimetric Heats for CO and Oxygen Adsorption and for Catalytic CO Oxidation reaction on Pt(111). *Journal of Chemical Physics* **1997,** *106* (1), 392-401.

(277) Dumesic, J. A.; Rudd, D. F.; Aparicio, L. M.; Rekoske, J. E.; Trevino, A. A., *The Microkinetics of Heterogeneous Catalysis*. American Chemical Society Washington D.C., 1993.

(278) ReactionDesign *Chemkin III Data Files*.

(279) Design, R. *Thermodynamic Data Core Utility Manual*; 2003.

(280) Design, R. *Chemkin -III file Ther.dat*; 1997.